TÜBINGER
GEOWISSENSCHAFTLICHE
ARBEITEN (TGA)

Reihe C:
Hydro-, Ingenieur- und Umweltgeologie

Schriftleitung:
P. Grathwohl, G. Teutsch

Ralf Klingbeil

Outcrop Analogue Studies - Implications for Groundwater Flow and Contaminant Transport in Heterogeneous Glaciofluvial Quaternary Deposits

TGA, C43, 1998

Outcrop Analogue Studies
-
Implications for Groundwater Flow and Contaminant Transport in Heterogeneous Glaciofluvial Quaternary Deposits

RALF KLINGBEIL

Lehrstuhl für Angewandte Geologie
Institut für Geologie und Paläontologie
Universität Tübingen
Sigwartstraße 10
72076 Tübingen
FRG

Herausgeber: Institut und Museum für Geologie und Paläontologie der Universität Tübingen
Sigwartstraße 10, D-72076 Tübingen

Schriftleitung der Reihe C: Lehrstuhl für Angewandte Geologie
Prof. Dr. Peter Grathwohl & Prof. Dr. Georg Teutsch

Redaktion: Dr. Mike Herbert

ISSN 0935-4948

Tübinger Geowiss. Arbeiten	Reihe C	Nr. 43	111 S., 99 Abb., 28 Tab.	Tübingen, 1998

Outcrop Analogue Studies - Implications for Groundwater Flow and Contaminant Transport in Heterogeneous Glaciofluvial Quaternary Deposits

RALF KLINGBEIL[1]

Abstract: Groundwater from gravel-filled valley aquifers is an important source for drinking water supplies in many regions. At the same time these aquifers are endangered by different sources of pollution from industrial and agricultural activities commonly located within these valleys. As experience shows, the subsurface characterisation of such heterogeneous sand and gravel aquifers is often insufficient for detailed reactive transport predictions. In particular, high resolution, hydraulic and hydrogeochemical aquifer data is required for accurate groundwater risk assessments, clean-up studies or the optimisation of investigation methods. However, these saturated aquifers are not directly accessible. Thus one option to evaluate relevant parameters are aquifer or outcrop analogue studies of accessible outcrops, which represent similar stratigraphy and lithology.

For this purpose sand and gravel outcrops were investigated in the Quaternary of SW Germany, particularly in the area north and northwest of the Lake Constance. The outcrops were photographed and the internal structures interpreted and mapped by digitising, based on a scheme of 23 lithofacies adapted from the architectural element analysis and lithofacies classification commonly used in sedimentology. The resulting high resolution 2D sedimentological data sets each covering an area of approximately 25 m by 5 m were combined in a database. To provide hydrogeological parameters for the different lithofacies various measurements were performed. Characteristic hydraulic conductivities and porosities for the lithofacies types were derived from *in situ* and laboratory gas tracer and pneumatic experiments, water permeameter tests and sieve analysis data. For the gas tracer and pneumatic experiments a new technique was developed.

The sedimentological data sets were extended by the incorporation of the hydrogeological parameters. Regrouping of the lithofacies types led to five relevant hydrofacies types (bimodal, open framework, planar/trough/horizontal and massive gravels, and sands).

Consequences for the hydraulics of groundwater flow and for contaminant transport in such subsurface heterogeneities, comprising of homogeneous hydrofacies elements, were discussed on the basis of one example outcrop. It was found that in the environments investigated it is very unlikely that the local high conductivity zones described by open framework gravels are connected regionally to preferential flow paths. Furthermore the simulation of sorptive transport of a hydrocarbon contaminant demonstrated the importance of incorporating kinetic sorption into the transport model. Under natural flow conditions the contact time of contaminated water with the aquifer material is so short that only in finer grained material, such as sand, can equilibrium sorption conditions be achieved. Hence, the effective retardation of a contaminant front depends highly on the proportion of sands through which it passes.

---

[1] Dissertation at the Geowissenschaftliche Fakultät, Universität Tübingen

Author's address: Geologisch-Paläontologisches Institut, Sigwartstr. 10, 72076 Tübingen, FRG

Tübinger Geowiss. Arbeiten	Reihe C	Nr. 43	111 S., 99 Abb., 28 Tab.	Tübingen, 1998

Kurzfassung: Grundwasser aus kieshaltigen Talaquiferen stellt in vielen Regionen eine bedeutende Trinkwasserresource dar. Gleichzeitig sind diese Grundwasserleiter aber auch bedroht durch verschiedene Verunreinigungsquellen von in den Tälern angesiedelter industrieller und landwirtschaftlicher Nutzung. Wie die Erfahrung zeigt, ist die Characterisierung des Untergrunds dieser heterogenen Sand- und Kiesaquifere für detailierte Vorhersagen reaktiven Transports oft unzureichend. Für eine genaue grundwasserbezogenen Risikoabschätzung, Sanierungsuntersuchungen oder die Optimierung von Untersuchungsmethoden sind insbesondere hochaufgelöste hydraulische und hydrogeochemische Aquiferdaten notwendig. Diese Grundwasserleiter sind jedoch nicht direkt zugänglich, daher muß die Bestimmung relevanter Parameter durch die Nutzung von Aquifer-, bzw. Aufschlußanalogverfahren, die die Stratigraphie und Lithographie des Aquifers representieren, erfolgen.

Zu diesem Zweck wurden Sand- und Kiesaufschlüsse im Quartär SW Deutschlands, insbesondere in der Region nördlich und nordwestlich des Bodensees, untersucht. Die Aufschlüsse wurden photographiert und die internen Strukturen anhand einer Aufstellung von 23 Lithofazies, die aus den in der Sedimentologie gebräuchlichen Architekturelementanalyse und Lithofazies Klassifizierungen abgeleitet wurden, interpretiert und mittels Digitalisierung kartiert. Die erhaltenen hochaufgelösten 2D sedimentologischen Datensätze von jeweils ca. 25 m mal 5 m wurden in einer Datenbank zusammengefaßt. Um hydrogeologische Parameter für die Lithofazies zur Verfügung zu stellen, wurden verschiedene Messungen durchgeführt. Charakteristische hydraulische Durchlässigkeiten und Porositäten für die Lithofazies Typen wurden von *in situ* und Labor-, Gastracer und -pneumatik Versuchen, sowie Wasserpermeameter Experimenten und Siebanalysendaten ermittelt. Für die Gastracer- und -pneumatikversuche wurde ein neues Meßverfahren entwickelt.

Die sedimentologischen Datensätze wurden unter Einbeziehung der hydrogeologischen Parameter erweitert. Dabei konnten durch eine Neugruppierung der Lithofaziestypen fünf relevante Hydrofazies definiert werden (bimodale Kiese, Rollkiese, planare/trogförmige/horizontale und massive Kiese, sowie Sande).

Konsequenzen für die Hydraulik der Grundwasserströmung und für den Schadstofftransport in derartigen, aus homogenen Hydrofazieselementen bestehenden Untergrundheterogenitäten wurden auf der Basis eines Beispielaufschlusses diskutiert. In den untersuchten Regionen ist es demnach sehr unwahrscheinlich, daß lokal hochdurchlässige Zonen, die durch Rollkieslagen beschrieben werden, regional zu bevorzugten Fließwegen verbunden sind. Außerdem wurde durch die Simulation sorptiven Schadstofftransports einer Kohlenwasserstoffverbindung die Wichtigkeit der Berücksichtigung von kinetischem Sorptionsverhalten im Transportmodell demonstriert. Unter natürlichen Grundwasserfließbedingungen ist die Kontaktzeit des kontaminierten Grundwassers mit dem Aquifermaterial so gering, daß nur in feinkörnigem Material, wie z.B. Sand, die Bedingungen für Gleichgewichtssorption erreicht werden können. D.h. die effektive Retardation einer Kontaminantionsfront hängt stark von den durchströmten Sandanteilen ab.

Acknowledgements

This work is part of the special research programme SFB 275, project C3 "Quaternary Valley Fills: Climatic History, Sediment Content and Hydrogeology" funded by the German Science Foundation (DFG).

I would like to thank my advisor, Prof. Dr. Georg Teutsch, for his continuous support and examination of this thesis.

Likewise I feel obliged to PD Dr. Martin Sauter and Dr. Rudi Liedl for many contributions in respect to different applied, theoretical and computational aspects of this work. Particularly I am thankful for the advice in sedimentological questions by Prof. Dr. Thomas Aigner.

My special thanks deserve my colleagues and friends for the many discussions of the sedimentology (Ulrich Asprion and Sybille Kleineidam), the physical aspects of the gas flow, its description by analytical solutions and the simulation of gas and groundwater flow and transport (Dr. Janet Whittaker and Renate Jaritz), the support during the GIS application and all soft- and hardware problems (Gerhard Lörcher and Markus Siegl).

Furthermore, I am indebted to the following students or former students, Thomas Hölz, Christoph Danner, Jakob Sierig, Thomas Weiß and Mischa Hagmeier, without their help I would not have been able to conduct the field work and who helped me a lot during the laboratory measurements and by the digitisation of the outcrop photographs.

I appreciate very much the sedimentological and Quaternary discussions I had at various occasions in the field with Dr. Peter Huggenberger from the University of Basel (formerly EAWAG Dübendorf), Dr. Ellwanger and Christa Szenkler from the Geological Survey (GLA) of Baden-Württemberg.

For all the practical help during the development of the field equipment and the field measurements I would like to thank the workshop of the Geological Department, in particular Herrn Stumpp, Herrn Kurz and Herrn Kürner, the quarry companies in Steißlingen, Böhringen, Birkenbühl, Bittelschieß, Tettnang and Hirschau, in particular Dr. Mohr, Herrn Hellstern and his conductors of the shovel dredgers.

Finally I thank Dr. Janet Whittaker for reading, commenting and correcting the manuscript and the endless patience she - and many other friends - have shown.

Table of Contents

1 Introduction 1
1.1 Objectives 2
1.2 Methodology and Approach 2
1.3 Review of Literature 3

2 Project Area 6
2.1 Quaternary Geology and Sedimentology 6
2.2 Quaternary Stratigraphy in the Field Areas 8
2.2.1 Tettnang 8
2.2.2 Bittelschieß 8
2.2.3 Friedingen, Steißlingen, Böhringen and Birkenbühl (Singen Basin) 8
2.3 Architectural Elements 9
2.4 Sedimentological Classification - Lithofacies Types 11
2.5 Hydrogeology 13

3 Flow and Transport of Water and Gas in Unconsolidated Porous Formations (Theory) 15
3.1 Fluid Flow in Porous Formations 15
3.1.1 Flow of Water 15
3.1.2 Flow of Gas 15
3.1.2.1 Turbulence 16
3.1.2.2 Slip Flow (Klinkenberg) 18
3.1.2.3 Compressibility 18
3.1.2.4 Saturation by Air/Water 19
3.2 Transport of Gas - Use of Gas as a Tracer 20
3.2.1 Advection and Dispersion 20
3.2.2 Diffusion 20
3.2.3 Analytical Solutions for Gas Tracer Breakthrough Curves 21
3.3 Parameters of Gas Tracers 21
3.4 Hydraulic Conductivity from Gas Measurements 22
3.4.1 Gas Pneumatic Tests 22
3.4.1.1 Laboratory Tests 22
3.4.1.2 *In Situ* Field Tests 22
3.4.2 Gas Tracer Tests 23
3.4.2.1 Laboratory Tests 23
3.4.2.2 *In Situ* Field Tests 23

4 Simulating Steady State Gas Flow and Transport 25
4.1 Modelling of 3D Gas Flow 26
4.1.1 Modelling Compressible Gas Flow 26
4.1.2 Modelling Incompressible Gas Flow 26
4.1.3 Comparison of Compressible and Incompressible Modelling and Analytical Solutions 27
4.2 3D Modelling of Pathlines of Gas Particles 27
4.2.1 Comparison of Effective Permeabilities Derived from Particle Travel Times with Harmonic Mean Permeabilities 28

5 Development of Field and Laboratory Equipment for Pneumatic Tests 29
5.1 Concept 29
5.2 Hardware 30
5.2.1 Measurement Devices 30
5.2.1.1 Source of Carrier and Tracer Gas 30
5.2.1.2 Mass Flow Controller 30
5.2.1.3 Overpressure Meter 31
5.2.1.4 Pressure Difference Controller 31

5.2.1.5 Mass Flow Meter 31
5.2.1.6 Control Valve 31
5.2.1.7 Vacuum Pump 31
5.2.1.8 Infrared Detector for Tracer Gas 31
5.2.2 Field Equipment 31
5.2.2.1 Hollow Metal Rods 31
5.2.2.2 Pulling Equipment 32
5.2.2.3 Excavator 33
5.2.2.4 Hydraulic Hammer 33
5.2.3 Laboratory Equipment 33
5.3 Software 34
5.3.1 Program for Tracer Tests 34
5.3.2 Program for Pneumatic Tests 35

6 Hydraulic Parameters - Measurements and Results 36
6.1 *In Situ* Field Gas Tests 36
6.1.1 Tracer Tests 37
6.1.2 Pneumatic Pumping Tests 39
6.1.3 Comparison between *In Situ* Tracer and Pneumatic Pumping Tests 39
6.2 Laboratory Gas Tests 39
6.2.1 Tracer Tests 39
6.2.2 Pneumatic Pumping Tests 40
6.2.3 Comparison between Laboratory Tracer and Pneumatic Pumping Tests 40
6.3 Laboratory Water Tests (Darcy Experiments) 40
6.3.1 Comparison between Laboratory Gas and Water Tests 40
6.4 Evaluation of Sieve Analysis Data 41
6.5 Porosity Measurements 41
6.6 Comparison of All Measurements 41
6.6.1 Data Measured During this Project 41
6.6.2 Data from Literature 42
6.7 Lithofacies to Hydrofacies Relationship 43

7 Digital-Photographic Approach for Sedimentological and Hydrogeological Database (Regionalisation) 44
7.1 Digital-Photographic Approach 44
7.1.1 Camera 44
7.1.2 Slide Scanner 44
7.2 Sedimentological Database 44
7.3 Database to Grid Transfer 45
7.3.1 Transfer of Gridded ASCII Data for Geostatistical Analysis 45
7.3.2 Transfer of Gridded ASCII Data for Groundwater Flow and Transport Modelling 45

8 2D Groundwater Flow and Transport Modelling 47
8.1 The Example Data Set 47
8.1.1 Statistical Parameters 47
8.1.1.1 Histograms 48
8.1.1.2 Semi-Variograms 48
8.2 Groundwater Flow Modelling 48
8.2.1 Effective Hydraulic Conductivity 49
8.3 Transport Modelling 49
8.3.1 Advective Transport Only, Conservative Tracer 49
8.3.2 Advective Transport with Equilibrium Sorption 51
8.3.2.1 Equilibrium Distribution Coefficients 51
8.3.2.2 Incorporating Equilibrium Sorption into the Model 51
8.3.3 Advective Transport with Kinetic Sorption 51
8.3.3.1 Kinetic Distribution Coefficients 51
8.3.3.2 Incorporating Kinetic Sorption into the Model 52
8.4 Comparison of Different Transport Mechanisms 52

9 Conclusions 56

References 58

Annex 1: Derivation of Analytical Solutions for Gas Flow 63
A 1.1 One Dimensional Differential Equation 63
A 1.1.1 Compressibility Assumption 63
A 1.1.2 Incompressibility Assumption 64
A 1.1.3 Comparison 64
A 1.2 Two Dimensional Radially Symmetric Differential Equation 65
A 1.2.1 Compressibility Assumption 65
A 1.2.2 Incompressibility Assumption 66
A 1.2.3 Comparison 66
A 1.3 Three Dimensional Spherically Symmetric Differential Equation 66
A 1.3.1 Compressibility Assumption 67
A 1.3.2 Incompressibility Assumption 67
A 1.3.3 Comparison 68

Annex 2: Analytical Solutions for Gas Tracer Breakthrough Curve Evaluation 69
A 2.1 Dirac or Slug Input 70
A 2.1.1 One Dimensional Transport 70
A 2.1.2 Two Dimensional Transport 70
A 2.1.3 Three Dimensional Transport 70
A 2.1.4 Convergent Radial Flow 70
A 2.2 Continuous Input 71
A 2.2.1 One Dimensional Transport 71
A 2.2.2 Two Dimensional Transport 71
A 2.2.3 Three Dimensional Transport 71
A 2.2.4 Convergent Radial Flow 71
A 2.3 Input over a Time Interval Δt 72
A 2.3.1 Häfner Solution (constant concentration) 72
A 2.3.2 Van Genuchten Solution (constant mass flux) 73
A 2.3.3 Program DTTRACER 73

Annex 3: Listing of Program DTTRACER 77

Annex 4: Listing of Input File for DTTRACER 79

Annex 5: Derivation of k_c, k_i, k_i/k_c Formulas for 1D and 3D Tracer Test Evaluation 80
A 5.1 Laboratory Tests (1D) 80
A 5.2 Field Tests (3D) 81

Annex 6: Analogy between Groundwater and Gas Flow Modelling 82

Annex 7: Measurement Data 83
A 7.1 *In Situ* Gas Tracer Data 83
A 7.2 *In Situ* Gas Pneumatic Data 85
A 7.3 Laboratory Gas Tracer Data 87
A 7.4 Laboratory Gas Pneumatic Data 87

Annex 8: Collection of 2D Sedimentological Outcrop Studies 89

Annex 9: Listing of Program ARCTOGS 106

Annex 10: Listing of Program PREMFLOW 107

Annex 11: Listing of Program RETARD 110

List of Figures

Fig. 2.1: Location map of field area in southwest Germany 6

Fig. 2.2: Extent of the last glaciation (Würm) in the area of the Alps (Ehlers, 1994) 7

Fig. 2.3: Location of field sites in the Quaternary environment north and northwest of Lake Constance, Baden-Württemberg. The outermost extent of different ice ages are shown (We: Würm, Re: Riß; based on a map from Villinger, 1989) 7

Fig. 2.4: Detailed map of location of field sites in the Quaternary environment of the Singen basin, small arrows indicating the direction of meltwater streams at the end of the last (Würm) glaciation (based on a map from Schreiner, 1992) 7

Fig. 2.5: Three-dimensional sketch of extent of the Würm iceage in the Singen basin (Schreiner, 1992) 8

Fig. 2.6: Three-dimensional sketch of today's landscape and subsurface geology in the Singen basin (Schreiner, 1992) 8

Fig. 2.7: Different types of architectural elements, the "eight basic architectural elements" in fluvial deposits (Miall, 1985) 9

Fig. 2.8: Models illustrating the composition of different architectural elements in a river's depositional environment, a: gravel-bed braided river showing dissected lobes of sediment-gravity-flow deposits (SG), b: gravel-bed river dominated by traction-current deposits (GB), c: deep, gravel-bed braided river with well-defined topographic levels (models 1, 2, 3 from Miall, 1985, 1996) 10

Fig. 2.9: Model of depositional environment for glaciofluvial deposits, glacial series (Schreiner, 1992, originally from Penck and Brückner, 1909) 11

Fig. 2.10: Conceptual hydrogeological model for actual water budget in the Singen basin, values in 10^6 m^3/y if not stated otherwise (Koziorowski, 1986) 13

Fig. 3.1: Conversion factors for gas conductivity, K_g, hydraulic conductivity, K_f, and intrinsic permeability, k, for a temperature of 10 °C 16

Fig. 3.2: Pressure gradient (Druckgradient [Pa/m]) versus velocity (Q/A, Volumenstromdichte [$m^3/m^2/a$]) for different uniform sands (Ruiz-Rodriguez, 1994; Kretzer, 1989) 17

Fig. 3.3: Validity of Darcy's law: Permeability (Permeabilität [m^2]) depending on Reynolds number, Re = Re_k, for various effective grain sizes, d_{10} (Ruiz-Rodriguez, 1994; Kretzer, 1989) 17

Fig. 3.4: Reciprocal mean pressure, 1/p, versus apparent permeability, k_{app}, "Klinkenberg plot" (after Klinkenberg, 1942) 18

Fig. 3.5: Deviation of apparent permeability, k_{app}, from intrinsic permeability, k, caused by not correcting for slip flow (adapted from Jaritz, 1998) 18

Fig. 3.6: Differences of three-dimensional pressure distribution (incompressible to compressible) for various pressure differences and radii applied in the field 19

Fig. 3.7: Differences of three-dimensional pressure gradient distribution (incompressible to compressible) for various pressure differences and radii applied in the field 19

Fig. 3.8: Dependence of the specific permeability, k_s, from saturation for gas, k_g, (CO_2) and water, k_l, (Carman, 1956, original from Wyckoff and Botset, 1936) 20

Fig. 3.9: Comparison of calculations of intrinsic permeability, considering compressible (k_c), assuming incompressible (k_i) gas flow for different pressure differences Δp from one-dimensional tracer breakthrough curves in the laboratory 23

Fig. 3.10: Comparison of calculations of intrinsic permeability, considering compressible (k_c), assuming incompressible (k_i) gas flow for different pressure differences Δp from three-dimensional tracer breakthrough curves in the field (r_l = 0.01 m, r_{sph} = 1 m) 24

Fig. 4.1: Comparison of steady state gas flow modelling considering compressibility - AIR (Lin and Kinzelbach, 1991), or assuming incompressibility - MODFLOW (McDonald and Harburgh, 1984) with the respective analytical solutions: abstraction flow rate Q_{out} = 0.564 l/s, permeability k = $8.0 \cdot 10^{-12}$ m^2, representing a pressure difference (drop) from atmospheric pressure of Δp = 100 HPa 25

Fig. 4.2: Vertical section through schematic model of 2D geological structure of two different hydraulic conductivities for models of high permeability unit (k_1) in low permeable environment (k_2) and vice versa 26
Fig. 4.3: Gridded vertical profile of 2D heterogeneous geological structures (cell width 0.05 m), representing a section of a gravel outcrop, hydraulic conductivities based on Jussel (1992), isolines of modelled 3D pressure distribution (interval of 5 Pa) due to abstraction of 4 l/s from the centre, example of particle pathline 27

Fig. 5.1: General concept for field and laboratory pneumatic and tracer tests: controlled injection concentration, controlled flow and pressure difference, measured extraction concentration 29
Fig. 5.2: Detailed measurement concept, here for the field pneumatic and tracer tests 30
Fig. 5.3: Field setup 30
Fig. 5.4: Field setup: interior of the van, foreground: vacuum pump, flow and pressure control unit, PC with input and output boards, background: compressor 30
Fig. 5.5: Photograph of tip (top) and end (centre) of inner and outer hollow metal rods with outlet openings and connection for tubing after use in the field, withdrawal tools (bottom) 32
Fig. 5.6: Technical drawing of inner and outer hollow metal rods with dimensions in mm, a: overview, b: detailed tip and end of inner rod with dimensions in mm 32
Fig. 5.7: Photograph of pulling equipment to withdraw hollow metal rods in the field 33
Fig. 5.8: Detailed photograph of pulling equipment to withdraw hollow metal rods in the field 33
Fig. 5.9: Technical drawing of different parts of pulling equipment with dimensions in mm 33
Fig. 5.10: Photograph of small excavator, driving hollow metal rods into outcrop wall 33
Fig. 5.11: Photograph of hammer, inserting hollow metal rods into outcrop wall 33
Fig. 5.12: Photograph of measurement equipment in the laboratory 34
Fig. 5.13: Front panel of GAS TRACER CONTROL PROGRAM, developed under LabVIEW®, allowing the online control of measurement data in the field and laboratory 34

Fig. 6.1: Correction chart for pressure drop, Δp_{in}, due to injection of flow rate, Q_{in}, through metal rod and tubing, as a function of tube length 36
Fig. 6.2: Correction chart for pressure drop, Δp_{out}, due to extraction of flow rate, Q_{out}, through metal rod and tubing, as a function of tube length 36
Fig. 6.3: Correction of measured arrival times: time, t_{meas}, versus relative concentration, $c(t)/c_{max}$, of breakthrough curves with the tubing only for different pressure differences compared to direct measurement of the injection pulse 37
Fig. 6.4: *In situ* gas tracer tests in Gcpo in an outcrop at Friedingen, SW Germany; tubing and hollow metal rods in the outcrop 38
Fig. 6.5: Examples of results from *in situ* gas tracer tests in Gcpo in an outcrop at Friedingen, SW Germany, with corresponding abstraction and injection flow rates, dotted: measured breakthrough curves, continuous line: fitted analytical solutions 38
Fig. 6.6: *In situ* gas tracer tests in Sh in an outcrop at Böhringen, SW Germany, tubing and hollow metal rods in the outcrop 38
Fig. 6.7: Examples of results from *in situ* gas tracer tests in Sh in an outcrop at Böhringen, SW Germany, with corresponding abstraction and injection flow rates, dotted: measured breakthrough curves, continuous line: fitted analytical solutions 38
Fig. 6.8: Comparison of results from all field gas tracer and pneumatic tests 39
Fig. 6.9: Results from laboratory gas pneumatic tests 40
Fig. 6.10: Comparison of results from all laboratory gas tracer and pneumatic tests 40
Fig. 6.11: Grain size distribution curves for different lithofacies (here combined to hydrofacies, s. Ch. 7) 41
Fig. 6.12: Comparison of results from laboratory gas pneumatic tests and sieve analysis data 41
Fig. 6.13: Comparison of hydraulic conductivities for all lithofacies categories with model parameters used by Jussel (1992) 43
Fig. 6.14: Relationship between lithofacies and hydrofacies, based on the comparison of all measurement results, P/T/H: planar, trough and horizontal gravel 43

Fig. 6.15: Comparison of horizontal and vertical hydraulic conductivities for all hydrofacies categories with the model parameters used by Jussel (1992) 43

Fig. 7.1: Outcrop analysis: lithofacies interpreted from a wide angle photograph, hydrofacies and horizontal hydraulic conductivities based on the field and laboratory measurements, here: ST2 from Steißlingen, SW Germany 46

Fig. 8.1: The example data set: lithofacies in outcrop ST2 from Steißlingen, SW Germany, gridded with a cell size of 0.025 m, resulting in a grid of 890 x 178 cells 47

Fig. 8.2: The example data set: gridded hydraulic conductivity distribution, K_h(m/s), displayed as natural logarithm, $\ln K_h$ 47

Fig. 8.3: Histogram of the number of cells (percentage) in each of the 23 lithofacies classes of the example data set 48

Fig. 8.4: Histogram of the number of cells (percentage) in each of the 5 hydrofacies classes in the example data set 48

Fig. 8.5: Semi-variogram of hydraulic conductivities ($\ln K_h$ and $\ln K_v$) in x direction in the example data set 48

Fig. 8.6: Semi-variogram of hydraulic conductivities ($\ln K_h$ and $\ln K_v$) in z direction in the example data set 48

Fig. 8.7: Pathlines of 25 particles tracked through the example data set on the groundwater head distribution from chapter 8.2, initial distribution of particles flux dependent on left hand side 50

Fig. 8.8: Cumulative particle arrival times (breakthrough curves) from 400 particles, representing advective transport only, advective transport with kinetic sorption and advective transport with equilibrium sorption 50

Fig. 8.9: Histogram plot of log of particle arrival times of 400 particles from advective transport only 50

Fig. 8.10: Grain size distribution curves for samples from the outcrop ST2 in Steißlingen, SW Germany (thin lines) on which the input data for the intra-particle diffusion model (thick lines) is based 52

Fig. 8.11: Distribution coefficients, K_d [l/kg], versus contact time t [s] calculated with an intra-particle diffusion model (Jäger, 1996) 52

Fig. 8.12: Histograms of contact times of particles in the different hydrofacies types after kinetic retardation 53

Fig. 8.13: Histogram of contact pathlength of particles in the different hydrofacies types 53

Fig. 8.14: Path lengths per particle, divided up into parts of contributions by the different hydrofacies, particles numbered according to their spatial position so that particle number 1 is that nearest the top of the aquifer and 400 that nearest the base 54

Fig. 8.15: Arrival times per particle as sum of contact times per cell along the flow path of each particle, divided up into different parts representing the contributions of the different hydrofacies, particles numbered according to their spatial position so that particle no. 1 is that nearest the top of the aquifer and 400 that nearest the base. Different transport scenarios: a - advection only, b - advection and equilibrium sorption, c - advection and kinetic sorption 54

Fig. 8.16: Arrival times per particle as sum of contact times per cell along the flow path of each particle, divided up into different parts representing the contributions of the different hydrofacies, vertical order of particles sorted according to total arrival times, normalised to mean arrival time. Different transport scenarios: a - advection only, b - advection and equilibrium sorption, c - advection and kinetic sorption 54

Fig. A1.1: Pressure, p_c, and pressure gradient, p'_c, distribution over a one dimensional column of 1 m length with a total pressure drop of $100 \cdot 10^2$ Pa from analytical solution, considering compressible steady state gas flow 64

Fig. A1.2: Pressure, p_i, and pressure gradient, p'_i, distribution over a one dimensional column of 1 m length with a total pressure drop of $100 \cdot 10^2$ Pa from the analytical solution, assuming incompressible steady state gas flow 64

Fig. A1.3: Error of pressure, p, and pressure gradient, p', distribution over a one dimensional column of 1 m length with a total pressure drop of $100 \cdot 10^2$ Pa relative to the analytical solution considering compressible steady state gas flow 64

Fig. A1.4: Pressure, p_c, and pressure gradient, p'_c, distribution over a two dimensional radial flow field of 1 m radius with total pressure drop of $100 \cdot 10^2$ Pa from the analytical solution, considering compressible steady state gas flow 65

Fig. A1.5: Pressure, p_i, and pressure gradient, p'_i, distribution over a two dimensional radial flow field of 1 m radius with total pressure drop of $100 \cdot 10^2$ Pa from the analytical solution, assuming incompressible steady state gas flow 65

Fig. A1.6: Error of pressure, p, and pressure gradient, p', distribution over a two dimensional radial flow field of 1 m radius with a total pressure drop of $100 \cdot 10^2$ Pa relative to the analytical solution considering compressible steady state gas flow 66

Fig. A1.7: Pressure, p_c, and pressure gradient, p'_c, distribution over a three dimensional radial flow field of 1 m radius with a total pressure drop of $100 \cdot 10^2$ Pa from the analytical solution, considering compressible steady state gas flow 67

Fig. A1.8: Pressure, p_i, and pressure gradient, p'_i, distribution over a three dimensional radial flow field of 1 m radius with a total pressure drop of $100 \cdot 10^2$ Pa from the analytical solution, assuming incompressible steady state gas flow 67

Fig. A1.9: Error of pressure, p, and pressure gradient, p', distribution over a three dimensional radial flow field of 1 m radius with a total pressure drop of $100 \cdot 10^2$ Pa relative to the analytical solution considering compressible steady state gas flow 68

Fig. A2.1: Analytical solutions, after Häfner et al. (1992) and van Genuchten (1981), for breakthrough curves calculated by DTTRACER with input parameters: distance $x = 0.5$ m, injection time interval $\Delta t = 10$ s, tracer velocity $v_a = 0.02$ m/s, dispersivity $\alpha = 0.005$ m, diffusion coefficient $Diff = 1.69 \cdot 10^{-5}$ m²/s, retardation factor $R = 1$ 75

Fig. A2.2: Analytical solutions after Häfner et al. (1992) for breakthrough curves calculated by DTTRACER with different injection time intervals $\Delta t = t_{in}$. Other parameters similar to those in Fig. A 2.1 75

Fig. A2.3: Analytical solutions after Häfner et al. (1992) for breakthrough curves calculated by DTTRACER with different tracer velocities v_a. Other parameters similar to those in Fig. A 2.1 75

Fig. A2.4: Analytical solutions after Häfner et al. (1992) for breakthrough curves calculated by DTTRACER with different dispersivities α. Other parameters similar to those in Fig. A 2.1 75

Fig. A2.5: Analytical solutions after Häfner et al. (1992) for breakthrough curves calculated by DTTRACER with different coefficients of molecular diffusion D_m. Other parameters similar to those in Fig. A 2.1 76

Fig. A2.6: Analytical solutions after Häfner et al. (1992) for breakthrough curves calculated by DTTRACER with different retardation factors R. Other parameters similar to those in Fig. A 2.1 76

List of Tables

Tab. 2.1: Simplified Quaternary stratigraphy of northwest Europe and the Alps, *italic*: interglacials (after Ehlers, 1994; Murawski, 1983) 6
Tab. 2.2: Architectural elements in fluvial deposits (after Miall, 1985, 1996) 10
Tab. 2.3: Lithofacies codes (after Miall, 1977, 1978, 1996) 12
Tab. 2.4: Major and minor classification for lithofacies codes (after Keller, 1996) 12
Tab. 2.5: Lithofacies code used in this project 13
Tab. 2.6: 23 sedimentologically reasonable lithofacies types, as a combination of lithofacies codes from Tab. 2.5 13
Tab. 2.7: Hydraulic conductivities and porosities for Pleistocene Rhine gravels from (Jussel, 1992) 14

Tab. 3.1: Analytical solutions for one-, two-, three-dimensional (radïal) steady state gas flow considering compressibility or assuming incompressibility 19
Tab. 3.2: Linear approximations of the non-linear general flow equation for gas, depending on assumptions for the total pressure difference $\Delta p = p_1 - p_2$, p_0 represents the initial (gas) pressure, mostly atmospheric (after Massmann, 1989) 19
Tab. 3.3: Diffusion coefficients of CO_2 in air, calculated from equation 3.26 21
Tab. 3.4: Parameters for different potential tracer gases and air (Perry and Green, 1984, * Olschewski et al., 1995) 21

Tab. 4.1: Comparison between particle tracking effective permeabilities, k_{mod}, and cell averaged permeabilities, k_{calc}, -: pathlines do not represent straight lines 28

Tab. 6.1: Averaged horizontal and vertical hydraulic conductivities measured with gas tracer tests in the field for various lithofacies 38
Tab. 6.2: Averaged horizontal and vertical hydraulic conductivities measured with gas pneumatic tests in the field for various lithofacies 39
Tab. 6.3: Averaged hydraulic conductivities measured with gas tracer and pneumatic tests in the laboratory for different lithofacies 40
Tab. 6.4: Averaged hydraulic conductivities measured with water (permeameter experiments) in the laboratory, K_{water}, and calculated on the basis of sieve analysis data (after Beyer, 1964) for different lithofacies, K_{sieve} 40
Tab. 6.5: Porosities, n, for different lithofacies 41
Tab. 6.6: Comparison of all measured and assigned data (*in situ* and laboratory) for all lithofacies types, bold: measured, standard: assigned 42
Tab. 6.7: Final parameter table for all lithofacies and corresponding hydrofacies categories, based on the comparison of values in Tab. 6.6, parameters will be used in the outcrop analysis studies (Ch. 7) and in the modelling (Ch. 8) 42

Tab. 8.1: Comparison of different averages for the horizontal and vertical hydraulic conductivities of the example data set 49
Tab. 8.2: Typical equilibrium distribution coefficients, K_d^{eq}, for hydrofacies for 100 µg/l phenanthrene in a pulverised sample 51

Tab. A7.1: Listing of all measured *in situ* gas tracer data, Böhringen, SW Germany, bold: data used in further evaluation 83
Tab. A7.2: Listing of all measured *in situ* gas tracer data, Friedingen, SW Germany, bold: data used in further evaluation 84
Tab. A7.3: Listing of all measured *in situ* gas pneumatic data, Böhringen, SW Germany, bold: data used in further evaluation 85
Tab. A7.4: Listing of all measured *in situ* gas pneumatic data, Friedingen, SW Germany, bold: data used in further evaluation 86
Tab. A7.5: Listing of all measured laboratory gas tracer data, samples from Friedingen and Böhringen, SW Germany 87

Tab. A7.6: Listing of all measured laboratory gas pneumatic data, based on gas tracer measurements, samples from Friedingen and Böhringen, SW Germany 87
Tab. A7.7: Listing of all measured laboratory gas pneumatic data, based on gas pneumatic measurements, samples from Friedingen and Böhringen, SW Germany 88

List of Abbreviations

α	[m]	dispersivity
β	[-]	Forchheimer turbulence factor
Φ	[m^2/s^2]	fluid potential, energy per unit mass
μ	[Pa·s = kg/m·s]	dynamic viscosity
μ_f	[$1.307 \cdot 10^{-3}$ Pa·s]	dynamic viscosity of water
μ_g	[$1.794 \cdot 10^{-5}$ Pa·s]	dynamic viscosity of gas
ν	[m^2/s]	kinematic viscosity
ν_g	[$1.45 \cdot 10^{-5}$ m^2/s]	kinematic viscosity of gas
π	[-]	pi
θ	[-]	angular coordinate
ρ	[kg/m^3]	density
ρ_f	[999.7 kg/m^3]	density of water
ρ_g	[1.23 kg/m^3]	density of gas
$(\Sigma\nu)_i$	[-]	atomic diffusion volume for gas i
A	[m^2]	cross section area
b	[1/Pa]	Klinkenberg constant
c	[mg/l or Vol.%]	concentration of a substance in water or air, respectively
c_0	[mg/l or Vol.%]	initial concentration of a substance in water or air, respectively
c_{max}	[Vol.%]	maximal concentration
c_{meas}	[Vol.%]	measured absolute concentration
d_{10}	[m]	effective grain size, 10 % of grain size distribution curve
d_{60}	[m]	60 % of grain size distribution curve
D	[m^2/s]	dispersion coefficient
D_L	[m^2/s]	longitudinal dispersion coefficient
D_T	[m^2/s]	transversal dispersion coefficient
D_m	[m^2/s]	coefficient of molecular diffusion
D_m^{air}	[m^2/s]	coefficient of molecular diffusion of gas in air
f	[-]	Freundlich coefficient
g	[m/s^2]	gravitational acceleration
h	[m]	hydraulic head
k	[m^2]	intrinsic permeability of porous material
k_{app}	[m^2]	apparent intrinsic permeability, not Klinkenberg corrected
k_c	[m^2]	intrinsic permeability from tracer tests, considering compressibility
k_{eff}	[m^2]	effective permeability, not saturation corrected
k_i	[m^2]	intrinsic permeability from tracer tests, assuming incompressibility
k_s	[-]	specific permeability with respect to saturation
K	[m/s]	fluid conductivity
K_d	[l/kg]	sorption distribution coefficient
K_f	[m/s]	hydraulic conductivity
K_g	[m/s]	air/gas conductivity
K_h	[m/s]	horizontal hydraulic conductivity
K_v	[m/s]	vertical hydraulic conductivity
l	[m]	height/length of cylinder, distance between extraction and injection, length of tubing
m	[kg]	mass
m_g	[kg]	mass of gas
M_i	[-]	molecular weight of substance i
n	[-]	porosity
n_{air}	[-]	air filled porosity
n_g	[mol]	no of moles
p	[Pa = 10^{-2} mbar]	pressure
p_0	[1 atm ≈ 10^5 Pa]	atmospheric pressure

Δp	[Pa = 10^{-2} mbar]	pressure difference
Δp_{in}	[Pa = 10^{-2} mbar]	pressure drop due to injection flow
Δp_{meas}	[Pa = 10^{-2} mbar]	measured pressure difference
Δp_{out}	[Pa = 10^{-2} mbar]	pressure drop due to extraction flow
Pe	[-]	Peclet number
q_f	[1/s]	flow rate of water per cell volume
q_g	[1/s]	flow rate of gas per cell volume
Q	[m^3/s]	flow rate
Q_{in}	[m^3/s]	injection flow rate
Q_{out}	[m^3/s]	outflow flow rate
r	[m]	distance (1D), radial distance (2D, 3D)
r_{cyl}	[m]	radius of cylinder
r_{sph}	[m]	radius of sphere of convergent flow field
R	[-]	retardation factor
R_g	[8.3145 J/mol·K]	molar or general gas constant
Re	[-]	Reynolds number
Re_{crit}	[-]	critical Reynolds number
s	[mg/kg]	concentration of a substance sorbed in or on the aquifer matrix
t	[s]	time
$t_{0.5}$	[s]	mean arrival time
t_{app}	[s]	lag time caused by apparatus, tubing and hollow metal rods
t_{meas}	[s]	measured time ($t + t_{app}$)
Δt	[s]	injection time interval for tracer injection (= t_{in})
T_g	[K]	absolute temperature
U	[-]	unconformity coefficient, d_{60}/d_{10}
v	[m/s]	Darcy velocity
v_a	[m/s]	tracer velocity (= v/n)
V	[m^3]	volume
W	[kg·m^2/s^2]	total energy
W_{pot}	[kg·m^2/s^2]	potential energy
W_{kin}	[kg·m^2/s^2]	kinetic energy
W_{el}	[kg·m^2/s^2]	elastic energy
x	[m]	distance in x direction, directional index
y	[m]	distance in y direction, directional index
z	[m]	distance in z direction, directional index, elevation

1 Introduction

The complex nature of sedimentational and erosional processes has resulted in an often highly heterogeneous distribution of hydrogeological parameters in aquifers. These heterogeneities of hydraulic conductivities, porosities and other hydrogeologically relevant parameters have long been seen as a major hurdle in the determination of actual flow paths. Subsurface investigations, e.g. pumping tests, are only able to deliver effective parameters at a scale much larger than the typical length of structures in a heterogeneous aquifer. However, the detailed information is necessary for accurate predictions of flow paths and local contaminant transport.

Results from many different field sites (e.g. Borden (Sudicky, 1986), Cape Cod (Hess, 1990; Hess et al., 1991), Twin Lake (Moltyaner and Killey, 1988), Horkheim (Ptak and Teutsch, 1994)) show that the required spatial resolution for predicting transport parameters cannot be achieved by standard subsurface investigation techniques such as pumping tests, flowmeter or core analysis. Although in the vertical direction flowmeter and core analysis data give enough details to characterise the heterogeneities, in the horizontal direction boreholes often have larger spacings so that they are not able to provide information on correlation at small scales. Thus the continuity of structures, especially in the horizontal direction, is often not known. Based on this experience more detailed information is needed, particularly on the small scale structure and distribution of heterogeneous parameters in aquifers. Anderson (1989) explains the specific need for investigations at a finer resolution:

> "Additional basic research is required to measure hydraulic conductivity variation within representative hydrogeologic facies and to develop statistical descriptions to represent the variations. Such detailed descriptions of hydraulic conductivity may be necessary to describe ground-water flow at a local scale for analysis of contaminant transport." (Anderson, 1989)

Throughout this work the term facies will be used for a homogeneous sedimentological or a homogeneous but not necessarily isotropic hydrogeological unit (Anderson, 1989), formed under characteristic conditions which lead to characteristic hydraulic properties.

The problems associated with the necessary transfer from basic geological field information into hydrologically interpretable data depend on the direction from which the task is approached by the geologist or hydrologist. Whereas the primary goal of a geologist is to describe an ancient depositional environment with observable patterns by formulating descriptions of the spatial patterns of sedimentological properties (so called "facies models"), the goal of the hydrologist is the opposite: to infer patterns of properties on the basis of some knowledge of the depositional environment (Scheibe and Freyberg, 1990). These fundamentally different goals may be a reason for the difficulties sometimes encountered in communication between geologists, hydrologists and hydrogeologists.

To describe the heterogeneities in sedimentary deposits three major approaches have been distinguished (Koltermann and Gorelick, 1992, 1996): structure-imitating, process-imitating and descriptive methods.

Structure-imitating models are aimed at the reproduction of geometric relations of sedimentary deposits. For example sequence stratigraphy is one kind of a structure-imitating approach as empirical relations between rates of sea level change, subsidence and sedimentation result in characteristic structures or forms of deposits. Another class relies on spatial statistics, correlated random fields and probabilistic rules to generate geometric patterns, sometimes with deterministic (process-based) constraints developed from facies relations. Those models which do not consider the sedimentological processes provide little understanding of geological environments and may lead to geologically impossible interpretations.

Process-imitating includes aquifer model calibration methods and geological process models. They comprise physical mechanisms which are formulated in terms of governing partial differential equations. This approach represents interactions of geological processes operating over spatial and temporal scales.

The descriptive approach classifies depositional environments, facies relations and sedimentary basins. It divides an aquifer into zones of characteristic hydraulic properties based on the connection from geological observations to facies relations. Descriptive models cannot be used to quantitatively test hypotheses regarding detailed geological history.

Generally real aquifers are not accessible for investigation to derive hydrogeological parameters at the scale required. An outcrop composed of similar stratigraphy and lithologies

as the aquifer may be viewed as analogue of this aquifer ("aquifer/outcrop analogue") representing an accessible formation for the examination of spatial geometries and for *in situ* measurements of hydrogeological parameters at smaller scale.

This project concentrates on fluvial Quaternary deposits such as braided river deposits, delta sediments and bed load systems. For the project area most of the sediments were deposited by the latest glaciation period north and northwest of Lake Constance in Baden-Württemberg, Southwest Germany.

The braided river systems are of special interest as (a) in Central Europe they are particularly endangered by pollution as many industrial sites and the major infrastructure (roads and railways) are situated on such valley fills, (b) four major hydrogeological investigations, including tracer tests (Borden (Sudicky, 1986), Cape Cod (Hess, 1990), Twin Lake (Moltyaner and Killey, 1988), Horkheim (Ptak and Teutsch, 1994)) were performed in glaciofluvial sediments made up of mainly braided stream deposits, (c) connected highly permeable units allowing the formation of preferential flow paths for contaminants in groundwater may be present in braided channel fill sequences, (d) distinct facies and elements have been mapped and interpreted for current and past braided stream environments, and (e) a large volume of sedimentological research exists in this area.

1.1 Objectives

Following the state of hydrogeological science in heterogeneous environments as described above, this work concentrates on basic data collection and evaluation. The objectives of this project are

- to use accessible glaciofluvial Quaternary deposits of gravel pits in Southwest Germany as an aquifer or outcrop analogue,
- to use *in situ* and laboratory gas measurements for the evaluation of permeabilities/hydraulic conductivities and other transport parameters for the specific sedimentological units under consideration in the outcrops,
- to gain high resolution two dimensional spatial distributions (data sets) of sedimentology and hydrogeological properties, i.e. lithological facies distributions, hydraulic conductivity and other transport parameter distributions from outcrop analysis, and
- to examine by modelling the consequences of heterogeneous distributions of hydraulic conductivities, porosities and retardation coefficients in these 2D data sets for groundwater flow and transport, especially with regard to effective parameter estimation at a scale larger than the heterogeneities present.

1.2 Methodology and Approach

As detailed mapping of hydrogeological parameters by subsurface groundwater testing methods is not possible, the intention is to measure, instead of in the saturated zone of a real aquifer, in an analogue of a real aquifer. The aquifer analogue shows similar distribution of hydrogeological parameters but is easier accessible for detailed facies mapping and measurements within the outcrops of the unsaturated zone.

Firstly a method has to be developed to measure hydraulic conductivities, porosities and other relevant hydrogeological parameters *in situ* in Quaternary outcrops of gravel pits. This method should be a tool, quick and easy to handle, to determine the parameters in question in the field. Techniques of hydraulic characterisation of sandstone environments by measuring the flow of gas through a probe into the potential reservoir rock (mini permeameters, Eijpe and Weber, 1971, Goggin et al., 1988) are widely used in the fields of sedimentology and petrology. In the Quaternary environments rocks are unconsolidated, therefore the general principles of mini permeameters are not applicable. The technique used in this work can be described as small scale pneumatic pumping tests and gas tracer tests. Two metal rods are driven into the outcrop walls by a small excavator and a hydraulic hammer. Control software measures and controls in- and outflow of gas and pressure drops through the tubing and the metal rods (chapter 5). This newly developed technique offers a unique possibility for detailed quantification of permeabilities of specific structures *in situ*, in unconsolidated outcrops. In the past this could only be achieved by taking mostly disturbed samples in the field and conducting tests, e.g. permeameter measurements in the laboratory.

The development of this method required fundamental knowledge of gas flow and transport in porous material and in particular of the relationship between gas and water flow, as the permeabilities measured were converted into hydraulic conductivities for further use in hydrogeological evaluation (chapter 3).

Furthermore, for numerical assessment prior to the *in situ* measurements, gas flow for specific homogeneous and heterogeneous cases was modelled with two different three dimensional finite difference programs: AIR (Lin and Kinzelbach, 1991) and MODFLOW (McDonald and Harburgh, 1984). Whereas AIR allows to model compressible and incompressible gas flow, MODFLOW is normally restricted to incompressible groundwater flow; advective transport may be calculated for the flow fields using MODPATH (Pollock, 1989). In this project it was adapted for the modelling of gas flow, assuming incompressibility. Advantages and disadvantages are discussed in chapter 4.

Beside the development of this new investigation technique, field measurements were conducted to measure the parameters of characteristic structures within the outcrops. To verify these measurements samples were taken and evaluated in the laboratory. For specific sedimentological structures data was collected and compared from *in situ* gas tracer tests, *in situ* gas pneumatic (pumping) tests, laboratory gas tracer tests, laboratory gas pneumatic (pumping) tests and - as a well known standard method - from sieve analysis data (chapter 6). The comparison led to mean characteristic parameters (e.g. hydraulic conductivities, porosities), which were viewed as the most plausible parameters for the specific structure. Incorporating the results from (Kleineidam, 1998) the data was extended to include hydrogeochemical parameters such as retardation factors (chapter 8).

Furthermore, a database was built up including photographic images of Quaternary outcrop walls, their sedimentological and their hydrogeological interpretations. The sedimentological facies analysis (e.g. Miall, 1978, 1996; Keller, 1996) was the basis for the lithological facies distribution of the outcrops evaluated (chapter 2) and led to interpreted sedimentological cross sections of photographed outcrop walls of around 25 by 5 m. The database was built up in the style of a GIS (Geographical Information System) format and allowed the input of further information, such as hydrogeological parameters (chapter 7).

The data of the database is accessible for further use such as geostatistical analysis or two dimensional groundwater flow and transport modelling. One outcrop was used for geostatistical characterisation and modelling of groundwater flow and conservative as well as sorptive transport to determine the importance of such sedimentological heterogeneities for effective hydrogeological parameters (e.g. hydraulic conductivity) over distances of up to 30 m (chapter 8).

1.3 Review of Literature

The review of literature is restricted to the two most important areas relevant to this project: the outcrop analysis studies of deposits of braided river, delta or bed load systems and the use of gas flow and transport for hydrogeological characterisation.

Literature on outcrop analysis studies

Literature on outcrop analysis studies can be subdivided into three main groups: fundamental sedimentological articles, Quaternary sedimentological papers and articles on the combination of hydrogeology and sedimentology.

The fundamental articles on sedimentology of braided river, delta and bed load systems comprise many field studies of ancient or present river systems, some overview articles and papers related to the general classification of these sediments. Most of the field studies describe the sediments present in a specific case or area, either in ancient or today's depositional environments. Often detailed cross sections are drawn (e.g. Bluck, 1979; Leopold and Wolman, 1957; Williams and Rust, 1969). Explanations about the processes leading to such fluvial deposits are given by Ashmore (1991), Best (1988), Carling and Glaister (1987) and Mosley (1976). These authors explain specifically the genesis of scour pools within channel confluences or the development of well-sorted bimodal structures during rapid sand and gravel deposition at a down gradient step along river flow directions. A good overview on the sedimentological science with respect to braided river environments is given by the article collection of Best and Bristow (1993). It shows how braided rivers are examined for a wide spectrum of purposes, such as understanding of sedimentological processes, a determination of the boundaries between architectural elements by ground penetrating radar, and aerial remote sensing methods. For the general classification of fluvial sediments at different scales the contributions of two particular authors are notable. Miall has described many different scenarios of fluvial depositional environments (Miall, 1977, 1978, 1980, 1981, 1985, 1996). Looking at an outcrop or sediment of fluvial deposits generally two distinctions can be made: the architectural element analysis and the lithofacies distribution. The architectural element analysis is mainly the splitting up of the whole

complex deposit into units of similar depositional systems on the basis of their erosional faces and sometimes their differences in stratification, i.e. whether it has been deposited in a cross stratified braided river or massive bed load system. Within a single architectural element different lithologies may be present. So a second classification code is necessary for the distribution of lithofacies over the whole profile or cross section. Whereas the first distinction (architectural element analysis) is often more important for the sedimentologists, the applied geologist or the hydrogeologist is often more interested in the composition of different lithologies, since they are directly connected to hydraulic properties such as permeabilities and porosities. In the German speaking region Keller (1996) has adapted the architectural element analysis of Miall to the Swiss Molasse Basin and the lithofacies codes to glaciofluvial sediments (Keller, 1992, 1996).

The connection to Quaternary sedimentology is often realised by adapting the general classifications after Miall (1985) to the specific Quaternary environment with glaciofluvial (pre- and postglacial) or glacial specifications. The fluvial lithofacies codes are expanded for gravel, sand, silt, mud and till structures (Eyles et al., 1983; Fraser and Bleuer, 1987; Fraser and Cobb, 1982). At some distance from the glacial source areas some authors are able to relate the grain size distribution in fluvial deposits to the Quaternary climate (Vittori and Ventura, 1995). However, Quaternary geology is more often related to stratigraphical and morphological terminology than to genetic classifications of glacial or glaciofluvial deposits (Goldthwait, 1988; Jurgaitis and Juozapavicius, 1988). In combination with shallow geophysical prospection with high resolution ground penetrating radar (GPR) sedimentological units can be mapped either in two dimensional sections or by connecting many sections in three dimensional blocks (Beres and Haeni, 1991; Huggenberger, 1993; Huggenberger et al., 1994; Asprion and Aigner, 1997; Asprion, 1998). Although the detailed lithofacies distribution may not be evaluated directly, this method allows the detection in three dimensions of architectural elements which comprise specific lithologies. In combination with two dimensional outcrop mapping the lithofacies can be identified, described and transferred into the third dimension. By describing the sedimentology and measuring the hydraulic parameters it is possible to connect the geophysical measurements to hydrogeological studies (Huggenberger et al., 1988; Huggenberger, 1994).

Hydrogeology and sedimentology are the basis of various studies related to groundwater flow and transport in heterogeneous aquifers. Related to the work of Huggenberger et al. (1988) are the statistical descriptions and stochastic numerical tracer experiments of Jussel (1992) and Jussel et al. (1994), which took place in highly heterogeneous glaciofluvial deposits of the Rhine glacier at the border between Switzerland and Germany. As the sediments are genetically similar to those under consideration in this project, the data from his work is cited frequently within this work. Jussel combines laboratory measurements of hydraulic parameters from mainly disturbed and some undisturbed (nitrogen-frozen) samples with statistical-sedimentological outcrop analysis. The results are used to model groundwater flow and transport in lenticular shaped sedimentological structures. Based on fluvial deposits of the Wabash River, USA, Scheibe (1992) developed a numerical aquifer of scroll bars, trough sets and mud drapes which was then also used for flow and transport modelling (Scheibe and Freyberg, 1990; Scheibe, 1992). Another attempt by Webb (1992) was based on the deterministic modelling of sedimentological genesis of a braided river deposit and led to a three dimensional hydraulic conductivity field for which the preferential flow paths for contaminants in groundwater flow were simulated (Webb, 1992, 1994; Webb and Anderson, 1996). Architectural element analysis and the interconnectedness of sedimentological units are discussed by Fogg (1990), Fogg et al. (1997), Carle and Fogg (1996). There the concept of a transition probability matrix in combination with indicator geostatistics is developed to describe the connection from one sedimentological unit to another: a way of overcoming the problems associated with geostatistics, as it enables the generation of sequences based on the order of their geological succession (e.g. couplets of x and y) instead of only descriptions of correlation length and variability of single structures. Statistical analysis of sedimentological or hydrogeological parameters by horizontal and vertical variograms are used by Davis et al. (1992, 1993). An approach to interpret hydrostratigraphy with indicator geostatistics is used by Johnson and Dreiss (1989). More basic estimations of permeabilities and porosities with respect to the lithofacies present in fluvial deposits are performed by Pryor (1973) and Weber (1982). For the general background of the importance of sedimentary heterogeneities to groundwater flow and transport Anderson (1989),

Koltermann and Gorelick (1992, 1996) are recommended.

Literature on gas flow and transport

The literature on gas flow and transport related to this work can be grouped into three categories: the fundamental literature on gas flow, advective (and dispersive) transport and diffusion in porous media; the field and laboratory experiments in different scales for various purposes and the articles on the modelling of gas flow.

The fundamental articles on gas flow may be subdivided into those restricted to diffusional processes and others dealing with advection and dispersion. The diffusion of gas in porous media with special emphasis to carbon disulphide (CS_2) is described in an early paper by Penman (1940). Diffusion and diffusion coefficients for gases in porous materials are derived in the diploma theses of Klein (1992) and Weiβ (1992). Fundamental information on gas diffusion can be found in Atkins (1986), Lyman et al. (1990), Perry and Green (1984) and Sallam et al. (1984). A dissertation dealing with *in situ* measurements of the characteristics of gas diffusion in unsaturated porous media is given by Kreamer (1982). The more fundamental work on advection, dispersion and diffusion of gas in porous media often deals with the questions of Darcy- or non-Darcy-flow with respect to turbulence, compressibility and slip flow problems (Carman, 1956; Dake, 1978; Dullien, 1992; Dranchuk and Flores, 1975; Firoozabadi and Katz, 1979; Houpeurt, 1959; Kidder, 1957; Klinkenberg, 1942). Examples of parameter evaluation (permeabilities in different rocks: low permeability sandstones or high permeability unconsolidated sands and gravels) with the help of gas flow and transport measurements are given by Abu-El-Sha'r and Abriola (1997), Dürbaum et al. (1969), Garbesi et al. (1996), Voigt et al. (1973), Kretzer (1989) and Pusch et al. (1986).

The papers related to field and laboratory measurements are often based on a specific application such as permeability and porosity parameterisation of reservoir rocks with mini permeameters or the design and monitoring of vapour extraction systems for groundwater and soil remediation. Mini permeameters and their use in mainly consolidated rock are discussed in Eijpe and Weber (1971) and Goggin et al. (1988). The specific questions related to the optimal design of vapour extraction systems, i.e. the evaluation of local unsaturated soil properties and of the radius of influence for such extraction systems are described either on the basis of *in situ* gas tracer tests at the scale of the extraction system under consideration or by modelling three dimensional gas pressure distribution, sometimes in combination with transport modelling. References for particular case studies, the use of tracer gases such as He, Rn, SF_6 or CO and practical advice for the design of extraction systems are given by Fierz et al. (1993), Johnson et al. (1990), Olschewski et al. (1995), Richardson et al. (1996) and Schmidt (1994). A more general article on the validity of Darcy's law in relation to soil venting operations is presented by Ruiz-Rodriguez (1994) which is based on the work of Kretzer (1989). Literature on modelling of gas flow and transport is often connected to the optimal design of vapour extraction systems. A fundamental reference is given by Massmann (1989), in which the opportunities of modelling gas flow with standard groundwater flow models is justified for specific boundary conditions. Others have developed models for the flow of gas, assuming compressibility or incompressibility, in either two dimensions (Mohr and Merz, 1995) or three dimensions (Marley, 1991; Marley et al., 1990, 1992; Lin and Kinzelbach, 1991; Borho, 1995). In this project one approach uses the model AIR (Lin and Kinzelbach, 1991) with a larger number of cells, needed to describe more complex heterogeneous three dimensional structures. The other approach presented is based on the groundwater flow model MODFLOW (McDonald and Harburgh, 1984).

2 Project Area

2.1 Quaternary Geology and Sedimentology

Quaternary sand and gravel deposits are found in different regions of Europe. The most important glaciations took place in northern Europe. The ice cover in the Alps during the ice ages was much smaller in comparison to the north European glaciers. The glacial periods in the Quaternary of Germany can therefore be divided geographically into those resulting from the Scandinavien and those from the Alpine glaciation. Two minor areas were covered by ice in the Black Forest and the Harz mountains. The ice cover led to glacial deposits such as till in the form of different moraines and in their melting phase to glaciofluvial sanders and various other structures composed of sandy and gravely, often heterogeneous deposits.

Whereas the sanders in northern Germany are situated at a larger distance from their source area and show often a more sandy than gravely composition, the glaciofluvial deposits in the surroundings of the Alps are often more gravely and heterogeneous. This results in different types of deposits: fluvial deposits of the glacial outwash in braided rivers with much steeper morphological gradients and at a closer distance to the source areas in the Alps, flood or debris flow deposits and delta sediments of meltwater streams discharging into near-ice-margin lakes (glaciofluvial-glaciolacustrine deposits; Menzies, 1995).

The Quaternary sediments investigated in this project are situated in southwest Germany, north and northwest of Lake Constance (Bodensee) in the federal state of Baden-Württemberg (Fig. 2.1). They were deposited by meltwaters of the Rhine glacier, which was resting at the site of today's Lake Constance during and after the last two Alpine glaciation periods (Riß and Würm).

The Quaternary stratigraphy varies for the two main regions of Quaternary deposits (NW Europe and the Alps). Although it is possible to correlate the different regional names during the later periods (Late Pleistocene), the corresponding interglacial and glacial stages in the earlier periods (Middle and Early Pleistocene) are much disputed within the field of Quaternary science. In table 2.1 a general overview is given, relating the periods to a starting age and to the general magneto-stratigraphy.

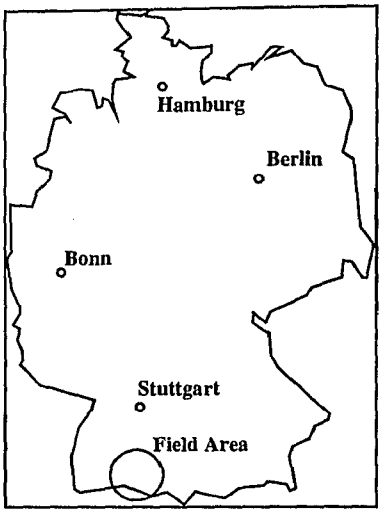

Fig. 2.1: Location map of field area in southwest Germany

Magneto-Stratigraphy	Age (years b.p.)	Chrono-Stratigraphy	NW Europe	Alpes
Brunhes	10000	Holocene		
	70000	Late	Weichsel	Würm
	120000	Pleistocene	*Eem*	*Riß/Würm*
	280000	Middle	Saale	Riß
	350000	Pleistocene	*Holstein*	*Mindel/Riß*
	500000		Elster	Mindel
			Cromer IV	*Haslach/Mindel*
			Cromer C	
			Cromer III	Haslach
			Cromer B	*Günz/Haslach*
			Cromer II	
	780000		Cromer A	Günz
Matuyama		Early	*Cromer I*	
		Pleistocene	*Bavel*	*Donau/Günz*
			Menap	Donau
			Waal	
	2600000		Eburon	Biber
Gauss		Tertiary		

Tab. 2.1: Simplified Quaternary stratigraphy of northwest Europe and the Alps, *italic*: interglacials (after Ehlers, 1994; Murawski, 1983)

It can be expected that the depositional environment resulting from the alpine glaciations was similar anywhere in the surroundings of the Alps. Results from this work, therefore, can probably be transferred to other areas, even south of the Alps (Fig. 2.2).

The deposits found in the direct (proximal) Quaternary environment are similar in terms of their heterogeneity to those in periglacial areas of e.g. river valleys further away (distal) from the former glacially covered areas. However, the composition of sands and gravels in the valleys may differ from those in the glaciofluvial environment. The results, particularly from the permeability measurements of specific lithological components within this project, and the digital photographic approach may thus be

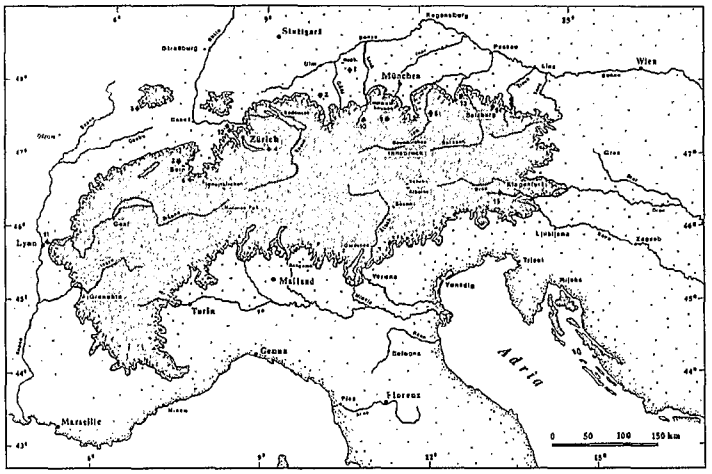

Fig. 2.2: Extent of the last glaciation (Würm) in the area of the Alps (Ehlers, 1994)

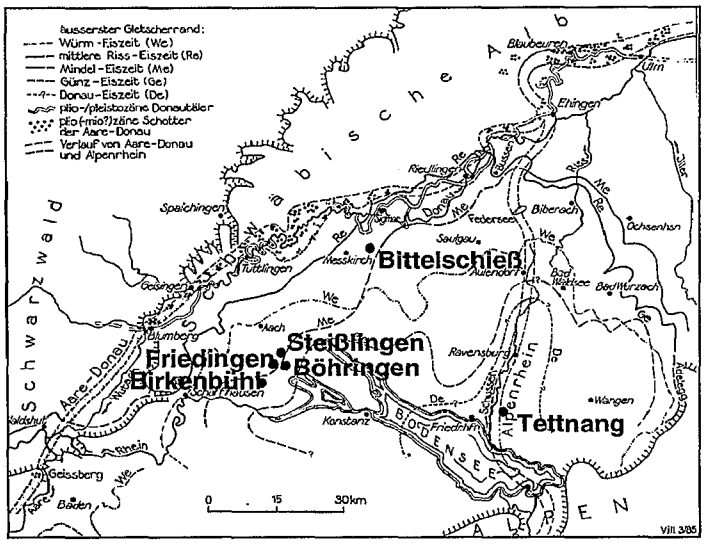

Fig. 2.3: Location of field sites in the Quaternary environment north and northwest of Lake Constance, Baden-Württemberg. The outermost extent of different ice ages are shown (We: Würm, Re: Riß; based on a map from Villinger, 1989)

transferred to hydrogeological parameter evaluation in the periglacial valley regions.

After various visits in the region north and northwest of Lake Constance for reasons of accessibility of outcrops three areas were defined for further investigation: the first area is situated 5 to 10 km north of the main part of the lake in the vicinity of Tettnang in the former valley of the Alprhine (Alpenrhein), today the valley of the river Schussen. A second area, 5 km south of the river Danube (Donau), is referred to as Bittelschieß, after the best conserved outcrop location. The largest and for this work most important area is the Singen basin, 5 km northwest of the western end of the lake. The locations here are Friedingen, Steißlingen, Böhringen and Birkenbühl. All six field locations are given in figure 2.3 with respect to their position in the Quaternary depositional environment (see also Ch. 2.2).

A more detailed map of the location of field sites in the Singen basin is given in figure 2.4 in connection with the different stages of the latest glaciation period and specific depositional directions of glaciofluvial meltwater streams.

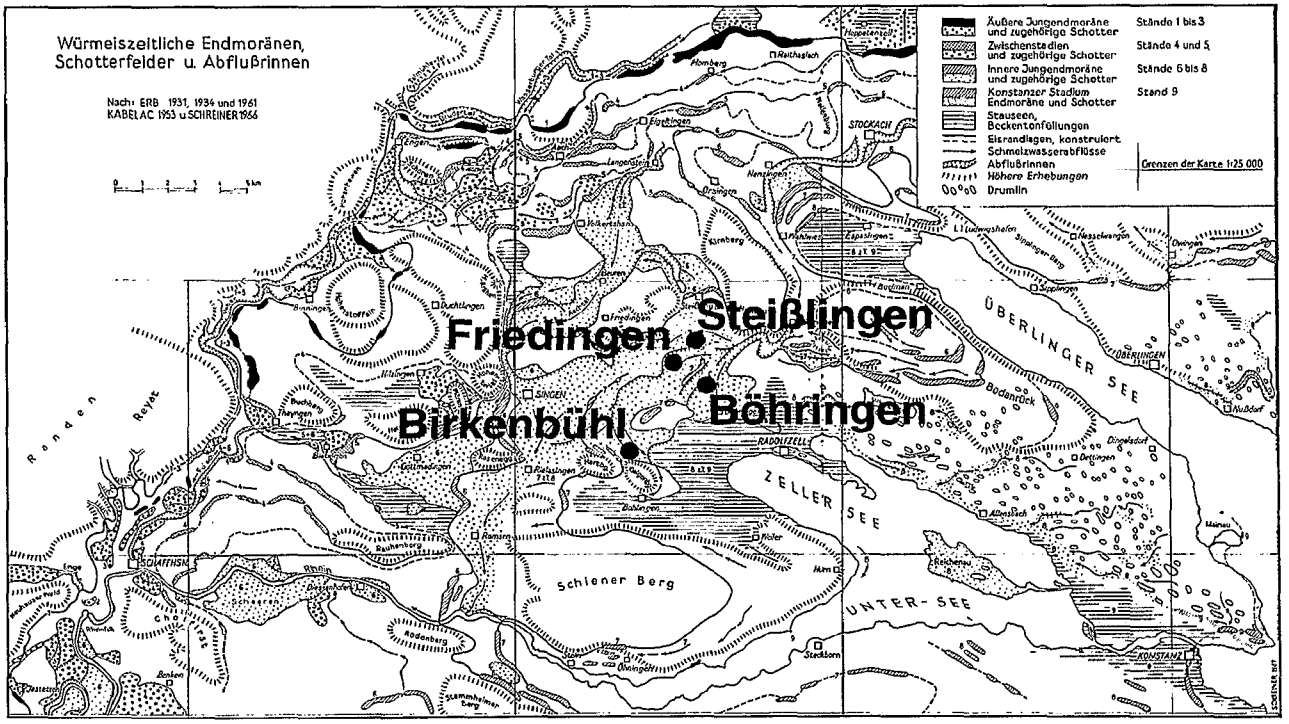

Fig. 2.4: Detailed map of location of field sites in the Quaternary environment of the Singen basin, small arrows indicating the direction of meltwater streams at the end of the last (Würm) glaciation (based on a map from Schreiner, 1992)

2.2 Quaternary Stratigraphy in the Field Areas

2.2.1 Tettnang

The Tettnang area (Fig. 2.3) today is characterised by the river Schussen discharging from the north into Lake Constance. At the times of the last ice ages the glacial outwash was flowing from the glacier situated at Lake Constance to the north, discharging into the Danube. In this way the river was a continuation of the Alprhine (Alpenrhein; Schreiner, 1978; Villinger, 1989).

The outcrops found in the gravel pits around Tettnang comprise mainly delta sediments with large, steep sloping foresets. Their origin is related to the deposition of coarse gravels and sands into a near-ice-margin lake, especially during the later stages of the last glaciation (Würm).

In the Tettnang area no suitable outcrops for *in situ* measurements or two-dimensional wide angle photographs were found. However, Asprion (1998) was able to detect the top- and foresets of the steep dipping delta structures with ground penetrating radar (GPR).

2.2.2 Bittelschieß

Bittelschieß (Fig. 2.3) is located at the confluence of the Kehlbach and Andelsbach valleys, two discharge areas at various stages of the Riß glaciation. During the Riß glaciation this region was more than once covered by glaciers, resulting in sediments related to prograding and downmelting glaciers (Ellwanger, 1990, 1994; Schmidt, 1994; Villinger, 1985, 1989).

The outcrop of Bittelschieß itself can be divided into different parts: the youngest, uppermost part comprises gravels and sands of glaciofluvial origin of the outwash of later stages of the Riß glaciation, interbedded with some - possibly till-like - structures, whose origin is still under discussion. In the lower parts of the outcrop very compact mud is found locally, possibly as a result of glaciolacustrine lake deposits at the margin of a glacier. In the lowest part highly heterogeneous deposits, resulting mainly from braided river but also from debris flow, are found. These originated from the melting of an earlier stage of the Riß glaciation.

The lowest part of the outcrop shows primarily deposits of a braided river environment. The channel deposits have only small lateral (up to 3 to 4 m) and vertical extent (up to 1 m), representing an often changing glaciofluvial environment. This part of the outcrop is used in this work to map the heterogeneous lithological facies composition by digital-photographic means (see Ch. 7). The outcrop is not suitable for *in situ* permeability measurements since it is inaccessible for the equipment.

2.2.3 Friedingen, Steißlingen, Böhringen and Birkenbühl (Singen Basin)

The field sites in Friedingen, Steißlingen, Böhringen and Birkenbühl are part of the Singen basin, deposited mainly by meltwaters of the downmelting Würm glacier in the western part of Lake Constance (Fig. 2.3). During the different stages of the Würm glaciation the ice cover extended as far northwest as indicated by the terminal moraines (Äußere Jungendmoräne, Fig. 2.4), leaving uncovered most of the tertiary volcanoes (to the northwest), Schiener Berg, Hartberg, Galgenberg (to the south), the Kirchberg and Homburg (to the northeast), and the Bodanrück (to the east of the Singen basin).

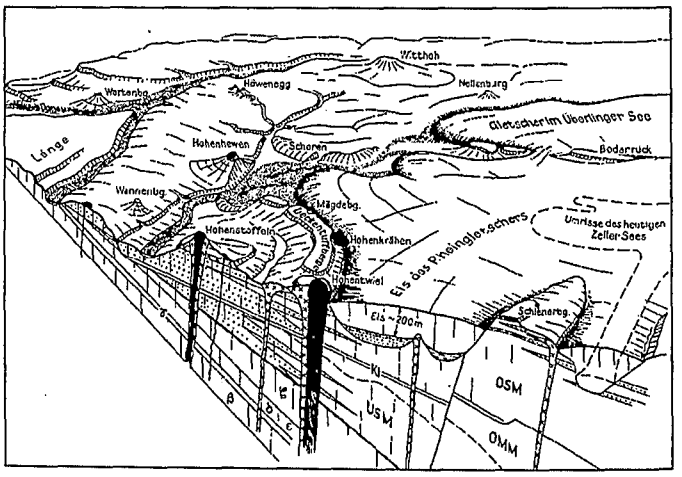

Fig. 2.5: Three-dimensional sketch of extent of the Würm iceage in the Singen basin (Schreiner, 1992)

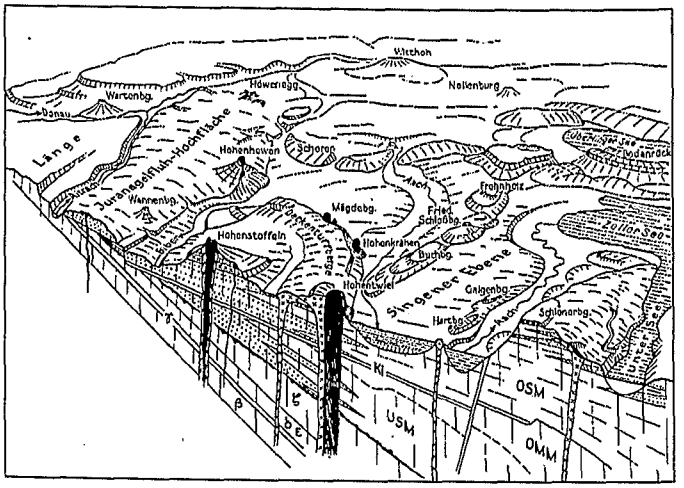

Fig. 2.6: Three-dimensional sketch of today's landscape and subsurface geology in the Singen basin (Schreiner, 1992)

A three-dimensional sketch of the location of the glacier in the Singen basin at the time of the Würm ice age is shown in figure 2.5. The view from the southwest represents an intermediate stage of the Würm glaciation (retreating/downmelting stage) with a coverage of the glacier of up to 200 m in the central Singen basin. The profile in northwest - southeast direction shows the general dipping of the geological subsurface towards the southeast. In some of the ice covered valleys glacial or glaciofluvial deposits of prograding or melting glaciers of earlier Würm stages or even from the Riß glaciation are found. These formed the base of today's Quaternary valley fills (Schreiner, 1989, 1992; Ellwanger et al., 1997; Szenkler et al., 1997).

Today (Fig. 2.6) the former glacier has retreated to the upper Rhine valley in Switzerland. The basin is filled with glaciofluvial sediments. Some Holocene deposits develop along the stream Aach, which discharges into the western Lake Constance (Zeller See).

The deposits in the Singen basin itself are composed of mainly braided river, debris flow and delta sediments. The cross-bedded troughs of the braided river sediments are larger than those discovered in Bittelschieß (up to 7 m horizontally and 3 m vertically) but still smaller than the braided river deposits in Hüntwangen, Switzerland (Huggenberger, 1993, 1994; Huggenberger et al., 1994; Jussel, 1992; Jussel et al., 1994). They originate from gravel-bed rivers discharging from the glaciers. The delta sediments, deposited by short but steep gravel-bed streams from the glaciers into near-ice-margin lakes, are often found in the same location as the braided river deposits. The main difference between the planar- (delta) and trough-like (braided) dipping structures, which can be observed in outcrops, is often hidden by scree at the bottom of the structure. The delta structures, deposited in the former flow direction, are normally of longer lateral extent than the braided river deposits, where the former flow direction was perpendicular to the trough-like structures. The debris flow sediments are given by mixed gravel and sand sheets of sometimes very long lateral extent (tens to hundreds of m) and up to 2 m in height.

2.3 Architectural Elements

For the classification of fluvial sediments Miall (1985) proposed a concept of hierarchical building stones, out of which the fluvial environment is constructed. This concept is directly connected to the concept of size hierarchy (Keller, 1992) in which sedimentological heterogeneities are described depending on the scale of observation:

giga scale: formation (> tens m),
mega scale: outcrop (m to hundreds m),
intermediate scale: architectural element (m to tens m),
macro scale: sample (tenths m to m),
micro scale: pores and grains (< tenths m).

An architectural element may be defined as a component of a depositional system equivalent in size to, or smaller than a channel fill, and larger than an individual facies unit. It is characterised by a distinctive facies assemblage, internal geometry and external form. Units belonging to the same architectural element are enclosed by bounding/erosional surfaces.

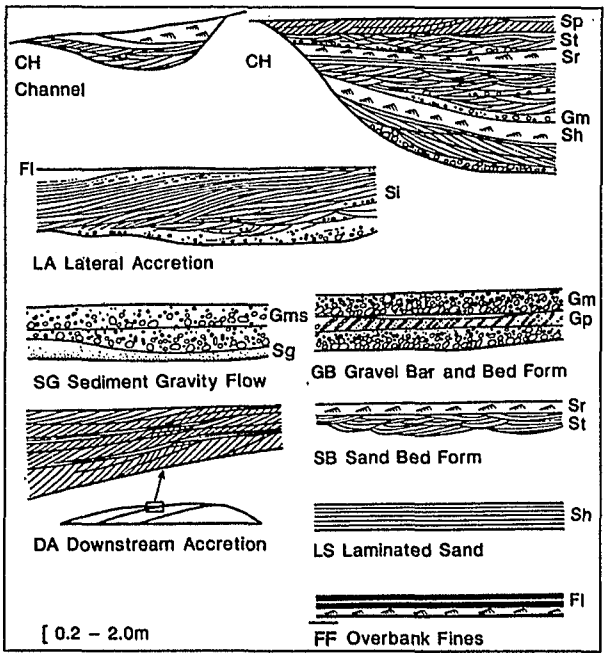

Fig. 2.7: *Different types of architectural elements, the "eight basic architectural elements" in fluvial deposits (Miall, 1985)*

The eight basic architectural elements, of which a fluvial depositional environment can be build up (Miall, 1981, 1985), are described in figure 2.7. Subsequent work added a ninth element (Tab. 2.2, after Miall, 1996). Often not all elements may be found at one field site, since it depends on the sedimentological setting present e.g. whether channel fills (CH) or overbank fines (FF) are deposited.

Element	Symbol	Principal Lithofacies	Geometry and Relationship
Channels	CH	any combination	finger, lens or sheet; concave-up erosional base; scale and shape highly variable; internal concave-up, 3rd order erosion surfaces common
Gravel bars and bedforms	GB	Gm, Gp, Gt	lens, blanket; usually tabular bodies; commonly interbedded with SB
Sandy bedforms	SB	St, Sp, Sh, Sl, Sr, Se, Ss	lens, sheet, blanket, wedge; occurs as channel fills, crevasses splays, minor bars
Downstream-accretion macroform	DA	St, Sp, Sh, Sl, Sr, Se, Ss	lens resting on flat or channelled base, convex-up 3rd order internal erosion surfaces and upper 4th order bounding surface
Lateral-accretion macroforms	LA	St, Sp, Sh, Sl, Se, Ss, less commonly Gm, Gt, Gp	wedge, sheet, lobe; characterised by internal lateral accretion 3rd order surfaces
Scour hollow	HO	Gh, Gt, St, Sl	scoop-shaped hollow with asymmetric fill
Sediment gravity flows	SG	Gmm, Gmg, Gci, Gcm	lobe, sheet; typically interbedded with GB
Laminated sand sheet	LS	Sh, Sl, minor Sp, Sr	sheet, blanket
Overbank fines	FF	Fm, Fl	thin to thick blankets; commonly interbedded with SB; may fill abandoned channels

Tab. 2.2: Architectural elements in fluvial deposits (after Miall, 1985, 1996)

In the case of Quaternary gravel and sand deposits from glacial outwash the combinations of architectural elements given by Miall (1985, 1996) can be limited to three different models. Although Miall (1985) emphasises that the models given there do "not represent an attempt to provide a comprehensive suite of fluvial models" and warns of "force-fitting ... field examples into any of these models". The glaciofluvial deposits found at the different field sites can generally be seen as a gradation between the first three of the twelve models from Miall (1985, 1996).

Those three models of gravel-dominated rivers (Fig. 2.8) are characterised by low sinuosity, high (to intermediate) braiding parameters, a main sediment type of gravel (minor sand) and characteristic architectural elements of the types gravel bars and bedforms (GB), sandy bedforms (SB) and downstream-accretion macroforms (DA). Model a (model 1 of Miall, 1985, Fig. 2.8a) represents a braided gravel river of proximal alluvial fans with sediment gravity flow lobes, model b (model 2 of Miall, 1985, Fig. 2.8b) a shallow braided gravel river of proximal alluvial fan or outwash braidplain and model c (model 3 of Miall, 1985, Fig. 2.8c) shows a deep braided gravel river of low sinuosity with well defined topographic levels.

This concept of architectural element analysis of fluvial deposits has been widely used in the sedimentological research (Best and Bristow, 1993; Bridge, 1993; Huggenberger et al., 1988; Keller, 1992; Menzies, 1995; Ori, 1982). For example Keller (1992) uses it to characterise the hydrogeological parameters of the Swiss Molasse basin (Tertiary), whereas the hydrogeological work from Jaritz (1998) is based on the sedimentological description by architectural element analysis of parts of the Keuper (Late Triassic) sandstones in southwest Germany.

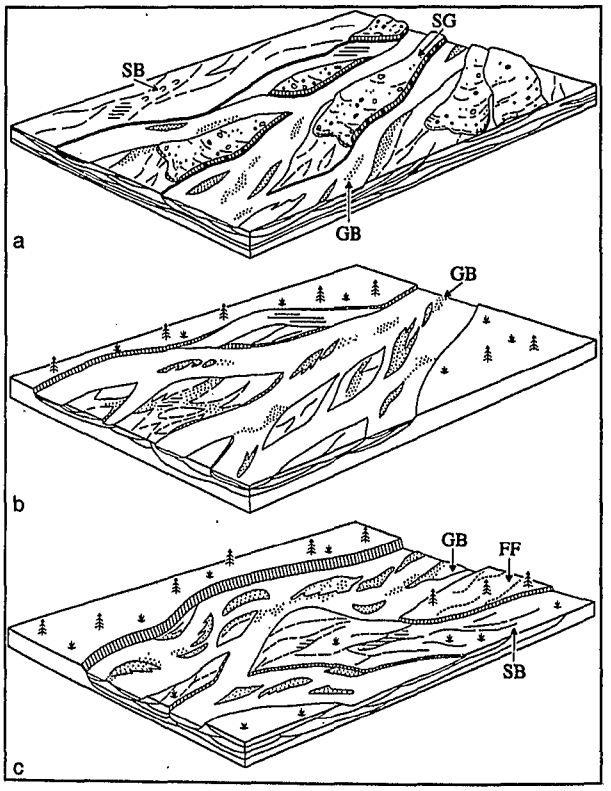

Fig. 2.8: Models illustrating the composition of different architectural elements in a river's depositional environment, a: gravel-bed braided river showing dissected lobes of sediment-gravity-flow deposits (SG), b: gravel-bed river dominated by traction-current deposits (GB), c: deep, gravel-bed braided river with well-defined topographic levels (models 1, 2, 3 from Miall, 1985, 1996)

For glaciofluvial Quaternary deposits the architectural element analysis may better follow the concept of the glacial series (Fig. 2.9, originally from Penck and Brückner, 1909), which is discussed by Ehlers (1994) and in more detail by Schreiner (1992). The term "glacial series" is used for the common appearance and the combination of different glacial, glaciofluvial or glaciolacustrine deposits of a glacial period. The prograding glacier builds a reservoir, in which glaciolacustrine sediments (gs1) are deposited and later overridden by the further prograding glacier. After filling-up of the

reservoir, meltwater deposits sands and gravels into earlier developed valleys, which are also overridden by the glacier (VS). Different glacial thrusts result in terminal (E) and basal (Gm) moraines. During the equilibrium stage of the glacier (accumulation equals ablation) the outer terminal moraine (here of the Würm glaciation) is built up (Em1). At the same time meltwater creates the sander and the sand and gravel deposits (Sf1). While the glacier melts (retreats) the basal moraine will be partly covered by near-ice-margin meltwater sediments (eS). A newly prograding glacier results in new glaciolacustrine sediments (gs2) and the cycle of sedimentation and erosion repeats.

With the help of the glacial series the existing gravel and sand deposits (braided river, delta and debris flow sediments) in the outcrops of the field areas can be explained. The braided river deposits result from multi-channel gravely river beds in the sander or sand/gravel regions (VS, Sf1) and lead to often trough-like sediment structures in the outcrops, perpendicular to the former flow direction. The delta sediments, often of planar structure in the outcrops, aligned with the former flow direction, are the remains of the deposits of gravely rivers into near-ice-margin lakes (VS, es1). The debris flow sediments, with sheet-like, massive appearance in the outcrops, originate from special high flood events.

2.4 Sedimentological Classification - Lithofacies Types

In addition to the architectural element classification it is often more important, not only for hydrogeological investigations, to know the exact lithological composition within one architectural element. This lithological description of sediment features such as rock type, layering, texture or fabric is referred to as lithological facies (lithofacies) classification. Normally the elements are seen as a specific sedimentological unit, which results from a particular depositional process. However, this does not describe different energy regimes at the time of deposition, which may lead to more sandy or gravely lithologies, according to low or high flow conditions. Similar architectural elements, e.g. scour hollows, may have the same layering but different properties of sandy or gravely facies types.

The first comprehensive collection of lithological facies types is given by Miall (1977). Later it was improved and adapted following subsequent research (Miall, 1978, 1980, 1996). The 21 codes represent a general lithological classification for a fluvial environment solely from the sedimentological point of view (Tab. 2.3).

Keller (1996) recognised that for the particular application to glacial deposits a more detailed minor classification is needed. This "Quaternary" lithofacies code is a letter combination of the major and minor classifications from table 2.4.

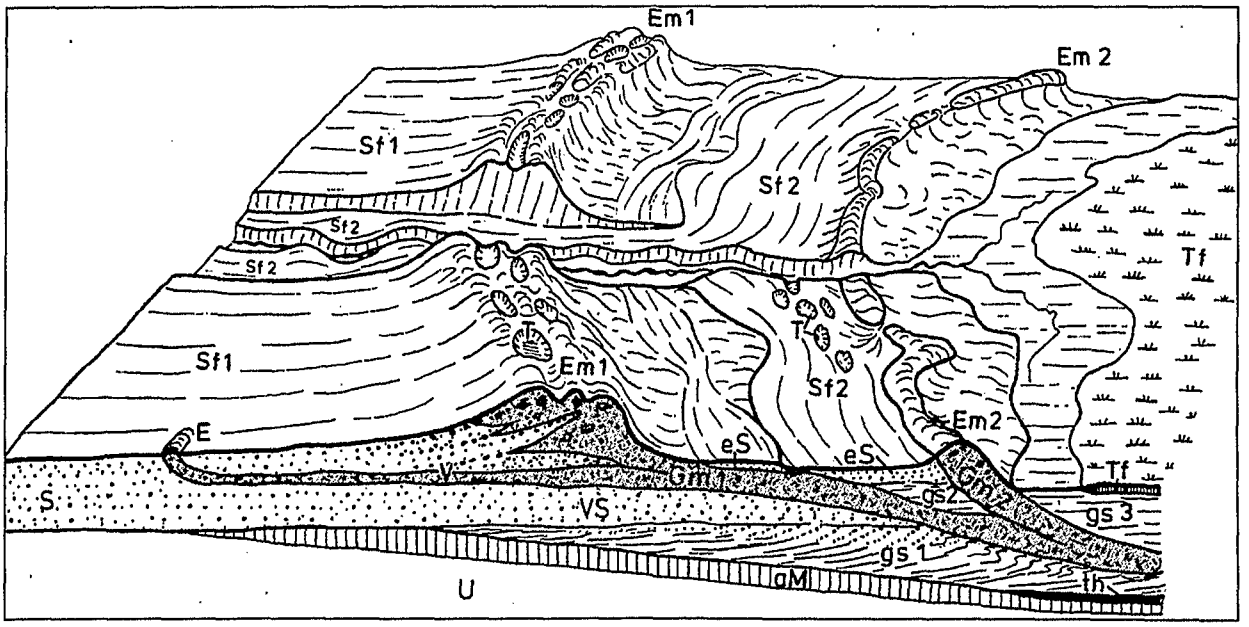

Fig. 2.9: Model of depositional environment for glaciofluvial deposits, glacial series (Schreiner, 1992, originally from Penck and Brückner, 1909)

Facies Code	Lithofacies	Sedimentary Structures	Interpretation
Gmm	matrix supported, massive gravel	weak grading	plastic debris flow (high strength, viscous)
Gmg	matrix-supported gravel	inverse to normal grading	pseudoplastic debris flow (low strength, viscous)
Gci	clast-supported gravel	inverse grading	clast-rich debris flow (high strength) or pseudoplastic debris flow (low strength)
Gcm	clast-supported, massive gravel		pseudoplastic debris flow (inertial bedload, turbulent flow)
Gh	clast-supported, crudely bedded gravel	horizontal bedding, imbrication	longitudinal bedforms, lag deposits, sieve deposits
Gt	gravel, stratified	trough crossbeds	minor channel fills
Gp	gravel, stratified	planar crossbeds	transverse bedforms, deltaic growths from older bar remnants
St	sand, fine to very coarse, may be pebbly	solitary or grouped trough crossbeds	sinuous-crested and linguoid (3D) dunes
Sp	sand, fine to very coarse, may be pebbly	solitary or grouped planar crossbeds	transverse and linguoid bedforms (2D dunes)
Sr	sand, very fine to coarse	ripple cross lamination	ripples (lower flow regime)
Sh	sand, very fine to coarse, may be pebbly	horizontal lamination, parting or streaming lineation	plane bed flow (critical flow)
Sl	sand, very fine to coarse, may be pebbly	low angle (< 15°) crossbeds	scour fills, humpback or washed-out dunes, antidunes
Se	erosional scours with intraclasts	crude crossbedding	scour fills
Ss	sand, fine to very coarse, may be pebbly	broad, shallow scours	scour fills
Sm	sand, fine to coarse	massive or faint lamination	sediment-gravity flow deposits
Fl	sand, silt, mud	fine lamination, very small ripples	overbank, abandoned channel or waning flood deposits
Fsm	silt, mud	massive	backswamp or abandoned channel deposits
Fm	mud, silt	massive, desiccation cracks	overbank, abandoned channel or drape deposits
Fr	silt, mud	massive, roots, bioturbation	root bed, incipient soil
C	carbonaceous mud, coal	plant, mud films	vegetated swamp deposits
P	paleosol carbonate (calcite, siderite)	pedogenic features: nodules, filaments	soil with chemical precipetation

Tab. 2.3: Lithofacies codes (after Miall, 1977, 1978, 1996)

For the hydrogeological objectives of this project (this work; Asprion, 1998; Kleineidam, 1998) even a combination of both lithofacies classification (Tab. 2.3 and 2.4) had to be extended to include in particular the trough, planar or horizontal gravel units, which can often be subdivided into bimodal sand-gravel units changing into open framework gravels. Although the structures might be seen as one unit from the perspective of their depositional origin, for hydrogeological flow and transport evaluations a differentiation is necessary. The expected differences in their hydraulic conductivities and chemical composition will result in variations of flow lines and different retardation to possible contaminants (s. Ch. 8). A similar separation has already been approved by different authors (Huggenberger et al., 1988, 1994; Huggenberger, 1993; Jussel, 1992; Jussel et al., 1994).

Major Classification		Minor Classification	
Facies Code	Lithofacies	Grain Size (Gravel/Scree)	
SC	grain-supported scree	g	gravel (2 - 60 mm)
Gc	grain-supported gravel	c	cobbles (60 - 200 mm)
Gm	matrix-supported gravel	b	boulders (> 200 mm)
Dc	grain-supported diamictite	Texture	
Dm	matrix-supported diamictite	m	matrix-supported
SSC	scree with sand matrix	c	clast-supported
GS	gravel-sand	Structure/Layering	
S	sand	l	laminated (< 1 cm)
H	heterolithic bedding	b	bedded (> 1 cm)
F	fines	m	massive
P	peat	p	planar crossbeds
C	carbonate	u	mud drapes
		g	graded
		d	deformed
		r	ripples
		t	trough cross-stratification
		Miscellaneous	
		d	drop stones
		o	organic
		p	pedogenised
		f	freshwater molluscs

Tab. 2.4: Major and minor classification for lithofacies codes (after Keller, 1996)

The bimodal gravels show a distinct grain size distribution with fine to coarse sands and fine to coarse gravels. Some of the middle fractions of sand or gravel are not present, resulting in the bimodal shape of the grain size distribution curve. The open framework gravel is of fine to coarse gravel units, normally without much variability and totally lacking fine (sand) particles.

Incorporating the bimodal and open framework structures in the present classification system of Miall and Keller results in the table of lithofacies codes used in this project (Tab. 2.5). Again the specific code for a lithofacies results from a combination of letters, representing the gravel or sand in question. The 23 sedimentologically reasonable combinations are given in table 2.6.

Gravel G		Sand S	
Layering		**Layering**	
p	planar	p	planar
t	trough	t	trough
h	horizontal	h	horizontal
m	massive	m	massive
g	graded	g	graded
Texture			
m	matrix supported		
c	component supported		
Miscellaneous			
b	bimodal		
o	open framework		

Tab. 2.5: Lithofacies code used in this project

Gravel, planar crossbedded		Gravel, trough crossbedded	
Gmp	matrix supported	Gmt	matrix supported
Gmpb	matrix supported, bimodal	Gmtb	matrix supported, bimodal
Gcp	component supported	Gct	component supported
Gcpb	component supported, bimodal	Gctb	component supported, bimodal
Gcpo	component supported, open framework	Gcto	component supported, open framework
Gravel, horizontal		**Gravel, massive**	
Gmh	matrix supported	Gmm	matrix supported
Gmhb	matrix supported, bimodal	Gcm	component supported
Gch	component supported	**Sand**	
Gchb	component supported, bimodal	Sp	planar crossbedded
Gcho	component supported, open framework	St	trough crossbedded
Gravel, graded		Sh	horizontal
Gg	component supported, mainly open framework, but of different grain size	Sm	massive
		Sg	graded

Tab. 2.6: 23 sedimentologically reasonable lithofacies types, as a combination of lithofacies codes from Tab. 2.5

2.5 Hydrogeology

For the field sites of this project detailed hydrogeological studies were only available for the Singen basin.

The Singen basin is an important source for the regional drinking water supply and, at the same time, the major resource for sand and gravel quarrying in the area. In the past this has often caused a conflict of interests.

The most comprehensive study of the hydrogeology of the Singen basin is presented by Koziorowski (1986). Although the local details in the outcrops are not taken into account, it was a very valuable data source for the planning of the regional water supply. The work separates the whole basin into two gravel layers (upper and lower) with an intermediate, sometimes interrupted low permeable zone. Characteristic hydraulic conductivity values are given from sieve analysis and pumping test data. For the upper gravel layer (sieve analysis data) four facies are observed: open framework gravel with a mean hydraulic conductivity of $1.5 \cdot 10^{-1}$ m/s, gravel $5.0 \cdot 10^{-4}$ m/s (varies from $1.9 \cdot 10^{-7}$ to $1.5 \cdot 10^{-1}$ m/s), sand from $9.0 \cdot 10^{-8}$ to $4.0 \cdot 10^{-4}$ m/s and silt from $2.4 \cdot 10^{-9}$ to $2.0 \cdot 10^{-6}$ m/s. The intermediate "impermeable" layer composes mud, silt and till of $1.9 \cdot 10^{-6}$ to $5.3 \cdot 10^{-10}$ m/s (permeameter measurements). By different pumping tests the upper and lower gravel layers were examined, leading to hydraulic conductivities for the upper gravel in the range of $6.2 \cdot 10^{-4}$ to $7.0 \cdot 10^{-3}$ m/s and the lower gravel $3.0 \cdot 10^{-4}$ to $4.2 \cdot 10^{-3}$ m/s.

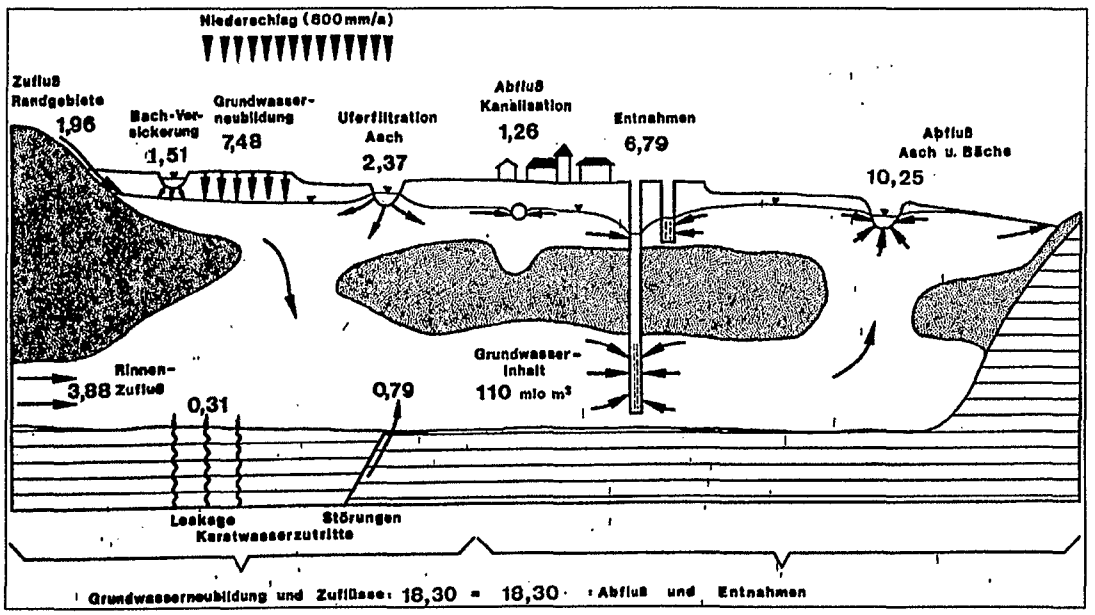

Fig. 2.10: Conceptual hydrogeological model for actual water budget in the Singen basin, values in 10^6 m³/y if not stated otherwise (Koziorowski, 1986)

Of particular interest is the water balance: Koziorowski (1986) concludes that in the western part of the Singen basin groundwater abstraction has reached its limits already, whereas in the eastern part possible further development of aquifers can be achieved up to a total of 300 l/s or $9.47 \cdot 10^6$ m^3/y (Fig. 2.10).

The new interpretation of the Quaternary depositional processes results in a more complicated structure of various basins of different depth and interconnections within the Singen basin (Szenkler et al., 1997). This concept will in the near future lead to a revised conceptual model and water balance of the whole basin. As the base of some of the connections between the basins is probably not as deep as was assumed in the past, the inflow through these connections is significantly reduced, in comparison to former assumptions, which will lead to less groundwater being available for abstraction than was previously predicted.

No data has been published for this region in the detail provided by this project and with the intention of understanding the importance of the locally heterogeneous conductivity compositions. Only the results of the work in the neighbouring region in Switzerland (Hüntwangen, about 50 km west of the Singen basin) can be compared to this project (Huggenberger et al., 1988; Jussel, 1992; Jussel et al., 1994). There, outcrops have been analysed for textural types and their hydraulic conductivities and porosities have been estimated mainly by laboratory measurements. The condensed results of their measurements with respect to their textural classification are given in table 2.7. A comparison with the results of this work will follow in chapter 6.4.

Textural type	K_F (m/s)	σ_{lnKF}	n (-)
Grey gravel (GG)	$1.5\ 10^{-4}$	0.5	0.20
Brown gravel (BG)	$2.0\ 10^{-5}$	0.6	0.14
Alternation (GG/BG)	$8.0\ 10^{-5}$	0.8	0.17
Open framework gravel (OW)	$1.0\ 10^{-1}$		0.35
Open framework/bimodal couplets (OW/BM)	$1.0\ 10^{-2}$		0.30
Sand (SA)	$2.6\ 10^{-4}$	0.4	0.43
Silt (SI)	$5.0\ 10^{-6}$		0.40

Tab. 2.7: Hydraulic conductivities and porosities for Pleistocene Rhine gravels from (Jussel, 1992)

3 Flow and Transport of Water and Gas in Unconsolidated Porous Formations (Theory)

For the hydrogeology of heterogeneous gravel and sand deposits the quantification of hydraulic conductivities is most important, as they are responsible for local changes in the flow regime and may lead to preferential flow paths for contaminants. Often the hydraulic parameterisation of specific architectural elements and units of similar lithofacies reaches its limits, where the local resolution of the subsurface investigation methods cannot resolve the hydraulically important small scale differences in lithology, e.g. regionalised parameters from pumping tests or surface geophysical measurements.

A way of overcoming these problems is the procedure of measuring porosities and permeabilities in reservoir analogues used in petroleum geology. Transferred to hydrogeology this means the detailed description of hydraulic parameters of lithofacies or architectural elements in the (unsaturated) outcrops of gravel/sand deposits, which reflect the characteristics of a real but saturated aquifer (i.e. the concept of an aquifer analogue). While the fluid of interest is groundwater, it is not feasible to saturate the whole outcrop to measure hydraulic conductivities directly. However, it is possible to measure conductivities for air/gas flow, K_g [m/s], in the unsaturated outcrops or at samples in the laboratory and to transfer these via intrinsic permeabilities, k [m^2], to hydraulic conductivities, K_f [m/s]. In this chapter the physical basis is described for this transfer and the measurements with gas instead of water.

3.1 Fluid Flow in Porous Formations

The basic equation describing single-phase fluid flow through a porous medium is given by Darcy's law

$$\bar{v} = -\frac{\overline{K}}{g} \cdot \mathrm{grad}\Phi = -\frac{\overline{K}}{g} \cdot \nabla\Phi \qquad 3.1$$

The fluid potential Φ (the mechanical energy per unit mass) is defined on the basis of the sum of potential, kinetic and elastic energy W (Bernoulli equation)

$$W = W_{pot} + W_{kin} + W_{el} \qquad 3.2$$

$$W = m \cdot g \cdot z + \frac{1}{2} \cdot m \cdot v^2 + m \cdot \int_{p_0}^{p} \frac{dp}{\rho} \qquad 3.3$$

$$\Phi = \frac{W}{m} = g \cdot z + \frac{v^2}{2} + \int_{p_0}^{p} \frac{dp}{\rho} \qquad 3.4$$

Natural flow conditions for water or gas are such that the flow velocities are extremely low, i.e. the second term (kinetic energy) can be neglected, resulting in the general fluid potential equation

$$\Phi = g \cdot z + \int_{p_0}^{p} \frac{dp}{\rho} \qquad 3.5$$

The fluid conductivity tensor $\overline{K}$ (Eq. 3.1) can be expressed in terms of the intrinsic permeability tensor $\overline{k}$ and the fluid dependent parameters density and dynamic viscosity as well as the gravitational constant

$$\overline{K} = \frac{\rho \cdot g}{\mu} \cdot \overline{k} \qquad 3.6$$

3.1.1 Flow of Water

In the case of water, which may be assumed to be an incompressible fluid, equation 3.5 reduces to

$$\Phi = g \cdot z + \frac{p - p_0}{\rho} \qquad 3.7$$

and by expressing p_0 as atmospheric pressure equal to zero and the fluid potential in terms of hydraulic head h (e.g. Freeze and Cherry, 1979) this becomes

$$\Phi = g \cdot z + \frac{p}{\rho} = g \cdot h \qquad 3.8$$

Introducing the fluid potential and conductivity with respect to water (index f) in equation 3.1 leads to Darcy's law for water

$$\bar{v} = -\overline{K}_f \cdot \nabla h = -\frac{\rho_f \cdot g}{\mu_f} \cdot \overline{k} \cdot \nabla\left(z + \frac{p}{\rho_f \cdot g}\right) \qquad 3.9$$

or, in terms of pressure, to

$$\bar{v} = -\frac{\overline{k}}{\mu_f} \cdot (\nabla p + \rho_f \cdot g \cdot \nabla z) \qquad 3.10$$

The hydraulic conductivity tensor $\overline{K}$ can be written as

$$\overline{K}_f = \frac{\rho_f \cdot g}{\mu_f} \cdot \overline{k} \qquad 3.11$$

3.1.2 Flow of Gas

Preconditions for using Darcy's law in the general form given by equation 3.1 for the flow of gas/air in porous media and the fluid potential in the form of equation 3.5 are that processes such as **turbulence** (Ch. 3.1.2.1) or **slip flow** (drift flow, Ch. 3.1.2.2) do not occur or can be neglected for the conditions of low flow velocities in unconsolidated gravels and sands. As long as the

compressibility of gas can be neglected for low pressure differences (Ch. 3.1.2.3), Darcy's law in terms of pressure for gas (index g, analogous to equation 3.10) is valid

$$\bar{v} = -\frac{\bar{k}}{\mu_g} \cdot (\nabla p + \rho_g \cdot g \cdot \nabla z) \qquad 3.12$$

Generally the flow due to potential energy (elevation z) is small compared to the flow due to pressure differences

$$\rho_g \cdot g \cdot \nabla z \ll \nabla p \qquad 3.13$$

resulting in a simpler form of equation 3.12

$$\bar{v} = -\frac{\bar{k}}{\mu_g} \cdot \nabla p \qquad 3.14$$

The gas conductivity tensor, analogous to the hydraulic conductivity (Eq. 3.11), although not often used, can be given by

$$\bar{K}_g = \frac{\rho_g \cdot g}{\mu_g} \cdot \bar{k} \qquad 3.15$$

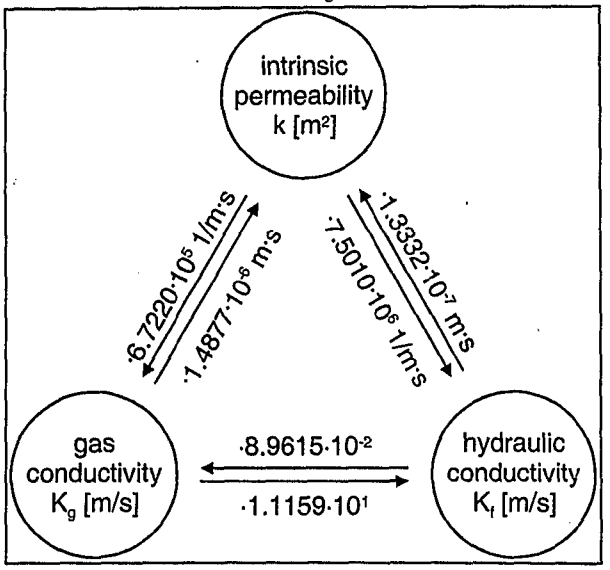

Fig. 3.1: Conversion factors for gas conductivity, K_g, hydraulic conductivity, K_f, and intrinsic permeability, k, for a temperature of 10 °C

Further details on the derivation of gas and water flow equations can be found in Freeze and Cherry (1979), Kretzer (1989) and Borho (1995). For comparison and easier conversion from gas conductivities to intrinsic permeabilities and hydraulic conductivities a simplified diagram of conversion factors for a temperature of 10 °C is given in figure 3.1.

3.1.2.1 Turbulence

The Darcy equation is only valid for laminar flow conditions. This restricts its application to fluid flow at low velocities. Up to which velocity the linear expression is valid depends on the critical Reynolds number, Re_{crit}, which describes the transition point from laminar to turbulent flow.

For higher velocities, i.e. higher Reynolds numbers, the flow rate is no longer proportional to the pressure difference. Forchheimer (1901) proposes the extension of the Darcy equation with a squared velocity term. For one-dimensional measurements along a column this is given by

$$-\frac{dp}{dx} = \frac{\mu_g}{\bar{k}} \cdot v + \beta \cdot \rho_g \cdot v^2 \qquad 3.16$$

where β is a turbulence factor.

The Reynolds number, Re, can either be calculated for specific flow conditions of flow through pipes or, more importantly in this case, for flow through porous media. Two formulas are given for the calculation of Reynolds numbers in porous media (de Marsily, 1986): the first depending on the intrinsic permeability, k, of the porous formation

$$Re = \frac{v_a \cdot \sqrt{k}}{\nu_g} = \frac{v_a \cdot \rho_g \cdot \sqrt{k}}{\mu_g} \qquad 3.17$$

and a second, following from the first, depending on the effective grain size, often used as 10 % of grain size distribution, d_{10},

$$Re = \frac{v_a \cdot d_{10}}{\nu_g} = \frac{v_a \cdot \rho_g \cdot d_{10}}{\mu_g} \qquad 3.18$$

However, in the literature a wide range of critical Reynolds numbers is given (Kister, 1994). Re varies for laminar flow from < 0.1 to < 75 and for turbulent flow from > 10 to > 600. Others explain that the validity of the Darcy expression depends not only on the Reynolds number but also on the effective grain size (Ruiz-Rodriguez, 1994; Kretzer, 1989): based on measurements with sands of only one grain size, Re_{crit} for fine to middle sand is given as 1 and for coarse sand to fine gravel as 10 (Fig. 3.2).

For poorly-sorted sands and gravels the critical Reynolds number cannot be given by tables. In this case it is advisable to measure the flow through samples in column experiments and plot the measured flow rate, Q, or velocity, v = Q/A, versus the pressure difference, Δp, applied along the column. As long as a linear relationship is found, the validity of the Darcy equation can be assumed. Ruiz-Rodriguez (1994) shows results of laboratory measurements with sands of only one grain size. The plots for different grain sizes deviate from the straight-line relationship the higher the pressure gradient and the velocity (Fig 3.3).

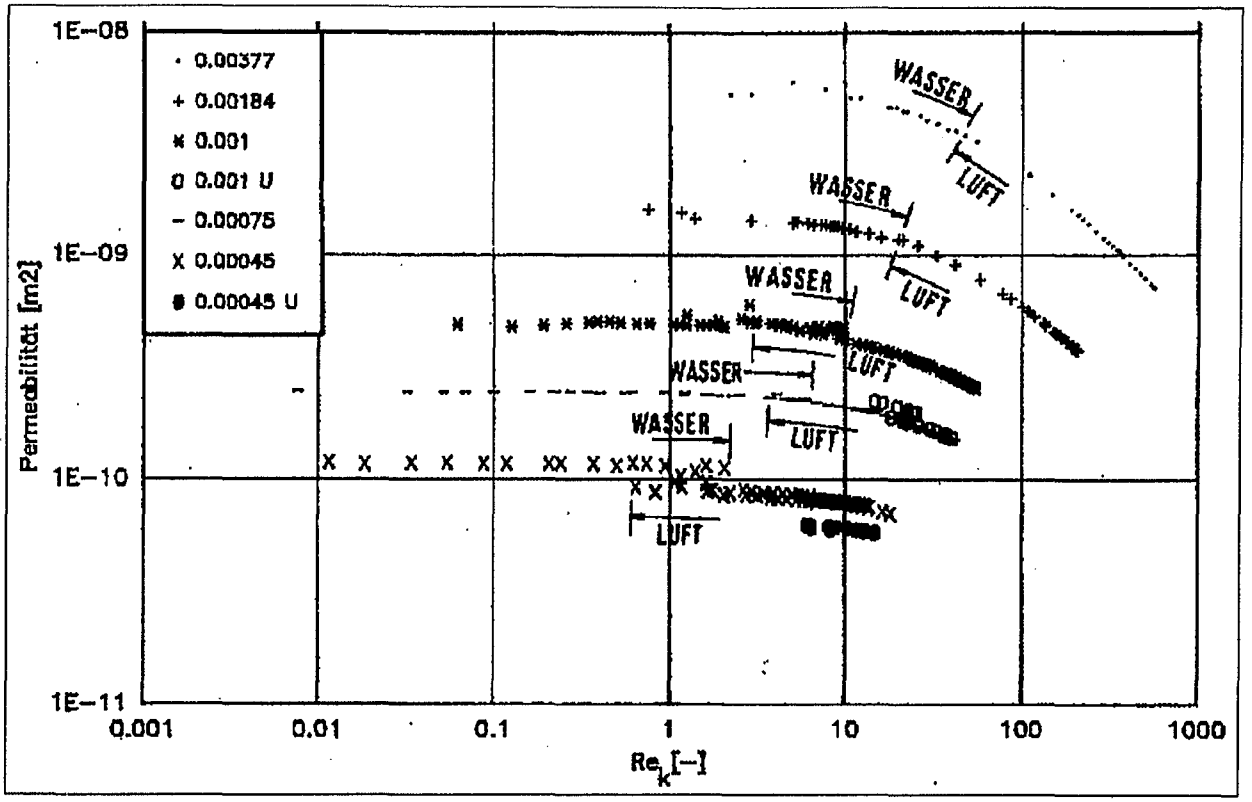

Fig. 3.3: Validity of Darcy's law: Permeability (Permeabilität [m^2]) depending on Reynolds number, Re = Re_k, for various effective grain sizes, d_{10} (Ruiz-Rodriguez, 1994; Kretzer, 1989)

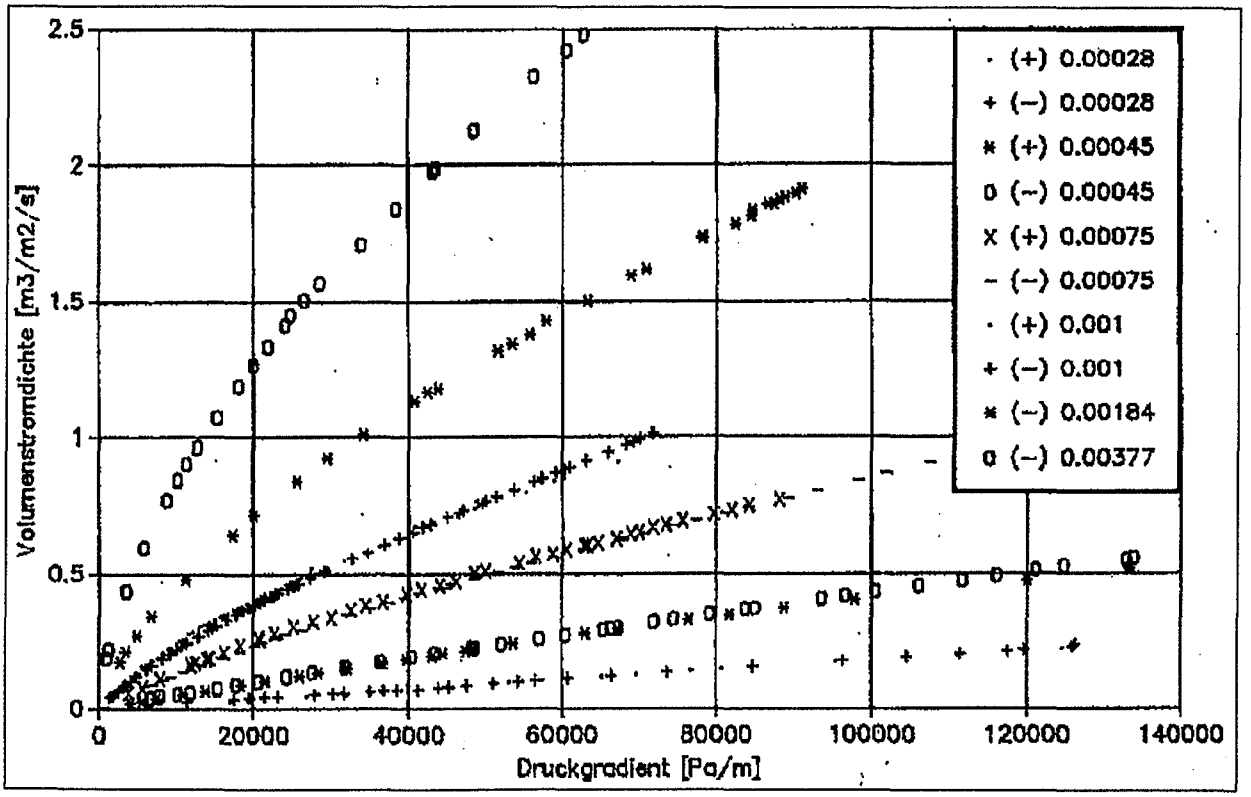

Fig. 3.2: Pressure gradient (Druckgradient [Pa/m]) versus velocity (Q/A, Volumenstromdichte [$m^3/m^2/a$]) for different uniform sands (Ruiz-Rodriguez, 1994; Kretzer, 1989)

The linearity of the Δp-Q or Δp-v relation of the measurements in this work is shown in chapter 6.2.2, results of pneumatic pumping tests. It clearly justifies the use of Darcy's equation for the flow of gas under the conditions of low pressure differences within this work. In comparison with Ruiz-Rodriguez (1994) and Kretzer (1989) the pneumatic tests of this work plot only in the low pressure gradient/low velocity region of figure 3.3.

3.1.2.2 Slip Flow (Klinkenberg)

One factor causing differences between measured hydraulic and gas conductivities is the slip flow. Slip flow can be interpreted as the bouncing of the gas molecules on the (grain) wall at low velocities when the mean free path of the molecules becomes the same order of magnitude as the pore diameter (see e.g. Jaritz, 1998). Klinkenberg (1942) demonstrated that the slip effect (Fig. 3.4) can be taken into account as follows: The apparent permeabilities, k_{app}, of the measurements can be transferred to intrinsic permeabilities, k, by extrapolating the straight-line relationship 1/p versus k_{app}

$$k_{app} = k \cdot \left(1 + \frac{b}{p}\right) \qquad 3.19$$

(p represents mean pressure) to an infinite mean pressure.

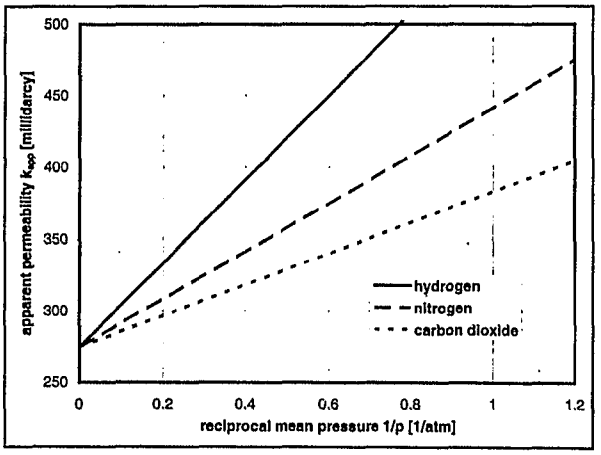

Fig. 3.4: Reciprocal mean pressure, 1/p, versus apparent permeability, k_{app}, "Klinkenberg plot" (after Klinkenberg, 1942)

The Klinkenberg constant, b, multiplied by k determines the slope of the straight-line relation in equation 3.19 and depends on the gas used. The comparison of different gases, such as hydrogen, nitrogen and carbon dioxide, shows that the latter results in the lowest slope, i.e. in the smallest differences between k_{app} and k values.

Experiments (Jaritz, 1998) show that laboratory measurements for sandstone samples result in permeabilities depending on the mean pressures. Thus, a permeability correction by incorporating the slip flow effect is necessary for low-permeability materials. However, the slip or drift flow (Dullien, 1992) can be neglected for grain sizes $> 10^{-3}$ mm, i.e. Darcy's law represents a good approximation for gas flow in sands and gravels (Massmann, 1989).

Thus, for the particular measurements performed in this work, slip flow is not important as the sediments under consideration range mainly from sands to gravels. Comparing the deviation caused by not correcting the apparent permeability to the real, intrinsic permeability (Fig. 3.5, after Jaritz, 1998) shows that for the expected permeabilities of $> 10^{-4}$ m/s the difference becomes very small.

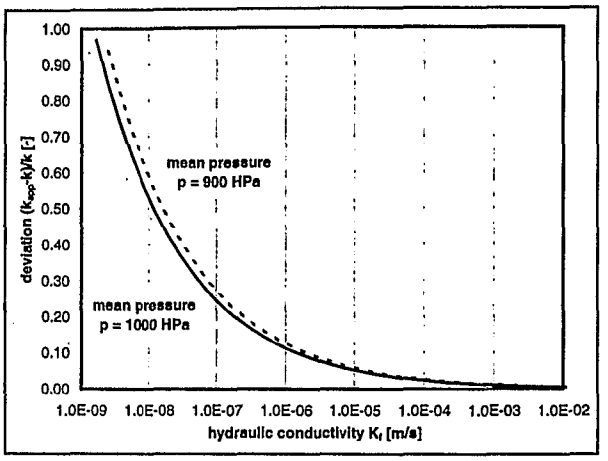

Fig. 3.5: Deviation of apparent permeability, k_{app}, from intrinsic permeability, k, caused by not correcting for slip flow (adapted from Jaritz, 1998)

3.1.2.3 Compressibility

The compressibility of gas means that the density, ρ, is a function of the pressure, p. In terms of the description of gas flow it results in a non-linear form of the general flow equation (e.g. Massmann, 1989)

$$\nabla \cdot \left(\frac{k}{\mu_g} p \nabla p\right) = n \frac{\partial p}{\partial t} + p_0 \cdot q \qquad 3.20$$

or, for steady state flow without sources or sinks,

$$\nabla \cdot \left(\frac{k}{\mu_g} p \nabla p\right) = 0 \qquad 3.21$$

For the specific case of equation 3.21 the detailed derivations of analytical solutions for 1D, 2D, 3D (radial) conditions are given in annex 1. Table 3.1 summarises the results in terms of pressure and pressure gradient distributions for compressible and incompressible conditions.

Furthermore, in annex 1 the errors of assuming an incompressible pressure and pressure gradient distribution instead of the compressible analytical solutions for the particular case of a distance of 1 m and a total pressure drop of $100 \cdot 10^2$ Pa, similar to field conditions (Ch. 6) are calculated: generally they are very small (maximal difference of pressure distribution 0.14 %, pressure gradient distribution ± 5 %).

	Compressible	Incompressible
1D	$p(r)=\sqrt{\frac{p_2^2-p_1^2}{r_2-r_1}\cdot(r-r_1)+p_1^2}$	$p(r)=\frac{p_2-p_1}{r_2-r_1}\cdot(r-r_1)+p_1$
	$\frac{\partial p(r)}{\partial r}=\frac{p_2^2-p_1^2}{2\cdot(r_2-r_1)\cdot p(r)}$	$\frac{\partial p(r)}{\partial r}=\frac{p_2-p_1}{r_2-r_1}$
2D	$p(r)=\sqrt{\frac{p_2^2-p_1^2}{\ln\frac{r_2}{r_1}}\cdot\ln\frac{r}{r_1}+p_1^2}$	$p(r)=\frac{p_2-p_1}{\ln\frac{r_2}{r_1}}\cdot\ln\frac{r}{r_1}+p_1$
	$\frac{\partial p(r)}{\partial r}=\frac{p_2^2-p_1^2}{2\cdot r\cdot\ln\frac{r_2}{r_1}\cdot p(r)}$	$\frac{\partial p(r)}{\partial r}=\frac{p_2-p_1}{r\cdot\ln\frac{r_2}{r_1}}$
3D	$p(r)=\sqrt{\frac{p_2^2-p_1^2}{r_2-r_1}\cdot r_2\cdot\left(1-\frac{r_1}{r}\right)+p_1^2}$	$p(r)=\frac{p_2-p_1}{r_2-r_1}\cdot r_2\cdot\left(1-\frac{r_1}{r}\right)+p_1$
	$\frac{\partial p(r)}{\partial r}=\frac{\left(p_2^2-p_1^2\right)\cdot r_1\cdot r_2}{2\cdot r^2\cdot(r_2-r_1)\cdot p(r)}$	$\frac{\partial p(r)}{\partial r}=\frac{p_2-p_1}{r^2\cdot(r_2-r_1)}\cdot r_1\cdot r_2$

Tab. 3.1: Analytical solutions for one-, two-, three-dimensional (radial) steady state gas flow considering compressibility or assuming incompressibility

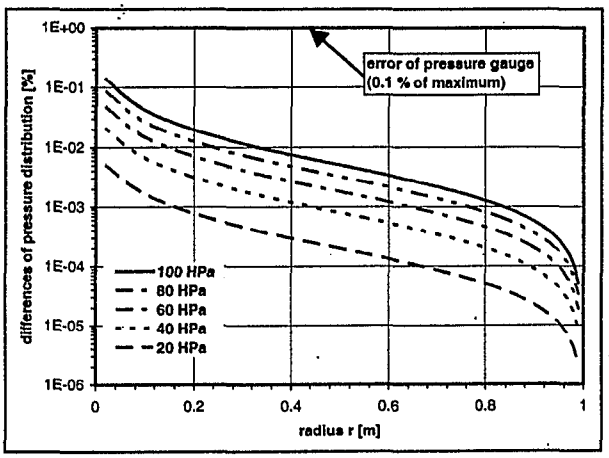

Fig. 3.6: Differences of three-dimensional pressure distribution (incompressible to compressible) for various pressure differences and radii applied in the field

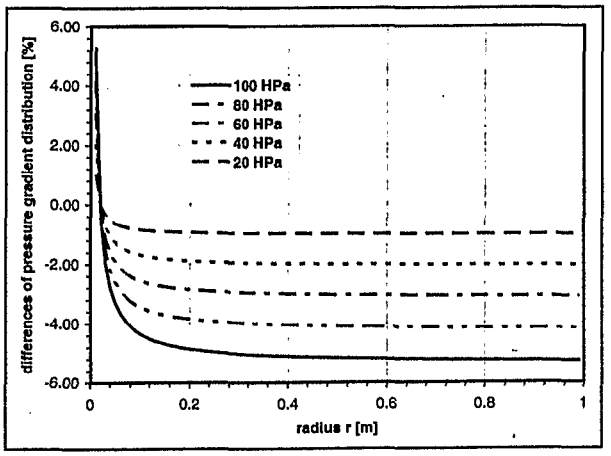

Fig. 3.7: Differences of three-dimensional pressure gradient distribution (incompressible to compressible) for various pressure differences and radii applied in the field

Examining the differences of the three-dimensional pressure distribution (between incompressible and compressible conditions) for various pressure differences applied in the field (Fig. 3.6) these are even smaller for lower pressure gradients. In particular the measurement error of the membrane to measure the pressure difference in the field or laboratory (see Ch. 5.2) is much higher (at about 1 % of $100 \cdot 10^2$ Pa). Similarly the differences of the three-dimensional pressure gradient distribution (incompressible to compressible) for various pressure differences applied in the field decrease with decreasing pressure as expected (Fig. 3.7).

On the basis of this comparison of the compressible and incompressible analytical solutions the effects of compressibility can be neglected for the pressure differences applied in this work.

Returning to the general flow equations, Massmann (1989) describes methods of overcoming the problem of non-linearity of Eq. 3.20 or 3.21 by linearising the flow equations based on assumptions about the total pressures involved (Tab. 3.2). These are useful for gas flow modelling under different pressure boundary conditions (Ch. 4).

	assumption 1	assumption 2
non-lin. gen. flow eq. w. source/sink	$n\frac{\partial p}{\partial t}=\nabla\cdot\left(\frac{k}{\mu}\cdot p\cdot\nabla p\right)-p_0\cdot q$	
non-lin. gen. flow equation w/o source/sink	$n\frac{\partial p}{\partial t}=\nabla\cdot\left(\frac{k}{\mu}\cdot p\cdot\nabla p\right)$	
	$\frac{p_2}{p_1}>0.8$ $p_1=10^3$HPa, $p_2>8\cdot10^2$HPa $\Rightarrow\Delta p<2\cdot10^2$HPa	$\frac{p_2}{p_1}>0.5$ $p_1=10^3$HPa, $p_2>5\cdot10^2$HPa $\Rightarrow\Delta p<5\cdot10^2$HPa
lin. approx. of gen. flow eq. w. source/sink	$n\frac{\partial p}{\partial t}=\nabla\cdot\left(\frac{k}{\mu}\cdot p_0\cdot\nabla p\right)-p_0\cdot q$	$n\frac{\partial p^2}{\partial t}=\nabla\cdot\left(\frac{k}{\mu}\cdot\nabla p^2\right)-p_0\cdot q$
lin. approx. of gen. flow eq. w/o source/sink	$n\frac{\partial p}{\partial t}=\nabla\cdot\left(\frac{k}{\mu}\cdot p_0\cdot\nabla p\right)$	$n\frac{\partial p^2}{\partial t}=\nabla\cdot\left(\frac{k}{\mu}\cdot\nabla p^2\right)$
steady state lin. approx. w. source/sink	$0=\nabla\cdot\left(\frac{k}{\mu}\cdot\nabla p\right)-q$	$0=\nabla\cdot\left(\frac{k}{\mu}\cdot\nabla p^2\right)-p_0\cdot q$
steady state lin. approx. w/o source/sink	$0=\nabla\cdot\left(\frac{k}{\mu}\cdot\nabla p\right)$	$0=\nabla\cdot\left(\frac{k}{\mu}\cdot\nabla p^2\right)$

Tab. 3.2: Linear approximations of the non-linear general flow equation for gas, depending on assumptions for the total pressure difference $\Delta p = p_1 - p_2$, p_0 represents the initial (gas) pressure, mostly atmospheric (after Massmann, 1989)

3.1.2.4 Saturation by Air/Water

The permeability measured by gas or water depends on the saturation of the pore space with the respective fluid (Carman, 1956). For the combination of CO_2 (as gas) and water the dependence on the saturations of both fluids of the specific permeability, k_s, of a fluid was examined in detail for four sands (Wyckoff and Botset, 1936, Fig. 3.8).

Within the range of sand grain sizes used it resulted in a relation between the intrinsic

permeability, k, and the measured, effective permeability, k_{eff},

$$k_{eff} = k_s \cdot k \qquad 3.22$$

Carman (1956) pointed out that since CO_2 occupies the larger pores its permeability is not much influenced as long as less than 15 % of the pore space is taken up by water. This differs remarkably from the case when water is displaced by a small amount of gas, which results in a strong decrease of water permeability (Fig. 3.8).

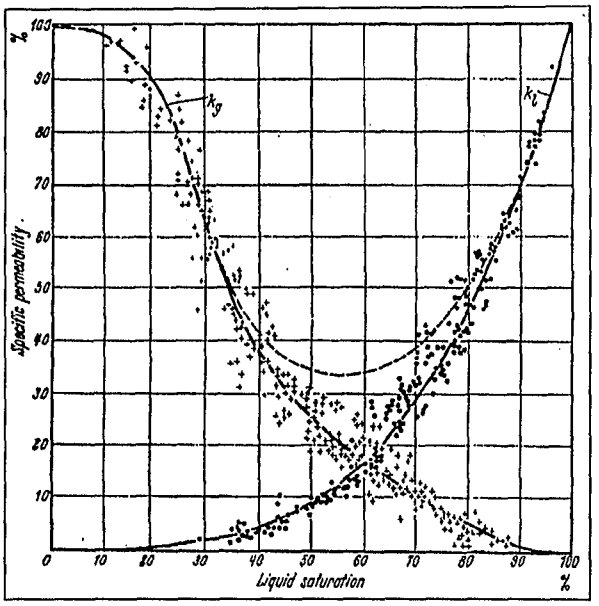

Fig. 3.8: Dependence of the specific permeability, k_s, from saturation for gas, k_g, (CO_2) and water, k_l, (Carman, 1956, original from Wyckoff and Botset, 1936)

In most field cases of gas tracer tests or vapour extraction systems the water saturation in the vadose zone of sands or gravels can be assumed to be smaller than 15 % of the pore space (10 %, Borho, 1995). Therefore, the effective permeability, k_{eff}, can be regarded as the intrinsic permeability, k.

3.2 Transport of Gas - Use of Gas as a Tracer

Analogous to transport in water, the transport of a specific gas (concentration) in soil air follows the same advection-dispersion-equation as long as the flow field can be assumed to follow Darcy's law (Ch. 3.1). However, one important difference to water is the higher molecular diffusion of a gas in comparison to its mechanical dispersion in mixing processes.

3.2.1 Advection and Dispersion

The general advection-dispersion equation

$$R \cdot \frac{\partial c}{\partial t} = \nabla \cdot (D \cdot \nabla c) - v_a \cdot \nabla c \qquad 3.23$$

is assumed to be valid for the case of gas tracers within unconsolidated and mainly air saturated porous formations.

For the purpose of this work the hydrodynamic dispersion, D, is seen as a combination of mechanical dispersion (dispersivity, α, multiplied with tracer velocity, v_a) and the coefficient of molecular diffusion, D_m,

$$D = \alpha \cdot v_a + D_m \qquad 3.24$$

3.2.2 Diffusion

For gas transport, diffusion cannot generally be neglected as it is often the case for transport in water.

The coefficient of molecular diffusion, D_m, in a porous media can be expressed in terms of diffusion of the specific gas in air, D_m^{air}, (Millington and Quirk, 1961; Klein, 1992) by

$$D_m = D_m^{air} \cdot \frac{n_{air}^{3.3}}{n^2} \qquad 3.25,$$

where the air filled porosity, n_{air}, is smaller or equal to the total porosity, n.

Assuming similar values for n_{air} and n, where n is < 0.43 for all lithological facies types, the quotient of porosities results to < 0.33. I.e. the diffusion coefficient is a factor of approximately 0.33 less than the diffusion coefficient in air alone. For smaller air filled porosities the factor would decrease further. Therefore, the maximal diffusion, D_m, is always smaller than a third of the diffusion in air, D_m^{air}.

The diffusion of gas in air can be estimated by

$$D_m^{air} = \frac{10^{-3} \cdot T_g^{1.75} \cdot \left(\frac{1}{M_1} + \frac{1}{M_2}\right)^{0.5}}{p\left[(\Sigma v)_1^{0.33} + (\Sigma v)_2^{0.33}\right]^2} \qquad 3.26$$

(Perry and Green, 1984; Lyman et al., 1990), where $M_{1,2}$ are the molecular weights of the two substances, here CO_2 and air (44.01 and 28.97, respectively), p is the absolute pressure in atmospheres [atm] and $(\Sigma v)_{1,2}$ the atomic diffusion volumes (26.9 and 20.1, respectively).

For CO_2 the diffusion coefficients in air, calculated on the basis of equation 3.26, are given in table 3.3 for different absolute temperatures and pressures.

T_g [K]		273	283	293
p [atm]	1.1	$1.22 \cdot 10^{-5}$ m²/s	$1.30 \cdot 10^{-5}$ m²/s	$1.38 \cdot 10^{-5}$ m²/s
	1.0	$1.34 \cdot 10^{-5}$ m²/s	$1.43 \cdot 10^{-5}$ m²/s	$1.52 \cdot 10^{-5}$ m²/s
	0.9	$1.49 \cdot 10^{-5}$ m²/s	$1.59 \cdot 10^{-5}$ m²/s	$1.69 \cdot 10^{-5}$ m²/s
	0.5	$2.69 \cdot 10^{-5}$ m²/s	$2.89 \cdot 10^{-5}$ m²/s	$3.04 \cdot 10^{-5}$ m²/s

Tab. 3.3: Diffusion coefficients of CO_2 in air, calculated from equation 3.26

For the evaluation of the measurements in this work the diffusion coefficient of CO_2 in the air of a porous media is assumed to be as high as the diffusion coefficient of CO_2 in air alone, for a temperature of 293 K, approximately 20 °C, and an absolute pressure of 0.9 atm, approximately 900 mbar = $900 \cdot 10^2$ Pa. This results in a diffusion, D_m, equal to $1.69 \cdot 10^{-5}$ m²/s. This overestimation is, comparing to the effective dispersion encountered in the measurements, still small enough to be neglected. However, in the evaluation of the tracer measurements in the laboratory and field the diffusion is taken into account in the calculations of the analytical solutions (Ch. 6, Annex 2).

3.2.3 Analytical Solutions for Gas Tracer Breakthrough Curves

Analytical solutions for the advection-dispersion equation in the form of equation 3.23 are given in annex 2 for different boundary conditions. A conservative, non-reactive tracer is assumed (with a retardation factor of R = 1) simplifying the equations substantially.

For this project the solutions for one-dimensional (and radial convergent) transport for tracer injections over a specific time interval are required as most field and laboratory situations can be represented only in this way. With respect to the boundary conditions given in annex 2 the solution by Häfner et al. (1992) is applied:

$$c(x,t) = \begin{cases} c_0 \cdot f(x,t) & \text{for } 0 < t \le \Delta t \\ c_0 \cdot [f(x,t) - f(x,t-\Delta t)] & \text{for } t > \Delta t \end{cases} \qquad 3.27$$

$$f(x,\tau) = \frac{1}{2} \cdot \left[\operatorname{erfc}\left(\frac{x - \frac{v_a \cdot \tau}{R}}{\sqrt{4 \cdot D_L \cdot \frac{\tau}{R}}} \right) + \exp\left(\frac{v_a \cdot x}{D_L} \right) \cdot \operatorname{erfc}\left(\frac{x + \frac{v_a \cdot \tau}{R}}{\sqrt{4 \cdot D_L \cdot \frac{\tau}{R}}} \right) \right] \qquad 3.28$$

The program DTTRACER is developed to calculate the breakthrough curves for the specific parameters in the laboratory or field. As a result from the manual curve fitting procedure parameters such as tracer velocity, v_a, and longitudinal dispersion, D_L, are given. Together with the other geometric dimensions of the experiment (Ch. 3.4) this results in conductivities for gas, K_g, intrinsic permeabilities, k, or directly in hydraulic conductivities, K_f.

3.3 Parameters of Gas Tracers

The choice of gas used as tracer in the low pressure gradient flow fields of air in the laboratory and field measurements of this work is determined mainly by its physical parameters.

One of the early references (Penman, 1940) uses CS_2 to determine diffusion values for gas. Later publications, concerning the design and monitoring of vapour extraction systems, prefer various other gases such as CH_4 (Marley et al., 1992), SF_6 (Marley et al., 1992; Olschewski et al., 1995), He (Marley et al., 1992; Fierz et al., 1993), Rn (Fierz et al., 1993) or CO (Richardson et al., 1996; Schmidt, 1994). A comparison of some physical parameters of gases is given in table 3.4.

Gas	CO	CO_2	CH_4	He	SF_6	N_2	air
M_g [g/mole]	28.0	44.0	16.0	4.0	146.1	28.0	28.6
μ_g [10^{-5} Pa·s] at 20 °C, 1 bar	1.75	1.46	1.09	1.95		1.77	1.81
solubility [10^3 g/m³·atm] at 20 °C	0.028	1.688			0.047* at 15 °C		
Henry const. [10^{-4} Pa] at 20 °C	4.88	3.5	3.76	12.5	132* at 15 °C	8.04	6.64
ρ_g [kg/m³] at 0 °C	1.25	1.98	0.72	0.18	6.5*	1.25	1.29
D_m^{air} [10^{-5} m²/s] at 20 °C	1.90	1.53		6.46	0.91	1.94	
detection method	electro chem. < 2 ppm	IR < 5 Vol%,			electr. capt.		
local price [DM/10 l]	506	36 10 kg, 4-6 m³		55	561	28	40

Tab. 3.4: Parameters for different potential tracer gases and air (Perry and Green, 1984, * Olschewski et al., 1995)

Probably the best tracer gas for field conditions would be SF_6 (Olschewski et al., 1995) since it is not easily soluble in water (high partitioning coefficient, Henry constant). However, its density and price are disadvantageous. Especially the high price reduces the feasibility for application of larger volumes. Another gas, CO, used by Richardson et al. (1996) and Schmidt (1994), has, beside that it is expensive, the disadvantage of being explosive and is therefore not suitable for transport to field measurement sites.

For this project the best compromise was found with the use of CO_2 as tracer gas. It is easily detectable with an infrared detector even under field conditions. Its main disadvantage, the high solubility in water, did not pose problems since the duration of the measurement (Ch. 6) was short (less than 1 minute) compared to the contact time

with the pore water, CO_2 needs to be dissolved. Furthermore, the costs for the volumes needed for various measurements in the field and laboratory were acceptable.

3.4 Hydraulic Conductivity from Gas Measurements

The field and laboratory gas measurements in this work result in relationships between the pressure difference and the volumetric flow rate (Δp-Q, pneumatic tests) and tracer breakthrough curves (tracer tests), from which intrinsic permeabilities and hydraulic conductivities may be derived (Ch. 3.1, Fig. 3.1). The major difference between the laboratory and field measurement is the flow field, which is one-dimensional in the case of a column experiment in the laboratory and three-dimensional, radial in the case of field experiments with a convergent flow field due to the extraction of soil air. Here the assumption of an incompressible gas is made, since, for the pressure differences applied in the measurements, the error in neglecting compressibility is small (An. 1). The description of the tracer breakthrough curves in both, the one- and three-dimensional (radial) cases is performed with the same analytical solution, as the convergent tracer tests can, under these conditions, be approximated by the one-dimensional solution (An. 2).

The results of the measurements, based on the formulas listed below, are presented in chapter 6.

3.4.1 Gas Pneumatic Tests

The proportionality of flow and pressure difference, represented by Darcy's law (Eq. 3.14), is valid under one- and three-dimensional conditions, such that

$$v = \frac{Q}{A} = -\frac{k}{\mu_g} \cdot \left(\frac{dp}{dr}\right) \qquad 3.29,$$

where r is the distance (1D) or radial distance (3D) and A the cross section area of flow: circle (1D) and surface of a sphere (3D).

Thus the intrinsic permeability is given by

$$k = -\frac{\mu_g}{A} \cdot \frac{Q}{\left(\frac{dp}{dr}\right)} \qquad 3.30$$

In this way the following estimations of k on the basis of the Δp-Q relation can be compared to the well-known Dupuit-Thiem formula (Δh-Q relation) for steady state pumping test evaluation in hydrogeology

$$Q = \underbrace{2 \cdot \pi \cdot r \cdot D}_{A} \cdot K_f \cdot \underbrace{\frac{h_2 - h_1}{r \cdot \ln\left(\frac{r_2}{r_1}\right)}}_{\frac{dh}{dr}} \qquad 3.31$$

However, the groundwater situation is only similar to the two-dimensional case of the incompressible assumption of the gas pressure distribution (Tab. 3.1), here the laboratory and field represent the one- and three-dimensional situations, respectively.

3.4.1.1 Laboratory Tests

Under one-dimensional laboratory conditions of controlled flow and pressure difference over a specific column the area, A, in equation 3.30 can be written as the cross section area of the cylinder

$$A = \pi \cdot r_{cyl}^2 \qquad 3.32$$

Under the assumption of incompressibility (s. Tab. 3.1) the pressure gradient dp/dr can be expressed as

$$\frac{\partial p(r)}{\partial r} = \frac{p_2 - p_1}{r_2 - r_1} = \frac{\Delta p}{l} \qquad 3.33$$

Knowing the column geometry (radius, r_{cyl}, length, l), the intrinsic permeability is proportional to the gradient of the Δp-Q relation

$$k = -\frac{\mu_g \cdot l}{\pi \cdot r_{cyl}^2} \cdot \frac{Q}{\Delta p} \qquad 3.34$$

3.4.1.2 *In Situ* Field Tests

For the field conditions of an assumed mainly three-dimensional convergent flow field from an outer injection point to the inner extraction point, which creates the convergent flow field, the cross-section area, A, is given by the surface of the outer sphere

$$A = 4 \cdot \pi \cdot r_{sph}^2 \qquad 3.35$$

Assuming incompressibility leads to an expression for dp/dr in the form of

$$\frac{\partial p(r)}{\partial r} = \frac{p_2 - p_1}{r^2 \cdot (r_2 - r_1)} \cdot r_1 \cdot r_2 = \frac{\Delta p}{r_{sph}^2 \cdot (r_{sph} - r_1)} \cdot r_1 \cdot r_{sph} \qquad 3.36$$

With the knowledge of the experimental geometry, i.e. known distance between injection and extraction points, r_{sph}, inner radius of the extraction rod, r_1, and under consideration of the dipole character of extraction and injection, i.e. the superposition of the convergent flow field, created by Q_{out} and the small contribution of the injection field Q_{in} ($Q = Q_{out} + Q_{in}$), the intrinsic permeability is given by

$$k = -\frac{\mu_g \cdot (r_{sph} - r_1)}{4 \cdot \pi \cdot r_{sph} \cdot r_1} \cdot \frac{Q}{\Delta p} \qquad 3.37$$

3.4.2 Gas Tracer Tests

The tracer velocity, v_a, estimated by fitting analytical solutions to the measured breakthrough curves (Annex 2), is given by

$$v_a = \frac{r_2 - r_1}{t_{0.5}} \qquad 3.38$$

The mean arrival time may be expressed as

$$t_{0.5} = \int_{r_1}^{r_2} \frac{1}{v_a} dr = \int_{r_1}^{r_2} \frac{n}{v} dr = -\frac{n \cdot \mu_g}{k} \cdot \int_{r_1}^{r_2} \frac{1}{\left(\frac{dp}{dr}\right)} dr \qquad 3.39$$

leading to an expression for the intrinsic permeability in the form of

$$k = -\frac{n \cdot \mu_g \cdot v_a}{r_2 - r_1} \cdot \int_{r_1}^{r_2} \frac{1}{\left(\frac{dp}{dr}\right)} dr \qquad 3.40$$

In the following sections this general equation is solved by inserting the appropriate analytical solution for the pressure gradient distribution (Tab. 3.1), considering compressible or assuming incompressible conditions and one- or three-dimensional flow, and solving the integral. Again the differences by considering compressible or assuming incompressible conditions are compared for the calculated intrinsic permeabilities.

3.4.2.1 Laboratory Tests

The one-dimensional analytical solution considering compressibility results in an intrinsic permeability

$$k_c = -\frac{2 \cdot n \cdot \mu_g \cdot v_a}{p_2^2 - p_1^2} \cdot \int_0^l \sqrt{\frac{p_2^2 - p_1^2}{l} \cdot r + p_1^2}\, dr \qquad 3.41,$$

where r is the one-dimensional distance along the column and l the total length of the column.

Assuming incompressibility, the intrinsic permeability is given by

$$k_i = -\frac{n \cdot \mu_g \cdot v_a \cdot l}{\Delta p} \qquad 3.42$$

The quotient k_i/k_c

$$\frac{k_i}{k_c} = \frac{3}{4} \cdot \left(\frac{(p_1 + p_2)^2}{(p_1 + p_2)^2 - p_1 \cdot p_2} \right) \qquad 3.43$$

can be plotted for different pressure differences, Δp, from atmospheric pressure, p_2 (Fig. 3.9). A detailed derivation of k_c, k_i and k_i/k_c is given in annex 5.

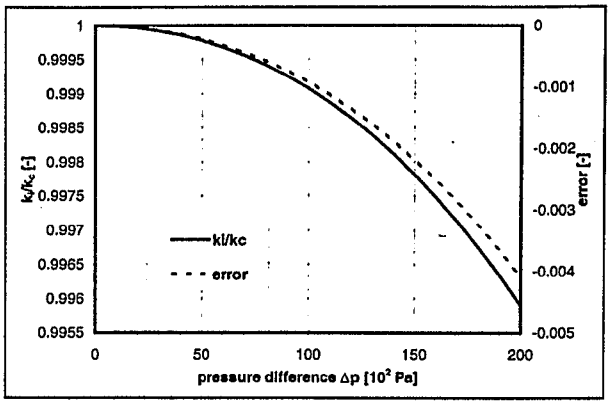

Fig. 3.9: Comparison of calculations of intrinsic permeability, considering compressible (k_c), assuming incompressible (k_i) gas flow for different pressure differences Δp from one-dimensional tracer breakthrough curves in the laboratory

The differences for an applied pressure difference of up to $50 \cdot 10^2$ Pa are small (< 0.05 %). Therefore, the evaluation of the laboratory measurements (Ch. 6) with the incompressibility assumption (Eq. 3.42) is reasonable.

3.4.2.2 *In Situ* Field Tests

The three-dimensional analytical solution considering compressibility results in an intrinsic permeability

$$k_c = -\frac{2n\mu_g v_a}{\left(p_2^2 - p_1^2\right) r_{sph} r_1} \int_{r_1}^{r_{sph}} r^2 \sqrt{\frac{p_2^2 - p_1^2}{r_{sph} - r_1} r_{sph}\left(1 - \frac{r_1}{r}\right) + p_1^2}\, dr \qquad 3.44,$$

where r is the radial distance in between extraction and injection point, $r_2 = r_{sph}$ the total radial distance and l the difference between total radial distance and inner radius of extraction rod.

Assuming incompressibility, the intrinsic permeability is given by

$$k_i = -\frac{n \cdot \mu_g \cdot v_a \cdot \left(r_{sph}^3 - r_1^3\right)}{3 \cdot \Delta p \cdot r_{sph} \cdot r_1} \qquad 3.45$$

The quotient k_i/k_c can be plotted for different pressure differences, Δp, from atmospheric pressure, p_2. Figure 3.10 shows the differences for a radius of the sphere $r_{sph} = 1$ m and an inner radius of the extraction rod, $r_1 = 0.01$ m, representing the field conditions described in chapter 6. A detailed derivation for k_c, k_i and k_i/k_c is given in annex 5.

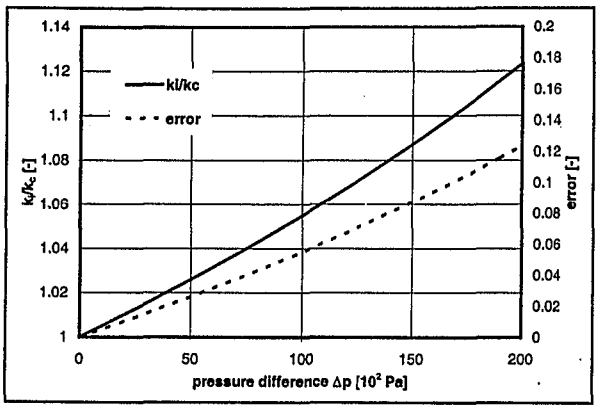

Fig. 3.10: Comparison of calculations of intrinsic permeability, considering compressible (k_c), assuming incompressible (k_i) gas flow for different pressure differences Δp from three-dimensional tracer breakthrough curves in the field ($r_i = 0.01$ m, $r_{sph} = 1$ m)

Even in the three-dimensional case the differences for an applied pressure difference of up to $50 \cdot 10^2$ Pa are small (< 2.5 %). Therefore, the evaluation of the field measurements (Ch. 6) with the incompressibility assumption (Eq. 3.45) is reasonable.

4 Simulating Steady State Gas Flow and Transport

The gas tracer tests may be applied in the field according to two objectives: (a) to provide characteristic hydraulic parameters for a single lithofacies unit, or (b) to define effective hydraulic parameters representing a region comprising more than one lithofacies unit. In approach (a) the measured the pressure differences, flow rate and breakthrough curves of gas flows may be analysed and interpreted using analytical solutions of flow and transport. For approach (b) the resulting effective values may be assessed by the use of numerical models incorporating heterogeneous 3D lithofacies units defined by 2D outcrop analysis (see Ch. 7), information in the third dimension being supplied by ground penetrating radar (GPR). This chapter details the gas flow and transport modelling tools that may be used for assessing the parameters derived in such heterogeneous environments; examples for simple scenarios (single lenses of different permeability) and a complex heterogeneous block (taken from 2D outcrop data) are given. Future acquisition of ground penetrating radar data will allow the incorporation of variation in the third dimension.

In this project the field measurements have been conducted mainly following approach (a), i.e. within single homogeneous units to estimate parameters for individual lithofacies types.

Modelling of steady state gas flow was initially conducted by comparing the model results from two programs, AIR (Lin and Kinzelbach, 1991) and MODFLOW (McDonald and Harburgh, 1984), with the analytical solutions for the three-dimensional pressure distribution due to abstraction from a homogeneous geological structure. AIR may be used for compressible and incompressible calculations, whereas MODFLOW is restricted to incompressible conditions.

For the pressure differences applied in the field it was found that it is sufficient to approximate the gas flow by an incompressible gas flow model (see chapter 3 and Massmann, 1989). Thus the pressure distribution and particle flow paths for different geologically heterogeneous cases at the

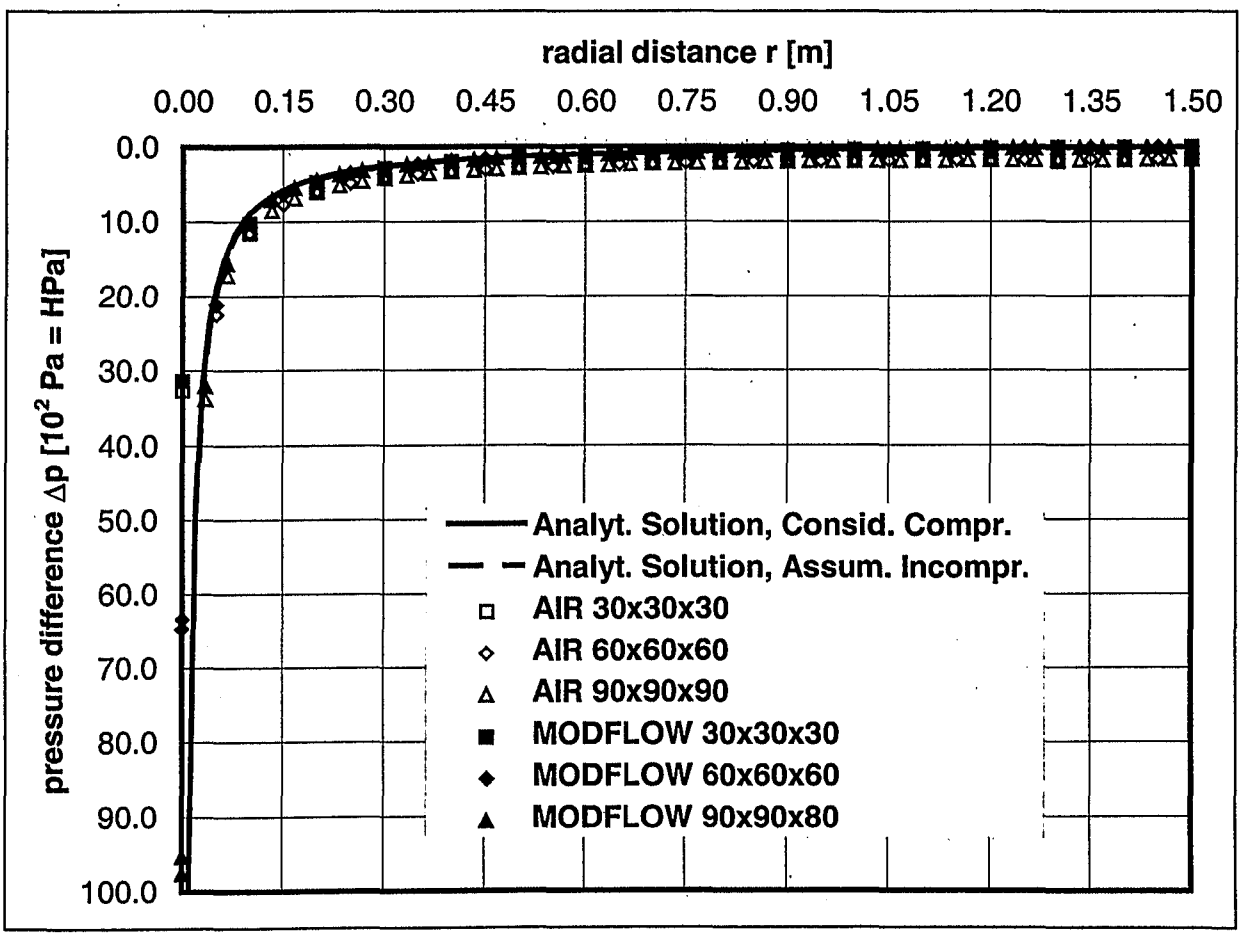

Fig. 4.1: Comparison of steady state gas flow modelling considering compressibility - AIR (Lin and Kinzelbach, 1991), or assuming incompressibility - MODFLOW (McDonald and Harburgh, 1984) with the respective analytical solutions: abstraction flow rate Q_{out} = 0.564 l/s, permeability k = $8.0 \cdot 10^{-12}$ m², representing a pressure difference (drop) from atmospheric pressure of Δp = 100 HPa

end of this chapter were calculated only with the programs MODFLOW/MODPATH (McDonald and Harburgh, 1984; Pollock, 1989). The permeabilities resulting from estimated tracer velocities on the basis of the particle arrival times are compared with the means of the permeabilities in the model.

4.1 Modelling of 3D Gas Flow

For the pressure distribution in a gas flow field due to abstraction, under the field conditions similar to those encountered in this work, the gas flow can be approximated by an incompressible fluid flow (Ch. 3, Massmann, 1989). To support the theoretical results the analytical solutions (compressible and incompressible) were compared with model calculations for a homogeneous case, conducted with two different programs: AIR, allowing compressible and incompressible gas flow modelling, and MODFLOW, allowing only incompressible fluid flow modelling.

4.1.1 Modelling Compressible Gas Flow

The program used to model the gas flow under consideration of its compressibility is AIR (AIR INDUCED REMEDIATION MODEL, Lin and Kinzelbach, 1991). This software package includes a preprocessing program, the program AIRSIM to calculate the pressure distributions, the program AIRPATH to calculate pathlines and postprocessing programs. The central finite difference program to calculate the 3D flow field (pressure distribution) is based on the mass flow equation

$$\nabla\cdot\left(\rho_g\cdot\frac{k}{\mu_g}\cdot\nabla p\right)=\nabla\cdot\left(\frac{m_g}{2\cdot n_g\cdot R_g\cdot T_g}\cdot\frac{k}{\mu_g}\cdot\nabla p^2\right)=m_g\cdot q_g \qquad 4.1.$$

Steady state laminar single phase gas flow is assumed. The free groundwater surface is an impervious boundary for gas and its location may change depending on the air pressure field. Within the node-centred, rectangular cells the air balance equations are established on the basis of Darcy's law, yielding a system of equations, which is solved for the unknown pressures. Pathlines are computed by means of particle tracking in the velocity field.

To be able to calculate the gas flow in a more complex, heterogeneous environment with a higher resolution and in order to compare the resulting pressure distributions from AIR with those from MODFLOW the original program (FORTRAN 77 source code AIRSIM.F) was adapted to allow modelling with up to 90 x 90 x 90 cells.

The air pressure distribution due to abstraction by pumping (100 HPa pressure drop: 0.564 l/s in a homogeneous permeability field of $8\cdot10^{-12}$ m^2) from the centre of a 3 x 3 x 3 m^3 unit was calculated for different grids with cubic grid cells (30 cells in each direction: 0.1 m cell size, 60 cells in each direction: 0.05 m cell size, 90 cells in each direction: 0.033 m cell size). The boundary conditions are given by a constant head (atmospheric pressure) at the top and horizontal sides and a no-flow boundary (groundwater surface) at the bottom. The results are compared with the analytical solutions (based on Ch. 3) and the results from gas flow modelling assuming incompressibility (Fig. 4.1).

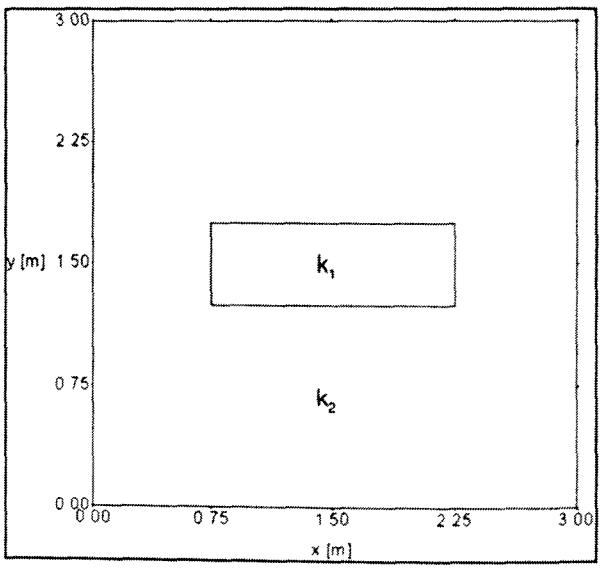

Fig. 4.2: Vertical section through schematic model of 2D geological structure of two different hydraulic conductivities for models of high permeability unit (k_1) in low permeable environment (k_2) and vice versa

4.1.2 Modelling Incompressible Gas Flow

The computation time for calculations by AIR were unsatisfactory long due to the repeated solving of the system of equations for the large number of cells used. Thus the gas flow modelling assuming incompressibility was carried out using MODFLOW (McDonald and Harburgh, 1984), since the gas flow equation is analogous to the equation for confined groundwater flow.

To use the groundwater flow model MODFLOW for the gas flow calculations the hydraulic conductivity, K_f, the flow rate, q_f, and the groundwater head, h, used normally by the model, have to be redefined for the purpose of modelling gas flow. The hydraulic conductivity, K_f, is exchanged with k/μ_g and the flow rate, q_f, with the gas flow rate, q_g. As a result the groundwater head distribution, h, can be interpreted as the pressure distribution, p (see annex 6).

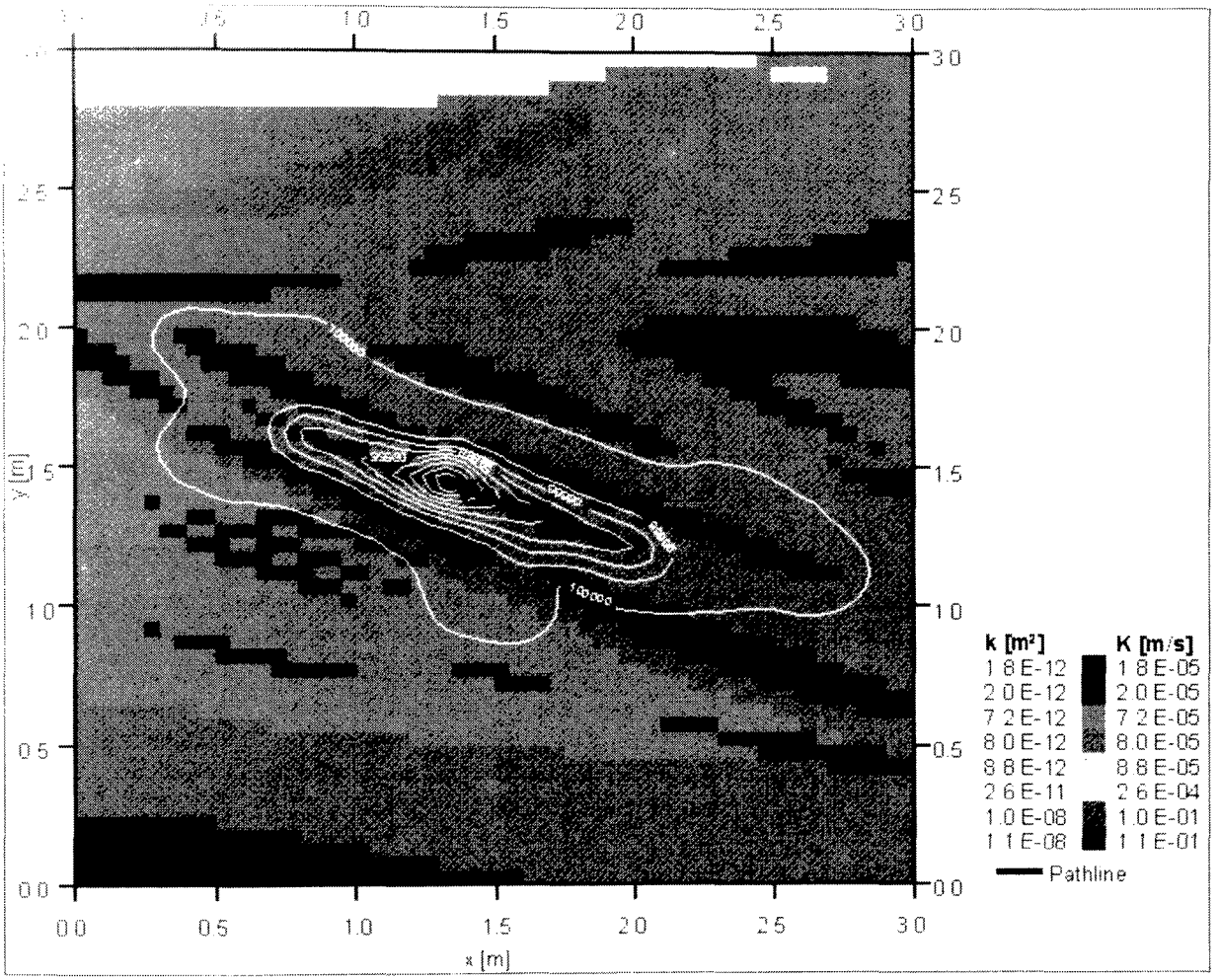

Fig. 4.3: Gridded vertical profile of 2D heterogeneous geological structures (cell width 0.05 m), representing a section of a gravel outcrop, hydraulic conductivities based on Jussel (1992), isolines of modelled 3D pressure distribution (interval of 5 Pa) due to abstraction of 4 l/s from the centre, example of particle pathline

The air pressure distribution is calculated for constant head (i.e. atmospheric pressure) boundary conditions at all sides of the model and the same abstraction rate as for the compressible case calculations (Ch. 4.1.1). The results are shown in figure 4.1.

4.1.3 Comparison of Compressible and Incompressible Modelling and Analytical Solutions

Both model calculations - AIR (Ch. 4.1.1) and MODFLOW (Ch. 4.1.2) - led to similar results (Fig. 4.1). With an increasing number of cells (thus decreasing cell size) the deviations from the analytical solutions became smaller. Under the specified conditions the differences between the analytical solutions (considering compressibility and assuming incompressibility) are negligible.

The pressure drop due to abstraction is small enough to use the incompressibility assumption for gas flow under the field conditions encountered during this project (Ch. 3). However, the modelling with AIR was not only much slower than that with MODFLOW, but also represents the bottom boundary by a no-flow boundary (groundwater table), which is not appropriate for the outcrop.

4.2 3D Modelling of Pathlines of Gas Particles

The simulated pressure distributions in 2D geological structures with MODFLOW were used as the basis for particle tracking (pathline calculations) with MODPATH (Pollock, 1989) within these flow fields. The particle tracking allows the estimation of conservative tracer velocities. The velocities can be used to derive effective permeabilities for the particular path. These can be compared with the means of the permeabilities in the cells along the pathlines.

Three different cases were studied:

- a high permeability unit ($k_1 = 1.0 \cdot 10^{-8}$ m^2) within a low permeability geological material ($k_2 = 8.0 \cdot 10^{-12}$ m^2, Fig. 4.2),
- a low permeability unit ($k_1 = 8.0 \cdot 10^{-12}$ m^2) within a high permeability ($k_2 = 1.0 \cdot 10^{-8}$ m^2, Fig. 4.2) and
- a heterogeneous model taken from an interpretation of a gravel and sand outcrop, composed of a variety of permeabilities ranging from $1.0 \cdot 10^{-12}$ m^2 to $1.1 \cdot 10^{-8}$ m^2 for the different lithofacies encountered (Fig. 4.3).

For each case 12 different injection/abstraction options have been considered for flow within a single lithofacies type or crossing the boundaries of different lithofacies units. The abstraction and injection coordinates and flow rates are listed in table 4.1.

4.2.1 Comparison of Effective Permeabilities Derived from Particle Travel Times with Harmonic Mean Permeabilities

For all 36 model setups (Tab. 4.1) pathlines of particles injected in the centre and at the sides of the injection cell were calculated. Figure 4.3 shows an example for the heterogeneous outcrop model.

For the comparison with the field cases, in which the particle pathline coordinates were assumed to connect the injection and abstraction ports with a straight line, reasonable estimations of the effective permeabilities of the area between both points were only obtained from pathlines which closely approximated a straight line.

The straight line of a particle path from the injection to the abstraction point and the particle travel time in combination with the injected/abstracted flow rate per cell size led to a modelled particle, i.e. tracer, velocity and hence to an effective permeability, k_{mod}. The harmonic mean of the permeabilities of the cells along the nearly straight line connection (flow path) led to a calculated permeability, k_{calc}.

The comparison of modelled and calculated permeabilities (Tab. 4.1) shows that in most cases the modelling led to similar permeability values. Thus the combination of modelling tools of MODFLOW and MODPATH, with parameters interpreted for gas flow (annex 6) confirmed the validity of the effective permeabilities gained from simulations of flow and transport in 3D heterogeneous environments such as gravel and sand outcrops.

No.	x,y coordinate [m]		inj. (+), abst. (-)		k_{mod}	k_{calc}
	point 1	point 2	Q_1 [l/s]	Q_2 [l/s]	[m^2]	[m^2]
1	1.225, 1.475	1.725, 1.475	-4.0	+0.0	5.96e-09	1.00e-08
2	1.225, 1.475	1.725, 1.475	-4.0	+2.0	-	-
3	1.225, 1.475	1.725, 1.475	-4.0	+4.0	1.57e-08	1.00e-08
4	1.225, 0.975	1.725, 0.975	-4.0	+0.0	2.85e-12	8.00e-12
5	1.225, 0.975	1.725, 0.975	-4.0	+2.0	-	-
6	1.225, 0.975	1.725, 0.975	-4.0	+4.0	6.43e-12	8.00e-12
7	1.475, 0.975	1.475, 1.475	-4.0	+0.0	-	-
8	1.475, 0.975	1.475, 1.475	-4.0	+2.0	-	-
9	1.475, 0.975	1.475, 1.475	-4.0	+4.0	2.13e-11	1.60e-11
10	1.475, 0.975	1.475, 1.475	-2.0	+4.0	-	-
11	1.475, 0.975	1.475, 1.475	0.0	+4.0	-	-
12	1.475, 0.975	1.475, 1.975	-4.0	+4.0	1.34e-11	1.60e-11
13	1.225, 1.475	1.725, 1.475	-4.0	+0.0	2.18e-12	8.00e-12
14	1.225, 1.475	1.725, 1.475	-4.0	+2.0	-	-
15	1.225, 1.475	1.725, 1.475	-4.0	+4.0	2.33e-12	8.00e-12
16	1.225, 0.975	1.725, 0.975	-4.0	+0.0	4.89e-09	1.00e-08
17	1.225, 0.975	1.725, 0.975	-4.0	+2.0	-	-
18	1.225, 0.975	1.725, 0.975	-4.0	+4.0	1.19e-08	1.00e-08
19	1.475, 0.975	1.475, 1.475	-4.0	+0.0	-	-
20	1.475, 0.975	1.475, 1.475	-4.0	+2.0	-	-
21	1.475, 0.975	1.475, 1.475	-4.0	+4.0	2.17e-11	1.60e-11
22	1.475, 0.975	1.475, 1.475	-2.0	+4.0	-	-
23	1.475, 0.975	1.475, 1.475	0.0	+4.0	-	-
24	1.475, 0.975	1.475, 1.975	-4.0	+4.0	-	-
25	1.325, 1.475	1.725, 1.325	-4.0	0.0	9.71e-09	1.1e-08
26	1.325, 1.475	1.725, 1.325	-4.0	+4.0	-	-
27	1.325, 1.475	1.725, 1.325	0.0	-4.0	1.11e-08	1.10e-08
28	1.325, 1.475	1.725, 1.325	+4.0	-4.0	1.16e-08	1.10e-08
29	1.225, 1.725	2.025, 1.475	-4.0	0.0	-	-
30	1.225, 1.725	2.025, 1.475	-4.0	+4.0	-	-
31	1.225, 1.725	2.025, 1.475	0.0	-4.0	-	-
32	1.225, 1.725	2.025, 1.475	+4.0	-4.0	-	-
33	1.325, 1.075	1.725, 1.875	-4.0	0.0	-	-
34	1.325, 1.075	1.725, 1.875	-4.0	+4.0	-	-
35	1.325, 1.075	1.725, 1.875	0.0	-4.0	-	-
36	1.325, 1.075	1.725, 1.875	+4.0	-4.0	-	-

Tab. 4.1: Comparison between particle tracking effective permeabilities, k_{mod}, and cell averaged permeabilities, k_{calc}. -: pathlines do not represent straight lines

During this project field gas measurements were only conducted within a single lithological facies, which was assumed to extend into the outcrop for some distance, allowing it to be seen as an internally homogeneous unit. Under these conditions the estimation of effective permeabilities and hydraulic conductivities from field measurements can be achieved by applying analytical solutions for the gas tracer breakthrough curves.

5 Development of Field and Laboratory Equipment for Pneumatic Tests

In the past, most simulations of groundwater flow and transport in heterogeneous gravel and sand deposits were carried out on averaged or generated permeability fields. These permeabilities were often based on field or laboratory data such as pumping tests, tracer tests, flowmeter measurements, column experiments, or sieve analysis data. The pumping and tracer tests in the groundwater saturated subsurface result in an integration over usually larger volumes than the volume of a single hydraulically uniform (lithofacies) structure. Thus, they average over a scale larger than that of the heterogeneity and cannot resolve the complexity in the subsurface. Furthermore, flowmeter measurements, although very detailed in the vertical direction, are unable to resolve any lateral changes at a short distance from the well. The experiments in laboratory flow cells are often conducted on disturbed samples, which might have different permeabilities than undisturbed, layered samples.

Beside the need for better vertical and horizontal resolution of subsurface structures based on sedimentologically interpreted two- and three-dimensional outcrop data (Ch. 7) this section of the work describes a method to measure the hydraulic conductivities of specific lithofacies components in the outcrops indirectly by gas flow and tracer experiments *in situ* (undisturbed samples) and in laboratory columns (disturbed samples).

5.1 Concept

The overall concepts for the field and laboratory measurements are essentially the same. For the pneumatic tests (Δp-Q relation) a stepwise increase of air flow, Q, is compared with its corresponding change in pressure difference, Δp. For the tracer tests a gas tracer, CO_2, is injected so that the total flow of air, Q_{AIR} plus Q_{CO2}, remains constant, resulting in a pulse input of CO_2 at the injection point in the sample or outcrop (Fig. 5.1). The flow, Q, and pressure difference, Δp, over the sample or outcrop is kept constant for the time of a single experiment. At the extraction point of the sample or outcrop the concentration of CO_2 in the air, c_{CO2}, is measured, leading to breakthrough curves, which can be analysed as described in chapter 3.

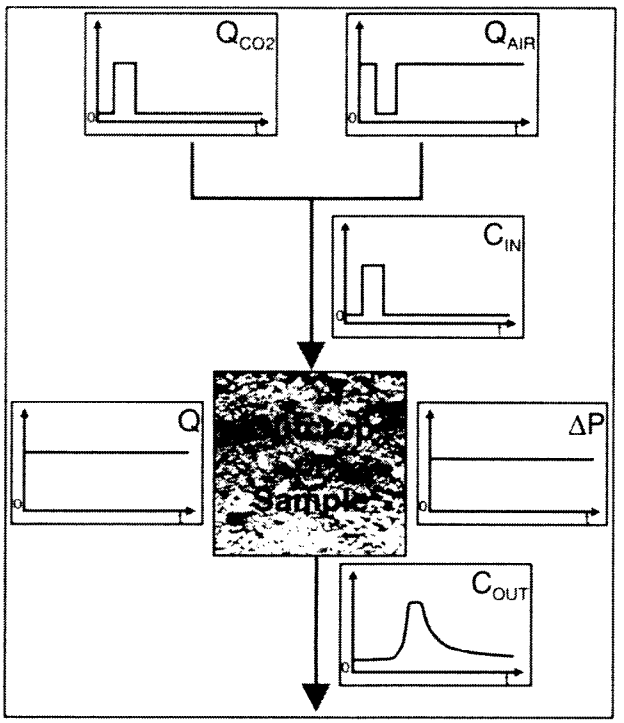

Fig. 5.1: General concept for field and laboratory pneumatic and tracer tests: controlled injection concentration, controlled flow and pressure difference, measured extraction concentration

In detail, the equipment comprises injection, extraction and control units in combination with the hardware to make measurements in the sample column or in a particular section of an outcrop.

The extraction is realised through suction by a vacuum pump. The volume extracted is much larger than the small volume of air and CO_2 injected. On the injection side a CO_2 gas-container, an air compressor and two mass flow controllers build a mixing cell. The overpressure, pressure over atmospheric, is measured by a pressure meter. The pressure difference between injection and extraction is measured with a pressure difference meter either over two separate connections to the column in the laboratory experiment or before injection (after extraction) into (from) the outcrop in the field experiments. The latter needs a correction of measured pressure differences as the pressure drop due to flow through the tubing and injection/extraction rods has to be considered (Ch. 6). The measured pressure difference controls a valve on the extraction side. The extracted mass flow of air is monitored by a mass flow meter. At the outlet of the vacuum pump the CO_2 concentration in the extracted air is detected online with an infrared detector. All measured data (injection mass flows

of CO_2 and air, overpressure, pressure difference, extraction mass flow and concentration of CO_2) is collected, controlled and saved on disk with LabVIEW® based control software (Fig. 5.2).

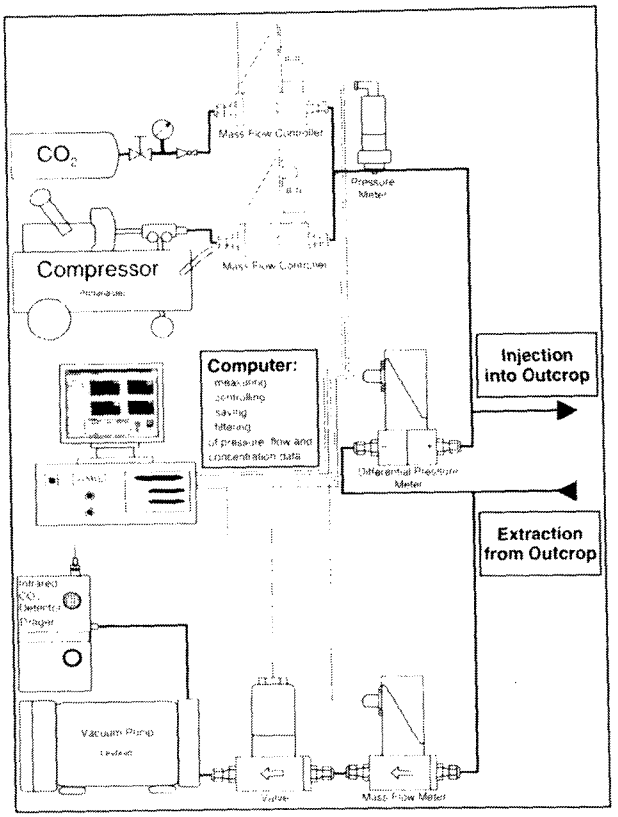

Fig. 5.2: Detailed measurement concept, here for the field pneumatic and tracer tests

In figures 5.3 and 5.4 the field setup is shown. The measurement equipment easily fits into a transit van.

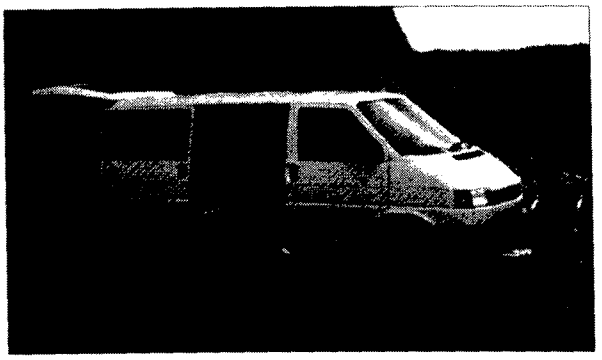

Fig. 5.3: Field setup

5.2 Hardware

5.2.1 Measurement Devices

A short description of the measurement devices used in the field or laboratory experiments is given in the following subsections. More detailed information on the measurement principles of the different sensors can be found in Hölz (1997) or in the corresponding supplier's information.

Fig. 5.4: Field setup: interior of the van, foreground: vacuum pump, flow and pressure control unit, PC with input and output boards, background: compressor

5.2.1.1 Source of Carrier and Tracer Gas

The carrier gas used for the pneumatic and tracer tests is compressed air, generated by an air compressor.

The tracer gas, CO_2, is taken from a 10 kg standard gas container, which is easily transportable to field sites.

5.2.1.2 Mass Flow Controller

The mass flow controllers (Bronkhorst F-201AC-FA-33-V, Bronkhorst F-201AC-FA-33-E) used to control the injected mass of air and CO_2, respectively, measure and compare the flow through the devices with the specified values given via the software and respond by opening or closing the connected valves to achieve the desired flow rate. In the flow sensors the flow is divided into a bypass and a laminar flow unit. The flow conditions in the laminar flow unit are proportional to the flow in the bypass unit. The bypass is heated: temperatures at the beginning and end of the bypass are controlled. The difference in temperature over the bypass is directly proportional to the mass flow as it depends on the number of molecules in the gas flow. It is amplified to an analogue output signal. Flow rates can be measured up to 30 standard l/min. The typical measurement accuracy is < 0.5 % of the maximal flow. For the CO_2 sensor a specific calibration is used. The integrated valve is a currentless closed proportional valve. The flow rates are recorded continuously. Data input and output to and from the computer occur via

analogue-digital (A/D) and digital-analogue (D/A) converter boards, respectively.

5.2.1.3 Overpressure Meter

The overpressure meter (Bronkhorst P-20-8400-270-004) measures the difference in pressure between the applied pressure and atmospheric pressure up to $600 \cdot 10^2$ Pa above atmospheric pressure. The measurement accuracy is 0.25 % of the maximal pressure. The sensor uses the piezoresistive effect, i.e. the characteristic of some materials to change its resistivity in response to a mechanical pressure. It can only be measured with an applied external voltage. Thus, the applied overpressure results in an analogue signal which is than transferred to the computer's A/D board.

5.2.1.4 Pressure Difference Controller

The pressure difference controller comprises a pressure difference meter directly connected to a control valve.

Similar to the overpressure meter, the pressure difference meter (Bronkhorst P-506C-FA-33-E) records the difference between two applied pressures up to a total pressure difference of $1000 \cdot 10^2$ Pa. The measurement accuracy is 0.5 % of the maximal pressure difference. The resulting analogue signal is transferred to the computer's A/D board and directly compared with the specified pressure value given via the computer's D/A board. Differences between measured and specified pressure differences result in an opening or closing of the extraction control valve to increase or lower the suction from the vacuum pump.

5.2.1.5 Mass Flow Meter

The mass flow meter (Hastings HFM-201) on the extraction side also measures the mass flow of air through the sensor. Flow rates can be measured up to 100 standard l/min. The typical measurement accuracy is 1 % of the maximal flow. The flow rate measured is continuously recorded via the computer's A/D board.

5.2.1.6 Control Valve

The control valve (Bronkhorst F-004AC-LU-33-E) as part of the pressure difference controller changes the pressure difference between injection and extraction points by reducing or increasing the suction from the vacuum pump, corresponding to the analogue signal given by the comparison of specified and measured pressure differences in the pressure difference meter. It is a proportional electromagnetic valve with a maximal flow rate of 60 standard l/min.

5.2.1.7 Vacuum Pump

The vacuum pump (Leybold Sogevac SV16) is a one-stage oil-sealed rotary slide pump. It can be used to evacuate up to $0.5 \cdot 10^2$ Pa. The maximal pumping rate is 14.5 m^3/h = 4.4 l/s. In the experiments the pump's suction, which creates the pumping rate, is reduced by the control valve, the mass flow meter and the extraction rod plus tubing.

5.2.1.8 Infrared Detector for Tracer Gas

The CO_2 concentrations in the extracted air are detected using an infrared detector (Dräger Multiwarn IR KAT CO_2-Ex). This mobile detector allows a simple and reliable online detection of the absolute concentrations of CO_2. The gas is extracted with an internal pump (pumping rate of about 4.4 to 5 ml/s) from the outlet of the vacuum pump into the measurement chamber. There the infrared absorption due to the number of CO_2 molecules present in the chamber results in a difference from a reference signal and thus in an analogue output voltage of 0 to 1 V, corresponding linearly to 0 to 5 Vol% CO_2. The signal is transferred to the computer's A/D board. Attempts to use the detector directly after the extraction rod and the tubing were not successful, since the pressure drop due to suction from the vacuum pump through the extraction system and the detector was too large to create a convergent flow field in the outcrop. For the evaluation of the measurements (Ch. 6) only the concentration of CO_2 relative to its maximum is used.

5.2.2 Field Equipment

Special equipment has been developed for the use in the field measurements.

Firstly, hollow metal rods were developed, having a rigidity and stiffness able of being driven horizontally into the target zones in the often highly compacted outcrop walls. The rods are driven and hammered using a small excavator and hydraulic hammer.

After the pneumatic or tracer experiment the rods have to be withdrawn from the outcrop without being damaged, for which purpose pulling equipment has been specially developed.

5.2.2.1 Hollow Metal Rods

The rods to inject air into and extract air from the outcrop comprise inner and outer hollow metal rods, which are only loosely connected (Fig. 5.5).

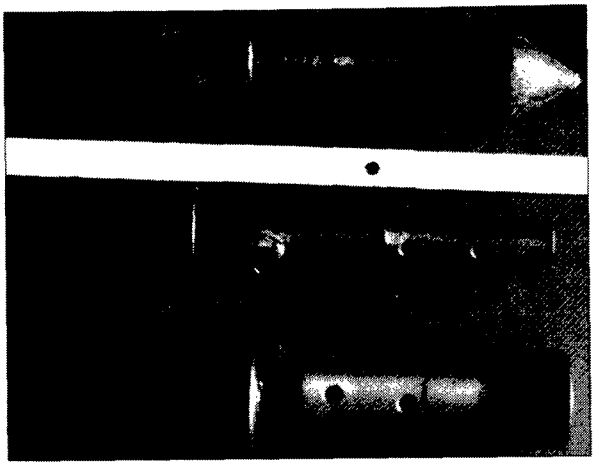

Fig. 5.5: Photograph of tip (top) and end (centre) of inner and outer hollow metal rods with outlet openings and connection for tubing after use in the field, withdrawal tools (bottom)

The outer hollow metal rod is driven into the wall, carrying with it the inner rod. To open the tip of the rod at the desired position the inner rod is pushed or hammered about 2 cm further into the wall, so that the tip of the rod is pushed out to expose the outlet openings. The connection for the tubing is then screwed into the inner rod and the testing for leaks or blocked openings can start. Similar to the development of a well, the openings of the rod have to be cleared with high air pressure and suction, so that the pressure drop over the rod and tubing reaches a minimum.

To prevent air leakage through the ring between the inner and outer rods, three well greased sealing rings of rubber are positioned on the outside of the inner rod.

After the measurements have been conducted the connection for the tubing has to be removed and the pulling equipment can be connected to the end of the rod. After withdrawal of the rods the openings and often the whole inner rod have to be cleaned and greased again to be prepared for the next injection.

The rods are made of standard, not specially hardened steel. In figure 5.6 a technical drawing with dimensions is given.

5.2.2.2 Pulling Equipment

While the insertion of the rods is not too difficult as long as the rods are stiff enough, the withdrawal is more complicated. A tool has been developed so that the hydraulic hammer in combination with the excavator is used to hammer the rods out of the wall.

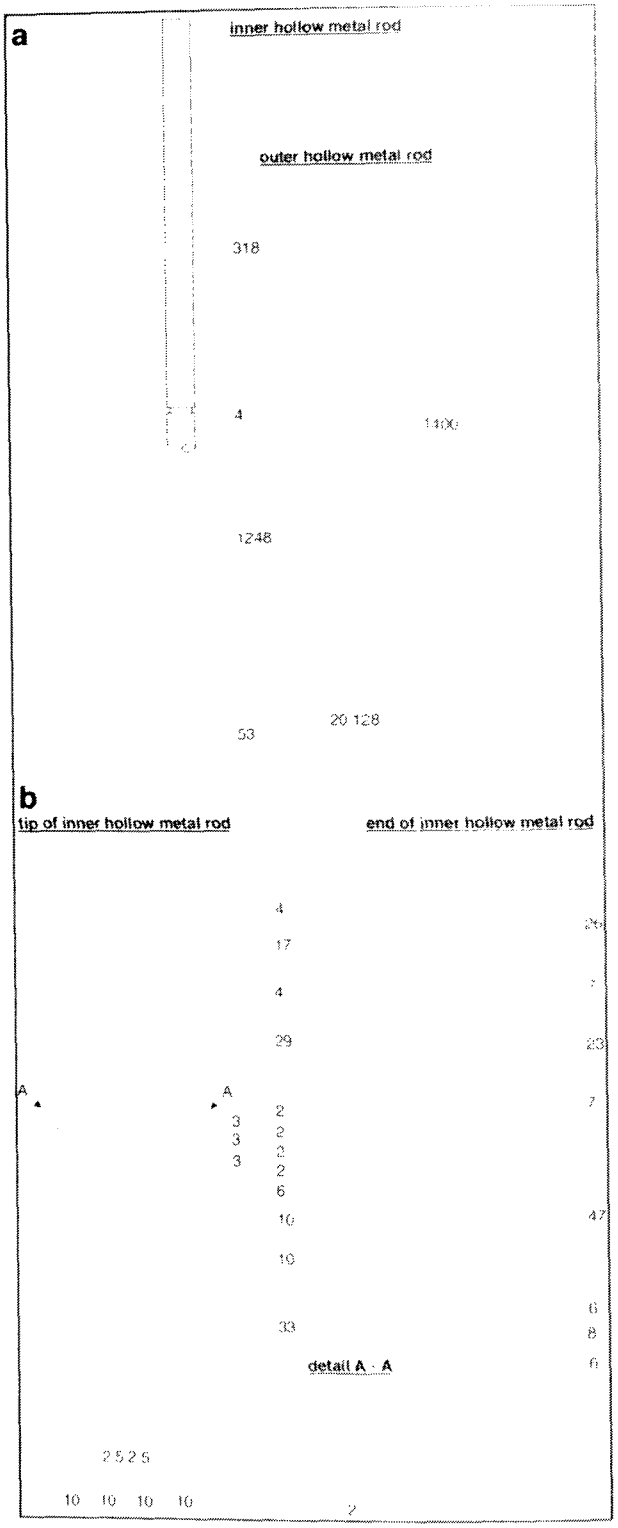

Fig. 5.6: Technical drawing of inner and outer hollow metal rods with dimensions in mm; a: overview, b: detailed tip and end of inner rod with dimensions in mm

To achieve this a small plate is connected on one side with an adapter and two split pins to the inner rod and on the other side to two metal slats. The slats again are connected with two split pins to a second stronger plate, which is mounted onto the hydraulic hammer (Fig. 5.7 and 5.8).

While the hydraulic hammer, driven by the excavator, is hammering in the reverse direction,

the inner rod is driven out of the outcrop wall, pulling the outer rod with it.

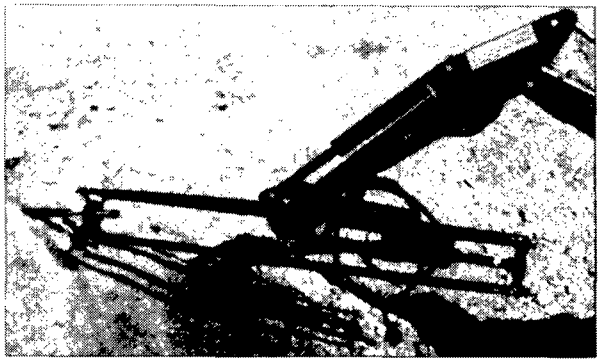

Fig. 5.7: Photograph of pulling equipment to withdraw hollow metal rods in the field

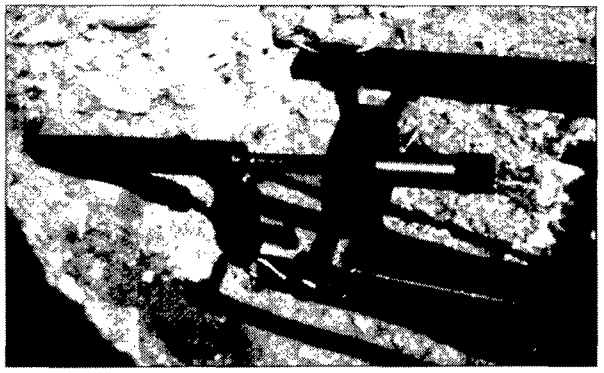

Fig. 5.8: Detailed photograph of pulling equipment to withdraw hollow metal rods in the field

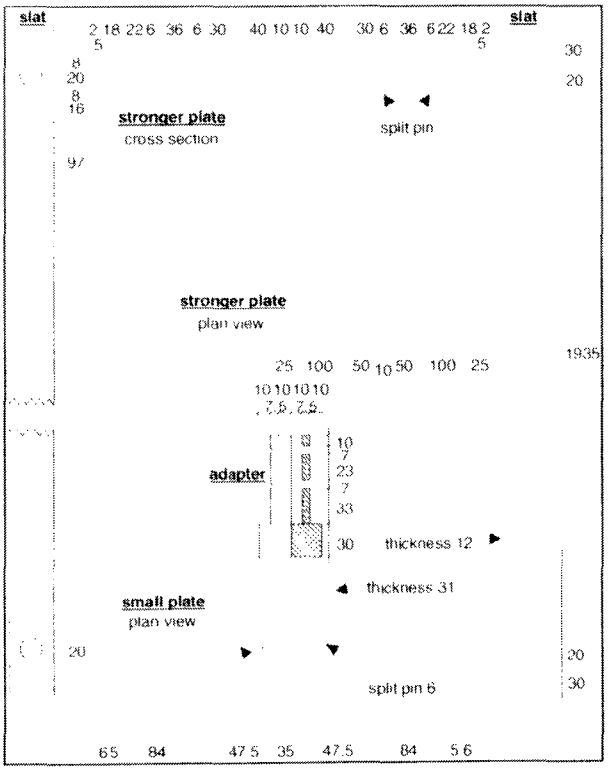

Fig. 5.9: Technical drawing of different parts of pulling equipment with dimensions in mm

A technical drawing with dimensions is given in figure 5.9.

5.2.2.3 Excavator

In the field a small excavator (O&K Orenstein & Koppel AG, RH1.15) is used in combination with the hydraulic hammer to drive in (withdraw) the rods into (out of) the outcrop (Fig. 5.10).

Before driving the rods into the wall the grading blade can be used to level out the working platform for the movement of the excavator and the backhoe collects the rubble at the foot of the outcrop.

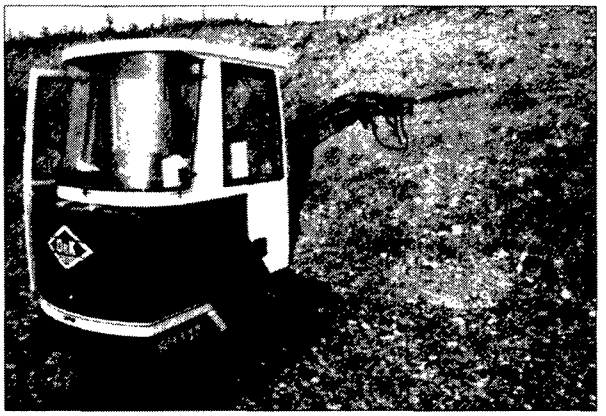

Fig. 5.10: Photograph of small excavator, driving hollow metal rods into outcrop wall

5.2.2.4 Hydraulic Hammer

The hydraulic hammer (Krupp HM 45) is used to insert or withdraw the rods. The specially hardened steel of the hammer tool has been bored open at the tip to fit in the end of the inner rod during insertion and the split pin of the larger plate during withdrawal (Fig. 5.11).

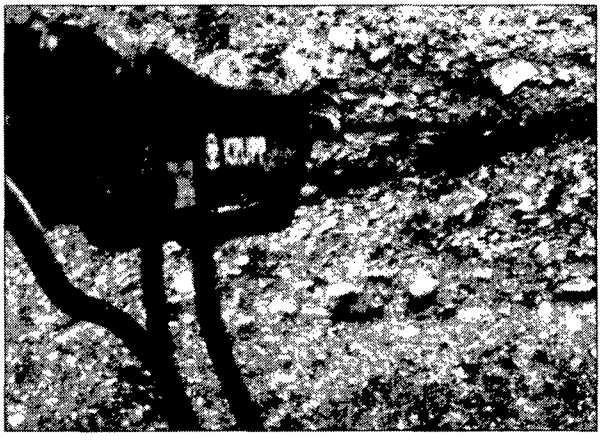

Fig. 5.11: Photograph of hammer, inserting hollow metal rods into outcrop wall

5.2.3 Laboratory Equipment

For the measurements in the laboratory a large cylindrical column was used. The inner diameter of the column is 0.19 m and its length is 0.76 m, resulting in a total volume of 0.0215 m^3 (Fig. 5.12).

Two separate connections are used to allow direct measurements of the pressure drop over the column.

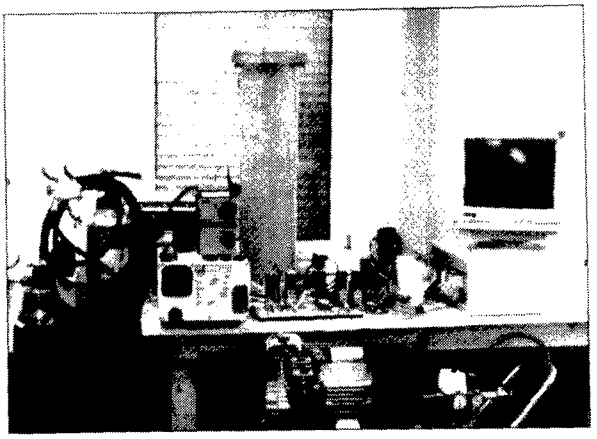

Fig. 5.12: Photograph of measurement equipment in the laboratory

5.3 Software

Software has been developed under LabVIEW® (National Instruments) to measure, control and save the data collected during the field and laboratory measurements. The different programs allow the data acquisition and display on the screen online during the experiments. All relevant parameters for the measurements can be changed by on-screen switches and control panels. At the same time all measured data is saved on disc in ASCII files for analysis (e.g. estimating tracer velocities and dispersivities from tracer tests with the program DTTRACER, plotting Δp-Q diagrams).

A short description of two programs is given in the following sections. Furthermore, automatic routines have been written to allow easy repetition of single measurements with different pressure differences. More details on the program structure and the basics of programming under LabVIEW® are given by Münch (1995) and Hölz (1997) or the LabVIEW® manuals from National Instruments.

5.3.1 Program for Tracer Tests

The GAS TRACER CONTROL PROGRAM has been developed for the tracer tests in the field and laboratory (Hölz, 1997). The front panel (Fig. 5.13), visual for the user on the screen after start-up, allows to control all relevant parameters for the measurements.

At the start the source code of the program is compiled and the program is set to run-mode. To start a particular measurement the ***program control*** panel has to be set to *start*, which initialises the internal clock and starts collecting data corresponding to the other setting parameters. At any instant it is possible to stop a running measurement with the *stop* button, which closes all open valves before leaving the run-mode. Initially in the ***injection*** panel a decision has to be made as to whether the tracer injection should be a *continuous* injection or *slug* injection over a specific *time interval*, which be specified. With the ***control*** panel it is possible to define the injected *total flow rate* (ml/s, compressed air and CO_2), which is kept constant during the time of the measurement, and the *CO_2 flow rate* (ml/s) for the time interval given in the injection panel. Furthermore, the overall *pressure difference* (mbar) has to be defined, with which the program should control the flow field. The last field is the ***data storage*** panel, instructs the program to *start* or *stop* saving the data of the running measurement to disk under a specified *path and filename*.

During a measurement the control data is send to the measurement and control devices (mass flow controllers and pressure difference controller) via the computers digital-analogue-converter board as an analogue voltage of 0 to 10 V (or 0 to 5 V, depending on the device). The comparison of the specified and measured values and the change of control voltage to open or close the respective valves occur in the electronic control units of each device.

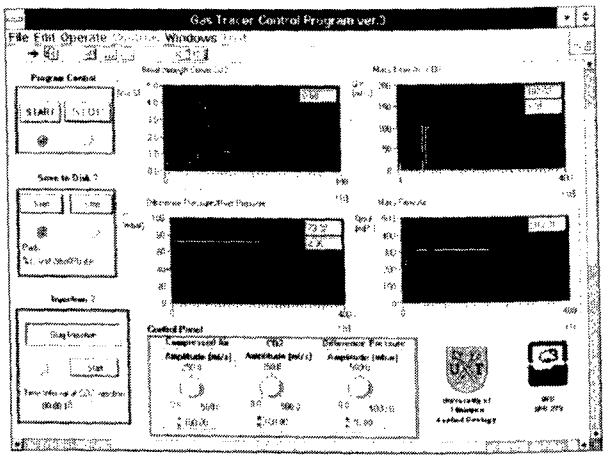

Fig. 5.13: Front panel of GAS TRACER CONTROL PROGRAM, developed under LabVIEW®, allowing the online control of measurement data in the field and laboratory

The actual measurements are the response to the current parameter setting due to the control panel parameters. They are collected as analogue signals and converted via the analogue-digital-converter board to digital signals. These are displayed and up-dated every second on the basis of an average of the data sampled at a 50 Hz sampling rate.

The display (Fig. 5.13) allows the online visual control of all measurements. On the right hand side the injection mass flows, $Q_{AIR}(t)$ and $Q_{CO2}(t)$,

(top) and the extraction mass flow, $Q_{OUT}(t)$, (bottom) are shown. The bottom left diagram displays the pressure difference, $\Delta p(t)$, and the overpressure, $p(t)-p_0$. In the remaining top left corner the current CO_2 breakthrough curve, $c_{CO2}(t)$, is given.

5.3.2 Program for Pneumatic Tests

Similarly a program has been written (Hölz, 1997) to measure the flow rate Q and the corresponding pressure difference Δp for the laboratory pneumatic tests. The flow rate is increased stepwise and the changing pressure differences are observed.

Before the start of the pneumatic measurements the two mass flow controllers on the injection side are both connected so that each measures a partial flow (one half) of the compressed air injected into the column. The addition of both mass flow readings results in the flow rate Q. The pressure difference Δp is measured with two separate connections to the column. The outlet of the column is left open to allow the direct outflow of air. Different Δp-Q data pairs are collected for each sample and saved to disc. They can be plotted to test the validity of Darcy's law and to evaluate the permeability of the sample (Ch. 6).

For the field measurements each Δp-Q pair is taken from the gas tracer data. After manual correction for the pressure drop due to rods and tubing, the corrected values are used to calculate the permeabilities for each measurement (Ch. 6).

6 Hydraulic Parameters - Measurements and Results

The hydraulic parameters for the different lithofacies types defined in chapter 2 were determined by various measurement methods in the field and in the laboratory. All measurement results are documented in the tables in annex 7. For those lithofacies, which could not be accessed with the equipment or sampled in the outcrops, the hydraulic parameters were taken to be equal to those of sedimentologically similar lithofacies, which could be measured (see Ch. 6.7).

The *in situ* (i.e from undisturbed samples) hydraulic conductivities for flow in horizontal and vertical directions were transferred from gas conductivities derived from field gas tracer and pneumatic tests. Similarly the hydraulic conductivities of disturbed samples were determined in the laboratory with gas tracer and pneumatic tests. For comparison the hydraulic conductivity of selected samples was measured in the laboratory directly with water (Darcy experiments) or by evaluating their grain size distribution curves. Furthermore the porosities of some disturbed samples were measured in the laboratory by weighing of specified volumes.

As a result of all measurements the 23 lithofacies types could be rearranged into 5 hydrofacies types, representing homogeneous, but not necessarily isotropic, hydraulic categories of different sedimentological origin. These hydrofacies units are characterised by horizontal and vertical hydraulic conductivities and porosities.

6.1 *In Situ* Field Gas Tests

In the field only gas tracer tests were conducted. For the gas pneumatic test evaluation the steady state data of the tracer tests is used.

The data collected in the field with the measurement equipment described in chapter 5 requires corrections of pressure differences, arrival times and concentrations.

Correction of Pressure Differences

The pressure difference is measured between two points situated before and after the measurement equipment. Thus it is a composition of the pressure differences resulting from the friction due to the injection flow through the tubing and one metal rod, the resistance of the outcrop material and the extraction flow through the other tubing and metal rod ($\Delta p_{tube\ flow}$ depends on Q, l). To determine the exact pressure difference over the outcrop material only, the two other pressure differences have to be quantified for various flow rates, Q, and length of tubing, l, such that

$$\Delta p = \Delta p_{meas} - \Delta p_{in}(Q_{in}, l) - \Delta p_{out}(Q_{out}, l) \qquad 6.1.$$

For both, injection and extraction, simple correction charts were determined in the laboratory. The pressure differences, Δp, were measured versus flow rates, Q, depending on the length of tubing, which varied from 1.0 to 5.0 m (Injection: Fig. 6.1, Extraction: Fig. 6.2).

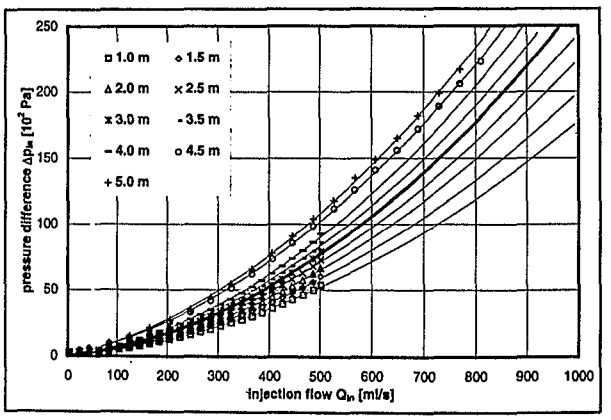

Fig. 6.1: Correction chart for pressure drop, Δp_{in}, due to injection of flow rate, Q_{in}, through metal rod and tubing, as a function of tube length

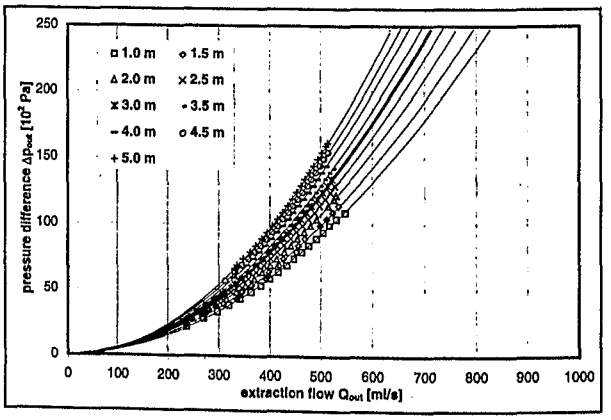

Fig. 6.2: Correction chart for pressure drop, Δp_{out}, due to extraction of flow rate, Q_{out}, through metal rod and tubing, as a function of tube length

For the field measurements the tubing had a length of 3.0 m, resulting in the following correction equations for Δp_{in} and Δp_{out} in terms of flow rates, Q_{in} and Q_{out}:

$$\Delta p_{in} = 0.0002 \cdot Q_{in}^2 + 0.0416 \cdot Q_{in} \qquad 6.2$$

$$\Delta p_{out} = 0.0005 \cdot Q_{out}^2 + 0.0027 \cdot Q_{out} \qquad 6.3.$$

Equation 6.2 and 6.3 are used in equation 6.1 to determine the exact pressure difference in the field measurements.

For some measurements the correction led to "negative" pressure differences, probably due to an overestimation of the pressure drop along the

tubing. In these cases instead of the "negative" pressure differences a minimal pressure difference of $0.1 \cdot 10^2$ Pa was assumed, leading to a lower boundary value (minimum value) for the permeabilities k and hence for the hydraulic conductivities K_f (s. Eq. 3.37 and 3.45).

Correction of Arrival Times

The measured travel times, t_{meas}, of the tracer concentration, c(t), are the sum of the travel times of the tracer through the injection (from the mass flow controllers to the tip of the injection rod), the geological medium and the extraction (from the tip of the extraction rod to the infrared detector). Thus, the actual time the tracer spends in the geological medium, t, is the measured time between injection through the mass flow controller and the detection in the infrared detector, t_{meas}, reduced by the time lag created by the apparatus, t_{app},

$$t = t_{meas} - t_{app} \qquad 6.4.$$

To determine the lag time, t_{app}, measurements without the geological medium (i.e. only apparatus, 2·3 m tubing, hollow metal rods directly connected to each other) were conducted. For the applied measured pressure differences the nearly rectangular shape of the injection pulse is represented by a slightly shifted, still nearly rectangular breakthrough curve (Fig. 6.3). The average shift of t_{app} = 7 s was used for the correction of all measured arrival times.

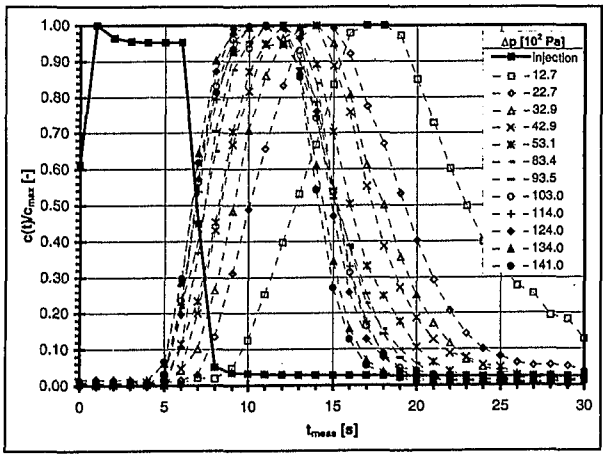

Fig. 6.3: Correction of measured arrival times: time, t_{meas}, versus relative concentration, $c(t)/c_{max}$, of breakthrough curves with the tubing only for different pressure differences compared to direct measurement of the injection pulse

Comparing the shape of the breakthrough curves with the shape of the curve of the injection pulse (Fig. 6.3) the dispersion caused by the possibly turbulent flow through the apparatus, the tubing or the rods is minimal, i.e. it could be neglected.

Correction of Concentrations

The measured concentrations of CO_2 are the result of the superposition of a background level (0.03 Vol.% in the atmosphere, approximately 0.13 Vol.% in the gravels and sands at the beginning of the measurements, slightly increasing with time) and the concentration change caused by the tracer. Therefore, the concentrations are firstly corrected by the background level at the beginning of each measurement, leading to the absolute measured concentration $c_{meas}(t)$.

For comparison with the calculated relative concentrations, the absolute concentrations are divided by the maximum concentration encountered during the specific measurement, leading to relative measured concentrations, $c_{meas}(t)/c_{max}$.

6.1.1 Tracer Tests

After the injection of the hollow metal rods, connecting up of tubing and apparatus, clean pumping of the rods (Ch. 5) the field measurements were conducted. In total 171 *in situ* tracer tests at 25 different locations in the outcrops of Friedingen and Böhringen were conducted. As described above the measured pressure differences and times were corrected to the pressure differences and time intervals over the geological media. The concentrations are converted into relative concentrations for comparison with the analytical solutions.

From the measured and fitted parameters the permeabilities (and hence the hydraulic conductivities) were calculated with equation 3.45.

An example of a measurement setup in a component-supported, planar, open framework gravel (Gcpo) is given in figure 6.4. Some of the corresponding measurement results are given as dotted (symbols) in figure 6.5. The best fit analytical solutions are shown as continuous lines.

A good fit with the analytical solutions could be achieved. The measurement and fitting parameters as well as the resulting hydraulic conductivities for the displayed three measurements are listed in tables A7.1 and A7.2 in annex 7. The hydraulic conductivities for these tracer measurements range from $3.26 \cdot 10^{-1}$ to $4.07 \cdot 10^{-1}$ m/s.

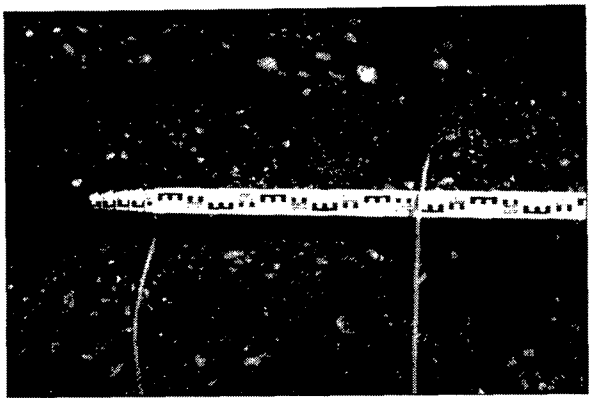

Fig. 6.4: *In situ* gas tracer tests in Gcpo in an outcrop at Friedingen, SW Germany; tubing and hollow metal rods in the outcrop

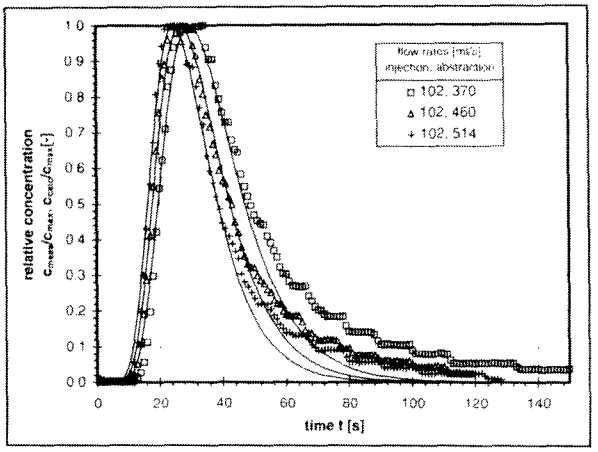

Fig. 6.5: Examples of results from *in situ* gas tracer tests in Gcpo in an outcrop at Friedingen, SW Germany, with corresponding abstraction and injection flow rates, dotted: measured breakthrough curves, continuous line: fitted analytical solutions

Another example of a measurement setup in a horizontal sand (Sh) is given in figure 6.6. Some of the corresponding measurement results are shown as dotted symbols in figure 6.7. The best fit analytical solutions - here only for the start of the breakthrough - are shown as continuous lines.

Here, the corrected pressure differences range from $28.70 \cdot 10^2$ to $45.38 \cdot 10^2$ Pa. The fitting of the tailing of the measured breakthrough curves is poor. This is believed to be due to the deviation of the tracer flow configuration from the assumed one-dimensional situation in the homogeneous sand. For almost all breakthrough curves the increase of the tracer concentration (tracer front) is well represented by the fitted analytical solutions. As a consequence the calculated permeabilities and hence hydraulic conductivities from the tracer tests, where only the start of the breakthrough curves could be fitted, represent an upper boundary value (maximum value). The measurement and fitting parameters as well as the resulting maximum hydraulic conductivities for the displayed three measurements are listed in tables A7.1 and A7.2 in annex 7. The hydraulic conductivities for these tracer measurements range from $7.74 \cdot 10^{-4}$ to $14.4 \cdot 10^{-4}$ m/s.

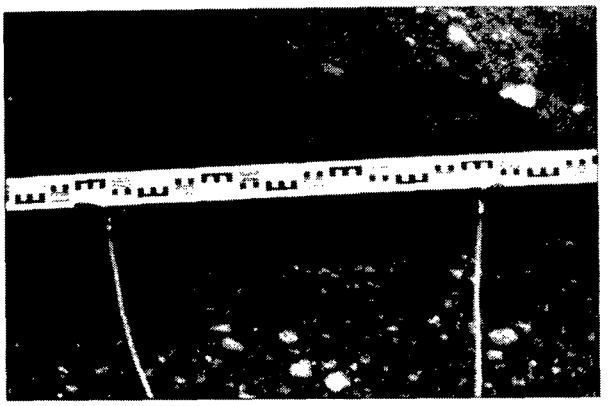

Fig. 6.6: *In situ* gas tracer tests in Sh in an outcrop at Böhringen, SW Germany, tubing and hollow metal rods in the outcrop

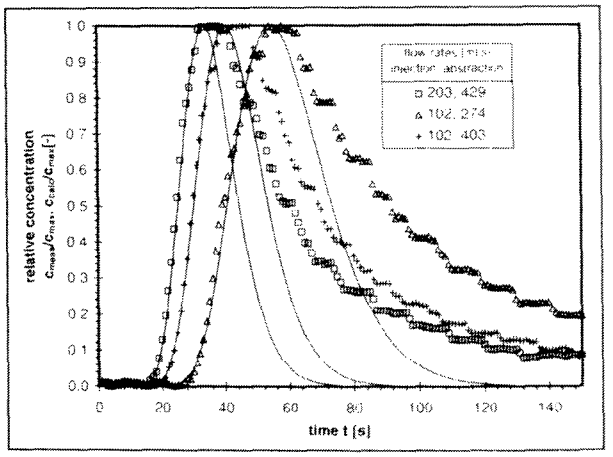

Fig. 6.7: Examples of results from *in situ* gas tracer tests in Sh in an outcrop at Böhringen, SW Germany, with corresponding abstraction and injection flow rates, dotted: measured breakthrough curves, continuous line: fitted analytical solutions

Overall horizontal hydraulic conductivities were estimated for nine different lithofacies encountered in the field. Vertical hydraulic conductivities were only estimated for three lithofacies types as the layers in the field were often too thin for two rods to be inserted (Tab. 6.1).

lithofacies	K_h [m/s]	K_v [m/s]
Gmpb	$1.16 \cdot 10^{-4}$	
Gcpo	$2.52 \cdot 10^{-4}$	
Gmh	$3.96 \cdot 10^{-4}$	$6.61 \cdot 10^{-5}$
Gmhb	$3.50 \cdot 10^{-4}$	
Gch	$4.61 \cdot 10^{-4}$	
Gcho	$2.97 \cdot 10^{-4}$	$1.39 \cdot 10^{-4}$
Gmm	$5.37 \cdot 10^{-4}$	
Gcm	$2.18 \cdot 10^{-4}$	$2.99 \cdot 10^{-5}$
Sh	$1.10 \cdot 10^{-4}$	

Tab. 6.1: Averaged horizontal and vertical hydraulic conductivities measured with gas tracer tests in the field for various lithofacies

6.1.2 Pneumatic Pumping Tests

The pneumatic measurements in the field are generally an offshoot of the tracer measurements. From the data files of the tracer measurements the pressure differences were corrected as described above and in combination with the abstraction and injection flow rates, Q_{in} and Q_{out}, the permeabilities (and hence the hydraulic conductivities) were calculated with equation 3.37.

The measurement parameters and results for all measurements are listed in tables A7.3 and A7.4 in annex 7. The averaged horizontal and vertical hydraulic conductivities for some lithofacies types are listed in table 6.2.

lithofacies	K_h [m/s]	K_v [m/s]
Gmpb	$3.85 \cdot 10^{-5}$	
Gcpo	$2.96 \cdot 10^{-2}$	
Gmh	$1.62 \cdot 10^{-4}$	$2.86 \cdot 10^{-4}$
Gmhb	$2.27 \cdot 10^{-4}$	
Gch	$2.63 \cdot 10^{-3}$	
Gcho	$3.07 \cdot 10^{-2}$	$2.82 \cdot 10^{-2}$
Gmm	$1.00 \cdot 10^{-4}$	
Gcm	$2.23 \cdot 10^{-3}$	$3.54 \cdot 10^{-4}$
Sh	$1.04 \cdot 10^{-4}$	

Tab. 6.2: Averaged horizontal and vertical hydraulic conductivities measured with gas pneumatic tests in the field for various lithofacies

6.1.3 Comparison between *In Situ* Tracer and Pneumatic Pumping Tests

To compare both sets of results, the hydraulic conductivities based on tracer and pneumatic tests of all measurements are plotted on a log-log scale (Fig. 6.8).

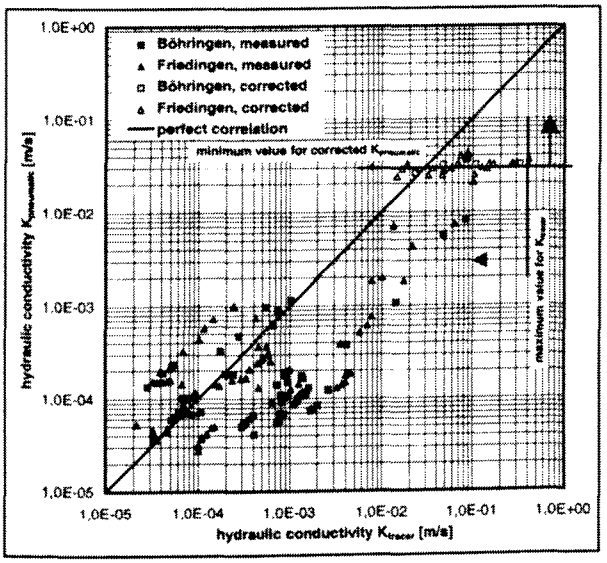

Fig. 6.8: Comparison of results from all field gas tracer and pneumatic tests

The comparison of the measured values with the expected perfect correlation shows that only the general trend of low and high conductivities could be recognised in both sets of results - values deviate sometimes by more than an order of magnitude.

The deviation can be best explained by the problems encountered with the pressure difference measurements, i.e. its correction and impact on the calculation of the permeabilities, which, for the corrected measurements, results in calculated minimum values for the hydraulic conductivity ($K_{pneumatic}$, Fig. 6.8). Furthermore the deviation of parts of the flow field from the assumed one-dimensional tracer flow conditions may be responsible for some of the differences, as it results in calculated maximum values for the hydraulic conductivities (K_{tracer}, Fig. 6.8).

6.2 Laboratory Gas Tests

In the case of the laboratory measurements the pressure differences were measured with a separate connection to the measurement column. Therefore the correction due to a pressure drop along the flow line (tubing) was not necessary in the laboratory.

In the same way the correction for the measured times could be omitted. The time, t_{app}, the tracer spends in the apparatus and in the tubing can be neglected in comparison to the time in the column filled with sample material.

The measured concentrations were again divided by the maximum concentration to yield relative concentrations which can be compared with the relative concentrations calculated with the analytical solution.

The column experiments were conducted as described in chapter 5.2.3 with the exception of a different column for the measurements of the open framework gravel. Only in a column with an inner diameter of 0.1 m and a length of 2.09 m (total volume of 0.0164 m^3) could pressure differences be measured for the highly conductive materials.

The samples used originated from the same outcrops in Friedingen and Böhringen, as those in which the *in situ* measurements took place.

6.2.1 Tracer Tests

With the measured and fitted parameters of the laboratory tracer tests the permeabilities (and hence the hydraulic conductivities) were calculated using equation 3.42.

Hydraulic conductivities were estimated as an average of measurements with varying pressure differences for five lithofacies (Tab. 6.3).

lithofacies	K_{tracer} [m/s]	$K_{pneumatic}$ [m/s]
Gmpb	$5.13 \cdot 10^{-4}$	$5.36 \cdot 10^{-4}$
Gcpo	$2.92 \cdot 10^{-1}$	$2.55 \cdot 10^{-1}$
Gmt	$9.68 \cdot 10^{-3}$	$4.64 \cdot 10^{-3}$
Sp	$9.57 \cdot 10^{-4}$	$1.11 \cdot 10^{-3}$
St	$3.14 \cdot 10^{-4}$	$4.85 \cdot 10^{-4}$

Tab. 6.3: Averaged hydraulic conductivities measured with gas tracer and pneumatic tests in the laboratory for different lithofacies

6.2.2 Pneumatic Pumping Tests

The pneumatic tests were conducted for the samples used in the tracer measurements with the software described in chapter 5.3.2. For a stepwise increasing flow rate, Q, the pressure difference was monitored and - after a steady state was reached - saved in the data file. Plotting the measured flow rate versus the pressure differences (Q-Δp plot, Fig. 6.9) led to a straight line relation ship, whose gradient was used in the determination of the permeabilities (and hence the hydraulic conductivities) in equation 3.34.

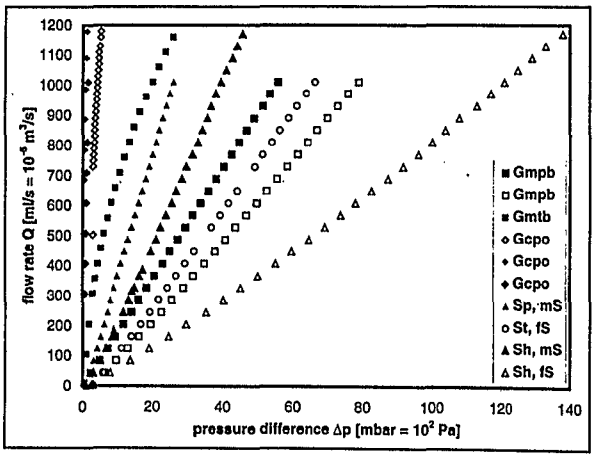

Fig. 6.9: Results from laboratory gas pneumatic tests

The linearity of the plots shows - in contrast to the measurements of Ruiz-Rodriguez (1994) and Kretzer (1989) - that Darcy's equation is valid and turbulence does not need to be taken into account for these measurements (s. Ch. 3.1.2.1). In this way it was possible to estimate the hydraulic conductivities for five different lithofacies (Tab. 6.3).

6.2.3 Comparison between Laboratory Tracer and Pneumatic Pumping Tests

To compare both sets of results, the hydraulic conductivities based on the single tracer and pneumatic tests are plotted on log-log scale (Fig. 6.10). Only minor differences between pneumatic and tracer measurements can be observed. In comparison to the field measurements (Fig. 6.8) the laboratory results are more reliable, due to the more accurate technique for the measurement of the pressure differences in the laboratory and the simplicity of the flow field.

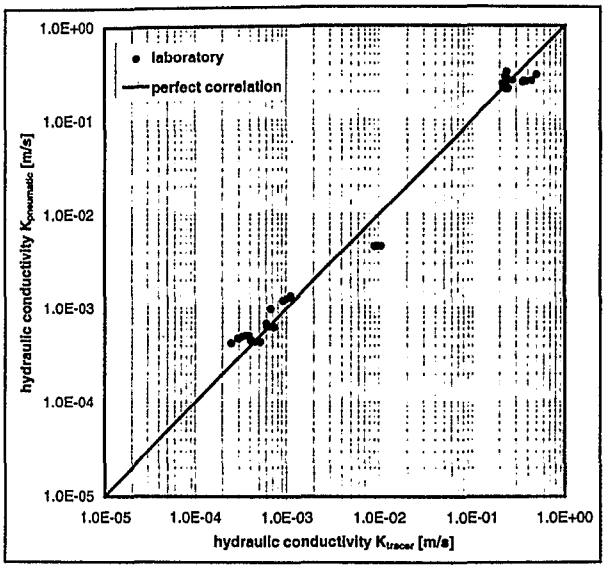

Fig. 6.10: Comparison of results from all laboratory gas tracer and pneumatic tests

6.3 Laboratory Water Tests (Darcy Experiments)

For three of the samples used in the gas tracer and pneumatic measurements, tests with water in a flow cell, i.e. constant head permeameter experiments, were conducted. The technique used for this laboratory water tests is described in Kleineidam (1998). The averaged results from various repeated measurements are listed in table 6.4.

lithofacies	K_{water} [m/s]	K_{sieve} [m/s]
Gmpb	$1.15 \cdot 10^{-4}$	$5.47 \cdot 10^{-4}$
Gcpo	$9.77 \cdot 10^{-2}$	$2.14 \cdot 10^{-1}$
Gmt		$6.29 \cdot 10^{-4}$
Gctb		$2.12 \cdot 10^{-3}$
Gcto		$9.78 \cdot 10^{-2}$
Gmm		$3.93 \cdot 10^{-4}$
Sp	$6.14 \cdot 10^{-4}$	$1.47 \cdot 10^{-3}$
St		$4.82 \cdot 10^{-4}$
Sm		$1.44 \cdot 10^{-4}$

Tab. 6.4: Averaged hydraulic conductivities measured with water (permeameter experiments) in the laboratory, K_{water}, and calculated on the basis of sieve analysis data (after Beyer, 1964) for different lithofacies, K_{sieve}

6.3.1 Comparison between Laboratory Gas and Water Tests

Generally the values from laboratory water tests are smaller than those from the gas tests. The factor between water and gas hydraulic conductivities varies from 4.66 for Gmpb to 2.99 for Gcpo and 1.81 for Sp (s. Tab. 6.3 and 6.4). Although only three samples could be compared this is a good agreement taking into account the different measurement setups: the different columns, the repacking of the samples and the

different techniques for the measurement of the pressure differences (digital pressure difference meter and manual constant head permeameter, respectively) with their corresponding measurement errors.

6.4 Evaluation of Sieve Analysis Data

The grain size distribution of most of the samples used in the laboratory was estimated by sieving in accordance with the German standard (DIN 4188). The resulting grain size distribution curves are plotted in figure 6.11.

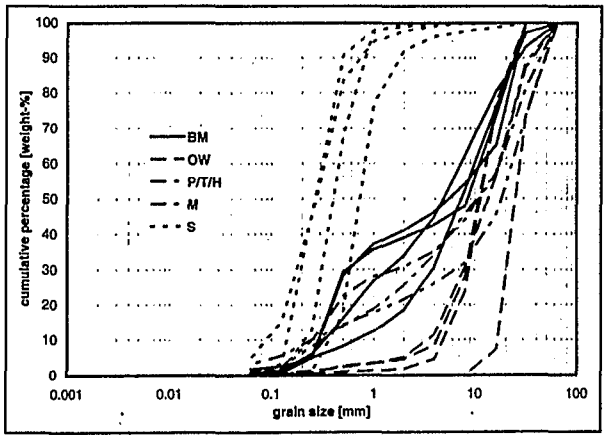

Fig. 6.11: Grain size distribution curves for different lithofacies (here combined to hydrofacies, s. Ch. 7)

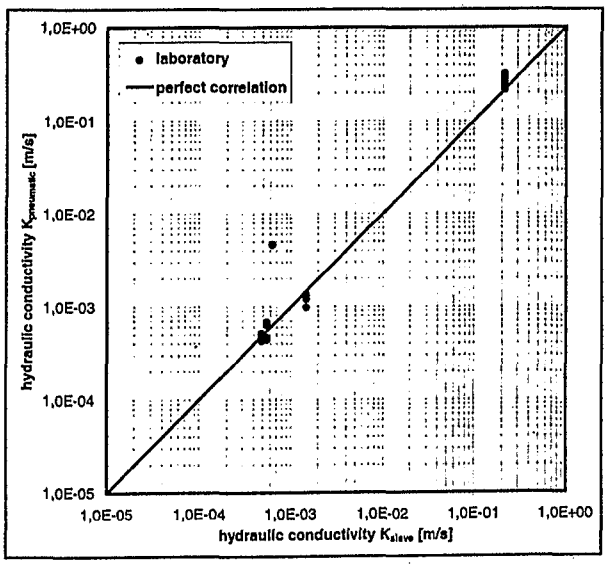

Fig. 6.12: Comparison of results from laboratory gas pneumatic tests and sieve analysis data

The hydraulic conductivities were estimated for each sample after the method of Beyer (1964). This is based on the rule of Hazen (1893) with an adjustment for different unconformity coefficients, U. It is strictly only valid for an effective grain size, $d_{10} < 0.6$ mm, and an unconformity coefficient, $U = d_{60}/d_{10} < 20$.

The results, listed in table 6.4, show generally a good agreement with the results of the laboratory gas tracer and pneumatic tests on the same samples (Tab. 6.3). In figure 6.12 the generally good correlation with the laboratory pneumatic measurements is shown. Even for the open framework gravels, which do not lie in the range of grain sizes for which Beyer's rule is approved, the data is in good agreement.

6.5 Porosity Measurements

For some of the disturbed samples in the laboratory, porosity measurements were performed by measuring the weight of a specified volume of the sample and calculating the porosity with the assumption of a constant grain density of 2.7 kg/m^3 (Tab. 6.5).

lithofacies	n [-]
Gmpb	0.30
Gcpo	0.36
Gmt	0.27
Sp	0.42
St	0.45

Tab. 6.5: Porosities, n, for different lithofacies

6.6 Comparison of All Measurements

6.6.1 Data Measured During this Project

Combining all measurement results from *in situ* and laboratory measurements for hydraulic conductivities and porosities (Tab. 6.6) it can be seen that measured hydraulic parameters are only available for a few lithofacies types. This is mainly due to the inaccessibility of the other lithofacies in the outcrops visited during this project. For none of the measurement techniques a full data set could be collected. On the basis of the sedimentological field interpretations during the project (i.e. the similarity of the depositional process of different lithofacies types and their grain sizes) and the above described hydraulic parameter estimations, hydraulic conductivity and porosity values were assigned to those lithofacies which could not be measured directly. In table 6.6 the bold values represent directly measured parameters, whereas the other values are assigned parameters.

	field				laboratory		water	sieve	porosity
	tracer		pneumatic		tracer	pneumatic			
lithofacies	K_h [m/s]	K_v [m/s]	K_h [m/s]	K_v [m/s]	K [m/s]	K [m/s]	K [m/s]	K [m/s]	n [-]
Gmp	$3.96 \cdot 10^{-03}$	$6.61 \cdot 10^{-05}$	$1.62 \cdot 10^{-04}$	$2.86 \cdot 10^{-04}$	$9.68 \cdot 10^{-03}$	$4.64 \cdot 10^{-03}$	$6.29 \cdot 10^{-04}$	$1.15 \cdot 10^{-04}$	0.27
Gmpb	$\mathbf{1.16 \cdot 10^{-04}}$	$1.16 \cdot 10^{-04}$	$\mathbf{3.85 \cdot 10^{-05}}$	$3.85 \cdot 10^{-05}$	$\mathbf{5.13 \cdot 10^{-04}}$	$\mathbf{5.36 \cdot 10^{-04}}$	$\mathbf{1.33 \cdot 10^{-03}}$	$\mathbf{1.15 \cdot 10^{-04}}$	**0.30**
Gcp	$3.96 \cdot 10^{-03}$	$6.61 \cdot 10^{-05}$	$1.62 \cdot 10^{-04}$	$2.86 \cdot 10^{-04}$	$9.68 \cdot 10^{-03}$	$4.64 \cdot 10^{-03}$	$6.29 \cdot 10^{-04}$	$1.15 \cdot 10^{-04}$	0.27
Gcpb	$1.16 \cdot 10^{-04}$	$1.16 \cdot 10^{-04}$	$3.85 \cdot 10^{-05}$	$3.85 \cdot 10^{-05}$	$5.13 \cdot 10^{-04}$	$5.36 \cdot 10^{-04}$	$1.33 \cdot 10^{-03}$	$1.15 \cdot 10^{-04}$	0.30
Gcpo	$\mathbf{2.52 \cdot 10^{-01}}$	$2.52 \cdot 10^{-01}$	$\mathbf{2.96 \cdot 10^{-02}}$	$2.96 \cdot 10^{-02}$	$\mathbf{2.92 \cdot 10^{-01}}$	$\mathbf{2.55 \cdot 10^{-01}}$	$\mathbf{8.93 \cdot 10^{-01}}$	$\mathbf{9.77 \cdot 10^{-02}}$	**0.36**
Gmt	$3.96 \cdot 10^{-03}$	$6.61 \cdot 10^{-05}$	$1.62 \cdot 10^{-04}$	$2.86 \cdot 10^{-04}$	$\mathbf{9.68 \cdot 10^{-03}}$	$\mathbf{4.64 \cdot 10^{-03}}$	$\mathbf{6.29 \cdot 10^{-04}}$	$1.15 \cdot 10^{-04}$	**0.27**
Gmtb	$1.16 \cdot 10^{-04}$	$1.16 \cdot 10^{-04}$	$3.85 \cdot 10^{-05}$	$3.85 \cdot 10^{-05}$	$5.13 \cdot 10^{-04}$	$5.36 \cdot 10^{-04}$	$1.33 \cdot 10^{-03}$	$1.15 \cdot 10^{-04}$	0.30
Gct	$3.96 \cdot 10^{-03}$	$6.61 \cdot 10^{-05}$	$1.62 \cdot 10^{-04}$	$2.86 \cdot 10^{-04}$	$9.68 \cdot 10^{-03}$	$4.64 \cdot 10^{-03}$	$6.29 \cdot 10^{-04}$	$1.15 \cdot 10^{-04}$	0.27
Gctb	$1.16 \cdot 10^{-04}$	$1.16 \cdot 10^{-04}$	$3.85 \cdot 10^{-05}$	$3.85 \cdot 10^{-05}$	$5.13 \cdot 10^{-04}$	$5.36 \cdot 10^{-04}$	$\mathbf{1.33 \cdot 10^{-03}}$	$1.15 \cdot 10^{-04}$	0.30
Gcto	$2.52 \cdot 10^{-01}$	$2.52 \cdot 10^{-01}$	$2.96 \cdot 10^{-02}$	$2.96 \cdot 10^{-02}$	$2.92 \cdot 10^{-01}$	$2.55 \cdot 10^{-01}$	$\mathbf{8.93 \cdot 10^{-01}}$	$9.77 \cdot 10^{-02}$	0.36
Gmh	$\mathbf{3.96 \cdot 10^{-03}}$	$\mathbf{6.61 \cdot 10^{-05}}$	$\mathbf{1.62 \cdot 10^{-04}}$	$\mathbf{2.86 \cdot 10^{-04}}$	$9.68 \cdot 10^{-03}$	$4.64 \cdot 10^{-03}$	$6.29 \cdot 10^{-04}$	$1.15 \cdot 10^{-04}$	0.27
Gmhb	$\mathbf{3.50 \cdot 10^{-04}}$	$3.50 \cdot 10^{-04}$	$\mathbf{2.27 \cdot 10^{-04}}$	$2.27 \cdot 10^{-04}$	$5.13 \cdot 10^{-04}$	$5.36 \cdot 10^{-04}$	$1.33 \cdot 10^{-03}$	$1.15 \cdot 10^{-04}$	0.30
Gch	$\mathbf{4.61 \cdot 10^{-03}}$	$6.61 \cdot 10^{-05}$	$\mathbf{2.63 \cdot 10^{-03}}$	$2.86 \cdot 10^{-04}$	$9.68 \cdot 10^{-03}$	$4.64 \cdot 10^{-03}$	$6.29 \cdot 10^{-04}$	$1.15 \cdot 10^{-04}$	0.27
Gchb	$3.50 \cdot 10^{-04}$	$3.50 \cdot 10^{-04}$	$2.27 \cdot 10^{-04}$	$2.27 \cdot 10^{-04}$	$5.13 \cdot 10^{-04}$	$5.36 \cdot 10^{-04}$	$1.33 \cdot 10^{-03}$	$1.15 \cdot 10^{-04}$	0.30
Gcho	$\mathbf{2.97 \cdot 10^{-01}}$	$\mathbf{1.39 \cdot 10^{-01}}$	$\mathbf{3.07 \cdot 10^{-02}}$	$\mathbf{2.82 \cdot 10^{-02}}$	$2.92 \cdot 10^{-01}$	$2.55 \cdot 10^{-01}$	$8.93 \cdot 10^{-01}$	$9.77 \cdot 10^{-02}$	0.36
Gmm	$\mathbf{5.37 \cdot 10^{-04}}$	$5.37 \cdot 10^{-04}$	$\mathbf{1.00 \cdot 10^{-04}}$	$1.00 \cdot 10^{-04}$	$9.68 \cdot 10^{-03}$	$4.64 \cdot 10^{-03}$	$\mathbf{6.29 \cdot 10^{-04}}$	$1.15 \cdot 10^{-04}$	0.27
Gcm	$\mathbf{2.18 \cdot 10^{-02}}$	$\mathbf{2.99 \cdot 10^{-04}}$	$\mathbf{2.23 \cdot 10^{-03}}$	$\mathbf{3.54 \cdot 10^{-04}}$	$9.68 \cdot 10^{-03}$	$4.64 \cdot 10^{-03}$	$6.29 \cdot 10^{-04}$	$1.15 \cdot 10^{-04}$	0.27
Gg	$2.52 \cdot 10^{-01}$	$2.52 \cdot 10^{-01}$	$2.96 \cdot 10^{-02}$	$2.96 \cdot 10^{-02}$	$2.92 \cdot 10^{-01}$	$2.55 \cdot 10^{-01}$	$8.93 \cdot 10^{-01}$	$9.77 \cdot 10^{-02}$	0.36
Sp	$1.10 \cdot 10^{-03}$	$1.10 \cdot 10^{-03}$	$1.04 \cdot 10^{-04}$	$1.04 \cdot 10^{-04}$	$\mathbf{9.57 \cdot 10^{-04}}$	$\mathbf{1.11 \cdot 10^{-03}}$	$\mathbf{5.61 \cdot 10^{-04}}$	$\mathbf{6.14 \cdot 10^{-04}}$	**0.42**
St	$1.10 \cdot 10^{-03}$	$1.10 \cdot 10^{-03}$	$1.04 \cdot 10^{-04}$	$1.04 \cdot 10^{-04}$	$\mathbf{3.14 \cdot 10^{-04}}$	$\mathbf{4.85 \cdot 10^{-04}}$	$\mathbf{5.61 \cdot 10^{-04}}$	$6.14 \cdot 10^{-04}$	**0.45**
Sh	$\mathbf{1.10 \cdot 10^{-03}}$	$1.10 \cdot 10^{-03}$	$\mathbf{1.04 \cdot 10^{-04}}$	$1.04 \cdot 10^{-04}$	$9.57 \cdot 10^{-04}$	$1.11 \cdot 10^{-03}$	$5.61 \cdot 10^{-04}$	$6.14 \cdot 10^{-04}$	0.42
Sm	$1.10 \cdot 10^{-03}$	$1.10 \cdot 10^{-03}$	$1.04 \cdot 10^{-04}$	$1.04 \cdot 10^{-04}$	$9.57 \cdot 10^{-04}$	$1.11 \cdot 10^{-03}$	$\mathbf{5.61 \cdot 10^{-04}}$	$6.14 \cdot 10^{-04}$	0.42
Sg	$1.10 \cdot 10^{-03}$	$1.10 \cdot 10^{-03}$	$1.04 \cdot 10^{-04}$	$1.04 \cdot 10^{-04}$	$9.57 \cdot 10^{-04}$	$1.11 \cdot 10^{-03}$	$5.61 \cdot 10^{-04}$	$6.14 \cdot 10^{-04}$	0.42

Tab. 6.6: Comparison of all measured and assigned data (*in situ* and laboratory) for all lithofacies types, bold: measured, standard: assigned

lithofacies	hydrofacies	K_h [m/s]	K_v [m/s]	n [-]
Gmp	P/T/H	$3.96 \cdot 10^{-3}$	$6.61 \cdot 10^{-5}$	0.27
Gmpb	BM	$1.16 \cdot 10^{-4}$	$1.16 \cdot 10^{-4}$	0.30
Gcp	P/T/H	$3.96 \cdot 10^{-3}$	$6.61 \cdot 10^{-5}$	0.27
Gcpb	BM	$1.16 \cdot 10^{-4}$	$1.16 \cdot 10^{-4}$	0.30
Gcpo	OW	$2.52 \cdot 10^{-1}$	$1.39 \cdot 10^{-1}$	0.36
Gmt	P/T/H	$3.96 \cdot 10^{-3}$	$6.61 \cdot 10^{-5}$	0.27
Gmtb	BM	$1.16 \cdot 10^{-4}$	$1.16 \cdot 10^{-4}$	0.30
Gct	P/T/H	$3.96 \cdot 10^{-3}$	$6.61 \cdot 10^{-5}$	0.27
Gctb	BM	$1.16 \cdot 10^{-4}$	$1.16 \cdot 10^{-4}$	0.30
Gcto	OW	$2.52 \cdot 10^{-1}$	$1.39 \cdot 10^{-1}$	0.36
Gmh	P/T/H	$3.96 \cdot 10^{-3}$	$6.61 \cdot 10^{-5}$	0.27
Gmhb	BM	$1.16 \cdot 10^{-4}$	$1.16 \cdot 10^{-4}$	0.30
Gch	P/T/H	$3.96 \cdot 10^{-3}$	$6.61 \cdot 10^{-5}$	0.27
Gchb	BM	$1.16 \cdot 10^{-4}$	$1.16 \cdot 10^{-4}$	0.30
Gcho	OW	$2.52 \cdot 10^{-1}$	$1.39 \cdot 10^{-1}$	0.36
Gmm	M	$5.37 \cdot 10^{-4}$	$2.99 \cdot 10^{-4}$	0.27
Gcm	M	$5.37 \cdot 10^{-4}$	$2.99 \cdot 10^{-4}$	0.27
Gg	OW	$2.52 \cdot 10^{-1}$	$1.39 \cdot 10^{-1}$	0.36
Sp	S	$1.10 \cdot 10^{-3}$	$1.10 \cdot 10^{-3}$	0.42
St	S	$1.10 \cdot 10^{-3}$	$1.10 \cdot 10^{-3}$	0.42
Sh	S	$1.10 \cdot 10^{-3}$	$1.10 \cdot 10^{-3}$	0.42
Sm	S	$1.10 \cdot 10^{-3}$	$1.10 \cdot 10^{-3}$	0.42
Sg	S	$1.10 \cdot 10^{-3}$	$1.10 \cdot 10^{-3}$	0.42

Tab. 6.7: Final parameter table for all lithofacies and corresponding hydrofacies categories, based on the comparison of values in Tab. 6.6, parameters will be used in the outcrop analysis studies (Ch. 7) and in the modelling (Ch. 8)

From table 6.6 the data judged to be the most reliable has been chosen for horizontal and vertical hydraulic conductivities and porosities (Tab. 6.7). Most of the field pneumatic test data was discarded in favour of the hydraulic conductivities derived from the field gas tracer tests, since the latter mostly compare well with the laboratory gas tracer and pneumatic tests and the sieve analysis data. In the process of translating lithofacies into hydrofacies it was necessary to define unique values for each hydrofacies type. Therefore the hydraulic conductivities of some lithofacies types (Gmhb, Gch, Gchb, Gcho and Gcm) were assigned the measured values of Gmpb, Gmh, Gmpb, Gcpo, Gmm, respectively.

This data is used as a standard data set for all lithofacies types encountered in any of the outcrop analysis studies (Ch. 7) and for the simulation of groundwater flow and transport (Ch. 8). Thus, it forms the fundamental parameter set for further application.

6.6.2 Data from Literature

The fundamental data set from table 6.7 is compared with hydraulic conductivities estimated in a similar sedimentary environment at Hüntwangen, Switzerland (Tab. 2.7, Jussel, 1992) by transferring the classifications used there to those used in this project, leading to figure 6.13. Generally the trend is similar. However, since during this project it was possible to measure the permeabilities in different directions, specific differences can be seen. Often the horizonal hydraulic conductivity is larger than the vertical (Tab. 6.7) as a result of the layering found in the sediments.

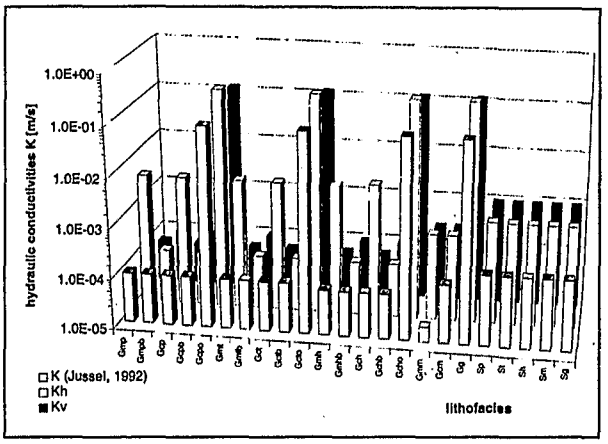

Fig. 6.13: Comparison of hydraulic conductivities for all lithofacies categories with model parameters used by Jussel (1992)

6.7 Lithofacies to Hydrofacies Relationship

The analysis of all measurements led to the conclusion that for the hydrogeological purposes of this project the wide variety of lithofacies used in the sedimentology can be adequately represented by five different facies of hydrogeological significance. These hydrofacies (bimodal, open framework, massive, planar/trough/horizontal gravels and sands) may be characterised by uniform hydrogeological parameters within each single facies type. A hydrofacies may comprise different lithofacies, and a specific lithofacies type can only belong to one hydrofacies (Fig. 6.14).

In table 6.7 the specific hydraulic parameters for the hydrofacies types were listed. Returning to the comparison with literature data a diagram plotting the horizontal and vertical hydraulic conductivities compared with the model parameters used by Jussel (1992) in Hüntwangen, Switzerland shows the simplification from the numerous sedimentological structures to the few hydrogeological facies (Fig. 6.15). The general trends for the different categories agree. However, the horizontal hydraulic conductivity of the P/T/H gravel and the horizontal and vertical hydraulic conductivities of the massive gravel are found to be larger than those from Hüntwangen. Furthermore, the horizontal and vertical hydraulic conductivities for the planar, trough and horizontal (P/T/H) gravels vary over more one order of magnitude (Fig. 6.15). This is due to the distinct layering in these facies which creates such a strong anisotropy in comparison to within the other facies.

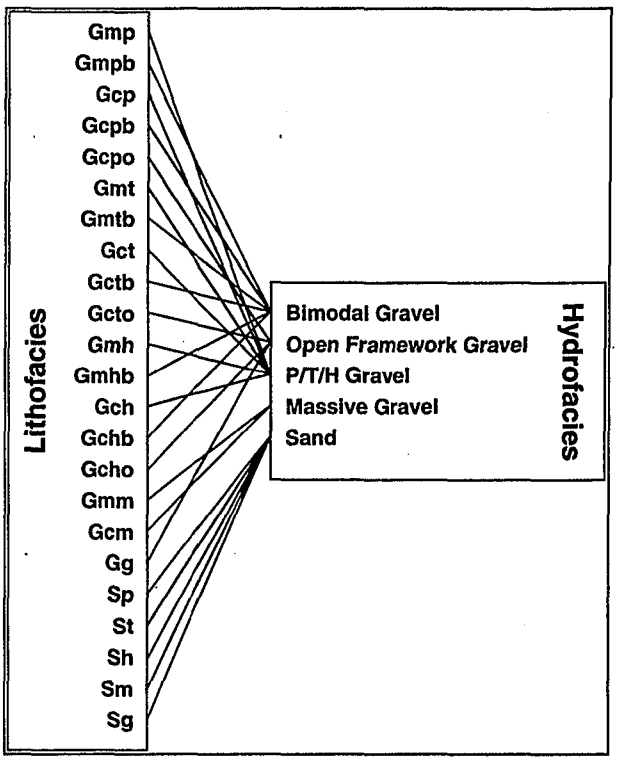

Fig. 6.14: Relationship between lithofacies and hydrofacies, based on the comparison of all measurement results, P/T/H: planar, trough and horizontal gravel

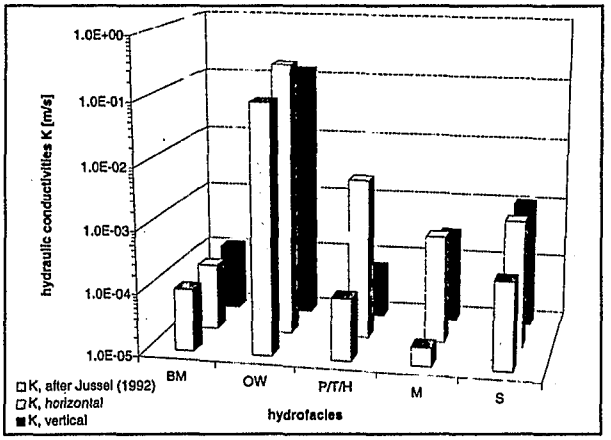

Fig. 6.15: Comparison of horizontal and vertical hydraulic conductivities for all hydrofacies categories with the model parameters used by Jussel (1992)

7 Digital-Photographic Approach for Sedimentological and Hydrogeological Database (Regionalisation)

In the past outcrops were often sedimentologically mapped by field studies and hand drawings (Bluck, 1979; Pryor, 1973), by tracing from outcrop photographs (Jussel, 1992; Jussel et al., 1994; Steel and Thompson, 1983; Fraser and Cobb, 1982; Ori, 1982) or by drawing from lacquer films (Basumallick, 1966). Recently ground penetrating radar (GPR) sections in gravel pits were interpreted with the help of outcrop photographs (Huggenberger et al., 1994; Asprion and Aigner, 1997; Asprion, 1998). In the GPR sections it is often possible to detect the erosional faces, separating different architectural elements, as these faces often represent strict boundaries for the physical properties detected by the GPR (Asprion, 1998). Unfortunately the resolution in the GPR sections is still not high enough to detect all changes in lithofacies types, which would lead to detailed three dimensional data sets of lithofacies units. Thus, within this project only two dimensional sections were interpreted.

A combination of an outcrop based sedimentological interpretation and directly or indirectly measured hydrogeological parameters is rarely found (Pryor, 1973; Jussel, 1992).

However, the methods used during this project allow a faster and more detailed mapping of outcrops than the techniques used in the past. Furthermore, the sedimentological data is collected and saved in a database. It is combined with the actual hydrogeological parameters measured in the outcrops and at samples from the same outcrops (Ch. 6) and will be used in geostatistical analysis and simulations of groundwater flow and transport (Ch. 8).

7.1 Digital-Photographic Approach

In the mapping procedure the following steps are taken: firstly a photograph (colour slide) is taken of the outcrop in the format 6 x 17 cm. This slide is scanned to obtain a high resolution coloured TIFF file. The TIFF file is imported as the screen background of the GIS software used and the boundaries of the different lithofacies types are digitised. The digitised boundaries are converted into polygons, which are classified sedimentologically. Any other database information can easily be related to the sedimentological classification of lithofacies.

7.1.1 Camera

The camera used to take the wide angle photographs of the outcrops is a Linhof Technorama 617 S in combination with a tripod and a Schneider centre filter. The colour slides taken by the camera are in the format 6 x 17 cm, therefore appropriately proportioned for the wide and thin outcrops. The centre filter is used to compensate the brightness differential between the (lighter) centre and the (darker) margins of the images.

Experience showed that generally the best weather to take outcrop photographs is a cloud covered sky. Any direct sunlight can easily hide some structures in the dark shadows. However, in some locations sunlight was found to be helpful as the contrast between lighter and darker components is enhanced.

The films used during this project had a lower sensitivity to light, i.e. finer grained/higher resolution films (Kodak Ektachrome 100 and Kodachrome 64 120 films).

7.1.2 Slide Scanner

The colour slides were scanned with the scanner Agfa Duoscan and the software Agfa Fototune and Adope Photoshop, allowing a non-interpolated resolution in horizontal and vertical direction of 1000 dpi. The RGB coloured or b/w images were saved as TIFF files.

7.2 Sedimentological Database

The digitisation and building-up of the database was carried out using the software ARCINFO. For the various field sites *workspaces* are defined, in which each outcrop interpretation is stored in a separate *coverage*.

The different subprograms of ARCINFO allow the fast on-screen digitisation as *arcs* of erosional or bounding faces between different architectural elements and lithofacies types from the high resolution coloured TIFF *images*. Following this procedure the topology is built by the connection of single bounding faces to *polygons*. Polygons are labelled with *IDs* according to their lithofacies types. The created *polygon attribute tables* are saved in files (*.pat, ARCEDIT). The coordinates of each coverage are transformed to real world coordinates.

Tables (*.def) similar to table 6.6 for each coverage are build up (INFO).

By linking (joining) the INFO tables to the *polygon attribute tables* the database for a *coverage* is completed.

The visual output of the *coverage* data can be achieved by plotting the TIFF *image* in combination with a *polygon coverage* or *grid* with a specified parameter on the screen or to any other output device (ARCPLOT).

An output example of the *coverage* st2 from the field site Steißlingen is shown in figure 7.1. Here the black and white *image* is described by two *polygon coverages* with the lithofacies types present and the horizontal hydraulic conductivities as defined in table 6.7.

A collection of sedimentological interpretations of all the outcrops analysed during this project - from Bittelschieß and Steißlingen and an example from Hüntwangen, Switzerlend - can be found in annex 8.

7.3 Database to Grid Transfer

The *polygon* based *coverages* can easily be transferred into a *grid* with specified cell sizes of the whole or parts of the *coverage*. The *grids* themselves can be exported to ASCII data files.

These include also the grid information such as number of cells and cell size in horizontal and vertical direction, as well as any specified information from the database, e.g. lithofacies codes, hydraulic conductivities. In this work grids were written with a numbers (1-23) corresponding to the lithofacies codes in the order of table 6.6 or 6.7. Special care has to be taken for grid regions which are not filled with data values, as these might lead to errors in other applications.

7.3.1 Transfer of Gridded ASCII Data for Geostatistical Analysis

For the geostatistical analysis (Ch. 8) of the two-dimensional outcrop information using GSLIB (Deutsch and Journel, 1992), the data needs to be converted into the software input format. The program transferring the ASCII data exported from ARCINFO to the input files used for GSLIB is called ARCTOGS. The Fortran 77 code is found in annex 9.

7.3.2 Transfer of Gridded ASCII Data for Groundwater Flow and Transport Modelling

The groundwater flow and transport modelling in chapter 8 is conducted with the software MODFLOW (McDonald and Harburgh, 1984) and MODPATH (Pollock, 1989). It requires various input files with grid information and information on the flow parameters. All input files are written with the program PREMFLOW. The FORTRAN 77 code of this preprocessing package is found in annex 10. More details of the preprocessing will be given in chapter 8.

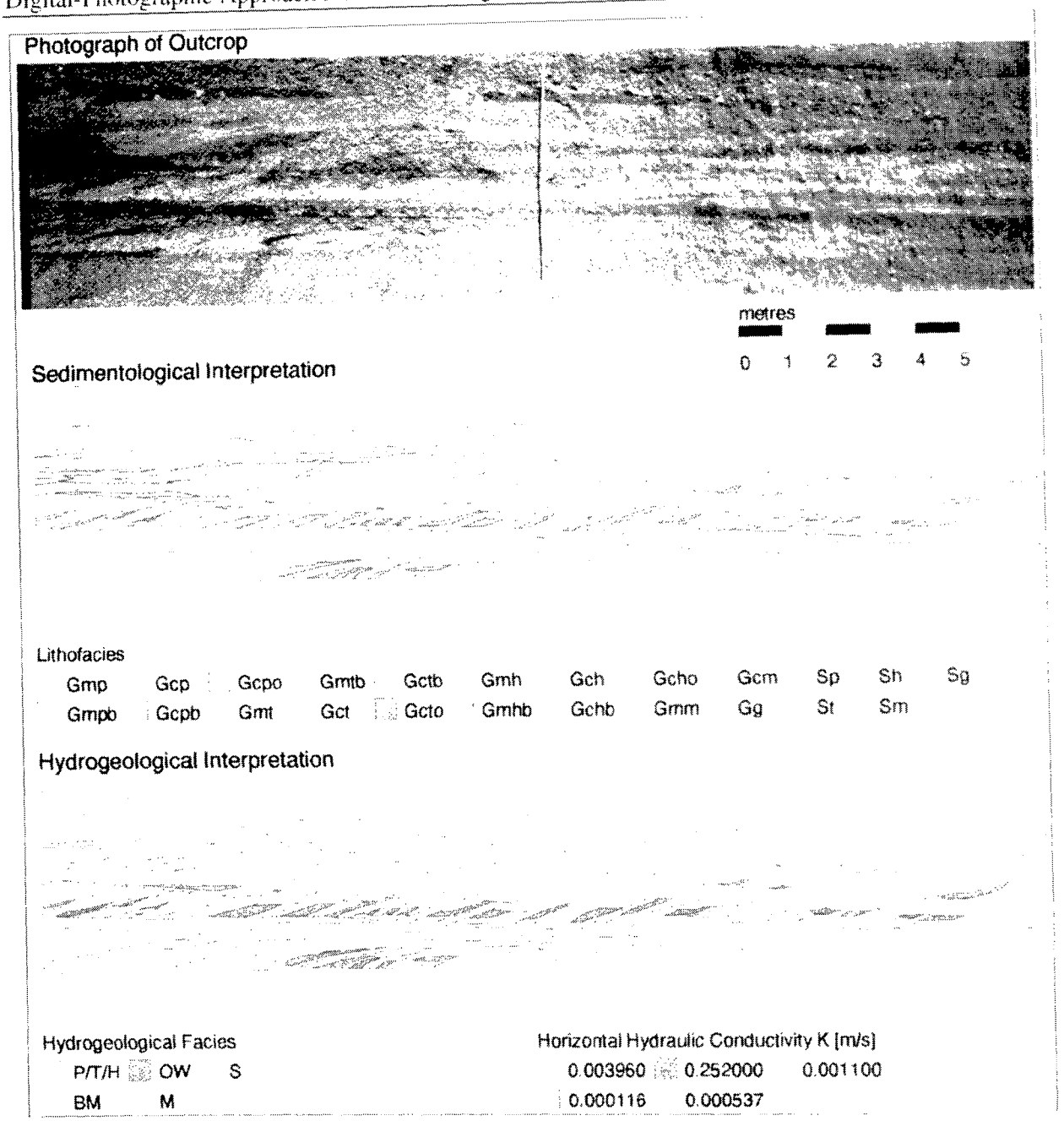

Fig. 7.1: Outcrop analysis: lithofacies interpreted from a wide angle photograph, hydrofacies and horizontal hydraulic conductivities based on the field and laboratory measurements, here: ST2 from Steißlingen, SW Germany

8 2D Groundwater Flow and Transport Modelling

The detailed sedimentological interpretations of outcrops offer the opportunity to evaluate the effect of small scale hydrogeological heterogeneities on the flow of groundwater and the transport of contaminants. Effective hydraulic conductivities and porosities for different hydrofacies can be estimated in a heterogeneous structure of the size of the outcrops (approximately 25 m x 5 m).

The modelling of confined groundwater flow and reactive transport in such heterogeneous environments leads to effective hydraulic conductivities, K_f^{eff}, for the 2D outcrop data sets. Incorporating the dependence of distribution coefficients, K_d, on the hydrofacies present and the contact time of the particle in a given cell, the following advective and sorptive transport calculations allow the estimation of effective parameters for porosities, n^{eff}, and retardation factors, R^{eff}, for specific contaminants.

In the following sections this is described at an example data set which represents well the heterogeneous structures encountered in the outcrops.

8.1 The Example Data Set

As an example data set, the outcrop ST2 from Steißlingen, SW Germany, was chosen (Fig. 7.1). It includes mainly braided river and debris flow sediments. The initial polygon-based lithofacies interpretation was gridded for the use with the finite difference groundwater flow model MODFLOW (McDonald and Harburgh, 1984) into cell sizes of 0.01 m, 0.025 m and 0.05 m resulting in different grids of 2227 x 446, 890 x 178 and 446 x 89 cells, respectively. The outcrop ST2, gridded with 0.025 m cell size, is shown in figure 8.1. The hydraulic conductivity distribution of the assigned lithofacies is shown as natural logarithm, lnK, in figure 8.2. The hydraulic conductivities and porosities used for the different hydrofacies are based on the laboratory and field measurements carried out during this work (Tab. 6.7).

8.1.1 Statistical Parameters

For comparison a statistical summary of the data set ST2, gridded with a cell size of 0.025 m, is given in terms of histograms and semi-variograms.

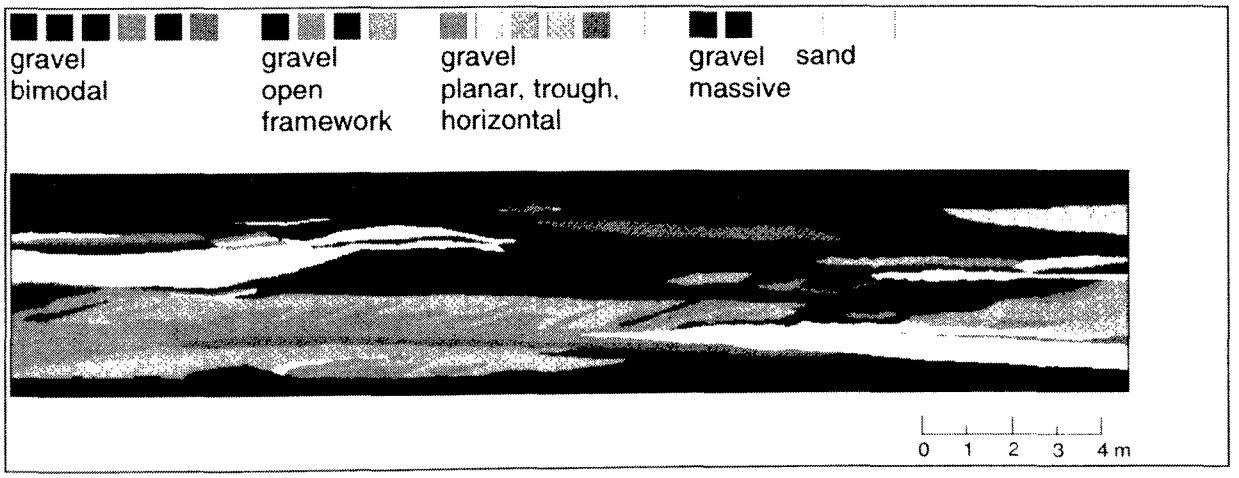

Fig. 8.1: The example data set: lithofacies in outcrop ST2 from Steißlingen, SW Germany, gridded with a cell size of 0.025 m, resulting in a grid of 890 x 178 cells

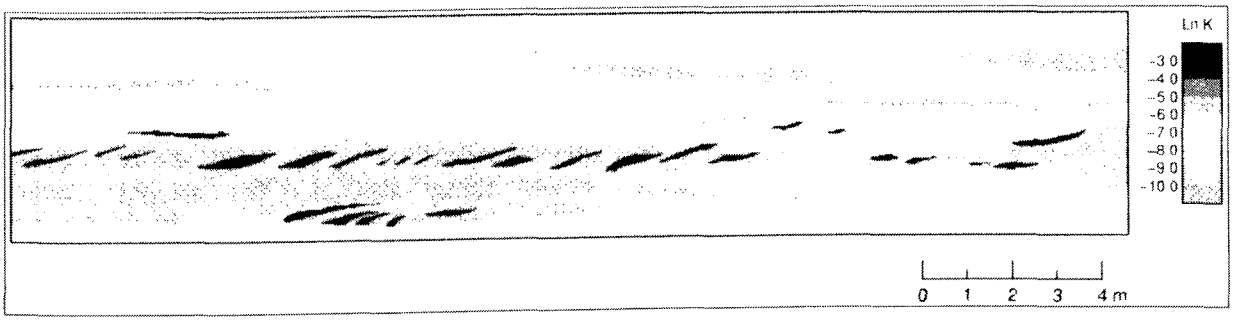

Fig. 8.2: The example data set: gridded hydraulic conductivity distribution, K_f(m/s), displayed as natural logarithm, lnK_f

8.1.1.1 Histograms

The histogram of the number of cells per lithofacies type is shown in figure 8.3. The total of 57.5 % of massive gravels (55908 + 35157 cells) indicates a high proportion of debris flow. It underlines the classification of the deposits as braided river and debris flow sediments.

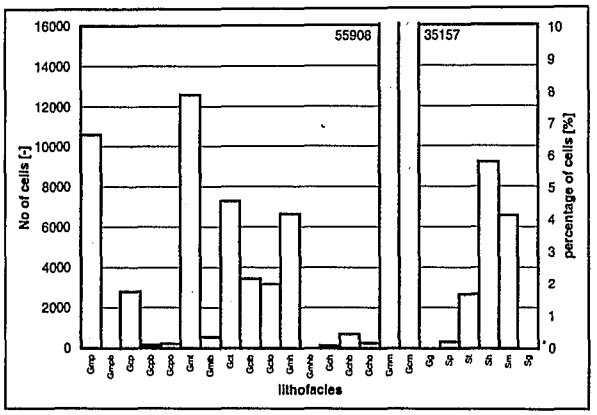

Fig. 8.3: Histogram of the number of cells (percentage) in each of the 23 lithofacies classes of the example data set

The histogram of hydrofacies types (Fig. 8.4) can be compared with the proportions in the sections of Hüntwangen, Switzerland, evaluated by Jussel et al. (1994). The fraction of 7.7 % (5.8 % + 1.9 %) open framework - bimodal couplets in Hüntwangen is only slightly higher than the 5.4 % in the section of Steißlingen. However, the Hüntwangen outcrop comprises more horizontal gravels and less sands than the data set ST2 from Steißlingen.

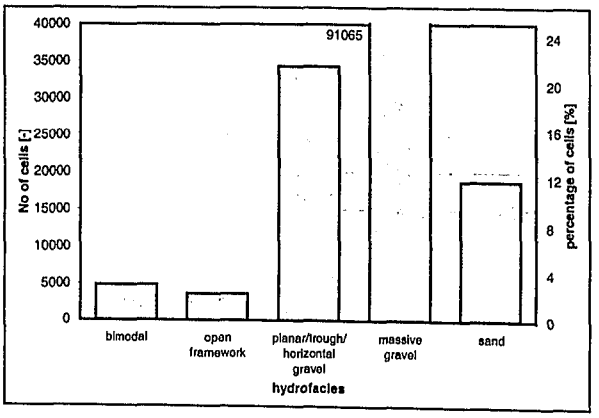

Fig. 8.4: Histogram of the number of cells (percentage) in each of the 5 hydrofacies classes in the example data set

8.1.1.2 Semi-Variograms

Semi-variograms, which were calculated using the software GSLIB (Deutsch and Journel, 1992), give an indication of the variances of the hydraulic conductivity fields and effective correlation lengths in horizontal (x) and vertical (z) directions.

As long as statistical stationarity applies, the variance of the natural logarithm of the horizontal hydraulic conductivities, $\ln K_h$ (1.55, Tab. 8.1), should be similar to the sill of the semi-variogram of $\ln K_h$ in the x direction (1.8, Fig. 8.5). The effective correlation length, defined as 1/3 of the range (Akin and Siemes, 1988) of K_h and K_v structures in x direction results in 1.1 m.

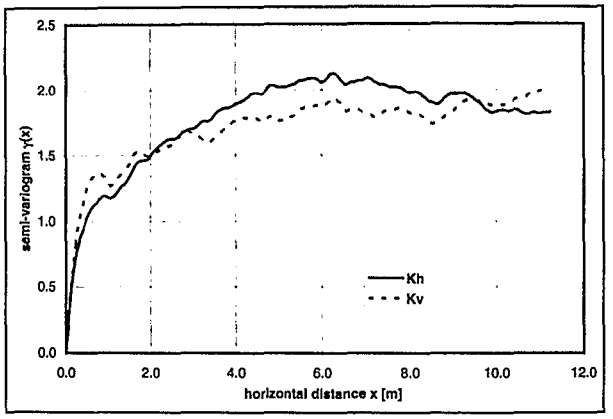

Fig. 8.5: Semi-variogram of hydraulic conductivities ($\ln K_h$ and $\ln K_v$) in x direction in the example data set

Similarly the variance of the vertical hydraulic conductivities $\ln K_v$ (1.66, Tab. 8.1) should equal the sill of the semi-variogram of $\ln K_v$ in the z direction (1.9, Fig. 8.6). From the semi-variogram the effective correlation length of structures in z direction may be approximated as 0.1 m.

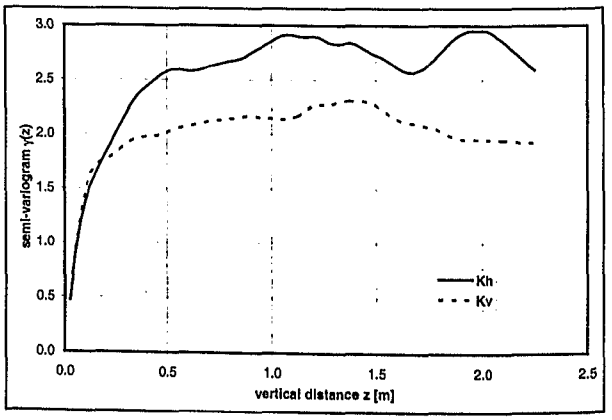

Fig. 8.6: Semi-variogram of hydraulic conductivities ($\ln K_h$ and $\ln K_v$) in z direction in the example data set

8.2 Groundwater Flow Modelling

On all three different grids (c.f. Ch. 8.1) 2D confined horizontal groundwater flow was simulated using MODFLOW (McDonald and Harburgh, 1984). The applied head gradients differ from 0.001 to 0.002, representing a minimum and a typical head gradient within fluvial valley aquifers. The steeper gradient (0.002) and a gridded section with 0.025 m cell sizes were chosen for the following flow evaluation.

8.2.1 Effective Hydraulic Conductivity

From the flow budget calculations and the geometry of the model an effective hydraulic conductivity, K_f^{eff}, can be calculated:

$$K_f^{eff} = -\frac{Q}{A}\cdot\frac{\Delta x}{\Delta h} \qquad 8.1$$

with

$$A = y \cdot z = 4.45 m^2 \qquad 8.2$$

$$Q = \frac{\text{total flow}}{\text{time interval}} = \frac{3.571\cdot 10^{-3} m^3}{300 s} = 1.190\cdot 10^{-5}\,\frac{m^3}{s} \qquad 8.3$$

$$\frac{\Delta h}{\Delta x} = -\frac{(10.044 - 10.0)m}{(22.25 - 0.025)m} = -1.980\cdot 10^{-3} \qquad 8.4$$

resulting in

$$K_f^{eff} = 1.35\cdot 10^{-3}\,\frac{m}{s} \qquad 8.5$$

This effective hydraulic conductivity, K_f^{eff}, is - as expected - nearer to the geometric mean than to the arithmetic mean of the horizontal hydraulic conductivities (Tab. 8.1). The positive skewness (Tab. 8.1) of the hydraulic conductivities represents a distribution such that the arithmetic mean is higher than the median. The means are calculated by the pre-processing with PREMFLOW (see Annex 10, also used in Whittaker and Teutsch, 1996, 1998).

mean	horizontal (x) direction	vertical (z) direction
eff. K_f [m/s] from budget analysis	$1.35\cdot10^{-3}$	-
geometric mean of K_f [m/s]	$1.07\cdot10^{-3}$	$2.67\cdot10^{-4}$
arithmetic mean of K_f [m/s]	$7.26\cdot10^{-3}$	$3.53\cdot10^{-3}$
variance	$1.42\cdot10^{-3}$	$4.34\cdot10^{-4}$
skew	6.34	6.34
neg. arithmetic mean of ln(K_f)	6.84	8.23
variance	1.55	1.66
skew	-1.97	-2.47

Tab. 8.1: *Comparison of different averages for the horizontal and vertical hydraulic conductivities of the example data set*

8.3 Transport Modelling

Transport of solutes in groundwater is often not restricted to pure advection. Many solutes show some kind of interaction with the aquifer material. In this thesis only the effect of sorption, particularly the sorption of a potential hydrocarbon contaminant, will be examined.

The sorptive process may occur fast compared to the flow velocity then it can be described by an equilibrium sorption isotherm: the solute concentration in the water is related to the amount sorbed onto the solid (linear, Freundlich or Langmuir isotherm). Or if the sorption is slow compared to the flow velocity, i.e. the solute comes not to an equilibrium with the sorbed phase, a kinetic sorption model is needed (Fetter, 1993).

Neglecting the effect of sorption, a contaminant transported by advection only leads to an early breakthrough of a contaminant front. Under conditions of equilibrium sorption the arrival time of a concentration front is retarded. Often the contact time of water with the aquifer is not long enough to allow equilibrium sorption of a hydrocarbon contaminant to be reached. Thus the arrival time of a concentration front is earlier than that arrival time given by a prediction based on the assumption of equilibrium sorption.

In the concept applied in this thesis particles were used (path lines and travel times) instead of concentrations. Local dispersion was ignored and only the arrival of a concentration front was examined. The tracking of particles was performed with MODPATH (Pollock, 1989) using the cell by cell fluxes calculated by MODFLOW (McDonald and Harburgh, 1984). The cumulative arrival times of the particle tracking by MODPATH were calculated by a specific post-processing program RETARD (see Annex 11), which accounts for the different sorption options described above: kinetic, equilibrium or none.

In the process applied to simulate kinetic sorption, generally the contact time of a single particle in a given cell - and thus the corresponding kinetic distribution coefficient for this particular cell and particle - depends on the flow velocity, i.e. the head gradient, the hydraulic conductivity and the cell size (discretisation).

It was found that by increasing the number of particles and/or by increasing the head gradient over the whole section the cumulative arrival times, interpreted as breakthrough curves, became more stable: For 400 or more particles and a head gradient of 0.002 or more the breakthrough curves were independent of the different grid sizes used. Therefore, for the following simulations 400 particles and a head gradient of 0.002 were used, corresponding to a typical groundwater head gradient often found in fluvial valley aquifers.

8.3.1 Advective Transport Only, Conservative Tracer

The transport simulation starts with the distribution of particles along the inflow boundary. The distribution of particles was based on the total inflow per cell along the inflow boundary, i.e. the flux between each pair of flow lines is the same.

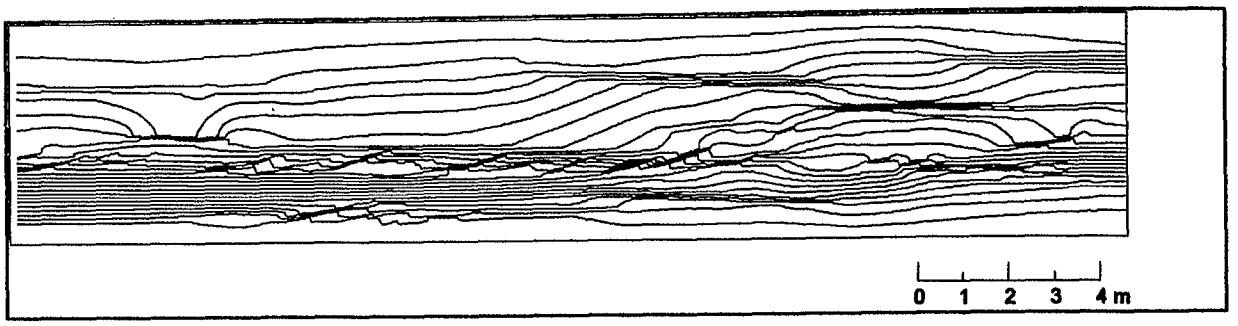

Fig. 8.7: Pathlines of 25 particles tracked through the example data set on the groundwater head distribution from chapter 8.2, initial distribution of particles flux dependent on left hand side

The result of the particle tracking from the advective transport modelling of a conservative tracer in terms of particle pathlines is presented in figure 8.7. For clarity the pathlines of only 25 out of 400 particle pathlines are shown. The high hydraulic conductivity units (i.e. open framework gravels) can clearly be identified as they "focus" the flow lines.

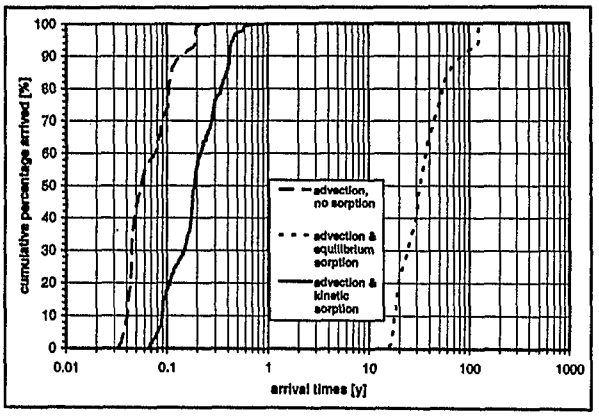

Fig. 8.8: Cumulative particle arrival times (breakthrough curves) from 400 particles, representing advective transport only, advective transport with kinetic sorption and advective transport with equilibrium sorption

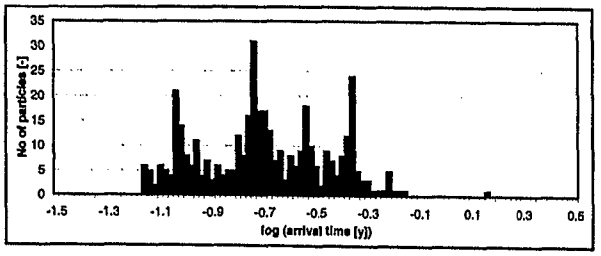

Fig. 8.9: Histogram plot of log of particle arrival times of 400 particles from advective transport only

To calculate the arrival times for each particle two methods were applied. Firstly a particular output file from MODPATH (ENDPOINT) was used, in which the times for each particle have been written out. Alternatively the contact times of each particle within the different cells along the pathline were calculated from another output file (PATHLINE) and added up. Both methods were implemented in the post-processing software RETARD (see Annex 11).

The cumulative particle arrival times are displayed in figure 8.8, which (due to the flux distribution of particles) resemble a concentration breakthrough curve. In figure 8.9 the arrival time distribution is displayed in the form of a histogram.

With the mean arrival time, t_{50}, obtained from the cumulative arrival time curve (Fig. 8.8) an effective porosity, n^{eff}, for the modelled section was calculated:

$$n^{eff} = \frac{v}{v_a} \qquad 8.6$$

$$n^{eff} = \frac{Q}{A} \cdot \frac{t_{0.5}}{x} = \frac{1.190 \cdot 10^{-5} \frac{m}{s}}{4.45 m^2} \cdot \frac{1.769 \cdot 10^{6} s}{(22.25 - 0.025) m} \qquad 8.7$$

$$n^{eff} = 0.213 \qquad 8.8$$

In the same way, taking the upper and lower quartiles, $t_{0.841}$ and $t_{0.159}$, from figure 8.8, an effective dispersion, D^{eff}, was calculated (Fetter, 1993):

$$D^{eff} = \frac{\left[v_a \cdot (t_{0.841} - t_{0.159})\right]^2}{8 \cdot t_{0.5}} \qquad 8.9$$

$$D^{eff} = \frac{\left[1.257 \cdot 10^{-5} \frac{m}{s} \cdot (3.442 - 1.332) \cdot 10^{6} s\right]^2}{8 \cdot 1.769 \cdot 10^{6} s} \qquad 8.10$$

$$D^{eff} = 4.972 \cdot 10^{-5} \frac{m^2}{s} \qquad 8.11$$

From the effective dispersion an effective dispersivity, α^{eff}, can be followed

$$\alpha^{eff} = \frac{D^{eff}}{v_a} = \frac{4.972 \cdot 10^{-5} \frac{m^2}{s}}{1.257 \cdot 10^{-5} \frac{m}{s}} \qquad 8.12$$

$$\alpha^{eff} = 3.9569 m \qquad 8.13$$

As advective transport only, i.e. a conservative behaviour of a contaminant, is not often encountered in the field it is necessary to incorporate sorption into the model. In the following sections equilibrium sorption and kinetic sorption were applied and their respective arrival time distributions were compared.

8.3.2 Advective Transport with Equilibrium Sorption

8.3.2.1 Equilibrium Distribution Coefficients

The process of sorption of a hydrophobic, polycyclic aromatic hydrocarbons (PAH), in this work represented by phenanthrene as an example of a PAH, can be described as absorption into the porous aquifer material by the process of diffusion into the grains and subsequent sorption onto interior surfaces (intra-particle diffusion; Grathwohl, 1998). Thus the time until equilibrium sorption is reached depends mainly on the grain sizes of the aquifer material present. However, the absolute value of equilibrium depends highly on the organic carbon fraction of the aquifer material. The arrival times of advective transport modelling with equilibrium sorption are retarded compared with the concentration front resulting from advective transport only.

Assuming that the sorption of a mass of solute (phenanthrene) onto and into the aquifer material is at equilibrium with the concentration in the groundwater and the relation between the sorbed concentration, s, and the concentration in the water, c, may be described by the Freundlich isotherm model (Grathwohl and Kleineidam, 1995)

$$s = K_d^{eq} \cdot c^{1/f} \qquad 8.14,$$

where f is the Freundlich coefficient. The equilibrium distribution coefficients, K_d^{eq}, were determined from pulverised samples (to accelerate the process of reaching equilibrium state) of the different litho-/hydrofacies types used in batch experiments in the laboratory (Kleineidam, 1998). Two hydrofacies types (planar, trough, horizontal and massive gravels) were regrouped into one single hydrochemical group. Typical K_d^{eq} values for the hydrofacies present are listed in table 8.2.

hydrofacies	distribution coefficient K_d^{eq} [l/kg]
bimodal (BM)	140
open framework (OW)	136
gravel (P/T/H &M)	87
sand (S)	19.9

Tab. 8.2: Typical equilibrium distribution coefficients, K_d^{eq}, for hydrofacies for 100 µg/l phenanthrene in a pulverised sample

8.3.2.2 Incorporating Equilibrium Sorption into the Model

The process of sorption can simply be incorporated into the particle tracking model if the isotherms can be approximated by linear isotherms, i.e. the Freundlich coefficient, f, of equation 8.14 is equal to 1.

In the post-processing of the MODPATH data (RETARD, Annex 11) equilibrium retardation factors, R^{eq}, were calculated from the distribution coefficients of each hydrofacies

$$R^{eq} = 1 + \rho \cdot K_d^{eq} \cdot \frac{1-n}{n} \qquad 8.15,$$

where ρ represents an average rock density of 2.7 g/cm^3.

For each of the advectively transported particles the contact time per cell and the cell type (hydrofacies type) were determined from the MODPATH output file PATHLINE. The cell type corresponds to a specific equilibrium retardation factor, which is multiplied with the contact time in the particular cell to provide a new, corrected (retarded) contact time. The sum of all retarded contact times along one pathline results in the arrival time of the particle due to advection and equilibrium sorption. The cumulative distribution of these arrival times is shown in figure 8.8.

Taking the mean arrival time of the equilibrium sorption breakthrough curve, $t_{0.5}^{eq}$, and comparing it with the mean arrival time of the advection only breakthrough curve, $t_{0.5}$, an effective equilibrium retardation factor, $R^{eq\text{-}eff}$, was estimated:

$$R^{eq-eff} = \frac{t_{0.5}^{eq}}{t_{0.5}} = \frac{1.024 \cdot 10^9 s}{1.769 \cdot 10^6 s} \qquad 8.16$$

$$R^{eq-eff} = 578.99 \qquad 8.17$$

8.3.3 Advective Transport with Kinetic Sorption

The contact times of water with contaminants under field conditions are often too short to allow equilibrium sorption to be assumed (Grathwohl and Kleineidam, 1995). Therefore the distribution coefficients, K_d, depend on the contact times, concentrations of contaminant and organic carbon fractions and grain sizes in the hydrofacies types. In this case the advective contact time of a particular concentration of a contaminant in a cell, comparable to the volume used in the laboratory batch experiments, have to be used to calculate a specific time, concentration and hydrofacies dependent kinetic distribution coefficient, K_d^{kin}(t, c, hydrofacies).

8.3.3.1 Kinetic Distribution Coefficients

The concentration and contact time dependent (kinetic) distribution coefficients can be calculated with an intra-particle diffusion model (Jäger, 1996). It solves the equation for diffusion of the PAH into the grains of the aquifer material

for the different hydrofacies. The information required for this model is the fraction of different grain sizes and lithological components, with particular respect to the carbon content of the hydrofacies type. Furthermore, the boundary conditions for the initial contaminant concentration in the water has to be defined. If the initial concentration decreases with time it is a closed system, if it is kept constant over time it is an open system.

The typical grain size fractions used within the model for the different hydrofacies are based on the grain size distributions from samples taken from the outcrop ST2 in Steißlingen, SW Germany (Fig. 8.10).

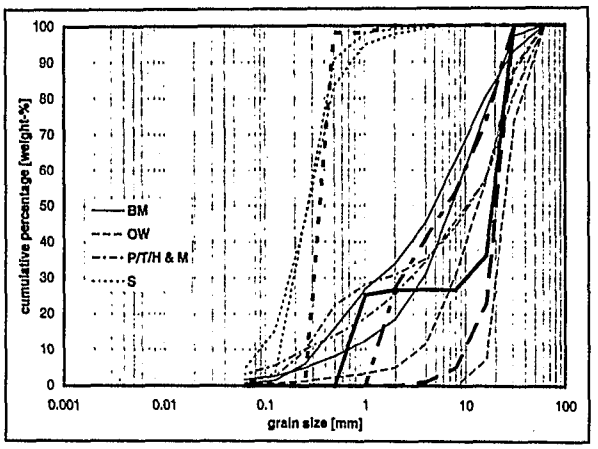

Fig. 8.10: Grain size distribution curves for samples from the outcrop ST2 in Steißlingen, SW Germany (thin lines) on which the input data for the intra-particle diffusion model (thick lines) is based

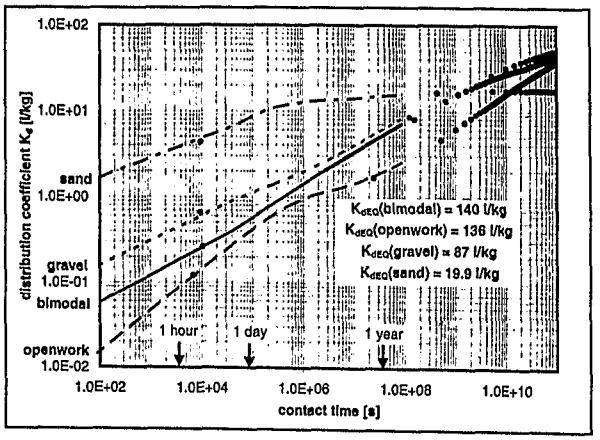

Fig. 8.11: Distribution coefficients, K_d [l/kg], versus contact time t [s] calculated with an intra-particle diffusion model (Jäger, 1996) for phenanthrene (PAH)

For this modelling exercise the concentration of phenanthrene in the water is assumed to be constant over time at 100 µg/l in all cells of the section, comparable to an "infinite bath" or open system.

The resulting functions for the distribution coefficients K_d(t, hydrofacies) are shown in figure 8.11. The longer the actual contact times, the closer the distribution coefficients come to the equilibrium values. However, only sand has a distribution coefficients which approaches its equilibrium value: after a contact time of approximately 10 to 20 days equilibrium is achieved. In all other hydrofacies, equilibrium is only reached after contact times of more than 1000 years.

8.3.3.2 Incorporating Kinetic Sorption into the Model

Similar to the incorporation of equilibrium distribution coefficients into the particle tracking approach, linear isotherms have to be assumed (Ch. 8.3.2.2). In the post-processing of the MODPATH data (RETARD, Annex 11) kinetic retardation factors, R^{kin}, were calculated for each particle with respect to its contact time in a particular cell as given in equation 8.15 and depending on its hydrofacies type of the particular cell, using the calculated functions of the kinetic distribution coefficients (Fig. 8.11).

For each of the particles, transported by advection only, the contact time per cell and the cell type (hydrofacies type) were determined from the MODPATH output file PATHLINE. The cell type and contact time result in a kinetic retardation factor, which is multiplied with the contact time in the particular cell to yield a new, corrected (kinetically retarded) contact time. The sum of all kinetically retarded contact times along one pathline results to the total arrival time of the particle (advection and kinetic sorption). The cumulative distribution of these arrival times is shown in figure 8.8.

Taking the mean arrival time of the kinetic sorption breakthrough curve, $t_{0.5}^{kin}$, and comparing it with the mean of the advection only breakthrough curve, $t_{0.5}$, an effective retardation factor, $R^{kin\text{-}eff}$, can be estimated:

$$R^{kin\text{-}eff} = \frac{t_{0.5}^{kin}}{t_{0.5}} = \frac{5.962 \cdot 10^6 s}{1.769 \cdot 10^6 s} \qquad 8.18$$

$$R^{kin\text{-}eff} = 3.37 \qquad 8.19$$

8.4 Comparison of Different Transport Mechanisms

The large overestimation (factor 171.8) of contaminant arrival times (breakthrough curves) under the assumption of equilibrium sorption becomes obvious when one compares the effective equilibrium and kinetic retardation factors, $R^{eq\text{-}eff}$ (578.99) and $R^{kin\text{-}eff}$ (3.37). This effect is mainly due to the high equilibrium distribution coefficients, K_d, in the gravels, bimodal and open framework gravels, which are

not reached under the flow conditions simulated. This is demonstrated by histograms and "particle dependent" plots of the contributions of the different hydrofacies to the total path lengths and travel times.

Summing up the advective cell contact times per particle in each of the hydrofacies (bimodal, open framework, gravel, sand) leads to different histograms for each hydrofacies (Fig. 8.12). Although not all particles have "seen" all hydrofacies, distinct differences in the means and width of the distributions can be found.

Particularly the large sums per particle of the contact times for gravels and sands show that the particles spend most of their time in gravels, followed by sands. In the advective case the gravels contribute most to the total arrival times, which is reasonable as the example data set comprises 57.5 % gravels (Fig. 8.3). The times are shorter, which are spend by the particles in the bimodal gravels and open framework gravels.

In the same way the sums of the path lengths per particle within a particular hydrofacies can be displayed as histograms (Fig. 8.13).

The longest path lengths are found in the gravels, followed by shorter path lengths in the sands and open framework gravels. Interesting are the shorter sums of path lengths in the bimodal gravels compared to those in the open framework gravels. Both normally appear only in bimodal - open framework couplets and are therefore similar in size. Whereas the sums of contact times the particles spend in both hydrofacies (bimodal and open framework) are similar (Fig. 8.12), the sums of the path lengths are about one order of magnitude different (Fig. 8.13).

Although the summarising histograms of figure 8.12 and 8.13 may give a good overview about the contributions of the different hydrofacies to the overall arrival times (here only for the advective case) much of the information contained in the "transport history" of each particle is not displayed. To overcome this problem a bar charts diagram of the path lengths, the advective, equilibrium and kinetic sorption contact times per particle was used.

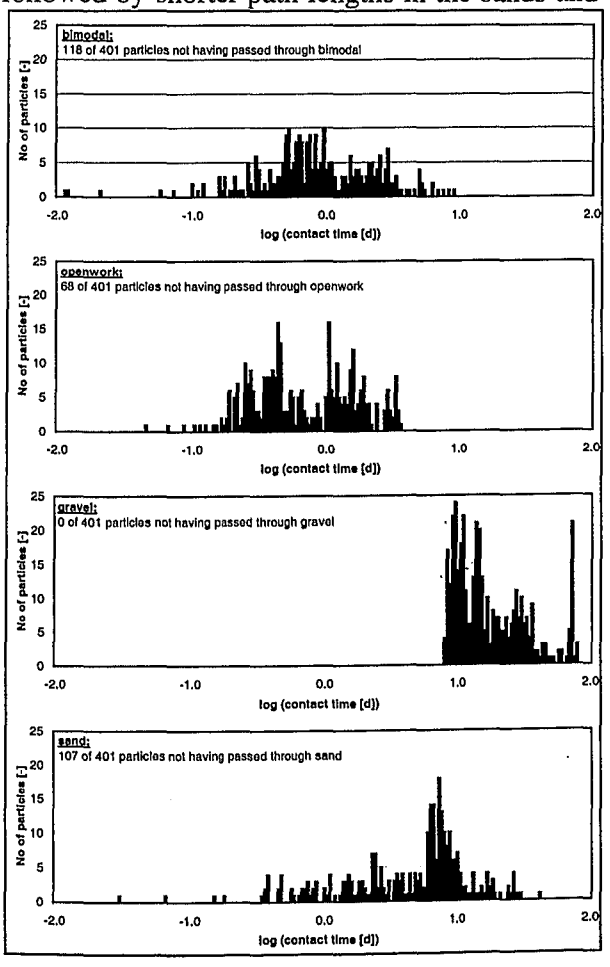

Fig. 8.12: Histograms of contact times of particles in the different hydrofacies types after kinetic retardation

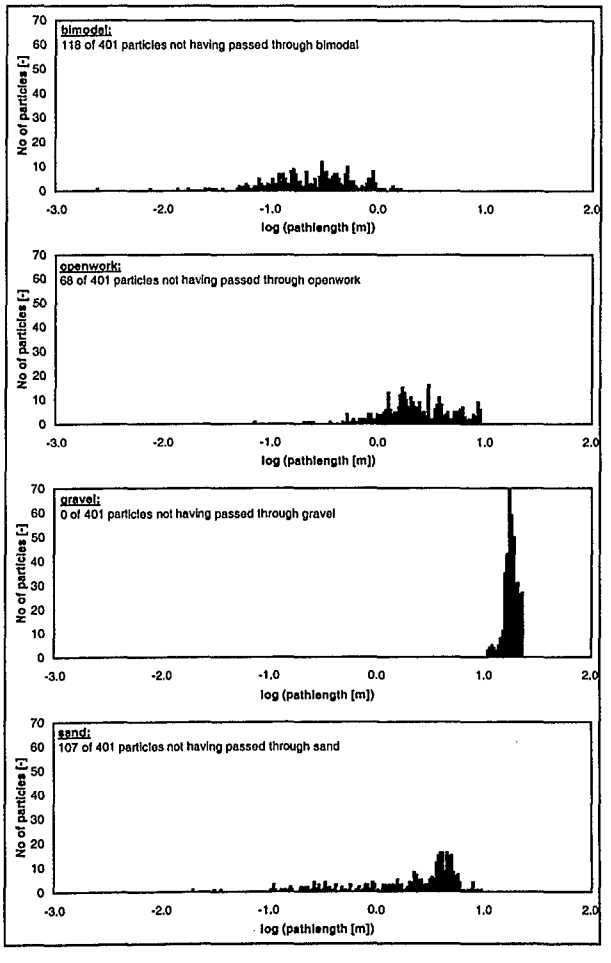

Fig. 8.13: Histogram of contact pathlength of particles in the different hydrofacies types

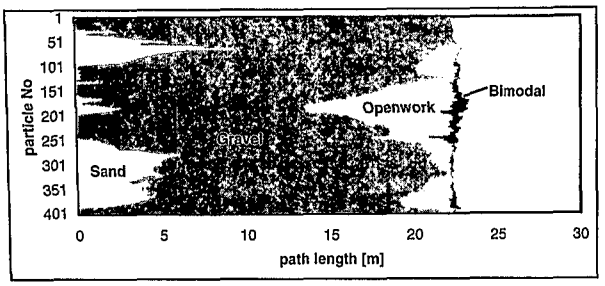

Fig. 8.14: Bar chart of path lengths per particle, divided up into parts of contributions by the different hydrofacies, particles numbered according to their spatial position so that particle number 1 is that nearest to the top of the aquifer and 400 that nearest to the base

In this way all four histograms of the sums of path lengths (Fig. 8.13) are combined in one bar chart (Fig. 8.14). Here the total path lengths per particle are shown as the sum of the contributions by the four different hydrofacies. Most of the total path lengths are only slightly longer than the total horizontal length of the section (22.225 m, Fig. 8.14).

Furthermore, the method of plotting the originally (in the section) flux dependent distributed particles in equal distance separation, numbered according to their spatial position so that particle number 1 is that nearest to the top of the aquifer and 400 that nearest to the base, takes into account the different hydraulic conductivities of the four hydrofacies. Thus, the mass of contaminant is better represented, as it is moved through the section (mass remains constant between two particle flow lines).

Similar to the path lengths, the sums of the advective only contact times (histogram displayed in figure 8.12), the sums of the contact times due to advection and equilibrium sorption and those due to advection and kinetic sorption can be presented for each particle, numbered according to their spatial position in the section (Fig. 8.15 a, b, c, respectively). These plots still represent the ordering according to their vertical positions. The arrival time is shown on the horizontal axis.

By resorting the particles according to their total arrival times and normalising to the mean of the arrival times it is possible to directly compare the three different transport scenarios (advection only, advection and equilibrium sorption, and advection and kinetic sorption, Fig. 8.16 a, b, c, respectively).

Comparing the transport scenarios a and b (Fig. 8.15 and 8.16) the effect of assuming

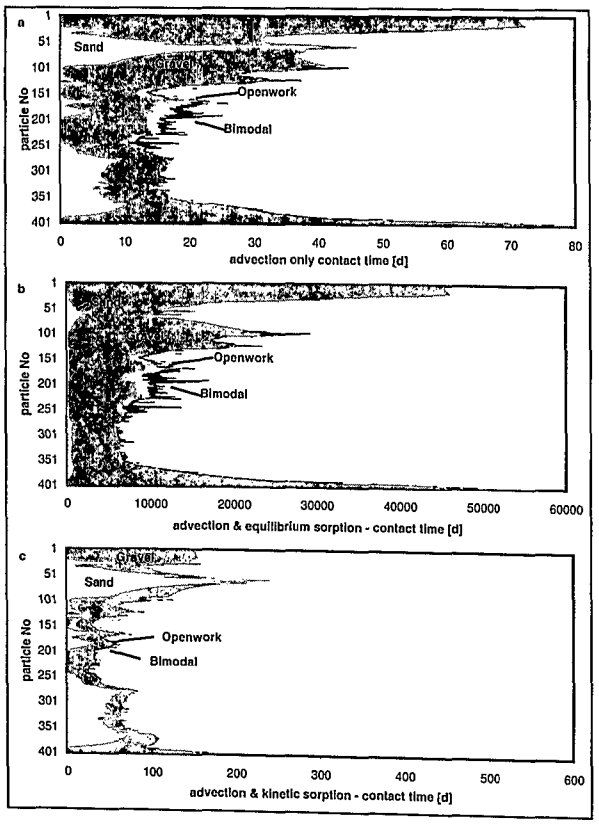

Fig. 8.15: Bar chart of arrival times per particle as sum of contact times per cell along the flow path of each particle, divided up into different parts representing the contributions of the different hydrofacies, particles numbered according to their spatial position so that particle no. 1 is that nearest the top of the aquifer and 400 that nearest the base. Different transport scenarios: a - advection only, b - advection and equilibrium sorption, c - advection and kinetic sorption

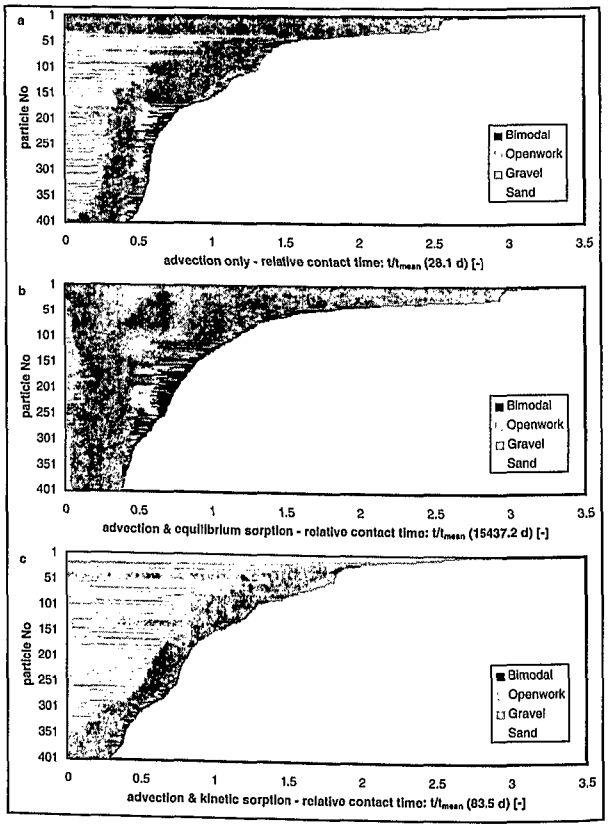

Fig. 8.16: Bar chart of arrival times per particle as sum of contact times per cell along the flow path of each particle, divided up into different parts representing the contributions of the different hydrofacies, vertical order of particles sorted according to total arrival times, normalised to mean arrival time. Different transport scenarios: a - advection only, b - advection and equilibrium sorption, c - advection and kinetic sorption

equilibrium sorption conditions in the cells can be observed. The total contact times particles spend in the gravels, bimodal and open framework gravels are much longer than the total contact times spend in the sand, as the equilibrium distribution coefficient for sand is much lower (Tab. 8.2, Fig. 8.11).

Taking into account the distribution coefficients, K_d, corresponding to the contact time a particle spends in a cell of a particular hydrofacies results in the third transport scenario c: "advection and kinetic sorption". Comparing this to the other scenarios underlines the importance of the sands for the retardation of the example PAH contaminant phenanthrene under realistic flow conditions. The sands reach their equilibrium sorption conditions much earlier than the other hydrofacies.

Furthermore, the bar charts of the particle's arrival times sorted according to their total arrival times (Fig. 8.16) may be used to explain which hydrofacies' retardation is represented in each part of the different breakthrough curves. In the case of advective transport only the contribution of the sands to the arrival times is nearly equally distributed over all particles (only the latest arrivals are due to particles which have not passed through sands). Under conditions of equilibrium sorption the retardation in the sands is lower than in the other hydrofacies, represented not only by an overall shorter length of the bars in the plot but also by the clustering of sand contributions at the fastest arrival times. For kinetic sorption the sand is the only hydrofacies for which the sorption reaches equilibrium conditions. Thus the latest arrivals are mainly due to the sorption in the sands, whereas the fastest arrival times are represented by particles not passing through sands.

9 Conclusions

For the accurate determination of flow paths and contaminant transport in heterogeneous sand and gravel aquifers such as valley fills an approach was used which combines the sedimentological information outcrop/aquifer analogues (outcrops of similar composition than the aquifer in question) with the hydrogeological properties of the sedimentological units mapped.

A sedimentological classification was developed for the lithological facies (lithofacies) encountered in the glaciofluvial Quaternary outcrops in the field areas of this project (in co-operation with Asprion, 1998 and Kleineidam, 1998). This classification is mainly adapted from the sedimentological work of Miall (1985, 1996) and Keller (1992, 1996). Beside the information about the main components (gravel or sand), the layering (planar, trough, horizontal, massive or graded) and the texture (matrix or component supported) the lithofacies types include also information on the characteristics of the grain size distribution curves (bimodal or open framework gravels) which are important for their hydraulic behaviour.

Typical hydrogeological parameters such as horizontal and vertical hydraulic conductivities, porosities and kinetic sorptive distribution coefficients were determined for the lithofacies types using various measurement techniques in the field and laboratory. On the basis of these estimated hydrogeological parameters the 23 lithofacies types were reduced to five relevant hydrofacies types (bimodal, open framework, massive and planar/trough/horizontal gravels and sands). From these five groups the massive and the planar/trough/horizontal gravels of each field site showed similar behaviour with respect to hydrocarbon contaminant sorption therefore both hydrofacies were assigned identical sorption characteristics.

The hydraulic conductivities were derived as a single, characteristic value for each hydrofacies type from water permeameter, sieve analysis, gas tracer and pneumatic measurements *in situ* and in the laboratory. Only the open framework gravels ($2.52 \cdot 10^{-1}$ m/s horizontally and $1.39 \cdot 10^{-1}$ m/s vertically) showed a significant difference by two to three orders of magnitude to the other hydrofacies. The *in situ* measured differences between horizontal and vertical hydraulic conductivities were larger for massive gravels ($5.37 \cdot 10^{-4}$ m/s horizontally and $2.99 \cdot 10^{-4}$ m/s vertically) and planar/through/horizontal gravels ($3.96 \cdot 10^{-3}$ m/s horizontally and $6.61 \cdot 10^{-5}$ m/s vertically). No anisotropy was detected for the sands and bimodal gravels ($1.10 \cdot 10^{-3}$ m/s and $1.16 \cdot 10^{-4}$ m/s, respectively).

The porosities measured in the laboratory resulted to 0.42 for sand, 0.36 for open framework gravels, 0.30 for bimodal gravels and 0.27 for planar/trough/horizontal and massive gravels.

The hydraulic conductivities were mainly determined using a newly developed gas tracer and pneumatic technique. The technique was applied both in the field (for direction dependent permeabilities of undisturbed outcrop material) and in the laboratory (column experiments on disturbed material). The field application proved to be successful for most hydrofacies types although the technical equipment is expensive and the measurement of pressure differences is difficult. As the difference between horizontal and vertical conductivities is often not large, future measurements should be based on a few *in situ* tests combined with further measurements in the laboratory. There the gas measurements allow a generally faster testing than using the water permeameter. However, often higher sample volumes are needed to achieve measurable pressure differences over the columns used.

To obtain a spatial distribution of hydrogeological parameters for a given outcrop analogue the lithofacies of the outcrop were identified and mapped digitising photographic images. Hydrogeological parameters were assigned to the lithofacies on the basis of their classification into hydrofacies and stored in a database. A gridded outcrop section was produced from the polygon-based database for the purpose of geostatistical analysis of hydraulic conductivities as well as groundwater flow and transport modelling.

From the modelling of confined groundwater flow and contaminant transport for a particular example data set a few general implications can be inferred.

Considering only the hydraulics of a heterogeneous gravel and sand aquifer the possibility of the existence of preferential flow paths for the advective transport of contaminants, created by the connection of different high conductivity structures, depends mainly on the frequency and individual length or width of open framework gravels. At any location where open framework gravels are interrupted by material of

two to three orders of magnitude lower conductivity, the local effective conductivity is a result of the geometric mean of both conductivities so that it is dominated by the low conductive material. For the two-dimensional outcrop sections evaluated during this work none showed such a high proportion of open framework gravels that preferential flow paths could exist (neither in horizontal nor in vertical direction). The individual length of open framework gravels rarely exceeded 2 m, the height was often less than 0.3 m and the fraction amounted to less than 8 % of the whole section. Even in three dimensions it is very unlikely that in such a glaciofluvial depositional environment any preferential flow paths may exist over longer distances. Preferential flow paths can probably only be expected in environments where open framework gravels represent a higher percentage of the total sections than that found in the area investigated during this project. Furthermore, the deposition of open framework gravels is sedimentologically coupled to the deposition of lower conductive bimodal gravels (bimodal - open framework gravel couplets), hence the probability of finding open framework gravels not interrupted by bimodal gravels is very low. Thus, in the absence of preferential flow paths over longer distances, the effective hydraulic conductivities in such environments may be estimated by the geometric mean of the conductivities of the single components.

For the transport of e.g. hydrocarbon contaminants in heterogeneous environments the effects of the hydrofacies are somewhat different. The movement of a concentration front of a contaminant is often retarded by sorption, depending on the different sorption characteristics of the hydrofacies. In particular the absorption into the grains of the aquifer material by intra-particle diffusion plays an important role in determining the arrival times of a contamination front. The proportion of a solute sorbed to the aquifer material is described by the distribution coefficient. The equilibrium distribution coefficients of the different hydrofacies depend on the fraction of organic carbon present. Thus the sands, which are mainly composed of quartz, have the lowest equilibrium distribution coefficients. However, this equilibrium state is rarely reached under natural flow conditions. In general due to the short contact times between the contaminated water and the aquifer material, sorption cannot be expected to reach its equilibrium. For a hydrophobic organic compound like the PAH phenanthrene, contact times of more than 1000 years are needed for larger grain sizes. Only the sands may allow to reach equilibrium conditions after only 10 to 20 days. This means that in the modelling case study presented here the effective retardation of the breakthrough of a contaminant front mostly depends on the proportion of sands encountered in the sections. In the example data set a proportion of approximately 12 % of sand led to an effective retardation factor of 3.4 (as compared to a retardation factor of 579 for equilibrium sorption).

Hence the statistical description of the sedimentology, i.e. lithofacies composition in outcrop analogues combined with *in situ* and laboratory measurements of hydrogeological parameters can be used to gain substantial information about the flow of groundwater and the transport of contaminants in heterogeneous environments. On the basis of a typical outcrop data set representing a proportion of an aquifer and with the help of some groundwater flow and contaminant transport simulations, effective hydraulic conductivities and effective retardation factors for specific contaminants were estimated.

References

Abramowitz, M. and Stegun, I.A. 1972. Handbook of Mathematical Functions with Formulas, Graphs and Mathematical Tables. 9th ed. New York, USA: Dover Publications. pp. 1046.

Abu-El-Sha'r, W. and Abriola, L.M. 1997. Experimental Assessment of Gas Transport Mechanisms in Natural Porous Media: Parameter Evaluation. *Water Resources Research*, 33 (4), pp. 505-516.

Akin, H. and Siemes, H. 1988. Praktische Geostatistik - Eine Einführung für den Bergbau und die Geowissenschaften. Berlin: Springer Verlag. pp. 304.

Anderson, M.P. 1989. Hydrogeological Facies Models to Delineate Large-Scale Spatial Trends in Glacial and Glaciofluvial Sediments. *Geological Society of America Bulletin*, 101, pp. 501-511.

Ashmore, P.E. 1991. How do Gravel-Bed Rivers Braid? *Canadian Journal of Earth Sciences*, 28, pp. 326-341.

Asprion, U. 1998. Ground Penetrating Radar (GPR) Analysis in Aquifer-Sedimentology: Case Studies with an Emphasis on Glacial Systems of SW Germany. Dissertation. Institute for Geology, University of Tübingen, Germany.

Asprion, U. and Aigner, T. 1997. Aquifer-Analogue Studies Using Ground Probing Radar: Examples from Fluvial Systems. In: Abstracts of the 18th IAS Regional European Meeting of Sedimentology, Heidelberg, 2.-4. September 1997, 1997. Bechstädt, T., Bengtson, P., Greiling, R. and Schweizer, V. (eds.). Heidelberg, Germany: Institute of Geology and Palaeontology, Ruprecht-Karls-University, Heidelberg. pp. 49-50.

Atkins, P.W. 1986. Physical Chemistry. 3rd ed. New York, USA: Freeman & Co. pp. 857.

Basumallick, S. 1966. Size Differentiation in a Cross-Stratified Unit. *Sedimentology*, 6, pp. 35-68.

Beres, M. and Haeni, F.P. 1991. Application of Ground-Penetrating-Radar Methods in Hydrogeologic Studies. *Ground Water*, 29 (3), pp. 375-386.

Best, J.L. 1988. Sediment Transport and Bed Morphology at River Channel Confluences. *Sedimentology*, 35, pp. 481-498.

Best, J.L. and Bristow, C.S. 1993. Braided Rivers. London: The Geological Society. pp. 432.

Beyer, W. 1964. Zur Bestimmung der Wasserdurchlässigkeit von Kiesen und Sanden aus der Kornverteilungs-Kurve. *WWT Wasserwirtschaft - Wassertechnik*, 14 (6), pp. 165-168.

Bluck, B.J. 1979. Structure of Coarse Grained Braided Stream Alluvium. *Transactions of the Royal Society of Edinburgh*, 70, pp. 181-221.

Borho, W. 1995. Vergleichende numerische Modellierung der Luftströmung zu Bodenluftabsaugbrunnen. Diplomarbeit. Applied Geology, University of Karlsruhe (TH), Germany.

Bridge, J.S. 1993. Description and Interpretation of Fluvial Deposits: A Critical Perspective. *Sedimentology*, 40, pp. 801-810.

Carle, S.F. and Fogg, G.E. 1996. Transition Probability-Based Indicator Geostatistics. *Mathematical Geology*, 28 (4), pp. 453-476.

Carling, P.A. and Glaister, M.S. 1987. Rapid Deposition of Sand and Gravel Mixtures Downstream of a Negative Step: The Role of Matrix-Infilling and Particle-Overpassing in the Process of Bar-Front Accretion. *Journal of the Geological Society*, 144, pp. 543-551.

Carman, P.C. 1956. Flow of Gases Through Porous Media. London: Butterworths Scientific Publications. pp. 200.

Dake, L.P. 1978. Fundamentals of Reservoir Engineering. Developments in Petroleum Science, Vol.: 8. Amsterdam: Elsevier.

Davis, J.M., Lohmann, R.C. and Love, D.W. 1992. A Sedimentological-Geostatistical Mode of Aquifer Heterogeneity Based on Outcrop Studies (abstract). *EOS Transactions of the American Geophysical Union*, 73 (14), pp. 122.

Davis, J.M., Lohmann, R.C., Phillips, F.M., Wilson, J.L. and Love, D.W. 1993. Architecture of the Sierra Ladrones Formation, Central New Mexico: Depositional Controls on the Permeability Correlation Structure. *Geological Society of America Bulletin*, 105, pp. 998-1007.

de Marsily, G. 1986. Quantitative Hydrogeology. Groundwater Hydrology for Engineers. San Diego: Academic Press. pp. 440.

Deutsch, C.V. and Journel, A.G. 1992. GSLIB Geostatistical Software Library and User's Guide, New York: Oxford University Press.

Dranchuk, P.M. and Flores, J. 1975. Non-Darcy Transient Radial Gas Flow Through Porous Media. *Society of Petroleum Engineers Journal*, pp. 129-139.

Dullien, F.A.L. 1992. Porous Media. Fluid Transport and Pore Structure. 2nd ed. San Diego: Academic Press, Inc. pp. 570.

Dürbaum, H., Mattheß, G. and Rambow, D. 1969. Untersuchungen der Gesteins- und Gebirgsdurchlässigkeit des Buntsandsteins in Nordhessen. *Notizblatt des hessischen Landesamtes für Bodenforschung*, 97, pp. 258-274.

Ehlers, J. 1994. Allgemeine und historische Quartärgeologie. Stuttgart: Enke. pp. 358.

Eijpe, R. and Weber, K.J. 1971. Mini-Permeameters for Consolidated Rock and Unconsolidated Sand. *The American Association of Petroleum Geologists Bulletin*, 55 (2), pp. 307-309.

Ellwanger, D. 1990. Zur Riß-Stratigraphie im Andelsbach-Gebiet (Baden-Württemberg). *Jahreshefte des Geologischen Landesamtes Baden-Württemberg*, 32, pp. 235-245.

Ellwanger, D. 1994. Vorläufige Geologische Karte von Baden-Württemberg, 1:25000, Blatt 8021, Pfullendorf mit Erläuterungen. Freiburg i. Br. GLA Baden-Württemberg.

Ellwanger, D., Fiebig, M. and Szenkler, C. 1997. Pleistocene Glaciations in the SW-German Alpine Foreland. In: Abstracts of the 18th IAS Regional European Meeting of Sedimentology, Heidelberg, 2.-4. September 1997, 1997. Bechstädt, T., Bengtson, P., Greiling, R. and Schweizer, V. (eds.). Heidelberg, Germany: Institute of Geology and Palaeontology, Ruprecht-Karls-University, Heidelberg. pp. 124-125.

Eyles, N., Eyles, C.H. and Miall, A.D. 1983. Lithofacies Types and Vertical Profile Models: An Alternative Approach to the Description and Environmental Interpretation of Glacial Diamict and Diamictite Sequences. *Sedimentology*, 30, pp. 393-410.

Fetter, C.W. 1993. Contaminant Hydrogeology. New Jersey, USA: Prentice-Hall. pp. 458.

Fierz, T., Fisch, H., Herklotz, K., Schwab, K., Bielesch, H. and Keppler, A. 1993. Durchführung eines Tracerversuches mit Helium und Radon in der ungesättigten Zone im Rahmen einer Bodenluftsanierung eines Altstandortes. *altlasten-spektrum* (4), pp. 189-198.

Firoozabadi, A. and Katz, D.L. 1979. An Analysis of High-Velocity Gas Flow Through Porous Media. *Journal of Petroleum Technology*, pp. 211-216.

Fogg, G.E. 1990. Architecture and Interconnectedness of Geological Media: Role of Low-Permeability Facies in Flow and Transport. In: Neuman and Neretnieks (eds.). Hydrogeology of Low Permeablity Environments: Heise Verlag.

Fogg, G.E., Carle, S.F., Weissmann, G.S. et al. 1997. New Markov/Geostatistical Approach for Modelling Sedimentary Heterogeneity: Implications for Transport Phenomena. In: Abstracts

of the 18th IAS Regional European Meeting of Sedimentology, Heidelberg, 2.-4. September 1997, 1997. Bechstädt, T., Bengtson, P., Greiling, R. and Schweizer, V. (eds.). Heidelberg, Germany: Institute of Geology and Palaeontology, Ruprecht-Karls-University, Heidelberg. pp. 132-133.

Forchheimer, P. 1901. Wasserbewegung durch Boden. *Zeitschrift des Vereins deutscher Ingenieure*, 45, p. 1731.

Fraser, G.S. and Bleuer, N.K. 1987. Use of Facies Models as Predictive Tools to Locate and Characterize Aquifers in Glacial Terrains. In: Proceedings of the NWWA Focus Conference on Midwestern Ground Water Issues, Dublin, Ohio, 1987: National Water Well Association. pp. 123-143.

Fraser, G.S. and Cobb, J.C. 1982. Late Wisconsin Proglacial Sedimentation Along the West Chicago Moraine of Northeastern Illinois. *Journal of Sedimentary Petrology*, 52 (2), pp. 473-491.

Freeze, R.A. and Cherry, J.A. 1979. Groundwater. Englewood Cliffs: Prentice-Hall. pp. 604.

Fried, J.J. 1975. Groundwater Pollution. Amsterdam: Elsevier. pp. 330.

Garbesi, K., Sextro, R.G., Robinson, A.L., Wooley, J.D., Owens, J.A. and Nazaroff, W.W. 1996. Scale Dependence of Soil Permeability to Air: Measurement Method and Field Investigation. *Water Resources Research*, 32 (3), pp. 547-560.

Gelhar, L.W., Mantoglou, A., Welty, C. and Rehfeldt, K.R. 1985. A Review of Field-Scale Physical Solute Transport Processes in Saturated and Unsaturated Porous Media. Report No: EPRI EA-4190. EPRI, Palo Alto, California, USA.

Goggin, D.J., Thrasher, R.L. and Lake, L.W. 1988. A Theoretical and Experimental Analysis of Minipermeameter Response Including Gas Slippage and High Velocity Flow Effects. *In Situ*, 12 (1&2), pp. 79-116.

Goldthwait, R.P. 1988. Classification of Glacial Morphologic Features. In: Goldthwait, R.P. and Matsch, C.L. (eds.). Genetic Classification of Glacigenic Deposits. Rotterdam: Balkema. pp. 267-277.

Grathwohl, P. 1998. Diffusion in Natural Porous Media: Contaminant Transport, Sorption/Desorption and Dissolution Kinetics. Boston, USA: Kluwer Academics Publisher. pp. 207.

Grathwohl, P. and Kleineidam, S. 1995. Impact of Heterogeneous Aquifer Materials on Sorption Capacities and Sorption Dynamics of Organic Contaminants. In: Proceedings of the Conference on Groundwater Quality: Remediation and Protection, Prague, Czech Republic, 1995: IAHS Publ. no. 225. pp. 79-86.

Häfner, F., Sames, D. and Voigt, H. 1992. Wärme- und Stofftransport: Mathematische Methoden. Berlin: Springer-Verlag. pp. 630.

Hazen, A. 1893. Some Physical Properties of Sands and Gravels with Special Reference to Their Use in Filtration. Report No: 34. 24th Annual Report Mass. State Board of Health Pub. Document 34. Boston, USA: Mass. State Board of Health. pp: 541-556.

Hess, K.M. 1990. Spatial Structure in a Glacial Outwash, Sand and Gravel Aquifer, Cape Cod, Massachusetts. *EOS Transactions of the American Geophysical Union*, 71 (17), pp. 509.

Hess, K.M., Wolf, S.H. and Celia, M.A. 1991. Estimation of Hydraulic Conductivity in a Sand and Gravel Aquifer, Cape Cod, Massachusetts, USGS Water Resources Investigation Report. Report No: 91-4034. USGS. pp. 15-22.

Hölz, T. 1997. Durchlässigkeitsbestimmungen in Lockersedimenten mittels einer regelbaren Gas-Tracer-Meßapparatur. Diplomarbeit. Applied Geology, University of Tübingen, Germany. p. 78

Houpeurt, A. 1959. On the Flow of Gases in Porous Media. *Revue de l'Institut Francaise du Pétrole*, 14 (11), pp. 1468-1497.

Huggenberger, P. 1993. Radar Facies: Recognition of Facies Paterns and Heterogeneities Within Pleistocene Rhine Gravels, NE Switzerland. In: Best, J.L. and Bristow, C.S. (eds.). Braided Rivers. London: The Geological Society. pp. 163-176.

Huggenberger, P. 1994. Field Trip. Die Rheinschotter: Ablagerung eines "Braided"-River Flusssystems (Rafzerfeld).

Huggenberger, P., Meier, E. and Pugin, A. 1994. Ground-Probing Radar as a Tool for Heterogeneity Estimation in Gravel Deposits: Advances in Data-Processing and Facies Analysis. *Journal of Applied Geophysics*, 31, pp. 171-184.

Huggenberger, P., Rauber, M. and Stauffer, F. 1994. Integration of Geophysical and Sedimentological Information in the Stochastic Description of Inhomogeneities in Fluvial Gravel Deposits. In: Proceedings of the IAHR/AIRH Symposium on Transport and Reactive Processes in Aquifers, Zürich, Switzerland, 11.-15.04.1994. Dracos, T. and Stauffer, F. (eds.). Rotterdam: Balkema. pp. 177-181.

Huggenberger, P., Siegenthaler, C. and Stauffer, F. 1988. Grundwasserströmung in Schottern; Einfluß von Ablagerungsformen auf die Verteilung der Grundwasserfließgeschwindigkeit. *Wasserwirtschaft*, 78 (5), pp. 202-212.

Jackson, R.E. 1980. Aquifer Contamination and Protection. Paris: unesco. pp. 440.

Jäger, R. 1996. Modellierung nichtlinearer Intra-Partikel-Diffusion in heterogenem Aquifermaterial. Diplomarbeit. University of Tübingen, Germany.

Jaritz, R. 1998. Quantifizierung der Heterogenität einer Sandsteinmatrix am Beispiel des Stubensandsteins. Dissertation. Applied Geology, University of Tübingen, Germany.

Johnson, N.M. and Dreiss, S.J. 1989. Hydrostratigraphic Interpretation Using Indicator Geostatistics. *Water Resources Research*, 25 (12), pp. 2501-2510.

Johnson, P.C., Stanley, C.C., Kemblowski, M.W., Byers, D.L. and Colthart, J.D. 1990. A Practical Approach to the Design, Operation, and Monitoring of In Situ Soil-Venting Systems. *Ground Water Monitoring Review*, Spring, pp. 159-178.

Jurgaitis, A. and Juozapavicius, G. 1988. Genetic Classification of Galciofluvial Deposits and Criteria for Their Recognition. In: Goldthwait, R.P. and Matsch, C.L. (eds.). Genetic Classification of Glacigenic Deposits. Rotterdam: Balkema. pp. 227-242.

Jussel, P. 1992. Modellierung des Transports gelöster Stoffe in inhomogenen Grundwasserleitern. Dissertation. Institute for Hydromechanics and Water Resources, ETH Zürich, Switzerland.

Jussel, P., Stauffer, F. and Dracos, T. 1994. Transport Modeling in Heterogeneous Aquifers: 1. Statistical Description and Numerical Generation of Gravel Deposits. *Water Resources Research*, 30 (6), pp. 1803-1817.

Jussel, P., Stauffer, F. and Dracos, T. 1994. Transport Modeling in Heterogeneous Aquifers: 2. Three-dimensional Transport Model and Stochastic Numerical Tracer Experiments. *Water Resources Research*, 30 (6), pp. 1819-1831.

Keller, B. 1992. Hydrogeologie des schweizerischen Molasse-Beckens: Aktueller Wissensstand und weiterführende Betrachtungen. *Eclogae geologica Helvetica*, 85 (3), pp. 611-651.

Keller, B. 1996. Lithofazies-Codes für die Klassifikation von Lockergesteinen. *Mitteilungen der Schweizerischen Gesellschaft für Boden- und Felsmechanik* (132), pp. 1-8.

Kidder, R.E. 1957. Unsteady Flow of Gas Through a Semi-Infinite Porous Media. *Journal of Applied Mechanics*, 24 (3), pp. 329-332.

Kister, B. 1994. Untersuchung der charakteristischen Gröben beim Bodenluftabsaugverfahren für Ein- und Mehrbrunnenanlagen durch Laborversuche und räumliche Finite-Elemente-Berechnungen. Dr. Institut für Bodenmechanik, Felsmechanik und Verkehrswesen, RWTH Aachen, Germany.

Klein, R. 1992. Labor- und Felduntersuchungen zum Schadstoffaustrag (LCKW) bei der Sanierung des Untergrunds mit

der Bodenluft-Kreislaufführung. Diplomarbeit. Applied Geology, University of Tübingen, Germany.

Kleineidam, S. 1998. Einfluss von Sedimentologie und Sedimentpetrographie auf den Transport organischer Schadstaoffe - Laborversuche. Dissertation. Applied Geology, University of Tübingen, Germany.

Klinkenberg, L.J. 1942. The Permeability of Porous Media to Liquids and Gases. *Drilling and Production Practice of the American Petroleum Institute*, pp. 200-213.

Koltermann, C.E. and Gorelick, S.M. 1992. Paleoclimatic Signature in Terrestrial Flood Deposits. *Science*, 256, pp. 1775-1782.

Koltermann, C.E. and Gorelick, S.M. 1996. Heterogeneity in Sedimentary Deposits: A Review of Structure-Imitating, Process-Imitating, and Descriptive Approaches. *Water Resources Research*, 32 (9), pp. 2617-2658.

Koziorowski, G. 1986. Hydrogeologische Untersuchungen im Singener Becken (Hegau/Südwestdeutschland). Dissertation. Applied Geology, University of Tübingen, Germany.

Kreamer, D.K. 1982. In Situ Measurements of Gas Diffusion Characteristics in Unsaturated Porous Media by Means of Tracer Experiments. Dissertation. University of Arizona, USA.

Kretzer, H. Unpublished Work. Luftströmung durch poröse Medien. Studienarbeit, Institut für konstruktiven Wasserbau und Wasserwirtschaft, TH Darmstadt.

Lallemand-Berrès, A. and Peaudecerf, P. 1978. Recherche des relations entre les valeurs mesurées de la dispersivité macroscopique d'un milieu aquifère, ses autres caractéristiques et les conditions de mesure. Etude bibliographic. *Bull. Bur. Rech. Géol. Min. Sér. 2, Sec. III* (4), pp. 277-284.

Lenda, A. and Zuber, A. 1970. Tracer Dispersion in Groundwater Experiments. In: Proceedings of a Symposium on Use of Isotopes in Hydrology, International Atomic Energy Agency, IAEA-SM-129/37, Vienna, Austria, 1970. pp. 619-941.

Leopold, L.B. and Wolman, M.G. 1957. River Channel Patterns: Braided, Meandering and Straight. *US Geological Survey Professional Paper* (282-B), pp. 39-85.

Lin, J.Y. and Kinzelbach, W. 1991. AIR - Air Induced Remediation Model, 2.0. Kassel, Germany: Technische Hydraulik und Ingenieurhydrologie, Gesamthochschule Kassel (Universität).

Lyman, W.J., Reehl, W.F. and Rosenblatt, D.H. 1990. Handbook of Chemical Property and Estimation Methods. Washington, DC, USA: American Chemical Society.

Marley, M.C. 1991. Development of Application of a Three-Dimensional Air Flow Model in the Design of a Vapor Extraction System. In: Proceedings National Research and Development Conference on the Control of Hazardous Materials, Anaheim, California, USA, Feb.1991. pp. 360-364.

Marley, M.C., Cody, R.J., Polonsky, J.D. et al., 1992. Application of Tracer Gas Studies in the Optimal Design of Soil Vapor Extraction Systems. In: Proceedings of the 6th National Outdoor Conference on Aquifer Restoration, Ground Water Monitoring, Geophysical Mathods. Ground Water Management II, USA. Stanley, A. (ed.). pp. 543-557.

Marley, M.C., Richter, S.D., Cody, R.J. et al., 1990. Modeling for In-Situ Evaluation of Soil Properties and Engineered Vapor Extraction System Design. In: Proceedings of Petroleum Hydrocarbons and Organic Chemicals in Groundwater Conference, Houston, Texas, USA, Nov. 1990: NWWA/API.

Massmann, J.W. 1989. Applying Groundwater Flow Models in Vapor Extraction System Design. *Journal of Environmental Engineering*, 115 (1), pp. 129-149.

McDonald, M.G. and Harbaugh, A.W. 1984. A Modular Three-Dimensional Finite-Difference Ground-Water Flow Model - MODFLOW. US Geological Survey Open-File Report 83-875, National Center Reston, Virginia, USA: US Geological Survey.

Menzies, J. 1995. Modern Glacial Environments - Processes, Dynamics and Sediments. Oxford, Great Britain: Butterworth-Heinemann Ltd. pp. 621.

Miall, A.D. 1977. A Review of the Braided-River Depositional Environment. *Earth Science Reviews*, 13, pp. 1-62.

Miall, A.D. 1978. Lithofacies Types and Vertical Profile Models in Braided Rivers: A Summary. In: Miall, A.D. (ed.). Fluvial Sedimentology. Calgary: Canadian Society of Petroleum Geologists Memoir. pp. 605-625.

Miall, A.D. 1980. Cyclicity and the Facies Model Concept in Fluvial Deposits. *Bull. Can. Petrol. Geol.* 28, pp. 59-80.

Miall, A.D. 1981. Alluvial Sedimentary Basins: Tectonic Settings and Basin Architecture. In: Miall, A.D. (ed.). Sedimentation and Tectonics in Alluvial Basins: Special Paper of the Geological Association of Canada. pp. 1-33.

Miall, A.D. 1985. Architectural-Element Analysis: A New Method of Facies Analysis Applied to Fluvial Deposits. *Earth Science Reviews*, 22, pp. 261-308.

Miall, A.D. 1996. The Geology of Fluvial Deposits - Sedimentary Facies Basin Analysis, and Petroleum Geology. Berlin: Springer-Verlag. pp. 582.

Millington, R.J. and Quirk, J.P. 1961. Permeability of Porous Solids. *Transactions of the Faraday Society*, 57, pp. 1200-1207.

Moench, A.F. 1989. Convergent Radial Dispersion: A Laplace Transform Solution for Aquifer Tracer Testing. *Water Resources Research*, 25 (3), pp. 439-447.

Mohr, D.H. and Merz, P.H. 1995. Application of a 2D Air Flow Model to Soil Vapor Extraction and Bioventing Case Studies. *Ground Water*, 33 (3), pp. 433-444.

Moltyaner, G.L. and Killey, R.W.D. 1988. The Twin Lake Tracer Tests: Longitudinal Dispersion. *Water Resources Research*, 24 (10), pp. 1613-1627.

Mosley, M.P. 1976. An Experimental Study of Channel Confluences. *Journal of Geology*, 84, pp. 535-562.

Münch, M. 1995. Tomographische Messungen an Bohrkernen. Diplomarbeit. Applied Geology, University of Tübingen, Germany.

Murawski, H. 1983. Geologisches Wörterbuch. 8th ed. Stuttgart, Germany: Enke. pp. 281.

Ogata, A. 1958. Dispersion in Porous Media. Dissertation. Northwestern University, Evanston, Illinois, USA.

Ogata, A. 1970. Theory of Dispersion in a Granular Medium - Fluid Movement in Earth Materials. Report No: 411-I. Geological Survey Professional Paper. Washington, USA: US Government Printing Office. p. 34.

Olschewski, A., Fischer, U., Hofer, M. and Schulin, R. 1995. Sulfur Hexafluoride as a Gas Tracer in Soil Venting Operations. *Environmental Science & Technology*, 29 (1), pp. 264-266.

Ori, G.G. 1982. Braided to Meandering Channel Patterns in Humid-Region Alluvial Fan Deposits, River Reno, Po Plain (Northern Italy). *Sedimentary Geology*, 31, pp. 231-248.

Penck, A. and Brückner, E. 1909. Die Alpen im Eiszeitalter. 3 Bände. Leipzig, Germany: Tauchnitz. pp. 1199.

Penman, H.L. 1940. Gas and Vapour Movements in the Soil. I. The Diffusion of Vapours Through Porous Solids. *Journal of Agricultural Science*, 30, pp. 437-462.

Perry, R.H. and Green, D.W. 1984. Perry's Chemical Engineers' Handbook. International Edition. 5th ed. Singapore: Mc Graw-Hill Book Co. pp. 3-285.

Pollock, D.W. 1989. Documentation of Computer Programs to Compute and Display Pathlines Using Results from the US Geological Survey Modular Three-Dimensional Finite Difference Ground-Water Flow Model - MODPATH. US Geological Survey

Open-File Report 83-381, National Center, Virginia, USA: US Geological Survey.

Pryor, W.A. 1973. Permeability-Porosity Patterns and Variations in Some Holocene Sand Bodies. *The American Association of Petroleum Geologists Bulletin*, 57 (1), pp. 162-189.

Ptak, T. and Teutsch, G. 1994. Forced and Natural Gradient Tracer Tests in a Highly Heterogeneous Porous Aquifer: Instrumentation and Measurements. *Journal of Hydrology*, 159, pp. 79-104.

Pusch, G., Schweitzer, P. and Gaminger, O. 1986. Stationäre und instationäre Gaspermeabilitätsmessung an niedrigpermeablen Gesteinen. *Erdöl Erdgas Kohle*, 102 (5), pp. 235-239.

Richardson, S., Schmidt, S. and Wohnlich, S. 1996. Kohlenmonoxid als Tracergas zur Optimierung von Bodenluftabsauganlagen. *Grundwasser*, 1 (1), pp. 39-45.

Ruiz-Rodriguez, E. 1994. Gültigkeitsgrenzen der Darcy-Gleichung bei Bodenluftabsaugverfahren. *Wasser & Boden*, 3, pp. 52-56.

Sallam, A., Jury, W.A. and Letey, J. 1984. Measurements of Gas Diffusion Coefficient Under Relatively Low Air-Filled Porosity. *Soil Science Society of America Journal*, 48, pp. 3-6.

Sauty, J. 1977. Contribution à l'Indification des Paramètres de Dispersion dans les Aquifèrs par l'Interpretation des Expériences de Tracage. Dissertation. Scientific and Medical University of Grenoble, France.

Sauty, J. 1978. Identification des Paramètres du Transport Hydrodispersif dans les Aquifères par Interprétation de Tracages en Écoulement Cylendrique Convergent ou Divergent. *Journal of Hydrology*, 39, pp. 69-103.

Sauty, J. 1980. An Analysis of Hydrodispersive Transport in Aquifers. *Water Resources Research*, 16 (1), pp. 145-158.

Scheibe, T.D. 1992. Characterization of the Spatial Structuring of Natural Porous Media and its Impacts on Subsurface Flow and Transport. Dissertation. Department of Civil Engineering, Stanford University, USA.

Scheibe, T.D. and Freyberg, D.L. 1990. Impacts of Geological Structure on Transport: Creating a Data Base. In: Parameter Identification and Estimation for Aquifer and Reservoir Characterization, Proceedings of the 5th Canadian/American Conference on Hydrology, Calgery, Canada: NWWA. pp. 56-71.

Schmidt, M. 1994. Geologische Karte von Baden-Württemberg, 1:25000, Blatt 7921, Sigmaringen mit Erläuterungen. Stuttgart: GLA Baden-Württemberg.

Schmidt, S. 1994. Geländeversuche und Reichweitenbestimmung einer Bodenluftabsauganlage mit Hilfe von Kohlenmonoxid als Tracergas. Diplomarbeit. Institute for General and Applied Geology, University of München, Germany.

Schreiner, A. 1978. Geologische Karte von Baden-Württemberg, 1:25000, Blatt 8323, Tettnang mit Erläuterungen. Stuttgart: GLA Baden-Württemberg.

Schreiner, A. 1989. Geologische Karte von Baden-Württemberg, 1:25000, Blatt 8219, Singen mit Erläuterungen. Stuttgart: GLA Baden-Württemberg.

Schreiner, A. 1992. Einführung in die Quartärgeologie. Stuttgart: Schweizerbart'sche Verlagsbuchhandlung. pp. 257.

Schreiner, A. 1992. Geologische Karte von Baden-Württemberg, 1:50000, Hegau und westlicher Bodensee mit Erläuterungen. Stuttgart: GLA Baden-Württemberg.

Steel, R.J. and Thompson, D.B. 1983. Structures and Textures in Triassic Braided Stream Conglomerates ("Bunter" Pebble Beds) in the Sherwood Sandstone Group, North Staffordshire, England. *Sedimentology*, 30, pp. 341-367.

Sudicky, E.A. 1986. A Natural Gradient Experiment on Solute Transport in a Sand Aquifer: Spatial Variability of Hydraulic Conductivity and Its Role in the Dispersion Process. *Water Resources Research*, 22 (13), pp. 2069-2082.

Szenkler, C., Bertleff, B. and Ellwanger, D. 1997. Glacial Sedimentology, Glaciotectonics and Erosional Events in the Singen Basin Complex and Its Hydrogeological Consequences (South German Alpine Foreland, Lake Constance Area). In: Abstracts of the 18th IAS Regional European Meeting of Sedimentology, Heidelberg, 2.-4. September 1997, 1997. Bechstädt, T., Bengtson, P., Greiling, R. and Schweizer, V. (eds.). Heidelberg, Germany: Institute of Geology and Palaeontology, Ruprecht-Kars-University, Heidelberg. pp. 328-329.

Szenkler, C., Sokol, G. and Bertleff, B. 1997. Ein vereinfachtes quartärgeologisches Modell als Grundlage für ein mathematisch-numerisches Grundwasserfliebmodell im Singener Beckenkomplex (Landkreis Konstanz). In: Herbert, M. and Teutsch, G. (eds.). Aquifersysteme Südwestdeutschlands - Eine Vorlesungsreihe an der Universität Tübingen. Tübingen, Germany: University of Tübingen, Applied Geology. pp. 109-136.

Van Genuchten, M.T. 1981. Analytical Solutions for Chemical Transport with Simultaneous Adsorption, Zero-Order Production and First-Order Decay. *Journal of Hydrology*, 49, pp. 213-233.

Van Genuchten, M.T. and Wierenga, P.J. 1976. Mass Transfer Studies in Sorbing Porous Media I. Analytical Solutions. *Soil Science Society of America Journal*, 40 (4), pp. 473-480.

Villinger, E. 1985. Geologie und Hydrogeologie der pleistozänen Donaurinnen im Raum Sigmaringen-Riedlingen (Baden-Württemberg). Unter Mitarbeit von J. Werner. *Abhandlungen des Geologischen Landesamtes Baden-Württemberg*, 11, pp. 141-203.

Villinger, E. 1989. Zur Fluß- und Landschaftsgeschichte im Gebiet von Aare-Donau und Alpenrhein. *Jahreshefte der Gesellschaft für Naturkunde Württembergs*, 144, pp. 5-27.

Vittori, E. and Ventura, G. 1995. Grain Size of Fluvial Deposits and Late Quarternary Climate: A Case Study in the Po River Valley (Italy). *Geology*, 23 (8), pp. 735-738.

Voigt, H., Häfner, F. and Förster, S. 1973. Simulation der Flüssigkeits- und Gasströmung in deformierbaren porösen Gesteinen unter Berücksichtigung der Abweichung vom Darcy-Gesetz. Teil I: Ermittlung der petrophysikalischen Parameter des Gesteins und deren Abhängigkeit von Überlagerungs- und Porenraumdruck - Ausgangsdaten für die mathematische Modellierung. *Zeitschrift für angewandte Geologie*, 19 (4), pp. 168-174.

Webb, E.K. 1992. Simulating the Spatial Heterogeneity of Sedimentological and Hydrogeological Characteristics for Braided Stream Deposits. Dissertation. University of Wisconsin-Madison, USA.

Webb, E.K. 1994. Simulating the Three-Dimensional Distribution of Sediment Units in Braided-Stream Deposits. *Journal of Sedimentary Research*, B64 (2), pp. 219-231.

Webb, E.K. and Anderson, M.P. 1996. Simulating of Preferential Flow in Three-Dimensional, Heterogeneous Conductivity Fields with Realistic Internal Architecture. *Water Resources Research*, 32 (3), pp. 533-545.

Weber, K.J. 1982. Influences of Common Sedimentary Structures on Fluid Flow in Reservoir Models. *Journal of Petroleum Technology*, 34, pp. 665-672.

Weiß, H. 1992. Erkundung einer Verunreinigung durch Steinkohleteeröl im Untergrund eines ehemaligen Gaswerkstandorts mit Hilfe von CO_2-, CH_4- und O_2-Messungen in der Bodenluft. Diplomarbeit. Applied Geology, University of Tübingen, Germany.

Whittaker, J. and Teutsch, G. 1996. The Simulation of Subsurface Characterization Methods Applied to a Natural Aquifer Analogue.

Whittaker, J. and Teutsch, G. 1998. Numerical Simulation of Subsurface Characterization Methods: Application to a Natural Aquifer Analogue. *accepted for publication in Advances in Water Resources.*

Williams, P.F. and Rust, B.R. 1969. The Sedimentology of a Braided River. *Journal of Sedimentary Petrology*, 39 (2), pp. 649-679.

Wyckoff, R.D. and Botset, H.G. 1936. The Flow of Gas-Liquid Mixtures Through Unconsolidated Sands. *Physics*, 7, pp. 325.

Annex 1: Derivation of Analytical Solutions for Gas Flow

Analytical solutions for the flow of gas in porous media are general solutions of the differential equations for the pressure distribution in one, two or three dimensions (radial symmetric). For the purpose of this study the differential equations are derived assuming mass continuity and steady state flow conditions. The individual functions of pressure distribution for the compressible or incompressible condition are then given respectively. The figures in this annex show cases, typical for the field conditions encountered, i.e. the pressure drop in the field rarely exceeds 10^4 Pa (= $100 \cdot 10^2$ Pa = 100 HPa = 100 mbar) and the distance r between extraction (r = 0 m) and injection points (r > 0 m) is not larger than 1 m.

A 1.1 One Dimensional Differential Equation

Steady state flow and continuity of the mass flux in one dimension are represented by

$$\frac{\partial}{\partial r}\left(\rho_g(r)\cdot Q\right)=\frac{\partial}{\partial r}\left(\rho_g(r)\cdot v(r)\cdot A\right)=\frac{\partial}{\partial r}\left(\rho_g(r)\cdot\left(-\frac{k\cdot A}{\mu_g}\cdot\frac{\partial p(r)}{\partial r}\right)\right)=0 \qquad \text{A1.1.}$$

A1.1 can be rewritten using the general state equation for gases,

$$p(r)\cdot V = n_g\cdot R_g\cdot T_g \qquad \text{A1.2}$$

$$\rho_g(r)=\frac{m_g\cdot p(r)}{n_g\cdot R_g\cdot T_g} \qquad \text{A1.3,}$$

as

$$\frac{\partial}{\partial r}\left(-\frac{k\cdot A}{\mu_g}\cdot\frac{m_g}{n_g\cdot R_g\cdot T_g}\cdot p(r)\cdot\frac{\partial p(r)}{\partial r}\right)=0 \qquad \text{A1.4.}$$

As all parameters (apart from the pressure) are assumed to be constant over r, for the one dimensional case of flow through a column the general differential equation is given by

$$\frac{\partial}{\partial r}\left(p(r)\cdot\frac{\partial p(r)}{\partial r}\right)=0 \qquad \text{A1.5.}$$

A 1.1.1 Compressibility Assumption

Considering the compressibility of gas, density is a function of the actual pressure present in the sample,

$$\rho(r)=\rho(p(r))\neq \text{const} \qquad \text{A1.6,}$$

leading to a general solution for A1.5 in the form

$$p(r)=\sqrt{2\cdot(A\cdot r+B)} \qquad \text{A1.7}$$

where A and B are constants.

Applying the boundary conditions

$$p(r)\big|_{r=r_1}=p_1 \quad \text{and} \quad p(r)\big|_{r=r_2}=p_2 \qquad \text{A1.8}$$

results in a pressure distribution of

$$p(r)=\sqrt{\frac{p_2^2-p_1^2}{r_2-r_1}\cdot(r-r_1)+p_1^2} \qquad \text{A1.9}$$

with the derivative given by

$$\frac{\partial p(r)}{\partial r}=\frac{p_2^2-p_1^2}{2\cdot(r_2-r_1)\cdot p(r)} \qquad \text{A1.10.}$$

Figure A1.1 shows the distribution of pressure and pressure gradient for compressible steady state gas flow in a column of 1 m length due to a total pressure drop of $100 \cdot 10^2$ Pa.

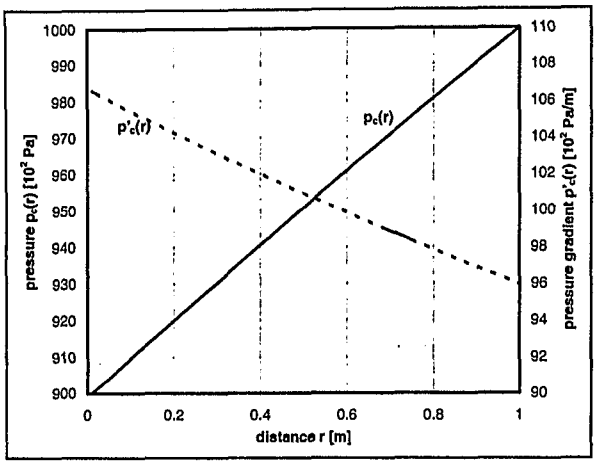

Fig. A1.1: Pressure, p_c, and pressure gradient, p'_c, distribution over a one dimensional column of 1 m length with a total pressure drop of $100 \cdot 10^2$ Pa from analytical solution, considering compressible steady state gas flow

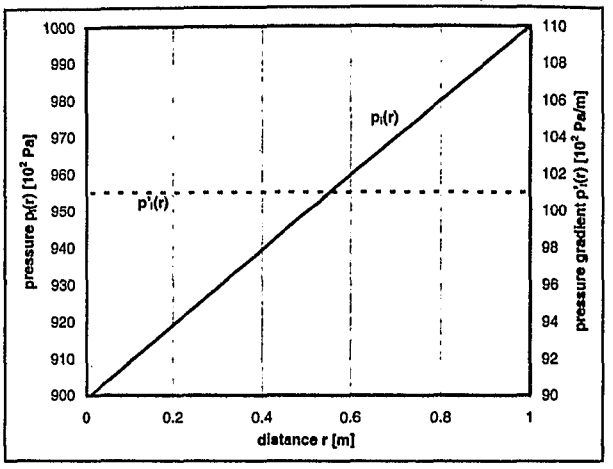

Fig. A1.2: Pressure, p_i, and pressure gradient, p'_i, distribution over a one dimensional column of 1 m length with a total pressure drop of $100 \cdot 10^2$ Pa from the analytical solution, assuming incompressible steady state gas flow

A 1.1.2 Incompressibility Assumption

Assuming incompressibility of the gas, density is not a function of the pressure present in the sample,

$$\rho(r) = \rho = \text{const} \qquad \text{A1.11,}$$

leading to a general solution of A1.5 in the form of

$$p(r) = A \cdot r + B \qquad \text{A1.12,}$$

where A and B are constants.

Applying the boundary conditions of A1.8 leads to

$$p(r) = \frac{p_2 - p_1}{r_2 - r_1} \cdot (r - r_1) + p_1 \qquad \text{A1.13}$$

with the derivative

$$\frac{\partial p(r)}{\partial r} = \frac{p_2 - p_1}{r_2 - r_1} \qquad \text{A1.14.}$$

Figure A1.2 shows the distribution of the pressure and pressure gradient for incompressible steady state gas flow in a column of 1 m length due to a total pressure drop of $100 \cdot 10^2$ Pa.

A 1.1.3 Comparison

Comparing both pressure distributions (Fig. A1.1 and Fig. A1.2), the resulting errors in assuming incompressible flow are minimal with respect to the analytically calculated compressible pressure and pressure gradient.

In Figure A1.3 the errors in the pressure and pressure gradient distribution, resulting from the assumption of incompressible gas flow, are plotted versus distance and relative to the analytical solution of compressible steady state gas flow. The comparison of pressure distributions shows a maximum error of only 0.14 %, whereas the error of the pressure gradient distributions ranges linearly over distance from 5 % at r = 0 m to -5 % at r = 1 m.

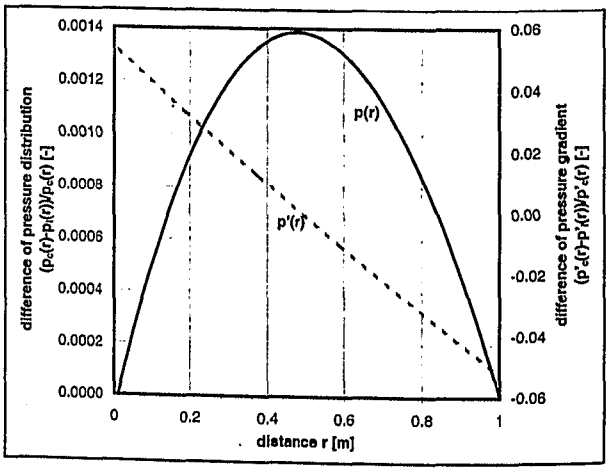

Fig. A1.3: Error of pressure, p, and pressure gradient, p', distribution over a one dimensional column of 1 m length with a total pressure drop of $100 \cdot 10^2$ Pa relative to the analytical solution considering compressible steady state gas flow

A 1.2 Two Dimensional Radial Symmetric Differential Equation

Steady state radial flow and continuity of the mass flux in two dimensions can again be represented by A1.1. Using the general state equation for gases (A1.2, A1.3) leads again to A1.4.

The flow passes through a cylindrical surface A. This cross-sectional area A does not remain constant over r, since

$$A = 2 \cdot \pi \cdot l \cdot r \qquad \text{A1.15.}$$

This leads to a differential equation of the form

$$\frac{\partial}{\partial r}\left(-\frac{2 \cdot \pi \cdot l \cdot k}{\mu_g} \cdot \frac{m_g}{n_g \cdot R_g \cdot T_g} \cdot r \cdot p(r) \cdot \frac{\partial p(r)}{\partial r} \right) = 0 \qquad \text{A1.16.}$$

All other parameters (apart from the pressure) are assumed to be constant over r, so that the general differential equation in the two dimensional case is given by

$$\frac{\partial}{\partial r}\left(r \cdot p(r) \cdot \frac{\partial p(r)}{\partial r} \right) = 0 \qquad \text{A1.17.}$$

A 1.2.1 Compressibility Assumption

Considering the compressibility of gas, density is a function of the pressure present in the sample (A1.6), leading to a general solution for A1.17 in the form

$$p(r) = \sqrt{2 \cdot (A \cdot \ln(r) + B)} \qquad \text{A1.18,}$$

where A and B are constants.

Applying the boundary conditions of A1.8 this results in

$$p(r) = \sqrt{\frac{p_2^2 - p_1^2}{\ln \frac{r_2}{r_1}} \cdot \ln \frac{r}{r_1} + p_1^2} \qquad \text{A1.19}$$

with the derivative

$$\frac{\partial p(r)}{\partial r} = \frac{p_2^2 - p_1^2}{2 \cdot r \cdot \ln \frac{r_2}{r_1} \cdot p(r)} \qquad \text{A1.20.}$$

Figure A1.4 shows the distribution of pressure and pressure gradient for compressible steady state gas flow in a two dimensional radial flow field over a radial distance of 1 m length due to a total pressure drop of $100 \cdot 10^2$ Pa.

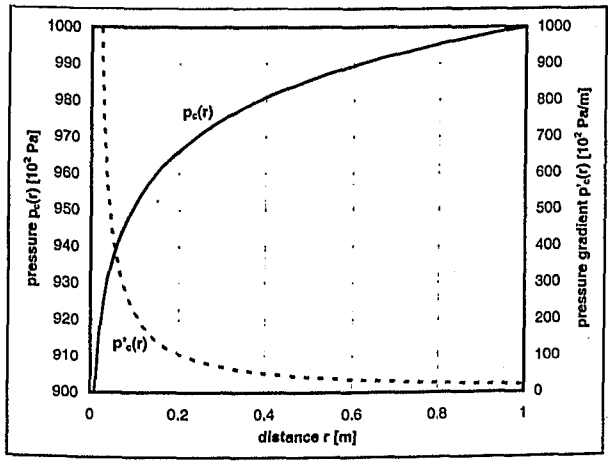

Fig. A1.4: Pressure, p_c, and pressure gradient, p'_c, distribution over a two dimensional radial flow field of 1 m radius with total pressure drop of $100 \cdot 10^2$ Pa from the analytical solution, considering compressible steady state gas flow

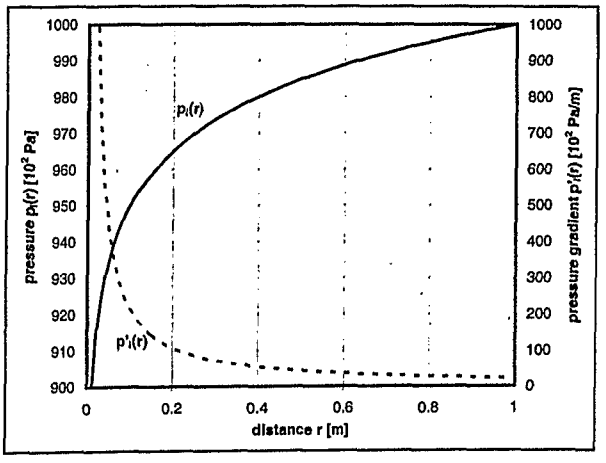

Fig. A1.5: Pressure, p_i, and pressure gradient, p'_i, distribution over a two dimensional radial flow field of 1 m radius with total pressure drop of $100 \cdot 10^2$ Pa from the analytical solution, assuming incompressible steady state gas flow

A 1.2.2 Incompressibility Assumption

Assuming incompressibility of gas, the density is not a function of the pressure present in the sample (A1.11), leading to a general solution of A1.18 in the form

$$p(r) = A \cdot \ln(r) + B \qquad \text{A1.21,}$$

where A and B are constants.

Applying the boundary conditions of A1.8 this results in

$$p(r) = \frac{p_2 - p_1}{\ln\frac{r_2}{r_1}} \cdot \ln\frac{r}{r_1} + p_1 \qquad \text{A1.22}$$

with the derivative

$$\frac{\partial p(r)}{\partial r} = \frac{p_2 - p_1}{r \cdot \ln\frac{r_2}{r_1}} \qquad \text{A1.23.}$$

Figure A1.5 shows the distribution of the pressure and pressure gradient for incompressible steady state gas flow in a two dimensional radial flow field over a radius of 1 m due to a total pressure drop of $100 \cdot 10^2$ Pa.

A 1.2.3 Comparison

Comparing both pressure distributions (Fig. A1.4 and Fig. A1.5), the resulting errors in assuming incompressible flow are minimal with respect to the analytically calculated compressible pressure or pressure gradient.

In Figure A1.6 the errors in the pressure and pressure gradient distribution, resulting from the assumption of incompressible gas flow, are plotted versus distance and relative to the analytical solution of compressible steady state gas flow. The comparison of pressure distributions shows a maximum error of only 0.14 %, whereas the error of the pressure gradient distribution ranges over distance from 5 % at r = 0 m to -5 % at r = 1 m.

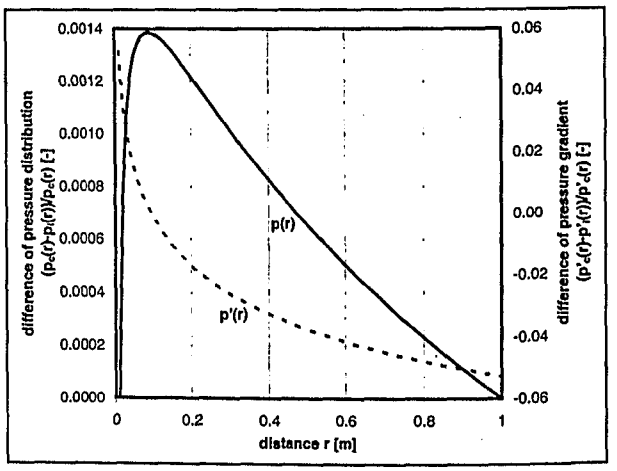

Fig. A1.6: Error of pressure, p, and pressure gradient, p', distribution over a two dimensional radial flow field of 1 m radius with a total pressure drop of $100 \cdot 10^2$ Pa relative to the analytical solution considering compressible steady state gas flow

A 1.3 Three Dimensional Spherically Symmetric Differential Equation

Steady state radial flow and continuity of the mass flux in three dimensions can again be represented by A1.1. With the general state equation for gases (A1.2, A1.3) this results in A1.4.

The flow passes through a spherical surface A. This cross-sectional area A does not remain constant over r, since

$$A = 4 \cdot \pi \cdot r^2 \qquad \text{A1.24.}$$

This leads to a differential equation of the form

$$\frac{\partial}{\partial r}\left(-\frac{4 \cdot \pi \cdot k}{\mu_g} \cdot \frac{m_g}{n_g \cdot R_g \cdot T_g} \cdot r^2 \cdot p(r) \cdot \frac{\partial p(r)}{\partial r}\right) = 0 \qquad \text{A1.25.}$$

All other parameters (apart from pressure) are assumed to be constant over r, so that the general differential equation in the three dimensional case is given by

$$\frac{\partial}{\partial r}\left(r^2 \cdot p(r) \cdot \frac{\partial p(r)}{\partial r}\right) = 0 \qquad \text{A1.26.}$$

A 1.3.1 Compressibility Assumption

Considering compressibility of gas, density is a function of the pressure present in the sample (A1.6), leading to a general solution for A1.26 in the form

$$p(r) = \sqrt{-\frac{2}{r}A + 2B} \qquad \text{A1.27,}$$

where A and B are constants.

Applying the boundary conditions from A1.8 this results in

$$p(r) = \sqrt{\frac{p_2^2 - p_1^2}{r_2 - r_1} \cdot r_2 \cdot \left(1 - \frac{r_1}{r}\right) + p_1^2} \qquad \text{A1.28}$$

with the derivative

$$\frac{\partial p(r)}{\partial r} = \frac{\left(p_2^2 - p_1^2\right) \cdot r_1 \cdot r_2}{2 \cdot r^2 \cdot (r_2 - r_1) \cdot p(r)} \qquad \text{A1.29.}$$

Figure A1.7 shows the distribution of the pressure and pressure gradient for compressible steady state gas flow in a three dimensional radial flow field over a radius of 1 m due to a total pressure drop of $100 \cdot 10^2$ Pa.

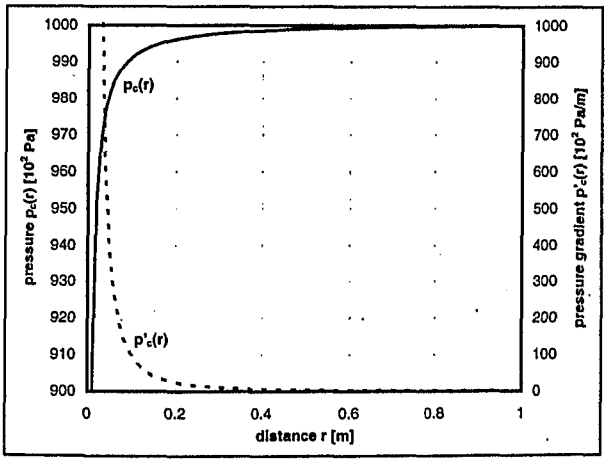

Fig. A1.7: Pressure, p_c, and pressure gradient, p'_c, distribution over a three dimensional radial flow field of 1 m radius with a total pressure drop of $100 \cdot 10^2$ Pa from the analytical solution, considering compressible steady state gas flow

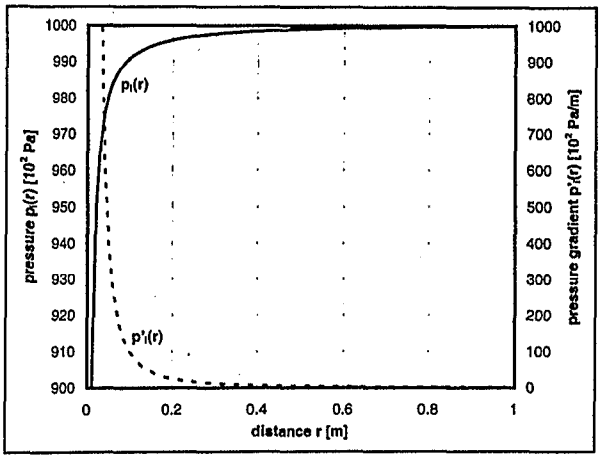

Fig. A1.8: Pressure, p_i, and pressure gradient, p'_i, distribution over a three dimensional radial flow field of 1 m radius with a total pressure drop of $100 \cdot 10^2$ Pa from the analytical solution, assuming incompressible steady state gas flow

A 1.3.2 Incompressibility Assumption

Assuming incompressibility of the gas, density is not a function of the pressure present in the sample (A1.11), leading to a general solution for A1.26 in the form

$$p(r) = -\frac{A}{r} + B \qquad \text{A1.30,}$$

where A and B are constants.

Applying the boundary conditions from A1.8 this results in

$$p(r) = \frac{p_2 - p_1}{r_2 - r_1} \cdot r_2 \cdot \left(1 - \frac{r_1}{r}\right) + p_1 \qquad \text{A1.31}$$

with the derivative

$$\frac{\partial p(r)}{\partial r} = \frac{p_2 - p_1}{r^2 \cdot (r_2 - r_1)} \cdot r_1 \cdot r_2 \qquad \text{A1.32.}$$

Figure A1.8 shows the distribution of pressure and pressure gradient for incompressible steady state gas flow in a three dimensional radial flow field over a radius of 1 m due to a total pressure drop of $100 \cdot 10^2$ Pa.

A 1.3.3 Comparison

Comparing both pressure distributions (Fig. A1.7 and Fig. A1.8), the resulting errors in assuming incompressible flow are minimal with respect to the analytically calculated compressible pressure or pressure gradient.

In Figure A1.9 the errors of the pressure and pressure gradient distribution, resulting from the assumption of incompressible gas flow, are plotted versus distance and relative to the analytical solution of compressible steady state gas flow. The comparison of pressure distributions shows a maximum error of only 0.14 %, whereas the error of the pressure gradient distributions ranges over distance from 5 % at r = 0 m to -5 % at r = 1 m.

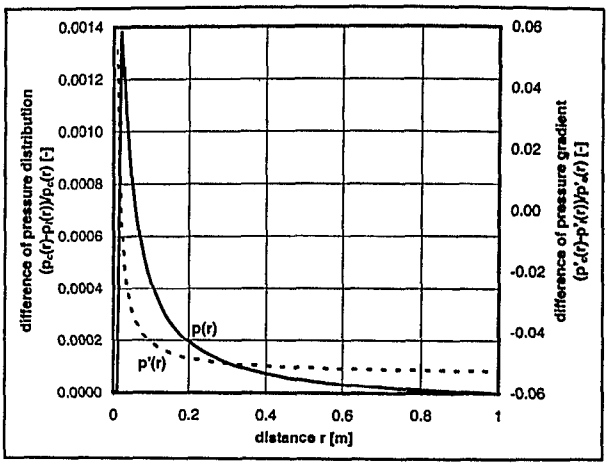

Fig. A1.9: Error of pressure, p, and pressure gradient, p', distribution over a three dimensional radial flow field of 1 m radius with a total pressure drop of $100 \cdot 10^2$ Pa relative to the analytical solution considering compressible steady state gas flow

Annex 2: Analytical Solutions for Gas Tracer Breakthrough Curve Evaluation

The analytical solutions for the transport of gas or water in porous material are derived from the advection-dispersion-equation (ADE) under specific flow conditions (one-, two-, three-dimensional or radial situation). In this annex a broad overview is given to the different forms of ADEs and their analytical solutions. However, for the purpose of this project only analytical solutions for one-dimensional flow fields need to be considered, as the convergent radial flow fields can be approximated by one-dimensional flow fields as long as the ratio of advection to dispersion is large enough, i.e. > 3. This ratio is described by the dimensionless Peclet number, Pe, (Sauty, 1980)

$$Pe = \frac{v_a \cdot d}{D} \qquad \text{A2.1}$$

where d is a characteristic length of the porous media (e.g. mean diameter of the grains or the pores).

The basic advection-dispersion-equation, which can be used to develop specific ADEs for the different flow conditions, is given by

$$R \cdot \frac{\partial c}{\partial t} = \nabla(D \cdot \nabla c) - v_a \cdot \nabla c \qquad \text{A2.2}$$

(Jackson, 1980; Sauty, 1980), where D is the tensor of the dispersion coefficient.

To describe the flow of a tracer in porous media along a stream line in x direction under steady state flow situations the following ADEs are used:

1D (Sauty, 1980) $$R \cdot \frac{\partial c}{\partial t} = D_L \cdot \frac{\partial^2 c}{\partial x^2} - v_a \cdot \frac{\partial c}{\partial x} \qquad \text{A2.3,}$$

2D (Sauty, 1980) $$R \cdot \frac{\partial c}{\partial t} = D_L \cdot \frac{\partial^2 c}{\partial x^2} + D_T \cdot \frac{\partial^2 c}{\partial y^2} - v_a \cdot \frac{\partial c}{\partial x} \qquad \text{A2.4,}$$

3D (Jackson, 1980) $$R \cdot \frac{\partial c}{\partial t} = D_x \cdot \frac{\partial^2 c}{\partial x^2} + D_y \cdot \frac{\partial^2 c}{\partial y^2} + D_z \cdot \frac{\partial^2 c}{\partial z^2} - v_a \cdot \frac{\partial c}{\partial x} \qquad \text{A2.5,}$$

2D-radial (Sauty, 1980) $$R \cdot \frac{\partial c}{\partial t} = D_L \cdot \frac{\partial^2 c}{\partial r^2} + \frac{D_T}{r^2} \cdot \frac{\partial^2 c}{\partial \theta^2} - v_a \cdot \frac{\partial c}{\partial r} \qquad \text{A2.6.}$$

In the case of a conservative tracer the retardation factor is unity, R = 1, simplifying these equations further.

The different one-, two-, three-dimensional or radial flow conditions are discussed here with respect to the three different initial and boundary conditions for the tracer input:

Dirac or slug input,
continuous injection,
injection over time interval Δt.

Various authors have applied these boundary conditions and developed the analytical solutions (Häfner et al., 1992; Jackson, 1980; Lenda and Zuber, 1970; Fried, 1975; Moench, 1989; Ogata, 1958; Ogata, 1970; Sauty, 1977; Sauty, 1978; Sauty, 1980; Van Genuchten and Wierenga, 1976; Van Genuchten, 1981). In the following sections the analytical solutions for the specific cases are given for reference.

A 2.1 Dirac or Slug Input

A 2.1.1 One Dimensional Transport

Initial and boundary conditions:

$$c(x,0)=0 \quad \text{for} \quad x>0$$
$$c(0,t)=\frac{M}{Q}\cdot\delta(t) \quad \text{with} \quad \delta(t)=0 \quad \text{for} \quad t\neq 0,\ \delta(t)=\infty \quad \text{for} \quad t=0 \qquad \text{A2.7}$$
$$\lim_{x\to\infty} c(x,t)=0$$

Analytical solution (Lenda and Zuber, 1970):

$$c(x,t)=\frac{M}{Q}\cdot\frac{v_a}{\sqrt{4\cdot\pi\cdot D_L\cdot t}}\cdot\exp\left(-\frac{\left(x-\frac{v_a\cdot t}{R}\right)^2}{4\cdot D_L\cdot\frac{t}{R}}\right) \qquad \text{A2.8}$$

A 2.1.2 Two Dimensional Transport

Initial and boundary conditions:

$$c(x,y,0)=0 \quad \text{for} \quad x>0,\ y>0$$
$$c(0,0,t)=\frac{M}{Q}\cdot\delta(t) \quad \text{with} \quad \delta(t)=0 \quad \text{for} \quad t\neq 0,\ \delta(t)=\infty \quad \text{for} \quad t=0 \qquad \text{A2.9}$$
$$\lim_{x,y\to\infty} c(x,y,t)=0$$

Analytical solution (Jackson, 1980):

$$c(x,y,t)=\frac{M}{4\cdot\pi\cdot n\cdot\sqrt{D_L\cdot D_T}}\cdot\frac{1}{t}\cdot\exp\left(-\frac{\left(x-\frac{v_a\cdot t}{R}\right)^2}{4\cdot D_L\cdot\frac{t}{R}}-\frac{y^2}{4\cdot D_T\cdot\frac{t}{R}}\right) \qquad \text{A2.10}$$

A 2.1.3 Three Dimensional Transport

Initial and boundary conditions:

$$c(x,y,z,0)=0 \quad \text{for} \quad x>0,\ y>0,\ z>0$$
$$c(0,0,0,t)=\frac{M}{Q}\cdot\delta(t) \quad \text{with} \quad \delta(t)=0 \quad \text{for} \quad t\neq 0,\ \delta(t)=\infty \quad \text{for} \quad t=0 \qquad \text{A2.11}$$
$$\lim_{x,y,z\to\infty} c(x,y,z,t)=0$$

Analytical solution (Freeze and Cherry, 1979):

$$c(x,y,z,t)=\frac{M}{8\cdot(\pi\cdot n)^{3/2}\cdot\sqrt{D_x\cdot D_y\cdot D_z}}\cdot\exp\left(-\frac{\left(x-\frac{v_a\cdot t}{R}\right)^2}{4\cdot D_x\cdot\frac{t}{R}}-\frac{y^2}{4\cdot D_y\cdot\frac{t}{R}}-\frac{z^2}{4\cdot D_z\cdot\frac{t}{R}}\right) \qquad \text{A2.12}$$

A 2.1.4 Convergent Radial Flow

The transport in diverging and converging radial flow can be approximated by the analytical solution of one-dimensional transport (Sauty, 1977; Sauty, 1978; Sauty, 1980) as long as the Peclet number, Pe, is larger than 1 and 3, respectively. This leads to the following initial and boundary conditions:

$$c(r,0)=0 \quad \text{for} \quad r>0$$
$$c(0,t)=\frac{M}{Q}\cdot\delta(t) \quad \text{with} \quad \delta(t)=0 \quad \text{for} \quad t\neq 0,\ \delta(t)=\infty \quad \text{for} \quad t=0 \qquad \text{A2.13}$$
$$\lim_{r\to\infty} c(r,t)=0$$

Analytical solution (Sauty, 1977; Sauty, 1978; Sauty, 1980):

$$c(r,t) = \frac{M}{Q} \cdot \frac{v_a}{\sqrt{4 \cdot \pi \cdot D_L \cdot t}} \cdot \exp\left(- \frac{\left(r - \frac{v_a \cdot t}{R} \right)^2}{4 \cdot D_L \cdot \frac{t}{R}} \right) \qquad \text{A2.14}$$

A 2.2 Continuous Input

A 2.2.1 One Dimensional Transport

Initial and boundary conditions:

$$\begin{aligned} &c(x,0) = 0 \quad \text{for} \quad x > 0 \\ &c(0,t) = c_0 \quad \text{for} \quad t > 0 \\ &\lim_{x \to \infty} c(x,t) = 0 \end{aligned} \qquad \text{A2.15}$$

Analytical solution (Ogata, 1958; Ogata, 1970):

$$c(x,t) = \frac{c_0}{2} \cdot \left[\operatorname{erfc}\left(\frac{x - \frac{v_a \cdot t}{R}}{\sqrt{4 \cdot D_L \cdot \frac{t}{R}}} \right) + \exp\left(\frac{v_a \cdot x}{D_L} \right) \cdot \operatorname{erfc}\left(\frac{x + \frac{v_a \cdot t}{R}}{\sqrt{4 \cdot D_L \cdot \frac{t}{R}}} \right) \right] \qquad \text{A2.16}$$

using the complementary error function, erfc, which is defined as

$$\operatorname{erfc}(y) = \frac{2}{\sqrt{\pi}} \cdot \int_y^\infty \exp\left(-u^2\right) \cdot du \qquad \text{A2.17.}$$

When transport is strongly dominated by advection (Peclet number Pe > 10) equation A2.16 can be approximated (Sauty, 1980) by

$$c(x,t) = \frac{c_0}{2} \cdot \operatorname{erfc}\left(\frac{x - \frac{v_a \cdot t}{R}}{\sqrt{4 \cdot D_L \cdot \frac{t}{R}}} \right) \qquad \text{A2.18.}$$

A 2.2.2 Two Dimensional Transport

Initial and boundary conditions:

$$\begin{aligned} &c(x,y,0) = 0 \quad \text{for} \quad x > 0, \quad y > 0 \\ &c(0,0,t) = c_0 \quad \text{for} \quad t > 0 \\ &\lim_{x,y \to \infty} c(x,y,t) = 0 \end{aligned} \qquad \text{A2.19}$$

Analytical solution (Fried, 1975; Sauty, 1980):

$$c(x,y,t) = \frac{c_0 \cdot q}{4 \cdot \pi \cdot n \cdot \sqrt{D_L \cdot D_T}} \cdot \exp\left(\frac{v_a \cdot x}{2 \cdot D_L} \right) \cdot W\left[\frac{a^2 \cdot R \cdot D_T}{v_a^2 \cdot t}, a \right] \qquad \text{A2.20}$$

where

$$a = \frac{v_a}{2} \cdot \sqrt{\frac{x^2}{D_L^2} + \frac{y^2}{D_L \cdot D_T}} \qquad \text{A2.21}$$

and

$$W[u,\beta] = \int_u^\infty \frac{\exp\left(-y - \frac{\beta^2}{u \cdot y} \right)}{y} dy \qquad \text{A2.22}$$

W is the well-known Hantush function for the drawdown around a well in a leaky aquifer.

A 2.2.3 Three Dimensional Transport

No analytical solutions have been found.

A 2.2.4 Convergent Radial Flow

The transport in diverging and converging radial flow can be approximated by the analytical solution of one-dimensional transport (Sauty, 1977; Sauty, 1978; Sauty, 1980) as long as the Peclet number, Pe, is larger than 10 and 3, respectively. This leads to the following initial and boundary conditions:

$$c(r,0) = 0 \quad \text{for} \quad r > 0$$
$$c(0,t) = c_0 \quad \text{for} \quad t > 0$$
$$\lim_{r\to\infty} c(r,t) = 0 \qquad \text{A2.23}$$

Analytical solution after (Ogata, 1958; Ogata, 1970):

$$c(r,t) = \frac{c_0}{2} \cdot \left[\operatorname{erfc}\left(\frac{r - \frac{v_a \cdot t}{R}}{\sqrt{4 \cdot D_L \cdot \frac{t}{R}}} \right) + \exp\left(\frac{v_a \cdot r}{D_L} \right) \cdot \operatorname{erfc}\left(\frac{r + \frac{v_a \cdot t}{R}}{\sqrt{4 \cdot D_L \cdot \frac{t}{R}}} \right) \right] \qquad \text{A2.24}$$

A 2.3 Input over a Time Interval Δt

In cases where the interval of the injection time is long in comparison to the time until breakthrough occurs, both aforementioned conditions (slug and continuous input) are not appropriate. It is then necessary to use one of the following analytical solutions. Both solve the equation by assuming a superposition of two continuous injections. The first injection with the concentration c_0 and the second with a delay of Δt (the injection time interval) and a concentration $-c_0$. The resulting analytical solutions are used in a FORTRAN 77 code to fit the measured data values from field and laboratory measurements. The difference of both analytical solutions lies only in the different boundary conditions assumed.

The following descriptions are restricted to the case of one dimensional transport with the variable x. The method is, however, applicable for transport in a radial flow field (see above).

A 2.3.1 Häfner Solution (constant concentration)

Initial and boundary conditions:

$$c(x,0) = 0 \quad \text{for} \quad x \geq 0$$
$$c(0,t) = \begin{cases} c_0 & \text{for } 0 < t \leq \Delta t \\ 0 & \text{for } t > \Delta t \end{cases}$$
$$\lim_{x\to\infty} c(x,t) = 0 \quad \text{for} \quad t \geq 0 \qquad \text{A2.25}$$

The boundary condition is given by a concentration step function representing a sudden change in concentration at the times t = 0 s and t = Δt.

Analytical solution (Fried, 1975):

$$c(x,t) = \frac{c_0}{\sqrt{2 \cdot \pi}} \cdot \int_{\frac{x - v_a \cdot t}{\sqrt{2 \cdot D_L \cdot t}}}^{\frac{x - v_a \cdot (t - \Delta t)}{\sqrt{2 \cdot D_L \cdot (t - \Delta t)}}} \exp\left(\frac{-\eta^2}{2} \right) \cdot d\eta \qquad \text{A2.26}$$

Equation A2.26 can be written in a non-integral form (Häfner et al., 1992):

$$c(x,t) = \begin{cases} c_0 \cdot f(x,t) & \text{for } 0 < t \leq \Delta t \\ c_0 \cdot [f(x,t) - f(x,t - \Delta t)] & \text{for } t > \Delta t \end{cases} \qquad \text{A2.27}$$

$$f(x,\tau) = \frac{1}{2} \cdot \left[\operatorname{erfc}\left(\frac{x - \frac{v_a \cdot \tau}{R}}{\sqrt{4 \cdot D_L \cdot \frac{\tau}{R}}} \right) + \exp\left(\frac{v_a \cdot x}{D_L} \right) \cdot \operatorname{erfc}\left(\frac{x + \frac{v_a \cdot \tau}{R}}{\sqrt{4 \cdot D_L \cdot \frac{\tau}{R}}} \right) \right] \qquad \text{A2.28}$$

A 2.3.2 Van Genuchten Solution (constant mass flux)

Initial and boundary conditions:

$$c(x,0) = 0 \quad \text{for} \quad x \geq 0$$

$$\lim_{x \to 0}\left[c(x,t) - \frac{D_L}{v_a} \cdot \frac{\partial}{\partial x} c(x,t)\right] = \begin{cases} c_0 & \text{for } 0 < t \leq \Delta t \\ 0 & \text{for } t > \Delta t \end{cases}$$

$$\lim_{x \to \infty} c(x,t) = 0 \quad \text{for} \quad t \geq 0 \qquad \text{A2.29}$$

The boundary condition is given as a mass flux boundary representing a reservoir supplying a mass flux into the medium/aquifer.

Analytical solution (Van Genuchten, 1981; Van Genuchten and Wierenga, 1976):

$$c(x,t) = \begin{cases} c_0 \cdot g(x,t) & \text{for } 0 < t \leq \Delta t \\ c_0 \cdot [g(x,t) - g(x,t-\Delta t)] & \text{for } t > \Delta t \end{cases} \qquad \text{A2.30}$$

$$g(x,\tau) = \frac{1}{2} \cdot \operatorname{erfc}\left(\frac{x - \frac{v_a \cdot \tau}{R}}{\sqrt{4 \cdot D_L \cdot \frac{\tau}{R}}}\right) - \frac{1}{2} \cdot \left(1 + \frac{v_a \cdot x}{D_L} + \frac{v_a^2 \cdot \tau}{R \cdot D_L}\right) \cdot \exp\left(\frac{v_a \cdot x}{D_L}\right) \cdot \operatorname{erfc}\left(\frac{x + \frac{v_a \cdot \tau}{R}}{\sqrt{4 \cdot D_L \cdot \frac{\tau}{R}}}\right) \qquad \text{A2.31}$$

$$+ v_a \cdot \sqrt{\frac{\tau}{\pi \cdot R \cdot D_L}} \cdot \exp\left(-\frac{\left(x - \frac{v_a \cdot \tau}{R}\right)^2}{4 \cdot D_L \cdot \frac{\tau}{R}}\right)$$

A 2.3.3 Program DTTRACER

The numerical simulation of both analytical solutions (Ch. A 2.3.1 and A 2.3.2) is not straight forward, since the FORTRAN 77 coding of the expressions for the complementary error function and the multiplicative combination of a complementary error function and an exponential function required the use of more complex series expansions. Otherwise numerical overflow results.

After Häfner et al. (1992) the complementary error function, erfc (Eq. A2.17), can be approximated by a series expansion in the form of

$$\operatorname{erfc}(y) = A \cdot \exp(-y^2) \quad \text{for} \quad y \geq 0 \qquad \text{A2.32}$$

$$\operatorname{erfc}(-y) = 2 - \operatorname{erfc}(y) \quad \text{for} \quad y < 0 \qquad \text{A2.33}$$

where A is a series expansion

$$A = p_1 \cdot z + p_2 \cdot z^2 + p_3 \cdot z^3 + p_4 \cdot z^4 + p_4 \cdot z^4 + p_5 \cdot z^5 \qquad \text{A2.34}$$

$$z = \frac{1}{1 + p_0 \cdot y} \qquad \text{A2.35}$$

and the coefficients

$$\begin{aligned} p_0 &= 0.327591000 \\ p_1 &= 0.254829592 \\ p_2 &= -0.284496736 \\ p_3 &= 1.421413741 \\ p_4 &= -1.453152027 \\ p_5 &= 1.061405429 \end{aligned} \qquad \text{A2.36}$$

The multiplicative combination of a complementary error function and an exponential function can be approximated similarly:

$$\operatorname{erc}(y_1, y_2) = \exp(y_1) \cdot \operatorname{erfc}(y_2) \qquad \text{A2.37,}$$

$$\operatorname{erc}(y_1, y_2) = A \cdot \exp(y_1 - y_2^2) \qquad \text{A2.38,}$$

where

$$z = \frac{1}{1 + p_0 \cdot y_2} \qquad \text{A2.39.}$$

A as in equation A2.34 and the coefficients as in equation A2.36.

Furthermore it was necessary to rewrite the van Genuchten (1981) solution (Ch. A2.32) in a form more suitable for program coding. The last two terms of equation A2.31 can thus be combined

$$-\frac{1}{2}\cdot\left(1+\frac{v_a\cdot x}{D_L}+\frac{v_a^2\cdot\tau}{R\cdot D_L}\right)\cdot\exp\left(\frac{v_a\cdot x}{D_L}\right)\cdot\operatorname{erfc}\left(\frac{x+\frac{v_a\cdot\tau}{R}}{\sqrt{4\cdot D_L\cdot\frac{\tau}{R}}}\right)+v_a\cdot\sqrt{\frac{\tau}{\pi\cdot R\cdot D_L}}\cdot\exp\left(-\frac{\left(x-\frac{v_a\cdot\tau}{R}\right)^2}{4\cdot D_L\cdot\frac{\tau}{R}}\right)$$

$$=-\frac{1}{2}\cdot\left(1+\frac{v_a\cdot x}{D_L}+\frac{v_a^2\cdot\tau}{R\cdot D_L}\right)\cdot A\cdot\exp\left(\frac{v_a\cdot x}{D_L}-\frac{\left(x+\frac{v_a\cdot\tau}{R}\right)^2}{4\cdot D_L\cdot\frac{\tau}{R}}\right)+v_a\cdot\sqrt{\frac{\tau}{\pi\cdot R\cdot D_L}}\cdot\exp\left(-\frac{\left(x-\frac{v_a\cdot\tau}{R}\right)^2}{4\cdot D_L\cdot\frac{\tau}{R}}\right)$$

$$=-\frac{1}{2}\cdot\left(1+\frac{v_a\cdot x}{D_L}+\frac{v_a^2\cdot\tau}{R\cdot D_L}\right)\cdot A\cdot\exp\left(\frac{4\cdot v_a\cdot x\cdot\frac{\tau}{R}-\left(x+\frac{v_a\cdot\tau}{R}\right)^2}{4\cdot D_L\cdot\frac{\tau}{R}}\right)+v_a\cdot\sqrt{\frac{\tau}{\pi\cdot R\cdot D_L}}\cdot\exp\left(-\frac{\left(x-\frac{v_a\cdot\tau}{R}\right)^2}{4\cdot D_L\cdot\frac{\tau}{R}}\right)$$

$$=-\frac{1}{2}\cdot\left(1+\frac{v_a\cdot x}{D_L}+\frac{v_a^2\cdot\tau}{R\cdot D_L}\right)\cdot A\cdot\exp\left(-\frac{\left(x-\frac{v_a\cdot\tau}{R}\right)^2}{4\cdot D_L\cdot\frac{\tau}{R}}\right)+v_a\cdot\sqrt{\frac{\tau}{\pi\cdot R\cdot D_L}}\cdot\exp\left(-\frac{\left(x-\frac{v_a\cdot\tau}{R}\right)^2}{4\cdot D_L\cdot\frac{\tau}{R}}\right)$$

$$=\exp\left(-\frac{\left(x-\frac{v_a\cdot\tau}{R}\right)^2}{4\cdot D_L\cdot\frac{\tau}{R}}\right)\cdot\left\{-\frac{1}{2}\cdot\left(1+\frac{v_a\cdot x}{D_L}+\frac{v_a^2\cdot\tau}{R\cdot D_L}\right)\cdot A+v_a\cdot\sqrt{\frac{\tau}{\pi\cdot R\cdot D_L}}\right\} \qquad \text{A2.40}$$

resulting in a new form of equation A2.31

$$g(x,\tau)=\frac{1}{2}\cdot\operatorname{erfc}\left(\frac{x-\frac{v_a\cdot\tau}{R}}{\sqrt{4\cdot D_L\cdot\frac{\tau}{R}}}\right)+\exp\left(-\frac{\left(x-\frac{v_a\cdot\tau}{R}\right)^2}{4\cdot D_L\cdot\frac{\tau}{R}}\right)\cdot\left\{-\frac{1}{2}\cdot\left(1+\frac{v_a\cdot x}{D_L}+\frac{v_a^2\cdot\tau}{R\cdot D_L}\right)\cdot A+v_a\cdot\sqrt{\frac{\tau}{\pi\cdot R\cdot D_L}}\right\} \qquad \text{A2.41}$$

The resulting FORTRAN 77 program DTTRACER allows the calculation of breakthrough curves either after the solution of Häfner et al. (1992) or van Genuchten (1981) with respect to different input parameters:

distance x [m],
injection time interval Δt [s],
duration of tracer test t_{max} [s],
tracer velocity v_a [m/s],
dispersivity α [m],
coefficient of molecular diffusion D_m [m^2/s] and
retardation factor R [-],

which are specified in a separate file called INPUT.DAT. A program listing of DTTRACER.F and a listing of an example input file INPUT.DAT are given in the annexes A 3 and A 4, respectively.

To display the fitting results on the screen the program UNIGRAPH 2000 was used. To simplify the process of manual iteration the graphics program was run in a batch mode, which allows the execution of a series of different commands. Another, more automatic iterative procedure (based on regression analysis) to fit the measured data with calculated data is described in Hölz (1997).

In figure A 2.1 the differences of the two analytical solutions after Häfner et al. (1992) and van Genuchten (1981) are displayed for an example case similar to the breakthrough curves resulting from field tracer tests. It is obvious that the differences in these cases are very small. In some cases the numerical evaluation of the van Genuchten (1981) solution gives numerical errors, i.e. the numerical evaluation of the solution after Häfner et al. (1992) is more stable under extreme input parameters such as very small velocities or dispersion coefficients.

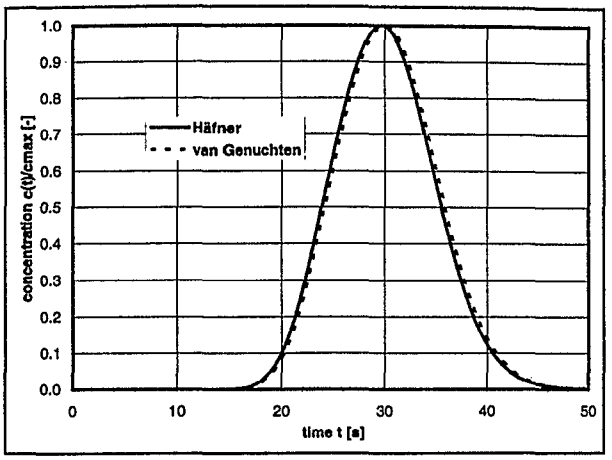

Fig. A2.1: Analytical solutions, after Häfner et al. (1992) and van Genuchten (1981), for breakthrough curves calculated by DTTRACER with input parameters: distance $x = 0.5$ m, injection time interval $\Delta t = 10$ s, tracer velocity $v_a = 0.02$ m/s, dispersivity $\alpha = 0.005$ m, diffusion coefficient Diff = $1.69 \cdot 10^{-5}$ m²/s, retardation factor R = 1

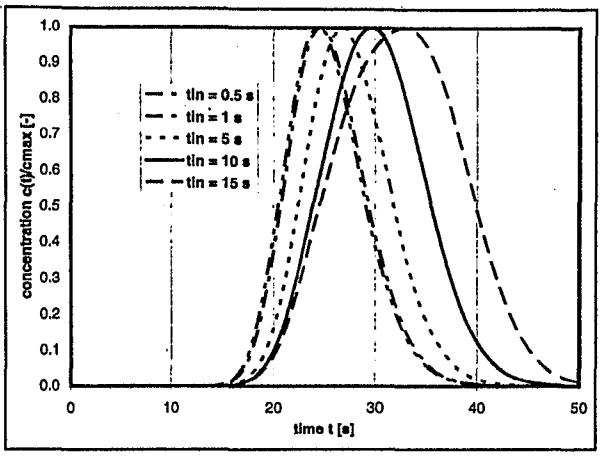

Fig. A2.2: Analytical solutions after Häfner et al. (1992) for breakthrough curves calculated by DTTRACER with different injection time intervals $\Delta t = t_{in}$. Other parameters similar to those in Fig. A 2.1

To compare the effect of different injection time intervals $\Delta t = t_{in}$ with respect to the length of measurement it can be shown (Fig. A 2.2) that not only the widths of the breakthrough curves are change relative to the duration of injection but also the time of maximum concentration decreases with shorter injection intervals.

Different tracer velocities v_a change only the position of the breakthrough curve along the time axis (Fig. A 2.3), whereas a change in dispersivity α (Fig. A 2.3) affects only the width of the curve (without change of position; maximum concentration remains nearly at the same time).

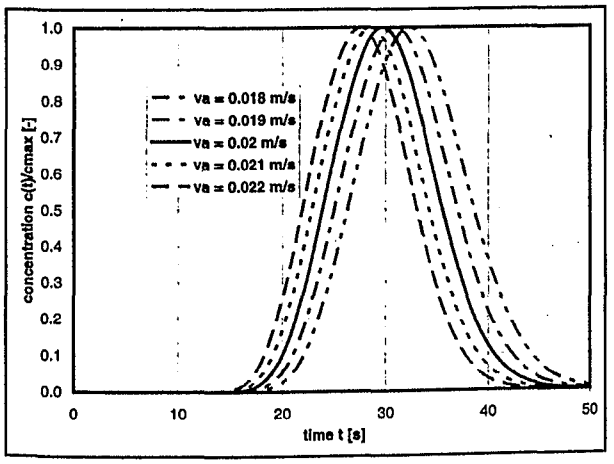

Fig. A2.3: Analytical solutions after Häfner et al. (1992) for breakthrough curves calculated by DTTRACER with different tracer velocities v_a. Other parameters similar to those in Fig. A 2.1

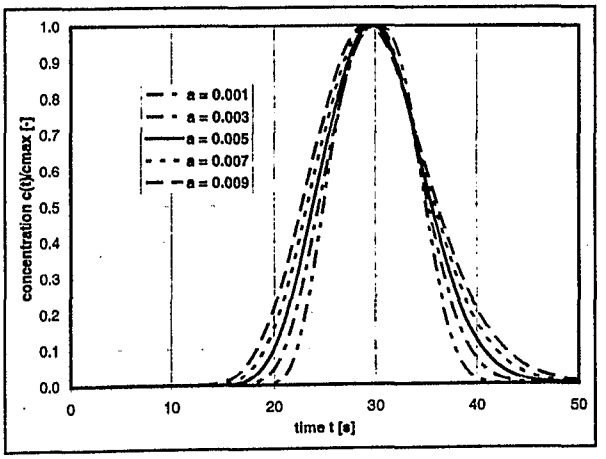

Fig. A2.4: Analytical solutions after Häfner et al. (1992) for breakthrough curves calculated by DTTRACER with different dispersivities α. Other parameters similar to those in Fig. A 2.1

Figure A 2.5 shows the effect of differing coefficients of molecular diffusion D_m. For values of less than that for diffusion of CO_2 in air ($1.69 \cdot 10^{-5}$ m²/s) - diffusion of CO_2 in a porous media should result in even smaller values (Ch. 3.4) - there are only minor differences to be observed.

Finally in figure A 2.6 the sensitivity to retardation factors R is shown. The shift of the whole curve to later times with increasing retardation factors can be observed.

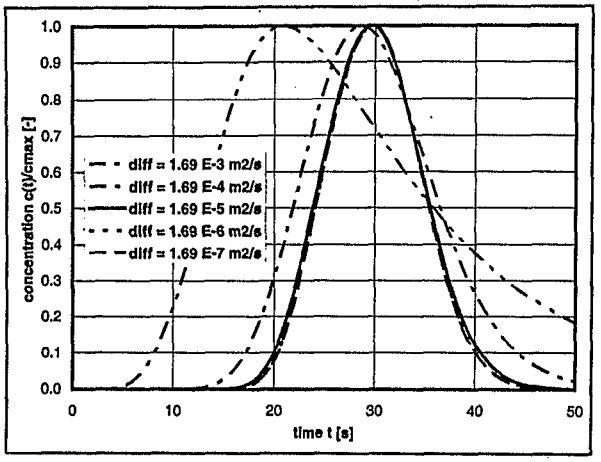

Fig. A2.5: Analytical solutions after Häfner et al. (1992) for breakthrough curves calculated by DTTRACER with different coefficients of molecular diffusion D_m. Other parameters similar to those in Fig. A 2.1

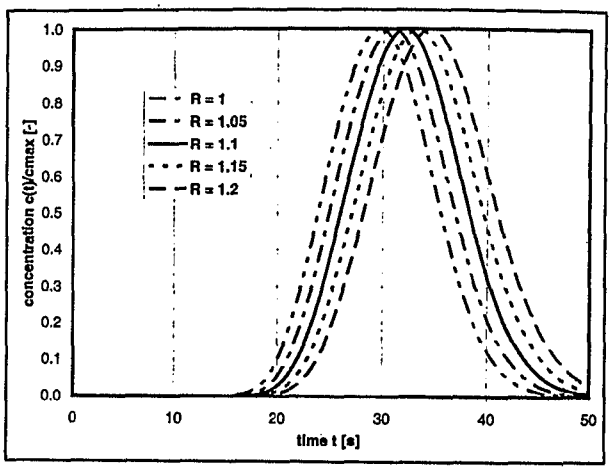

Fig. A2.6: Analytical solutions after Häfner et al. (1992) for breakthrough curves calculated by DTTRACER with different retardation factors R. Other parameters similar to those in Fig. A 2.1

Annex 3: Listing of Program DTTRACER

```
      PROGRAM DTTRACER
C
C     Author:       Ralf Klingbeil, Janet J. Whittaker
C     Version:      3
C     Date:         18.04.97
C     Language:     Fortran 77
C
C     Files:        will be read/created by the program
C                   INPUT.DAT contains all input data
C                   CONC.DAT   time (s), relative concentration (-)
C
C     Arrays:       C (NTIME)  DP rel. conc. for each time step
C                   T (NTIME)  DP actual time (s)
C
C     Subroutines: at the end of program
C                   HAESUB calculates Haefner solution
C                   VANSUB calculates van Genuchten solution
C
C     Functions:    at the end of program
C                   ERC    calculates EXP(X)*ERFC(Y)
C                   ERFC   calculates ERFC(X)
C                   HAEFCT calculates ERFC+EXP*ERFC
C                   VANFCT calculates ERFC-EXP*ERFC+SQRT*EXP
C
C     Variables:    ALPHA  DP (dynamic) dispersivity (m)
C                   CMAX   DP max. conc. of calculated concentrations C
C                   DIFF   DP molecular diffusion (m2/s)
C                   DISP   DP (dynamic) dispersion (m2/s)
C                   DT     DP interval between time steps (s)
C                   G1     DP C(T)=G1(T) for T<TIN
C                   G2     DP C(T)=G1(T)-G2(T) for T>TIN
C                   NIDENT I  0 van Genuchten, 1 Haefner solution
C                   NTIME  I  No. time steps
C                   PI     DP 3.14...
C                   R      DP retardation factor (-)
C                   TIN    DP time interval of const. tracer inj. (s)
C                   TMAX   DP max. time of observation (s)
C                   VA     DP tracer velocity (q/n)
C                   V1     DP variable
C                   V2     DP variable
C                   V3     DP variable
C                   V4     DP variable
C                   V5     DP variable
C                   V6     DP variable
C                   X      DP distance (m)
C
C-----------------------------------------------------------------------
C     this program calculates the tracer breakthrough curves 'C(T)/CMAX'
C     for any tracer for an input over any kind of time interval 'TIN'
C     teking a retardation coefficient 'R' into account as VAN GENUCHTEN
C     or HAEFNER solution
C-----------------------------------------------------------------------
      INTEGER imax,nident,ntime
      PARAMETER (ntime=1000)
      DOUBLE PRECISION alpha,diff,disp,dt,pi,r,tin,tmax,va,x
      DOUBLE PRECISION c(ntime),t(ntime)

C-----------------------------------------------------------------------
C >>>> DATA INPUT
C-----------------------------------------------------------------------
      OPEN (3,FILE='input.dat')
      REWIND (3)

      READ (3,*) x
      READ (3,*) tin
      READ (3,*) tmax
      READ (3,*) dt
      READ (3,*) va
      READ (3,*) alpha
      READ (3,*) diff
      READ (3,*) r
      READ (3,*) nident

      CLOSE (3)

      disp=alpha*va+diff
      pi=4.0*ATAN(1.0)

C-----------------------------------------------------------------------
C >>>> TIME STEPS
C-----------------------------------------------------------------------
      t(1)=dt
      imax=1
      DO 10 I=2,ntime
         t(I)=t(I-1)+dt
         IF (t(I) .GT. tmax) GOTO 15
         imax=imax+1
 10   CONTINUE
 15   CONTINUE

C-----------------------------------------------------------------------
C >>>> INITIALIZING CONCENTRATIONS
C-----------------------------------------------------------------------
      DO 17 J=1,ntime
         c(J)=0.0
 17   CONTINUE

C-----------------------------------------------------------------------
C >>>> CALCULATIONS
C-----------------------------------------------------------------------
      IF (nident .EQ. 0) CALL vansub (imax,t,tin,x,va,disp,pi,c,r)

      IF (nident .EQ. 1) CALL haesub (imax,t,tin,x,va,disp,pi,c,r)

      IF ((nident .NE. 0) .AND. (nident .NE. 1)) THEN
         WRITE (*,*) 'Error in INPUT.DAT file'
      ENDIF

C-----------------------------------------------------------------------
C >>>> DATA OUTPUT
C-----------------------------------------------------------------------
      OPEN (3,FILE='conc.dat')
      REWIND (3)

      DO 90 J=1,imax
         WRITE (3,900) t(J), c(J)
 90   CONTINUE

      CLOSE (3)

C-----------------------------------------------------------------------
C >>>> FORMATS
C-----------------------------------------------------------------------
 900  FORMAT(2F9.4)

      STOP
      END

C***********************************************************************
C >>>> SUBROUTINES
C-----------------------------------------------------------------------
C     VAN GENUCHTEN SOLUTION:
C-----------------------------------------------------------------------
      SUBROUTINE vansub (imax,t,tin,x,va,disp,pi,c,r)
      DOUBLE PRECISION x,tin,va,disp,pi,r
      DOUBLE PRECISION t(*),c(*)
      DOUBLE PRECISION cmax,g1,g2,vanfct
      INTEGER imax

      DO 10 I=1,imax
         IF (t(I) .LE. tin) THEN
            g1=vanfct(t(I),x,va,disp,pi,r)
            g2=0.0
         ELSE
            g1=vanfct(t(I),x,va,disp,pi,r)
            g2=vanfct(t(I)-tin,x,va,disp,pi,r)
         ENDIF
         c(I)=g1-g2
 10   CONTINUE

      cmax=0.0
      DO 20 I=1,imax
         IF (c(I) .GT. cmax) cmax=c(I)
 20   CONTINUE

      DO 30 I=1,imax
         c(I)=c(I)/cmax
 30   CONTINUE

      RETURN
      END

C-----------------------------------------------------------------------
C     HAEFNER SOLUTION:
C-----------------------------------------------------------------------
      SUBROUTINE haesub (imax,t,tin,x,va,disp,pi,c,r)
      DOUBLE PRECISION x,tin,va,disp,pi,r
      DOUBLE PRECISION t(*),c(*)
      DOUBLE PRECISION cmax,g1,g2,haefct
      INTEGER imax

      DO 10 I=1,imax
         IF (t(I) .LE. tin) THEN
            g1=haefct(t(I),x,va,disp,pi,r)
            g2=0.0
         ELSE
            g1=haefct(t(I),x,va,disp,pi,r)
            g2=haefct(t(I)-tin,x,va,disp,pi,r)
         ENDIF
         c(I)=g1-g2
 10   CONTINUE

      cmax=0.0
      DO 20 I=1,imax
         IF (c(I) .GT. cmax) cmax=c(I)
 20   CONTINUE

      DO 30 I=1,imax
         c(I)=c(I)/cmax
 30   CONTINUE

      RETURN
      END

C***********************************************************************
C >>>> FUNCTIONS
C-----------------------------------------------------------------------
c      FUNCTION vanfct(t,x,va,d,pi,r)
c      DOUBLE PRECISION vanfct,t,x,va,disp,pi,v1,v2,v3,v4,v5,v6,erfc,
c     +erc,r
c      v1=(x-va*t/r)/sqrt(4.0*disp*t/r)
c      v2=x*va/disp
c      v3=0.5*(1.0+v2+va*va*t/disp)
c      v4=(x+va*t/r)/sqrt(4.0*disp*t/r)
c      v5=t/(pi*disp)
c      v6=(x-va*t)*(x-va*t)/(-4.0*disp*t)
c      vanfct=0.5*erfc(v1)-v3*erc(v2,v4)+va*sqrt(v5)*exp(v6)
c      RETURN
c      END
c this vanfct creates numerical errors for small disp values

C-----------------------------------------------------------------------
      FUNCTION vanfct(t,x,va,disp,pi,r)
      DOUBLE PRECISION vanfct,t,x,va,disp,pi,v1,v2,v3,v4,v5,v6,erfc,r
      DOUBLE PRECISION coeff,a,aa
      v1=(x-va*t/r)/sqrt(4.0*disp*t/r)
      v2=x*va/disp
      v3=0.5*(1.0+v2+va*va*t/disp)
      v4=(x+va*t/r)/sqrt(4.0*disp*t/r)
      v5=t/(pi*disp)
      v6=(x-va*t)*(x-va*t)/(-4.0*disp*t)
      aa=a(v4)
      coeff=-v3*aa+va*sqrt(v5)
      vanfct=0.5*erfc(v1)+coeff*exp(v6)
      RETURN
      END

C-----------------------------------------------------------------------
      FUNCTION a(y)
      DOUBLE PRECISION a,y,z,p0,p1,p2,p3,p4,p5
c     a valid only for y positive
      p0=0.327591000
      p1=0.254829592
      p2=-0.284496736
      p3=1.421413741
      p4=-1.453152027
      p5=1.061405429
      z=1./(1.+p0*y)
      IF (y .lt. 3.0) THEN
         a=((((p5*z+p4)*z+p3)*z+p2)*z+p1)*z
      ELSE
         a=.5641896/(y+0.5/(y+1./(y+1.5/(y+2./(y+2.5/(y+1.))))))
      ENDIF
      RETURN
      END

C-----------------------------------------------------------------------
      FUNCTION haefct(t,x,va,disp,pi,r)
      DOUBLE PRECISION haefct,t,x,va,disp,pi,v1,v2,v4,erfc,erc,r
      v1=(x-va*t/r)/sqrt(4.0*disp*t/r)
      v2=x*va/disp
      v4=(x+va*t/r)/sqrt(4.0*disp*t/r)
      haefct=0.5*(erfc(v1)+erc(v2,v4))
      RETURN
      END

C-----------------------------------------------------------------------
      FUNCTION erfc(x)
      DOUBLE PRECISION erfc,x,expmax,xa,t
      PARAMETER (expmax=87.5)
      xa=ABS(x)
c      p0=0.327591000
      p1=0.254829592
      p2=-0.284496736
```

```
      p3=1.421413741
      p4=-1.453152027
      p5=1.061405429
      IF (xa .LT. 3.) THEN
         t=1./(1.+0.3275911*xa)
c         t=1./(1.+p0*xa)
         erfc=((((p5*t+p4)*t+p3)*t+p2)*t+p1)*t*exp(-min(x**2,expmax))
      ELSE
         erfc=.5641896/(xa+0.5/(xa+1./(xa+1.5/(xa+2./(xa+
     +   2.5/(xa+1.))))))*exp(-min(x**2,expmax))
      ENDIF
      IF (x.lt.0.) erfc=2.-erfc
      RETURN
      END
c from Haefner

C-----------------------------------------------------------------------
c      FUNCTION erc(x,y)
c      DOUBLE PRECISION erc,expmax,x,y,z,xa,t
c      PARAMETER (expmax=87.5)
c      xa=ABS(x)
c      z=y-x*x
c      IF (z .GT. expmax) THEN
c         PRINT *, 'Error in ERC: y-x**2 zu groß'
c         STOP
c      ENDIF
cc      p0=0.327591000
c      p1=0.254829592
c      p2=-0.284496736
c      p3=1.421413741
c      p4=-1.453152027
c      p5=1.061405429
c      IF (xa .LT. 3.) THEN
c         t=1./(1.+0.3275911*xa)
cc         t=1./(1.+p0*xa)
c         erc=((((p5*t+p4)*t+p3)*t+p2)*t+p1)*t*exp(max(z,-expmax))
c      ELSE
c         erc=.5641896/(xa+0.5/(xa+1./(xa+1.5/(xa+2./(xa+
c     +   2.5/(xa+1.)))))))*exp(max(z,-expmax))
c      ENDIF
c      IF (x .LT. 0.) THEN
c         IF (y .GT. expmax) THEN
c            PRINT *, 'Error in ERC: y zu groß'
c            STOP
c         ENDIF
c         erc=2.*exp(max(y,-expmax)) -erc
c      ENDIF
c      RETURN
c      END
c from Haefner but creates numerical errors

C-----------------------------------------------------------------------
      FUNCTION erc(x,y)
      DOUBLE PRECISION erc,x,y,z
      p0=0.327591000
      p1=0.254829592
      p2=-0.284496736
      p3=1.421413741
      p4=-1.453152027
      p5=1.061405429
      z=1./(1.+p0*y)
      erc=((((p5*z+p4)*z+p3)*z+p2)*z+p1)*z*exp(x-y**2)
      RETURN
      END
```

Annex 4: Listing of Input File for DTTRACER

INPUT.DAT:

```
0.5          # x      - distance (m)
10           # tin    - injection time (s)
150.0        # tmax   - max. time to calculate c(t) for
0.1          # dt     - time step how to increase t (s)
0.02         # va     - tracer velocity (m/s)
0.005        # alpha  - dispersion coefficient (m)
0.0000169    # diff   - diffusion (m2/s), <=0.0000169
1.2          # r      - retardation factor (-), >=1.0
1            # nident - 0 - van Genuchten, 1 - Haefner
```

Annex 5: Derivation of k_c, k_i, k_i/k_c Formulas for 1D and 3D Tracer Test Evaluation

The general equation to calculate the intrinsic permeability, k, from gas tracer measurements either in the laboratory or in the field is given by equation 3.40

$$k = -\frac{n \cdot \mu_g \cdot v_a}{r_2 - r_1} \cdot \int_{r_1}^{r_2} \frac{1}{\left(\frac{dp}{dr}\right)} \cdot dr \qquad \text{A5.1.}$$

To compare the differences for the permeability calculations, resulting from not considering compressibility (k_c) but assuming incompressibility (k_i) of gas/air flow in the expression of dp/dr, the appropriate analytical solutions (Ch. 3, Annex 1) have to be inserted and the quotient k_i/k_c has to be compared for different pressure differences applied.

A 5.1 Laboratory Tests (1D)

The one-dimensional analytical solution for the pressure gradient distribution (Ch. 3, Annex 1) considering compressibility

$$\frac{\partial p(r)}{\partial r} = \frac{p_2^2 - p_1^2}{2 \cdot (r_2 - r_1) \cdot \sqrt{\frac{p_2^2 - p_1^2}{r_2 - r_1} \cdot (r - r_1) + p_1^2}} \qquad \text{A5.2}$$

leads with equation A5.1 to k_c in the form of

$$k_c = -\frac{2 \cdot n \cdot \mu_g \cdot v_a}{p_2^2 - p_1^2} \cdot \int_{r_1}^{r_2} \sqrt{\frac{p_2^2 - p_1^2}{r_2 - r_1} \cdot (r - r_1) + p_1^2} \cdot dr \qquad \text{A5.3.}$$

The one-dimensional analytical solution for the pressure gradient distribution (Ch. 3, Annex 1) assuming incompressibility

$$\frac{\partial p(r)}{\partial r} = \frac{p_2 - p_1}{r_2 - r_1} \qquad \text{A5.4}$$

leads with equation A5.1 to k_i in the form of

$$k_i = -\frac{n \cdot \mu_g \cdot v_a \cdot (r_2 - r_1)}{p_2 - p_1} \qquad \text{A5.5.}$$

Thus, the quotient k_i/k_c follows to

$$\frac{k_i}{k_c} = \frac{(r_2 - r_1)(p_2 + p_1)}{\underbrace{2 \cdot \int_{r_1}^{r_2} \sqrt{\frac{p_2^2 - p_1^2}{r_2 - r_1} \cdot (r - r_1) + p_1^2} \cdot dr}_{I}} \qquad \text{A5.6.}$$

The specific solution for the integral I can be given by substituting

$$R = \frac{p_2^2 - p_1^2}{r_2 - r_1} \cdot (r - r_1) + p_1^2 \qquad \text{A5.7}$$

$$dR = \frac{p_2^2 - p_1^2}{r_2 - r_1} \cdot dr$$

$$\Rightarrow dr = \frac{r_2 - r_1}{p_2^2 - p_1^2} \cdot dR \qquad \text{A5.8}$$

$$\text{if } r = r_1 \Rightarrow R = p_1^2$$

$$\text{if } r = r_2 \Rightarrow R = p_2^2 \qquad \text{A5.9}$$

$$I = \frac{r_2 - r_1}{p_2^2 - p_1^2} \cdot \int_{p_1^2}^{p_2^2} R^{1/2} \cdot dR = \frac{2}{3} \cdot \frac{r_2 - r_1}{p_2^2 - p_1^2} \cdot \left[p_2^3 - p_1^3\right] = \frac{2}{3} \cdot \frac{(r_2 - r_1) \cdot \left(p_1^2 + p_1 \cdot p_2 + p_2^2\right)}{p_1 + p_2} \qquad \text{A5.10}$$

leading to an expression for the quotient in the form of

$$\frac{k_i}{k_c} = \frac{(r_2 - r_1)(p_2 + p_1)}{2 \cdot \frac{2}{3} \cdot \frac{(r_2 - r_1) \cdot (p_1^2 + p_1 \cdot p_2 + p_2^2)}{p_1 + p_2}} = \frac{3}{4} \cdot \frac{(p_1 + p_2)^2}{p_1^2 + p_1 \cdot p_2 + p_2^2} = \frac{3}{4} \cdot \frac{(p_1 + p_2)^2}{(p_1 + p_2)^2 - p_1 \cdot p_2} \qquad \text{A5.11.}$$

The resulting differences (k_i/k_c and percentage error $(k_i-k_c)/k_c$) from equation A5.11 for typical parameters of the laboratory measurements are shown in figure 3.10 (Ch. 3).

A 5.2 Field Tests (3D)

The three-dimensional radial analytical solution for the pressure gradient distribution (Ch. 3, Annex 1) considering compressibility

$$\frac{\partial p(r)}{\partial r} = \frac{\left(p_2^2 - p_1^2\right) \cdot r_1 \cdot r_2}{2 \cdot r^2 \cdot (r_2 - r_1) \cdot \sqrt{\frac{p_2^2 - p_1^2}{r_2 - r_1} \cdot r_2 \cdot \left(1 - \frac{r_1}{r}\right) + p_1^2}} \qquad \text{A5.12}$$

leads with equation A5.1 to k_c in the form of

$$k_c = -\frac{2 \cdot n \cdot \mu_g \cdot v_a}{\left(p_2^2 - p_1^2\right) \cdot r_1 \cdot r_2} \cdot \int_{r_1}^{r_2} r^2 \cdot \sqrt{\frac{p_2^2 - p_1^2}{r_2 - r_1} \cdot r_2 \cdot \left(1 - \frac{r_1}{r}\right) + p_1^2} \cdot dr \qquad \text{A5.13.}$$

The three-dimensional radial analytical solution for the pressure gradient distribution (Ch. 3, Annex 1) assuming incompressibility

$$\frac{\partial p(r)}{\partial r} = \frac{p_2 - p_1}{r^2 \cdot (r_2 - r_1)} \cdot r_1 \cdot r_2 \qquad \text{A5.14}$$

leads with equation A5.1 to k_i in the form of

$$k_i = -\frac{n \cdot \mu_g \cdot v_a \cdot \left(r_2^3 - r_1^3\right)}{3 \cdot (p_2 - p_1) \cdot r_1 \cdot r_2} \qquad \text{A5.15.}$$

Thus, the quotient k_i/k_c follows to

$$\frac{k_i}{k_c} = \frac{\left(r_2^3 - r_1^3\right)(p_2 + p_1)}{6 \cdot \int_{r_1}^{r_2} r \cdot \sqrt{\underbrace{\left(\frac{p_2^2 - p_1^2}{r_2 - r_1} \cdot r_2 + p_1^2\right)}_{a} \cdot r^2 \cdot \underbrace{\frac{p_2^2 - p_1^2}{r_2 - r_1}}_{b} \cdot r_1 \cdot r_2 \cdot r} \cdot dr} \qquad \text{A5.16}$$

$$\frac{k_i}{k_c} = \frac{1}{f \cdot \underbrace{\int_{r_1}^{r_2} r \cdot \sqrt{a \cdot r^2 \cdot b \cdot r} \cdot dr}_{I}} \qquad \text{A5.17,}$$

where

$$f = \frac{6}{\left(r_2^3 - r_1^3\right)(p_2 + p_1)} \qquad \text{A5.18.}$$

A general solution for the integral I is given by Abramowitz and Stegun (1972):

$$\text{if } a > 0, b \neq 0 \quad I = \frac{3b^3 \log\left(2\sqrt{a}\sqrt{ar^2 + br} + 2ar + b\right) + \sqrt{a}\sqrt{ar^2 + br} \cdot \left(16 \cdot a^2 r^2 + 4abr - 6b^2\right)}{48 \cdot a^{5/2}} \qquad \text{A5.19,}$$

$$\text{if } a < 0, b \neq 0 \quad I = \frac{\sqrt{-a} \cdot \sqrt{ar^2 + br} \cdot \left(16 \cdot a^2 \cdot r^2 + 4 \cdot a \cdot b \cdot r - 6 \cdot b^2\right) - 3 \cdot b^3 \cdot \operatorname{asin}\left(\frac{2 \cdot a \cdot r + b}{|b|}\right)}{48 \cdot \sqrt{-a} \cdot a^2} \qquad \text{A5.20,}$$

$$\text{if } a > 0, b = 0 \quad I = \frac{r^3 \cdot \sqrt{a}}{3} \qquad \text{A5.21.}$$

The resulting differences (k_i/k_c and percentage error $(k_i-k_c)/k_c$) from equation A5.17 for typical parameters of the field measurements are shown in figure 3.10 (Ch. 3).

Annex 6: Analogy between Groundwater and Gas Flow Modelling

To use a standard groundwater flow modelling package, such as MODFLOW, for the flow modelling of gases in porous media requires some boundary conditions for the gas flow which allow a comparison with the modelled flow equation in these programs.

In the case of MODFLOW the general mass flow equation for steady state groundwater flow with sources/sinks

$$\nabla.(\rho_f \cdot \vec{v}) = -\rho_f \cdot q_f \qquad \text{A6.1}$$

can be transferred with Eq. 3.9 to

$$\nabla.(K_f \cdot \nabla h) = q_f \qquad \text{A6.2}$$

which will be solved for groundwater heads, h.

For the gas pneumatic and tracer tests the general mass flow equation for steady state gas flow with sources/sinks

$$\nabla.(\rho_g \cdot \vec{v}) = -\rho_g \cdot q_g \qquad \text{A6.3}$$

would lead to a non-linear form

$$\nabla.\left(\frac{k}{\mu_g} \cdot p \cdot \nabla p\right) = q_g \qquad \text{A6.4.}$$

Under the field and laboratory conditions of a pressure difference of $\Delta p < 2 \cdot 10^2$ HPa the assumption of an incompressible gas is permitted (Tab. 3.2, Massmann, 1989) and leads to

$$\nabla.\left(\frac{k}{\mu_g} \cdot \nabla p\right) = q_g \qquad \text{A6.5.}$$

Comparing the both equation A 6.2 for water and A 6.5 for gas shows that the use of MODFLOW for the gas flow modelling is possible as long as the hydraulic conductivities, K_f, used in MODFLOW are exchanged with k/μ_g parameters. The resulting groundwater head distribution, h, has to be taken as the air pressure distribution, p. This implies that the initial values for the potential distribution are set to relatively high values, e.g. 10^5 Pa as atmospheric pressure, to avoid negative pressures due to extraction/suction of gas.

The advective transport modelling of particles in a groundwater flow field (groundwater head distribution, h) with MODPATH can similarly be used for the transport modelling of gas particles on an air flow field (air pressure distribution, p) resulting from the use of MODFLOW.

Annex 7: Measurement Data

A 7.1 *In Situ* Gas Tracer Data

filename	lithofacies	Δp_{max} [10^2 Pa]	Q_{in} [ml/s]	Δp_{in} [10^2 Pa]	Q_{out} [ml/s]	Δp_{out} [10^2 Pa]	Δp [10^2 Pa]	Δp_{min} [10^2 Pa]	l [m]	v_a [m/s]	α [m]	Diff [m^2/s]	3 dimensional k [m^2]	K_t [m/s]	k_{max} [m^2]	$K_{t\,max}$ [m/s]
1bo070	Gmm, hori.	73.4	102.0	6.3	274.0	38.3	28.8	0.1	0.500	6.90E-03	7.00E-03	1.69E-05	*5.37E-11*	4.03E-04	*1.55E-08*	1.16E-01
1bo105	Gmm, hori.	109.0	102.0	6.3	354.0	63.6	39.1	0.1	0.500	8.30E-03	7.00E-03	1.69E-05	*4.77E-11*	3.57E-04	*1.86E-08*	1.40E-01
1bo140	Gmm, hori.	144.0	102.0	6.3	418.0	88.5	49.2	0.1	0.500	9.60E-03	7.00E-03	1.69E-05	*4.36E-11*	3.28E-04	*2.15E-08*	1.62E-01
1bo170	Gmm, hori.	172.0	102.0	6.3	481.0	107.5	58.2	0.1	0.500	1.02E-02	7.00E-03	1.69E-05	*3.93E-11*	2.95E-04	*2.29E-08*	1.72E-01
1bo170b	Gmm, hori.	165.0	102.0	6.3	453.0	103.8	54.8	0.1	0.500	1.02E-02	7.00E-03	1.69E-05	*4.17E-11*	3.13E-04	*2.29E-08*	1.72E-01
2bo070	Gmm, hori.	73.4	102.0	6.3	319.0	51.7	15.3	0.1	0.500	6.60E-03	7.00E-03	1.69E-05	*9.65E-11*	7.24E-04	*1.48E-08*	1.11E-01
2bo105	Gmm, hori.	109.0	102.0	6.3	418.0	87.7	15.0	0.1	0.500	8.00E-03	7.00E-03	1.69E-05	*1.19E-10*	8.96E-04	*1.79E-08*	1.35E-01
2bo120	Gmm, hori.	124.0	102.0	6.3	452.0	103.4	14.3	0.1	0.500	8.30E-03	7.00E-03	1.69E-05	*1.30E-10*	9.76E-04	*1.86E-08*	1.40E-01
3bo070	Sh, hori.	73.4	203.0	16.7	261.0	34.8	21.9	0.1	0.820	3.90E-03	1.00E-03	1.69E-05	*1.07E-10*	8.04E-04	*2.35E-08*	1.76E-01
3bo120	Sh, hori.	121.0	102.0	6.3	444.0	99.8	14.9	0.1	0.820	2.90E-03	4.00E-03	1.69E-05	*1.17E-10*	8.80E-04	*1.75E-08*	1.31E-01
3bo130	Sh, hori.	134.0	203.0	16.7	434.0	95.3	22.0	0.1	0.820	4.60E-03	1.00E-03	1.69E-05	*1.26E-10*	9.48E-04	*2.78E-08*	2.08E-01
4bo070	Sh, hori.	73.4	203.0	16.7	258.0	34.0	22.7	0.1	0.820	4.30E-03	1.00E-03	1.69E-05	*1.14E-10*	8.56E-04	*2.59E-08*	1.95E-01
4bo120	Sh, hori.	124.0	102.0	6.3	425.0	91.5	26.2	0.1	0.820	5.30E-03	1.00E-03	1.69E-05	*1.22E-10*	9.15E-04	*3.20E-08*	2.40E-01
4bo140	Sh, hori.	141.0	203.0	16.7	430.0	93.6	30.7	0.1	0.820	6.50E-03	1.00E-03	1.69E-05	*1.28E-10*	9.58E-04	*3.92E-08*	2.94E-01
5bo110	Sh, hori.	114.0	1.3	0.1	422.0	90.2	23.8	0.1	0.820	4.30E-03	2.00E-03	1.69E-05	*1.09E-10*	8.19E-04	*2.59E-08*	1.95E-01
6bo070	Sh > Gcm, vert.	73.3	203.0	16.7	293.0	43.7	12.9	0.1	0.270	1.10E-03	1.00E-03	1.69E-05	*5.58E-12*	4.18E-05	*7.19E-10*	5.39E-03
6bo105	Sh > Gcm, vert.	109.0	203.0	16.7	395.0	79.1	13.2	0.1	0.270	1.40E-03	1.00E-03	1.69E-05	*6.92E-12*	5.19E-05	*9.15E-10*	6.87E-03
6bo110	Sh > Gcm, vert.															
6bo120	Sh > Gcm, vert.	124.0	203.0	16.7	431.0	94.0	13.3	0.1	0.270	1.45E-03	1.00E-03	1.69E-05	*7.14E-12*	5.36E-05	*9.48E-10*	7.11E-03
7bo110	Sh < Gcm, vert.	113.0	102.0	6.3	416.0	87.7	19.0	0.1	0.270	1.10E-03	1.00E-04	1.69E-05	*3.78E-12*	2.84E-05	*7.19E-10*	5.39E-03
7bo120	Sh < Gcm, vert.	124.0	203.0	16.7	414.0	86.8	20.5	0.1	0.270	1.50E-03	1.00E-04	1.69E-05	*4.78E-12*	3.59E-05	*9.81E-10*	7.36E-03
8bo070	Sh > Gcm, diag.	73.3	102.0	6.3	291.0	43.1	23.8	0.1	0.540	2.45E-02	4.00E-02	1.69E-05	*2.69E-10*	2.02E-03	*6.41E-08*	4.81E-01
8bo105	Sh > Gcm, diag.	109.0	102.0	6.3	374.0	70.9	31.7	0.1	0.540	2.90E-02	4.00E-02	1.69E-05	*2.39E-10*	1.79E-03	*7.59E-08*	5.69E-01
8bo120	Sh > Gcm, diag.	124.0	102.0	6.3	407.0	83.9	33.8	0.1	0.540							
8bo120b	Sh > Gcm, diag.	124.0	102.0	6.3	404.0	82.7	35.0	0.1	0.540	3.00E-02	4.00E-02	1.69E-05	*2.24E-10*	1.68E-03	*7.85E-08*	5.89E-01
9bo070	Sh < Gcm, diag.	73.3	102.0	6.3	312.0	49.5	17.5	0.1	0.540	2.35E-02	4.00E-02	1.69E-05	*3.52E-10*	2.64E-03	*6.15E-08*	4.61E-01
9bo110	Sh < Gcm, diag.	114.0	102.0	6.3	413.0	86.4	21.3	0.1	0.540	2.85E-02	4.00E-02	1.69E-05	*3.50E-10*	2.63E-03	*7.46E-08*	5.59E-01
10bo020	Sh, hori.	22.5	102.0	6.3	77.3	3.2	13.3	0.1	0.590	4.50E-03	2.50E-02	1.69E-05	*1.06E-10*	7.94E-04	*1.41E-08*	1.05E-01
10bo030	Sh, hori.	32.9	102.0	6.3	149.0	11.5	15.1	0.1	0.590	7.00E-03	2.00E-02	1.69E-05	*1.45E-10*	1.09E-03	*2.19E-08*	1.64E-01
10bo040	Sh, hori.	43.0	102.0	6.3	198.0	20.1	16.5	0.1	0.590	8.40E-03	2.00E-02	1.69E-05	*1.59E-10*	1.19E-03	*2.62E-08*	1.97E-01
10bo050	Sh, hori.	53.1	102.0	6.3	237.0	28.7	18.1	0.1	0.590	9.30E-03	2.00E-02	1.69E-05	*1.61E-10*	1.21E-03	*2.90E-08*	2.18E-01
10bo060	Sh, hori.	63.2	102.0	6.3	272.0	37.7	19.1	0.1	0.590	1.00E-02	2.00E-02	1.69E-05	*1.63E-10*	1.22E-03	*3.12E-08*	2.34E-01
10bo070	Sh, hori.	73.3	102.0	6.3	304.0	47.0	19.9	0.1	0.590	1.10E-02	2.00E-02	1.69E-05	*1.72E-10*	1.29E-03	*3.44E-08*	2.58E-01
10bo080	Sh, hori.	83.4	102.0	6.3	333.0	56.3	20.7	0.1	0.590	1.30E-02	2.00E-02	1.69E-05	*1.86E-10*	1.47E-03	*4.06E-08*	3.05E-01
10bo100	Sh, hori.	104.0	102.0	6.3	385.0	75.2	22.5	0.1	0.590	1.30E-02	2.00E-02	1.69E-05	*1.80E-10*	1.35E-03	*4.06E-08*	3.05E-01
10bo110	Sh, hori.	114.0	102.0	6.3	410.0	85.2	22.5	0.1	0.590	1.40E-02	2.00E-02	1.69E-05	*1.94E-10*	1.46E-03	*4.37E-08*	3.28E-01
10bo120	Sh, hori.	121.0	102.0	6.3	430.0	93.6	21.1	0.1	0.590	1.45E-02	2.00E-02	1.69E-05	*2.15E-10*	1.61E-03	*4.53E-08*	3.40E-01
10bo130	Sh, hori.	131.0	162.0	12.0	428.0	92.7	26.3	0.1	0.590	1.70E-02	2.00E-02	1.69E-05	*2.02E-10*	1.52E-03	*5.31E-08*	3.98E-01
10bo140	Sh, hori.	140.0	203.0	16.7	429.0	93.2	30.1	0.1	0.590	1.85E-02	2.00E-02	1.69E-05	*1.92E-10*	1.44E-03	*5.78E-08*	4.33E-01
11bo070	Sh, hori.	73.3	102.0	6.3	274.0	38.3	28.7	0.1	0.590	1.05E-02	2.00E-02	1.69E-05	*1.14E-10*	8.57E-04	*3.28E-08*	2.46E-01
11bo130	Sh, hori.	134.0	102.0	6.3	403.0	82.3	45.4	0.1	0.590	1.50E-02	2.00E-02	1.69E-05	*1.03E-10*	7.74E-04	*4.68E-08*	3.51E-01
12bo140c	Sh, hori.	144.0	152.0	10.9	398.0	80.3	52.8	0.1	0.590	1.65E-02	2.00E-02	1.69E-05	*9.76E-11*	7.32E-04	*5.15E-08*	3.87E-01
13bo050	Gcm, vert.	52.9	102.0	6.3	297.0	44.9	1.7	0.1	0.190	7.00E-03	5.00E-02	1.69E-05	*1.36E-10*	1.02E-03	*2.26E-09*	1.70E-02
13bo070	Gcm, vert.	73.1	102.0	6.3	362.0	66.5	0.3	0.1	0.190							
13bo070b	Gcm, vert.	73.1	102.0	6.3	356.0	64.3	2.4	0.1	0.190	7.50E-03	5.00E-02	1.69E-05	*9.82E-11*	7.44E-04	*2.43E-09*	1.82E-02
13bo100	Gcm, vert.	98.9	102.0	6.3	428.0	92.7	-0.2	0.1	0.190	9.50E-03	5.00E-02	1.69E-05	*-1.79E-09*	-1.34E-02	*3.07E-09*	2.31E-02
13bo100b	Gcm, vert.	99.0	102.0	6.3	428.0	92.7	-0.1	0.1	0.190							
13bo100c	Gcm, vert.	102.0	102.0	6.3	424.0	91.0	4.6	0.1	0.190							
13bo100d	Gcm, vert.	101.0	102.0	6.3	423.0	90.6	4.1	0.1	0.190	1.10E-02	3.00E-02	1.69E-05	*8.75E-11*	6.56E-04	*3.56E-09*	2.67E-02
13bo100e	Gcm, vert.	101.0	102.0	6.3	423.0	90.6	4.1	0.1	0.190	1.10E-02	3.00E-02	1.69E-05	*8.75E-11*	6.56E-04	*3.56E-09*	2.67E-02
14bo050	Gcm, vert.	53.1	102.0	6.3	218.0	24.4	22.4	0.1	0.190	8.00E-03	1.40E-02	1.69E-05	*1.15E-11*	8.66E-05	*2.59E-09*	1.94E-02
14bo070	Gcm, vert.	73.3	102.0	6.3	282.0	40.5	26.5	0.1	0.190	8.00E-03	2.50E-02	1.69E-05	*9.78E-12*	7.34E-05	*2.59E-09*	1.94E-02
14bo100	Gcm, vert.	104.0	102.0	6.3	406.0	84.3	13.3	0.1	0.190	1.10E-02	2.00E-02	1.69E-05	*2.67E-11*	2.00E-04	*3.56E-09*	2.67E-02
14bo100b	Gcm, vert.	104.0	102.0	6.3	383.0	66.9	30.8	0.1	0.190	1.35E-02	2.00E-02	1.69E-05	*1.42E-11*	1.06E-04	*4.37E-09*	3.28E-02
17bo100	Gcm, vert.	103.0	102.0	6.3	406.0	83.5	13.2	0.1	0.190	1.30E-02	2.00E-02	1.69E-05	*3.20E-11*	2.40E-04	*4.21E-09*	3.15E-02
15bo050	Gcm, vert.	53.1	102.0	6.3	206.0	21.8	25.0	0.1	0.210	4.30E-03	2.00E-02	1.69E-05	*8.80E-12*	5.10E-05	*1.70E-09*	1.28E-02
15bo070	Gcm, vert.	73.3	102.0	6.3	273.0	38.0	29.0	0.1	0.210	5.30E-03	2.00E-02	1.69E-05	*7.23E-12*	5.42E-05	*2.10E-09*	1.57E-02
15bo100	Gcm, vert.	104.0	102.0	6.3	362.0	66.5	31.2	0.1	0.210	6.40E-03	2.00E-02	1.69E-05	*8.12E-12*	6.09E-05	*2.53E-09*	1.90E-02
15bo120	Gcm, vert.	124.0	102.0	6.3	413.0	86.4	31.3	0.1	0.210	7.30E-03	2.00E-02	1.69E-05	*9.23E-12*	6.92E-05	*2.89E-09*	2.16E-02
15bo070	Gcm, vert.	73.3	102.0	6.3	357.0	64.7	2.3	0.1	0.210	4.20E-03	1.00E-02	1.69E-05	*7.26E-11*	5.44E-04	*1.66E-09*	1.25E-02
15bo100	Gcm, vert.	99.0	102.0	6.3	410.0	85.2	7.5	0.1	0.210	4.40E-03	2.00E-02	1.69E-05	*2.31E-11*	1.74E-04	*1.74E-09*	1.30E-02
16bo100b	Gcm, vert.	98.7	102.0	6.3	410.0	85.2	5.2	0.1	0.210	4.90E-03	1.00E-02	1.69E-05	*3.71E-11*	2.78E-04	*1.94E-09*	1.45E-02
18bo110	Gcm, vert.	113.0	102.0	6.3	405.0	83.1	23.6	0.1	0.210	5.40E-03	1.00E-02	1.69E-05	*9.06E-12*	6.79E-05	*2.13E-09*	1.60E-02
18bo100	Gcm, hori.	104.0	102.0	6.3	404.0	82.7	15.0	0.1	0.770	5.00E-03	6.00E-02	1.69E-05	*1.78E-10*	1.33E-03	*2.66E-08*	2.00E-01
18bo100b	Gcm, hori.	104.0	102.0	6.3	402.0	81.9	15.8	0.1	0.770	5.50E-03	6.00E-02	1.69E-05	*1.85E-10*	1.39E-03	*2.93E-08*	2.19E-01
18bo100c	Gcm, hori.	104.0	203.0	16.7	245.0	30.7	56.6	0.1	0.770	5.80E-03	6.00E-02	1.69E-05	*5.45E-11*	4.09E-04	*3.09E-08*	2.31E-01
19bo100	Gcm, hori.	98.1	102.0	6.3	409.0	84.7	7.0	0.1	0.770	7.30E-03	3.00E-02	1.69E-05	*5.52E-10*	4.14E-03	*3.88E-08*	2.91E-01
19bo100b	Gcm, hori.	104.0	203.0	16.7	406.0	84.3	3.0	0.1	0.770	1.05E-02	3.00E-02	1.69E-05	*1.87E-09*	1.41E-02	*5.59E-08*	4.19E-01
20bo100	Gcm, hori.	102.0	203.0	16.7	409.0	84.7	0.6	0.1	0.820	6.00E-03	7.00E-02	1.69E-05	*6.37E-09*	4.78E-02	*3.62E-08*	2.72E-01
21bo100	Gcm, hori.	101.0	203.0	16.7	407.0	83.9	0.4	0.1	0.820	7.20E-03	7.00E-02	1.69E-05	*1.11E-08*	8.35E-02	*4.34E-08*	3.26E-01
22bo100	Gcm, diag.	95.3	203.0	16.7	410.0	85.2	-6.5	0.1	0.800	2.50E-03	5.00E-02	1.69E-05	*-2.19E-10*	-1.65E-03	*1.44E-08*	1.08E-01
23bo100	Gcm, diag.	94.2	203.0	16.7	408.0	84.3	-6.8	0.1	0.800	*1.10E-03*	*1.50E-01*	1.69E-05	*-9.26E-11*	-8.95E-04	*6.32E-09*	4.74E-02
24bo100	Gcm, diag.	95.6	203.0	16.7	407.0	83.9	-5.0	0.1	0.830	7.00E-03	4.00E-02	1.69E-05	*-8.64E-10*	-6.48E-03	*4.33E-08*	3.25E-01

Tab. A7.1: Listing of all measured *in situ* gas tracer data, Böhringen, SW Germany, bold: data used in further evaluation

filename	lithofacies	Δp_{meas} [10^2 Pa]	Q_{in} [ml/s]	Δp_{in} [10^2 Pa]	Q_{out} [ml/s]	Δp_{out} [10^2 Pa]	Δp [10^2 Pa]	Δp_{min} [10^2 Pa]	l [m]	v_a [m/s]	α [m]	Diff [m^2/s]	3 dimensional k [m^2]	K_t [m/s]	k_{max} [m^2]	K_{tmax} [m/s]
1fr140	Gcho, hori.	144.0	102.0	6.3	506.0	129.4	8.3	0.1	0.980	4.50E-03	1.10E-01	1.69E-05	*4.68E-10*	3.51E-03	*3.88E-08*	2.91E-01
2fr105	Gcho, hori.	109.0	102.0	6.3	440.0	98.0	4.7	0.1	0.980	5.00E-03	1.10E-01	1.69E-05	*9.19E-10*	6.89E-03	*4.31E-08*	3.23E-01
2fr140	Gcho, hori.	144.0	102.0	6.3	510.0	131.4	6.2	0.1	0.980	5.60E-03	1.10E-01	1.69E-05	*7.72E-10*	5.79E-03	*4.83E-08*	3.62E-01
2fr105	Gcho, hori.	109.0	99.8	6.1	450.0	102.5	0.4	0.1	0.980	3.80E-03	1.00E-01	1.69E-05	*8.37E-09*	6.28E-02	*3.27E-08*	2.46E-01
3fr105	Gcho, hori.	109.0	99.8	6.1	450.0	102.5	0.4	0.1	0.980	3.80E-03	1.00E-01	1.69E-05	*-9.30E-08*	-6.97E-01	*3.53E-08*	2.65E-01
3fr140	Gcho, hori.	141.0	98.0	6.0	517.0	135.0	0.0	0.1	0.980	4.10E-03	1.00E-01	1.69E-05				
4fr035	Gch, hori.	38.0	102.0	6.3	248.0	31.4	0.3	0.1	0.380	3.50E-03	5.00E-01	1.69E-05	*1.78E-09*	1.34E-02	*4.53E-09*	3.40E-02
4fr070	Gch, hori.	73.1	102.0	6.3	377.0	72.1	-5.3	0.1	0.380	4.80E-03	5.00E-01	1.69E-05	*-1.17E-10*	-8.79E-04	*6.22E-09*	4.66E-02
4fr105	Gch, hori.	109.0	102.0	6.3	470.0	111.7	-9.0	0.1	0.380	6.00E-03	5.00E-01	1.69E-05	*-8.59E-11*	-6.45E-04	*7.77E-09*	5.83E-02
4fr140	Gch, hori.	144.0	102.0	6.3	547.0	151.1	-13.4	0.1	0.380	7.00E-03	5.00E-01	1.69E-05	*-6.76E-11*	-5.07E-04	*9.07E-09*	6.80E-02
5fr070	Gch, hori.	73.2	202.0	16.6	337.0	57.7	-1.1	0.1	0.380	5.00E-03	5.00E-01	1.69E-05	*-6.12E-10*	-4.59E-03	*6.48E-09*	4.86E-02
5fr105	Gch, hori.	109.0	202.0	16.6	440.0	98.0	-4.7	0.1	0.380	6.50E-03	5.00E-01	1.69E-05	*-1.68E-10*	-1.26E-03	*1.10E-08*	8.26E-02
5fr140	Gch, hori.	144.0	202.0	16.6	515.0	134.0	-6.6	0.1	0.380	9.00E-03	6.00E-01	1.69E-05	*-1.64E-10*	-1.23E-03	*1.17E-08*	8.75E-02
5fr150	Gch, hori.	154.0	202.0	16.6	535.0	144.6	-7.1	0.1	0.380	7.50E-03	5.00E-01	1.69E-05	*-2.94E-10*	-2.21E-03	*9.72E-09*	7.29E-02
6fr140	Gch, hori.	144.0	302.0	30.8	480.0	118.5	-3.3	0.1	0.380	9.00E-03	5.00E-01	1.69E-05	*-2.80E-10*	-2.10E-03	*1.17E-08*	8.75E-02
6fr150	Gch, hori.	154.0	302.0	30.8	502.0	127.4	-4.2	0.1	0.380	9.00E-03	2.00E+00	1.69E-05	*-5.51E-10*	-4.14E-03	*1.17E-08*	8.75E-02
7fr140	Gch, hori.	144.0	404.0	49.4	437.0	98.7	-2.1	0.1	0.380	9.00E-03	2.00E+00	1.69E-05	*8.62E-12*	4.97E-05	*1.68E-09*	1.26E-02
8fr140	Gch, hori.	144.0	475.0	64.9	325.0	53.7	25.4	0.1	0.380	1.30E-03	2.00E+00	1.69E-05	*5.56E-11*	4.17E-04	*1.30E-09*	9.72E-03
9fr035	Gch, hori.	38.1	102.0	6.3	240.0	29.4	2.3	0.1	0.380	1.00E-03	2.00E+00	1.69E-05	*-2.18E-10*	-1.64E-03	*1.94E-09*	1.46E-02
9fr070	Gch, hori.	73.4	102.0	6.3	366.0	68.0	-0.9	0.1	0.380	1.50E-03	2.00E+00	1.69E-05	*-6.40E-11*	-4.80E-04	*2.20E-09*	1.65E-02
9fr105	Gch, hori.	109.0	102.0	6.3	458.0	106.1	-3.4	0.1	0.380	1.70E-03	2.00E+00	1.69E-05	*-3.97E-11*	-2.98E-04	*2.46E-09*	1.85E-02
9fr140	Gch, hori.	142.0	102.0	6.3	530.0	141.9	-6.2	0.1	0.380	1.90E-03	2.00E+00	1.69E-05				
10fr070	Gcho, vert.	73.3	102.0	6.3	360.0	65.8	1.2	0.1	0.600	5.00E-03	1.20E-01	1.69E-05	*1.34E-09*	1.01E-02	*1.61E-08*	1.21E-01
10fr105	Gcho, vert.	109.0	102.0	6.3	452.0	103.4	-0.7	0.1	0.600	6.00E-03	1.20E-01	1.69E-05	*-2.78E-09*	-2.09E-02	*1.94E-08*	1.45E-01
10fr140	Gcho, vert.	141.0	102.0	6.3	521.0	137.1	-2.5	0.1	0.600	7.00E-03	1.20E-01	1.69E-05	*-9.22E-10*	-6.92E-03	*2.26E-08*	1.70E-01
11fr070	Gcho, vert.	73.4	102.0	6.3	360.0	65.8	1.3	0.1	0.600	4.20E-03	1.00E-01	1.69E-05	*1.04E-09*	7.80E-03	*1.36E-08*	1.02E-01
11fr105	Gcho, vert.	109.0	102.0	6.3	449.0	102.0	0.7	0.1	0.600	5.80E-03	1.00E-01	1.69E-05	*2.82E-09*	2.12E-02	*1.87E-08*	1.41E-01
11fr140	Gcho, vert.	141.0	102.0	6.3	516.0	134.5	0.2	0.1	0.600	6.50E-03	9.00E-02	1.69E-05	*1.36E-08*	1.02E-01	*2.10E-08*	1.57E-01
12fr140	Gmh, vert.	142.0	102.0	6.3	515.0	134.0	1.7	0.1	0.320							
13fr150	Gmh, vert.	151.0	102.0	6.3	508.0	130.4	14.3	0.1	0.320	1.00E-03	8.00E-02	1.69E-05	*6.44E-12*	4.83E-05	*9.19E-10*	6.89E-03
14fr190	Gmh, vert.	194.0	102.0	6.3	507.0	129.9	57.8	0.1	0.320	1.80E-03	8.00E-02	1.69E-05	*2.86E-12*	2.15E-05	*1.65E-09*	1.24E-02
15fr035	Gmhb, hori.	38.1	102.0	6.3	217.0	24.1	7.6	0.1	0.320	4.00E-03	6.00E-02	1.69E-05	*4.81E-11*	3.60E-04	*3.67E-09*	2.76E-02
15fr070	Gmhb, hori.	73.4	102.0	6.3	344.0	60.1	7.0	0.1	0.320	6.00E-03	6.00E-02	1.69E-05	*7.90E-11*	5.92E-04	*5.51E-09*	4.13E-02
15fr105	Gmhb, hori.	109.0	102.0	6.3	434.0	95.3	7.3	0.1	0.320	6.00E-03	9.00E-02	1.69E-05	*7.52E-11*	5.64E-04	*5.51E-09*	4.13E-02
15fr140	Gmhb, hori.	144.0	102.0	6.3	506.0	129.4	8.3	0.1	0.320	5.50E-03	1.30E-01	1.69E-05	*6.09E-11*	4.57E-04	*5.05E-09*	3.79E-02
16fr035	Gmhb, hori.	38.3	102.0	6.3	210.0	22.6	9.4	0.1	0.320	4.50E-03	6.00E-02	1.69E-05	*4.42E-11*	3.31E-04	*4.13E-09*	3.10E-02
16fr070	Gmhb, hori.	73.4	102.0	6.3	326.0	54.0	13.1	0.1	0.320	5.50E-03	7.00E-02	1.69E-05	*3.87E-11*	2.90E-04	*5.05E-09*	3.79E-02
16fr105	Gmhb, hori.	109.0	102.0	6.3	413.0	86.4	16.3	0.1	0.320	5.50E-03	1.00E-01	1.69E-05	*3.10E-11*	2.33E-04	*5.05E-09*	3.79E-02
16fr140	Gmhb, hori.	144.0	102.0	6.3	482.0	117.5	20.2	0.1	0.320	4.50E-03	1.70E-01	1.69E-05	*2.04E-11*	1.53E-04	*4.13E-09*	3.10E-02
16fr158	Gmhb, hori.	158.0	102.0	6.3	508.0	129.4	22.3	0.1	0.320	5.50E-03	1.40E-01	1.69E-05	*2.27E-11*	1.70E-04	*5.05E-09*	3.79E-02
17fr070	Gmh, vert.	73.3	102.0	6.3	333.0	56.3	10.6	0.1	0.190	1.70E-03	1.20E-01	1.69E-05	*5.17E-12*	3.88E-05	*5.50E-10*	4.13E-03
17fr105	Gmh, vert.	109.0	102.0	6.3	433.0	94.9	7.8	0.1	0.190	2.20E-03	1.20E-01	1.69E-05	*9.17E-12*	6.88E-05	*7.12E-10*	5.34E-03
17fr150a	Gmh, vert.	154.0	102.0	6.3	533.0	143.5	4.2	0.1	0.190	2.50E-03	1.20E-01	1.69E-05	*1.93E-11*	1.45E-04	*8.09E-10*	6.07E-03
17fr150b	Gmh, vert.	154.0	102.0	6.3	531.0	142.4	5.3	0.1	0.190	2.50E-03	1.20E-01	1.69E-05	*1.54E-11*	1.15E-04	*8.09E-10*	6.07E-03
17fr150c	Gmh, vert.	154.0	102.0	6.3	528.0	140.8	6.9	0.1	0.190	2.90E-03	1.20E-01	1.69E-05	*1.37E-11*	1.03E-04	*9.38E-10*	7.04E-03
18fr035	Gmh, vert.	38.1	102.0	6.3	205.0	21.6	10.2	0.1	0.190	2.60E-03	5.00E-02	1.69E-05	*8.87E-12*	6.66E-05	*9.06E-10*	6.79E-03
18fr070	Gmh, vert.	73.5	102.0	6.3	326.0	54.0	13.2	0.1	0.190	2.50E-03	1.00E-01	1.69E-05	*6.15E-12*	4.61E-05	*8.09E-10*	6.07E-03
18fr105	Gmh, vert.	109.0	102.0	6.3	413.0	86.4	16.3	0.1	0.190	2.80E-03	1.00E-01	1.69E-05	*5.57E-12*	4.17E-05	*9.06E-10*	6.79E-03
18fr150	Gmh, vert.	154.0	102.0	6.3	505.0	128.9	18.8	0.1	0.190	2.50E-03	1.90E-01	1.69E-05	*4.30E-12*	3.23E-05	*8.09E-10*	6.07E-03
19fr070	Gmh, diag.	73.3	102.0	6.3	336.0	58.0	8.9	0.1	0.600	2.30E-03	4.00E-01	1.69E-05	*8.31E-11*	6.23E-04	*7.43E-09*	5.57E-02
19fr105	Gmh, diag.	109.0	102.0	6.3	430.0	93.6	9.1	0.1	0.600	2.20E-03	5.00E-01	1.69E-05	*7.84E-11*	5.88E-04	*7.11E-09*	5.33E-02
19fr150	Gmh, diag.	150.0	102.0	6.3	512.0	132.5	11.2	0.1	0.600	2.40E-03	5.00E-01	1.69E-05	*6.91E-11*	5.18E-04	*7.75E-09*	5.81E-02
20fr070	Gmh, diag.	73.3	102.0	6.3	337.0	57.7	9.3	0.1	0.600	1.70E-03	5.00E-01	1.69E-05	*5.92E-11*	4.44E-04	*5.49E-09*	4.12E-02
20fr105	Gmh, diag.	109.0	102.0	6.3	427.0	92.3	10.4	0.1	0.600	2.10E-03	5.00E-01	1.69E-05	*6.55E-11*	4.91E-04	*6.78E-09*	5.09E-02
20fr140	Gmh, diag.	144.0	102.0	6.3	499.0	125.8	11.8	0.1	0.600	2.40E-03	5.00E-01	1.69E-05	*6.55E-11*	4.92E-04	*7.75E-09*	5.81E-02
20fr150	Gmh, diag.	149.0	102.0	6.3	509.0	130.9	11.8	0.1	0.600	2.40E-03	5.00E-01	1.69E-05	*6.59E-11*	4.94E-04	*7.75E-09*	5.81E-02
21fr070	Gmh, hori.	73.3	102.0	6.3	329.0	55.0	12.0	0.1	0.680	1.75E-02	5.00E-02	1.69E-05	*6.07E-10*	4.55E-03	*7.26E-08*	5.45E-01
21fr105	Gmh, hori.	109.0	102.0	6.3	417.0	88.1	14.6	0.1	0.680	2.00E-02	5.00E-02	1.69E-05	*5.68E-10*	4.26E-03	*8.30E-08*	6.22E-01
21fr150	Gmh, hori.	153.0	102.0	6.3	503.0	127.9	18.8	0.1	0.680							
21fr150b	Gmh, hori.	153.0	102.0	6.3	505.0	128.9	17.8	0.1	0.680							
21fr150c	Gmh, hori.	153.0	102.0	6.3	505.0	128.9	17.8	0.1	0.680	2.30E-02	5.00E-02	1.69E-05	*5.36E-10*	4.02E-03	*9.54E-08*	7.16E-01
22fr070	Gmh, hori.	73.4	102.0	6.3	321.0	52.4	14.7	0.1	0.680	1.90E-02	5.00E-02	1.69E-05	*5.37E-10*	4.03E-03	*7.88E-08*	5.91E-01
22fr105	Gmh, hori.	109.0	102.0	6.3	407.0	83.9	18.8	0.1	0.680	2.20E-02	5.00E-02	1.69E-05	*4.87E-10*	3.65E-03	*9.13E-08*	6.85E-01
22fr150	Gmh, hori.	154.0	102.0	6.3	495.0	123.8	23.8	0.1	0.680	2.50E-02	5.00E-02	1.69E-05	*4.35E-10*	3.27E-03	*1.04E-07*	7.78E-01
23fr150	Gmh, diag.	154.0	102.0	6.3	496.0	124.3	23.3	0.1	0.600	4.40E-03	7.00E-02	1.69E-05	*6.09E-11*	4.57E-04	*1.42E-08*	1.07E-01
24fr070	Gcpo, hori.	73.4	102.0	6.3	325.0	53.7	13.4	0.1	0.630	7.00E-03	3.00E-02	1.69E-05	*1.85E-10*	1.40E-03	*2.49E-08*	1.87E-01
24fr105	Gcpo, hori.	109.0	102.0	6.3	408.0	84.3	16.3	0.1	0.630	8.50E-03	3.00E-02	1.69E-05	*1.65E-10*	1.24E-03	*3.03E-08*	2.27E-01
24fr140	Gcpo, hori.	144.0	102.0	6.3	475.0	114.1	23.6	0.1	0.630	9.00E-03	3.50E-02	1.69E-05	*1.36E-10*	1.02E-03	*3.20E-08*	2.40E-01
24fr170	Gcpo, hori.	174.0	102.0	6.3	519.0	136.1	31.6	0.1	0.630	1.00E-02	3.50E-02	1.69E-05	*1.13E-10*	8.45E-04	*3.56E-08*	2.67E-01
24fr170b	Gcpo, hori.	174.0	102.0	6.3	517.0	135.0	32.6	0.1	0.630	1.00E-02	3.50E-02	1.69E-05	*1.09E-10*	8.18E-04	*3.56E-08*	2.67E-01
24fr170c	Gcpo, hori.	174.0	102.0	6.3	513.0	133.0	34.7	0.1	0.630	8.50E-03	5.00E-02	1.69E-05	*8.72E-11*	6.54E-04	*3.03E-08*	2.27E-01
25fr070	Gcpo, hori.	73.4	102.0	6.3	355.0	84.0	3.1	0.1	0.630	9.00E-03	5.00E-02	1.69E-05	*1.03E-09*	7.74E-03	*3.20E-08*	2.40E-01
25fr105	Gcpo, hori.	109.0	102.0	6.3	447.0	101.1	1.6	0.1	0.630	1.00E-02	5.00E-02	1.69E-05	*2.28E-09*	1.71E-02	*3.56E-08*	2.67E-01
25fr140	Gcpo, hori.	144.0	102.0	6.3	525.0	139.2	-1.6	0.1	0.630	1.00E-02	5.00E-02	1.69E-05	*-2.29E-09*	-1.72E-02	*3.56E-08*	2.67E-01
25fr140b	Gcpo, hori.	144.0	102.0	6.3	525.0	139.2	-1.6	0.1	0.630	1.10E-02	5.00E-02	1.69E-05	*-2.52E-09*	-1.89E-02	*3.92E-08*	2.94E-01
26fr070	Gcpo > Gmpb, vert.	73.4	102.0	6.3	284.0	41.1	26.0	0.1	0.280	3.30E-03	6.00E-03	1.69E-05	*8.93E-12*	6.70E-05	*2.32E-09*	1.74E-02
26fr105	Gcpo > Gmpb, vert.	109.0	102.0	6.3	334.0	58.7	46.0	0.1	0.280	4.00E-03	7.00E-03	1.69E-05	*6.12E-12*	4.59E-05	*2.81E-09*	2.11E-02
26fr140	Gcpo > Gmpb, vert.	144.0	102.0	6.3	375.0	71.3	56.4	0.1	0.280	4.50E-03	1.10E-02	1.69E-05	*4.77E-12*	3.58E-05	*3.16E-09*	2.37E-02
26fr180	Gcpo > Gmpb, vert.	184.0						0.1	0.280							
26fr180b	Gcpo > Gmpb, vert.	184.0	102.0	6.3	475.0	114.1	83.6	0.1	0.280	5.50E-03	1.40E-02	1.69E-05	*6.08E-12*	4.56E-05	*3.87E-09*	2.90E-02
27fr140	Gcpo < Gmpb, vert.	142.0	102.0	6.3	520.0	136.6	-0.9	0.1	0.280	1.50E-03	1.00E-02	1.69E-05	*-1.14E-10*	-8.53E-04	*1.05E-09*	7.91E-03
27fr140b	Gcpo < Gmpb, vert.	141.0	102.0	6.3	517.0	135.0	-0.4	0.1	0.280	1.50E-03	1.00E-02	1.69E-05	*-2.89E-10*	-2.17E-03	*1.05E-09*	7.91E-03
27fr150	Gcpo < Gmpb, vert.	148.0	102.0	6.3	520.0	136.6	3.1	0.1	0.280	1.40E-03	1.00E-02	1.69E-05	*3.20E-11*	2.40E-04	*9.84E-10*	7.38E-03
28fr070	Gmpb, hori.	73.3	102.0	6.3	248.0	31.4	35.8	0.1	0.380	5.50E-03	4.50E-02	1.69E-05	*2.00E-11*	1.50E-04	*7.12E-09*	5.34E-02
28fr105	Gmpb, hori.	109.0	102.0	6.3	318.0	51.4	51.3	0.1	0.380	6.50E-03	4.50E-02	1.69E-05	*1.64E-11*	1.23E-04	*8.42E-09*	6.32E-02
28fr140	Gmpb, hori.	144.0	102.0	6.3	389.0	76.7	61.0	0.1	0.380	7.50E-03	4.50E-02	1.69E-05	*1.59E-11*	1.20E-04	*9.72E-09*	7.29E-02
28fr190	Gmpb, hori.	194.0	102.0	6.3	466.0	109.8	77.8	0.1	0.380	8.50E-03	4.50E-02	1.69E-05	*1.41E-11*	1.06E-04	*1.10E-08*	8.26E-02
28fr190b	Gmpb, hori.	194.0	102.0	6.3	470.0	111.7	76.0	0.1	0.380	8.50E-03	4.50E-02	1.69E-05	*1.45E-11*	1.09E-04	*1.10E-08*	8.26E-02
29fr070	Gmpb, hori.	73.3	102.0	6.3	245.0	30.7	36.3	0.1	0.380	5.20E-03	4.50E-02	1.69E-05	*1.86E-11*	1.39E-04	*6.74E-09*	5.05E-02
29fr105	Gmpb, hori.	109.0	102.0	6.3	281.0	40.2	62.4	0.1	0.380	6.50E-03	4.50E-02	1.69E-05	*1.35E-11*	1.01E-04	*8.42E-09*	6.32E-02
29fr140	Gmpb, hori.	144.0	102.0	6.3	356.0	64.3	73.3	0.1	0.380	7.50E-03	4.50E-02	1.69E-05	*1.32E-11*	9.94E-05	*9.72E-09*	7.29E-02
29fr190	Gmpb, hori.	194.0	102.0	6.3	424.0	91.0	98.6	0.1	0.380	1.00E-02	3.00E-02	1.69E-05	*1.34E-11*	1.01E-04	*1.30E-08*	9.72E-02
30fr070	Gmpb > Gcpo, vert.	73.3	102.0	6.3	312.0	49.5	17.5	0.1	0.230	4.60E-03	1.20E-02	1.69E-05	*1.25E-11*	9.37E-05	*2.18E-09*	1.64E-02
30fr105	Gmpb > Gcpo, vert.	109.0	102.0	6.3	399.0	80.7	22.0	0.1	0.230	5.50E-03	1.20E-02	1.69E-05	*1.19E-11*	8.90E-05	*2.61E-09*	1.96E-02
30fr140	Gmpb > Gcpo, vert.	144.0	102.0	6.3	488.0	110.8	28.9	0.1	0.230	5.80E-03	1.50E-02	1.69E-05	*1.02E-11*	7.67E-05	*2.75E-09*	2.06E-02
30fr150	Gmpb > Gcpo, vert.	154.0	102.0	6.3	487.0	119.9	27.8	0.1	0.230	6.30E-03	1.20E-02	1.69E-05	*1.06E-11*	8.07E-05	*2.99E-09*	2.24E-02
30fr160	Gmpb > Gcpo, vert.	163.0	102.0	6.3	502.0	127.4	29.3	0.1	0.230	5.70E-03	1.60E-02	1.69E-05	*9.22E-12*	6.92E-05	*2.70E-09*	2.03E-02
31fr070	Gmpb < Gcpo, vert.	73.3	102.0	6.3	242.0	29.9	37.0	0.1	0.230	3.40E-03	2.40E-02	1.69E-05	*4.35E-12*	3.27E-05	*1.61E-09*	1.21E-02
31fr105	Gmpb < Gcpo, vert.	109.0	102.0	6.3	322.0	52.7	50.0	0.1	0.230	4.70E-03	2.40E-02	1.69E-05	*4.46E-12*	3.35E-05	*2.23E-09*	1.67E-02
31fr140	Gmpb < Gcpo, vert.	144.0	102.0	6.3	386.0	75.5	62.1	0.1	0.230	5.70E-03	2.40E-02	1.69E-05	*4.35E-12*	3.26E-05	*2.70E-09*	2.00E-02
31fr160	Gmpb < Gcpo, vert.	184.0	102.0	6.3	451.0	102.9	74.8	0.1	0.230	7.00E-03	2.20E-02	1.69E-05	*4.44E-12*	3.33E-05	*3.32E-09*	2.46E-02
32fr180c	Gmpb < Gcpo, vert.	184.0	202.0	16.6	399.0	80.7	86.8	0.1	0.230							
33fr070	Gcpo, hori.	73.3	102.0	6.3	373.0	70.6	-3.6	0.1	0.550	5.20E-03	1.00E-01	1.69E-05	*-3.92E-10*	-2.94E-03	*1.41E-08*	1.06E-01
33fr105	Gcpo, hori.	109.0	102.0	6.3	465.0	109.4	-8.7	0.1	0.550	6.30E-03	1.00E-01	1.69E-05	*-2.55E-10*	-1.92E-03	*1.71E-08*	1.28E-01
33fr140	Gcpo, hori.	144.0	102.0	6.3	524.0	138.7	-1.0	0.1	0.550	7.50E-03	1.00E-01	1.69E-05	*-1.98E-09*	-1.49E-02	*2.04E-08*	1.53E-01
33fr140b	Gcpo, hori.	140.0	102.0	6.3	526.0	139.8	-6.1	0.1	0.550	7.50E-03	1.00E-01	1.69E-05	*-3.35E-10*	-2.51E-03	*2.04E-08*	1.53E-01
34fr070	Gcpo, hori.	73.4	102.0	6.3	370.0	69.4	-2.4	0.1	0.550	1.60E-03	5.00E-02	1.69E-05	*-1.83E-10*	-1.37E-03	*4.34E-09*	3.26E-02
34fr105	Gcpo, hori.	109.0	102.0	6.3	460.0	107.0	-4.4	0.1	0.550	1.80E-03	5.00E-02	1.69E-05	*-1.12E-10*	-8.39E-04	*4.89E-09*	3.66E-02
34fr130	Gcpo, hori.	133.0	102.0	6.3	514.0	133.5	-6.6	0.1	0.550	2.00E-02	5.00E-02	1.69E-05	*-7.97E-10*	-5.98E-03	*5.43E-08*	4.07E-01
35fr140	Gcpo, hori.	144.0	202.0	16.6	508.0	130.4	-3.0	0.1	0.550	2.00E-02	8.00E-02	1.69E-05	*-1.83E-09*	-1.37E-02	*5.43E-08*	4.07E-01

Tab. A7.2: Listing of all measured *in situ* gas tracer data, Friedingen, SW Germany, bold: data used in further evaluation

A 7.2 *In Situ* Gas Pneumatic Data

filename	lithofacies	Δp_{max} [10^3 Pa]	Q_{in} [ml/s]	Δp_{in} [10^3 Pa]	Q_{out} [ml/s]	Δp_{out} [10^3 Pa]	Δp [10^3 Pa]	Δp_{min} [10^4 Pa]	l [m]	3 dimensional k [m^2]	K_P [m/s]	k_{MAX} [m^2]	K_{FMAX} [m/s]
1bo070	Gmm, hori.	73.4	102.0	6.3	274.0	38.3	28.8	0.1	0.500	8.95E-12	6.71E-05	2.59E-09	1.93E-02
1bo105	Gmm, hori.	109.0	102.0	6.3	354.0	63.6	39.1	0.1	0.500	8.00E-12	6.00E-05	3.13E-09	2.34E-02
1bo140	Gmm, hori.	144.0	102.0	6.3	418.0	88.5	49.2	0.1	0.500	7.25E-12	5.44E-05	3.56E-09	2.67E-02
1bo170	Gmm, hori.	172.0	102.0	6.3	461.0	107.5	58.2	0.1	0.500	6.63E-12	4.98E-05	3.86E-09	2.89E-02
1bo170b	Gmm, hori.	165.0	102.0	6.3	453.0	103.8	54.8	0.1	0.500	6.94E-12	5.20E-05	3.80E-09	2.85E-02
2bo070	Gmm, hori.	73.4	102.0	6.3	319.0	51.7	15.3	0.1	0.500	1.88E-11	1.41E-04	2.89E-09	2.16E-02
2bo105	Gmm, hori.	109.0	102.0	6.3	416.0	87.7	15.0	0.1	0.500	2.36E-11	1.77E-04	3.55E-09	2.66E-02
2bo120	Gmm, hori.	124.0	102.0	6.3	452.0	103.4	14.3	0.1	0.500	2.65E-11	1.99E-04	3.80E-09	2.85E-02
3bo070	Sh, hori.	73.4	203.0	16.7	261.0	34.8	21.9	0.1	0.820	1.47E-11	1.10E-04	3.23E-09	2.42E-02
3bo120	Sh, hori.	121.0	102.0	6.3	444.0	99.8	14.9	0.1	0.820	2.55E-11	1.91E-04	3.80E-09	2.85E-02
3bo130	Sh, hori.	134.0	203.0	16.7	434.0	95.3	22.0	0.1	0.820	2.02E-11	1.52E-04	4.44E-09	3.33E-02
4bo070	Sh, hori.	73.4	203.0	16.7	258.0	34.0	22.7	0.1	0.820	1.41E-11	1.06E-04	3.21E-09	2.41E-02
4bo120	Sh, hori.	124.0	102.0	6.3	425.0	91.5	28.2	0.1	0.820	1.40E-11	1.05E-04	3.67E-09	2.75E-02
4bo140	Sh, hori.	141.0	203.0	16.7	430.0	93.6	30.7	0.1	0.820	1.44E-11	1.08E-04	4.41E-09	3.31E-02
5bo110	Sh, hori.	114.0	1.3	0.1	422.0	90.2	23.8	0.1	0.820	1.24E-11	9.31E-05	2.95E-09	2.21E-02
6bo070	Sh > Gcm, vert.	73.3	203.0	16.7	293.0	43.7	12.9	0.1	0.270	2.54E-11	1.91E-04	3.28E-09	2.46E-02
6bo105	Sh > Gcm, vert.	109.0	203.0	16.7	395.0	79.1	13.2	0.1	0.270	2.99E-11	2.24E-04	3.95E-09	2.97E-02
6bo110	Sh > Gcm, vert.												
6bo120	Sh > Gcm, vert.	124.0	203.0	16.7	431.0	94.0	13.3	0.1	0.270	3.16E-11	2.37E-04	4.19E-09	3.14E-02
7bo110	Sh < Gcm, vert.	113.0	102.0	6.3	416.0	87.7	19.0	0.1	0.270	1.80E-11	1.35E-04	3.42E-09	2.57E-02
7bo120	Sh < Gcm, vert.	124.0	203.0	16.7	414.0	86.8	20.5	0.1	0.270	1.89E-11	1.49E-04	4.08E-09	3.06E-02
8bo070	Sh > Gcm, diag.	73.3	102.0	6.3	291.0	43.1	23.8	0.1	0.540	1.13E-11	8.50E-05	2.70E-09	2.03E-02
8bo105	Sh > Gcm, diag.	109.0	102.0	6.3	374.0	70.9	31.7	0.1	0.540	1.03E-11	7.74E-05	3.27E-09	2.45E-02
8bo120	Sh > Gcm, diag.	124.0	102.0	6.3	407.0	83.9	33.8	0.1	0.540	1.04E-11	7.78E-05	3.50E-09	2.63E-02
8bo120b	Sh > Gcm, diag.	124.0	102.0	6.3	404.0	82.7	35.0	0.1	0.540	9.95E-12	7.46E-05	3.48E-09	2.61E-02
9bo070	Sh < Gcm, diag.	73.3	102.0	6.3	312.0	49.5	17.5	0.1	0.540	1.63E-11	1.22E-04	2.85E-09	2.14E-02
9bo110	Sh < Gcm, diag.	114.0	102.0	6.3	413.0	86.4	21.3	0.1	0.540	1.66E-11	1.25E-04	3.54E-09	2.66E-02
10bo020	Sh, hori.	22.8	102.0	6.3	77.3	3.2	13.3	0.1	0.590	9.31E-12	6.99E-05	1.24E-09	9.28E-03
10bo030	Sh, hori.	32.9	102.0	6.3	149.0	11.5	15.1	0.1	0.590	1.15E-11	8.62E-05	1.73E-09	1.30E-02
10bo040	Sh, hori.	43.0	102.0	6.3	196.0	20.1	16.5	0.1	0.590	1.25E-11	9.38E-05	2.07E-09	1.55E-02
10bo050	Sh, hori.	53.1	102.0	6.3	237.0	28.7	18.1	0.1	0.590	1.30E-11	9.72E-05	2.34E-09	1.75E-02
10bo060	Sh, hori.	63.2	102.0	6.3	272.0	37.7	19.1	0.1	0.590	1.35E-11	1.01E-04	2.58E-09	1.94E-02
10bo070	Sh, hori.	73.3	102.0	6.3	304.0	47.0	19.9	0.1	0.590	1.40E-11	1.05E-04	2.80E-09	2.10E-02
10bo080	Sh, hori.	83.4	102.0	6.3	333.0	56.3	20.7	0.1	0.590	1.45E-11	1.09E-04	3.00E-09	2.25E-02
10bo100	Sh, hori.	104.0	102.0	6.3	385.0	75.2	22.5	0.1	0.590	1.49E-11	1.12E-04	3.36E-09	2.52E-02
10bo110	Sh, hori.	114.0	102.0	6.3	410.0	85.2	22.5	0.1	0.590	1.57E-11	1.18E-04	3.53E-09	2.65E-02
10bo120	Sh, hori.	121.0	102.0	6.3	430.0	93.6	21.1	0.1	0.590	1.74E-11	1.31E-04	3.67E-09	2.75E-02
10bo130	Sh, hori.	131.0	162.0	12.0	428.0	92.7	26.3	0.1	0.590	1.55E-11	1.16E-04	4.07E-09	3.05E-02
10bo140	Sh, hori.	140.0	203.0	16.7	429.0	93.2	30.1	0.1	0.590	1.45E-11	1.09E-04	4.36E-09	3.27E-02
11bo070	Sh, hori.	73.3	102.0	6.3	274.0	38.3	28.7	0.1	0.590	9.04E-12	6.78E-05	2.59E-09	1.95E-02
11bo130	Sh, hori.	134.0	102.0	6.3	403.0	82.3	45.4	0.1	0.590	7.68E-12	5.76E-05	3.48E-09	2.61E-02
12bo140c	Sh, hori.	144.0	152.0	10.9	398.0	80.3	52.8	0.1	0.590	7.19E-12	5.39E-05	3.79E-09	2.85E-02
13bo050	Gcm, vert.	52.9	102.0	6.3	297.0	44.9	1.7	0.1	0.190	1.53E-10	1.15E-03	2.55E-09	1.91E-02
13bo070	Gcm, vert.	73.1	102.0	6.3	362.0	66.5	0.3	0.1	0.190	1.07E-09	8.04E-03	2.96E-09	2.22E-02
13bo070b	Gcm, vert.	73.1	102.0	6.3	356.0	64.3	2.4	0.1	0.190	1.20E-10	8.97E-04	2.93E-09	2.19E-02
13bo100	Gcm, vert.	98.9	102.0	6.3	428.0	92.7	-0.2	0.1	0.190	-1.97E-09	-1.48E-02	3.39E-09	2.54E-02
13bo100b	Gcm, vert.	99.0	102.0	6.3	428.0	92.7	-0.1	0.1	0.190	-4.73E-09	-3.55E-02	3.39E-09	2.54E-02
13bo100c	Gcm, vert.	102.0	102.0	6.3	424.0	91.0	4.6	0.1	0.190	7.24E-11	5.43E-04	3.36E-09	2.52E-02
13bo100d	Gcm, vert.	101.0	102.0	6.3	423.0	90.6	4.1	0.1	0.190	8.24E-11	6.18E-04	3.35E-09	2.52E-02
13bo100e	Gcm, vert.	101.0	102.0	6.3	423.0	90.6	4.1	0.1	0.190	8.24E-11	6.18E-04	3.35E-09	2.52E-02
14bo050	Gcm, vert.	53.1	102.0	6.3	218.0	24.4	22.4	0.1	0.190	9.12E-12	6.84E-05	2.04E-09	1.53E-02
14bo070	Gcm, vert.	73.3	102.0	6.3	282.0	40.5	26.5	0.1	0.190	9.27E-12	6.96E-05	2.45E-09	1.84E-02
14bo100	Gcm, vert.	104.0	102.0	6.3	408.0	84.3	13.3	0.1	0.190	2.44E-11	1.83E-04	3.26E-09	2.44E-02
14bo100b	Gcm, vert.	104.0	102.0	6.3	383.0	68.9	30.8	0.1	0.190	9.64E-12	7.23E-05	2.97E-09	2.23E-02
17bo100	Gcm, vert.	103.0	102.0	6.3	406.0	83.5	13.2	0.1	0.190	2.47E-11	1.85E-04	3.25E-09	2.43E-02
15bo050	Gcm, vert.	53.1	102.0	6.3	206.0	21.8	25.0	0.1	0.210	7.96E-12	5.97E-05	1.99E-09	1.49E-02
15bo070	Gcm, vert.	73.3	102.0	6.3	273.0	38.0	29.0	0.1	0.210	8.36E-12	6.27E-05	2.42E-09	1.82E-02
15bo100	Gcm, vert.	104.0	102.0	6.3	362.0	66.5	31.2	0.1	0.210	9.61E-12	7.21E-05	3.00E-09	2.25E-02
15bo120	Gcm, vert.	124.0	102.0	6.3	413.0	86.4	31.3	0.1	0.210	1.06E-11	7.98E-05	3.33E-09	2.50E-02
18bo070	Gcm, vert.	73.3	102.0	6.3	357.0	64.7	2.3	0.1	0.210	1.30E-10	9.72E-04	2.97E-09	2.22E-02
18bo100	Gcm, vert.	99.0	102.0	6.3	410.0	85.2	7.5	0.1	0.210	4.40E-11	3.30E-04	3.31E-09	2.48E-02
18bo100b	Gcm, vert.	98.7	102.0	6.3	410.0	85.2	5.2	0.1	0.210	6.34E-11	4.75E-04	3.31E-09	2.48E-02
18bo110	Gcm, vert.	113.0	102.0	6.3	405.0	83.1	23.6	0.1	0.210	1.39E-11	1.04E-04	3.28E-09	2.46E-02
18bo100	Gcm, hori.	104.0	102.0	6.3	404.0	82.7	15.0	0.1	0.770	2.35E-11	1.76E-04	3.52E-09	2.64E-02
18bo100b	Gcm, hori.	104.0	102.0	6.3	402.0	81.9	15.8	0.1	0.770	2.22E-11	1.67E-04	3.51E-09	2.63E-02
18bo100c	Gcm, hori.	104.0	203.0	16.7	245.0	30.7	58.6	0.1	0.770	5.50E-12	4.13E-05	3.12E-09	2.34E-02
19bo100	Gcm, hori.	98.1	102.0	6.3	409.0	84.7	7.0	0.1	0.770	5.05E-11	3.79E-04	3.55E-09	2.67E-02
19bo100b	Gcm, hori.	104.0	203.0	16.7	408.0	84.3	3.0	0.1	0.770	1.43E-10	1.07E-03	4.25E-09	3.19E-02
20bo100	Gcm, hori.	102.0	203.0	16.7	409.0	84.7	0.6	0.1	0.820	7.50E-10	5.62E-03	4.26E-09	3.20E-02
21bo100	Gcm, hori.	101.0	203.0	16.7	407.0	83.9	0.4	0.1	0.820	1.09E-09	8.17E-03	4.25E-09	3.19E-02
22bo100	Gcm, diag.	95.3	203.0	16.7	410.0	85.2	-6.5	0.1	0.800	-6.52E-11	-4.89E-04	4.27E-09	3.20E-02
23bo100	Gcm, diag.	94.2	203.0	16.7	408.0	84.3	-6.8	0.1	0.800	-6.24E-11	-4.68E-04	4.25E-09	3.19E-02
24bo100	Gcm, diag.	95.6	203.0	16.7	407.0	83.9	-5.0	0.1	0.830	-8.46E-11	-6.36E-04	4.25E-09	3.19E-02

Tab. A7.3: Listing of all measured *in situ* gas pneumatic data, Böhringen, SW Germany, bold: data used in further evaluation

filename	lithofacies	Δp_{meas} [10^3 Pa]	Q_{in} [ml/s]	Δp_{in} [10^3 Pa]	Q_{out} [ml/s]	Δp_{out} [10^3 Pa]	Δp [10^3 Pa]	Δp_{min} [10^3 Pa]	l [m]	3 dimensional k [m^2]	K_z [m/s]	k_{MAX} [m^2]	$K_{f\,MAX}$ [m/s]
1fr140	Gcho, hori.	144.0	102.0	6.3	506.0	129.4	8.3	0.1	0.980	5.13E-11	3.85E-04	4.25E-09	3.19E-02
2fr105	Gcho, hori.	109.0	102.0	6.3	440.0	98.0	4.7	0.1	0.980	8.09E-11	6.07E-04	3.79E-09	2.84E-02
2fr140	Gcho, hori.	144.0	102.0	6.3	510.0	131.4	6.2	0.1	0.980	6.65E-11	5.14E-04	4.28E-09	3.21E-02
3fr105	Gcho, hori.	109.0	99.8	6.1	450.0	102.5	0.4	0.1	0.980	9.83E-10	7.37E-03	3.85E-09	2.88E-02
3fr140	Gcho, hori.	141.0	98.0	6.0	517.0	135.0	0.0	0.1	0.980	-1.13E-08	-8.49E-02	4.30E-09	3.23E-02
4fr035	Gch, hori.	38.0	102.0	6.3	248.0	31.4	0.3	0.1	0.380	9.31E-10	6.98E-03	2.37E-09	1.78E-02
4fr070	Gch, hori.	73.1	102.0	6.3	377.0	72.1	-5.3	0.1	0.380	-6.11E-11	-4.58E-04	3.24E-09	2.43E-02
4fr105	Gch, hori.	109.0	102.0	6.3	470.0	111.7	-9.0	0.1	0.380	-4.28E-11	-3.21E-04	3.87E-09	2.90E-02
4fr140	Gch, hori.	144.0	102.0	6.3	547.0	151.1	-13.4	0.1	0.380	-3.27E-11	-2.46E-04	4.39E-09	3.29E-02
5fr070	Gch, hori.	73.2	202.0	16.6	337.0	57.7	-1.1	0.1	0.380	-3.44E-10	-2.58E-03	3.65E-09	2.73E-02
5fr140	Gch, hori.	144.0	202.0	16.6	515.0	134.0	-8.6	0.1	0.380	-7.39E-11	-5.54E-04	4.85E-09	3.64E-02
5fr150	Gch, hori.	154.0	202.0	16.6	535.0	144.6	-7.1	0.1	0.380	-7.00E-11	-5.25E-04	4.99E-09	3.74E-02
6fr140	Gch, hori.	144.0	302.0	30.8	480.0	116.5	-3.3	0.1	0.380	-1.60E-10	-1.20E-03	5.29E-09	3.97E-02
6fr150	Gch, hori.	154.0	302.0	30.8	502.0	127.4	-4.2	0.1	0.380	-1.31E-10	-9.80E-04	5.44E-09	4.08E-02
7fr140	Gch, hori.	144.0	404.0	49.4	437.0	96.7	-2.1	0.1	0.380	-2.69E-10	-2.02E-03	5.69E-09	4.27E-02
8fr140	Gch, hori.	144.0	475.0	64.9	325.0	53.7	25.4	0.1	0.380	2.13E-11	1.60E-04	5.41E-09	4.06E-02
9fr035	Gch, hori.	38.1	102.0	6.3	240.0	29.4	2.3	0.1	0.380	9.94E-11	7.45E-04	2.31E-09	1.74E-02
9fr070	Gch, hori.	73.4	102.0	6.3	366.0	68.0	-0.9	0.1	0.380	-3.56E-10	-2.67E-03	3.17E-09	2.37E-02
9fr105	Gch, hori.	109.0	102.0	6.3	458.0	106.1	-3.4	0.1	0.380	-1.10E-10	-8.25E-04	3.79E-09	2.84E-02
9fr140	Gch, hori.	142.0	102.0	6.3	530.0	141.9	-6.2	0.1	0.380	-6.89E-11	-5.17E-04	4.27E-09	3.21E-02
10fr070	Gcho, vert.	73.3	102.0	6.3	360.0	65.8	1.2	0.1	0.600	2.65E-10	1.99E-03	3.19E-09	2.39E-02
10fr105	Gcho, vert.	109.0	102.0	6.3	452.0	103.4	-0.7	0.1	0.600	-5.49E-10	-4.12E-03	3.82E-09	2.87E-02
10fr140	Gcho, vert.	141.0	102.0	6.3	521.0	137.1	-2.5	0.1	0.600	-1.75E-10	-1.32E-03	4.30E-09	3.23E-02
11fr070	Gcho, vert.	73.4	102.0	6.3	360.0	65.8	1.3	0.1	0.600	2.45E-10	1.83E-03	3.19E-09	2.39E-02
11fr105	Gcho, vert.	109.0	102.0	6.3	449.0	102.0	0.7	0.1	0.600	5.73E-10	4.30E-03	3.80E-09	2.85E-02
11fr140	Gcho, vert.	141.0	102.0	6.3	516.0	134.5	0.2	0.1	0.600	2.76E-09	2.07E-02	4.27E-09	3.20E-02
12fr140	Gmh, vert.	142.0	102.0	6.3	515.0	134.0	1.7	0.1	0.320	2.47E-10	1.85E-03	4.13E-09	3.10E-02
13fr150	Gmh, vert.	151.0	102.0	6.3	508.0	130.4	14.3	0.1	0.320	2.86E-11	2.15E-04	4.06E-09	3.06E-02
14fr190	Gmh, vert.	194.0	102.0	6.3	507.0	129.9	57.8	0.1	0.320	7.05E-12	5.29E-05	4.06E-09	3.06E-02
15fr035	Gmhb, hori.	38.1	102.0	6.3	217.0	24.1	7.6	0.1	0.320	2.79E-11	2.09E-04	2.14E-09	1.60E-02
15fr070	Gmhb, hori.	73.4	102.0	6.3	344.0	60.1	7.0	0.1	0.320	4.28E-11	3.21E-04	2.99E-09	2.24E-02
15fr105	Gmhb, hori.	109.0	102.0	6.3	434.0	95.3	7.3	0.1	0.320	4.90E-11	3.67E-04	3.59E-09	2.69E-02
15fr140	Gmhb, hori.	144.0	102.0	6.3	506.0	129.4	8.3	0.1	0.320	4.91E-11	3.68E-04	4.07E-09	3.05E-02
16fr035	Gmhb, hori.	38.3	102.0	6.3	210.0	22.6	9.4	0.1	0.320	2.23E-11	1.67E-04	2.09E-09	1.57E-02
16fr070	Gmhb, hori.	73.4	102.0	6.3	326.0	54.0	13.1	0.1	0.320	2.19E-11	1.65E-04	2.86E-09	2.15E-02
16fr105	Gmhb, hori.	109.0	102.0	6.3	413.0	86.4	16.3	0.1	0.320	2.12E-11	1.59E-04	3.45E-09	2.59E-02
16fr140	Gmhb, hori.	144.0	102.0	6.3	482.0	117.5	20.2	0.1	0.320	1.93E-11	1.45E-04	3.91E-09	2.93E-02
16fr158	Gmhb, hori.	158.0	102.0	6.3	506.0	129.4	22.3	0.1	0.320	1.83E-11	1.37E-04	4.07E-09	3.05E-02
17fr070	Gmh, vert.	73.3	102.0	6.3	333.0	56.3	10.6	0.1	0.190	2.61E-11	1.96E-04	2.76E-09	2.08E-02
17fr105	Gmh, vert.	109.0	102.0	6.3	433.0	94.9	7.8	0.1	0.190	4.40E-11	3.30E-04	3.42E-09	2.56E-02
17fr150a	Gmh, vert.	154.0	102.0	6.3	533.0	143.5	4.2	0.1	0.190	9.68E-11	7.26E-04	4.06E-09	3.04E-02
17fr150b	Gmh, vert.	154.0	102.0	6.3	531.0	142.4	5.3	0.1	0.190	7.69E-11	5.76E-04	4.04E-09	3.03E-02
17fr150c	Gmh, vert.	154.0	102.0	6.3	528.0	140.8	6.9	0.1	0.190	5.87E-11	4.40E-04	4.02E-09	3.02E-02
18fr035	Gmh, vert.	38.1	102.0	6.3	205.0	21.6	10.2	0.1	0.190	1.92E-11	1.44E-04	1.96E-09	1.47E-02
18fr070	Gmh, vert.	73.5	102.0	6.3	326.0	54.0	13.2	0.1	0.190	2.08E-11	1.56E-04	2.73E-09	2.05E-02
18fr105	Gmh, vert.	109.0	102.0	6.3	413.0	86.4	16.3	0.1	0.190	2.02E-11	1.52E-04	3.29E-09	2.47E-02
18fr150	Gmh, vert.	154.0	102.0	6.3	505.0	128.9	18.8	0.1	0.190	2.06E-11	1.55E-04	3.88E-09	2.91E-02
19fr070	Gmh, diag.	73.3	102.0	6.3	338.0	58.0	8.9	0.1	0.600	3.40E-11	2.55E-04	3.04E-09	2.28E-02
19fr105	Gmh, diag.	109.0	102.0	6.3	430.0	93.6	9.1	0.1	0.600	4.05E-11	3.04E-04	3.67E-09	2.75E-02
19fr150	Gmh, diag.	150.0	102.0	6.3	512.0	132.5	11.2	0.1	0.600	3.78E-11	2.83E-04	4.24E-09	3.18E-02
20fr070	Gmh, diag.	73.3	102.0	6.3	337.0	57.7	9.3	0.1	0.600	3.26E-11	2.45E-04	3.03E-09	2.27E-02
20fr105	Gmh, diag.	109.0	102.0	6.3	427.0	92.3	10.4	0.1	0.600	3.52E-11	2.64E-04	3.65E-09	2.74E-02
20fr140	Gmh, diag.	144.0	102.0	6.3	499.0	125.8	11.8	0.1	0.600	3.51E-11	2.63E-04	4.15E-09	3.11E-02
20fr150	Gmh, diag.	149.0	102.0	6.3	509.0	130.9	11.8	0.1	0.600	3.59E-11	2.69E-04	4.22E-09	3.16E-02
21fr070	Gmh, hori.	73.3	102.0	6.3	329.0	55.0	12.0	0.1	0.680	2.50E-11	1.87E-04	2.99E-09	2.24E-02
21fr105	Gmh, hori.	109.0	102.0	6.3	417.0	88.1	14.6	0.1	0.680	2.46E-11	1.85E-04	3.60E-09	2.70E-02
21fr150	Gmh, hori.	153.0	102.0	6.3	503.0	127.9	18.8	0.1	0.680	2.23E-11	1.67E-04	4.19E-09	3.14E-02
21fr150b	Gmh, hori.	153.0	102.0	6.3	505.0	128.9	17.8	0.1	0.680	2.36E-11	1.77E-04	4.21E-09	3.16E-02
21fr150c	Gmh, hori.	153.0	102.0	6.3	505.0	128.9	17.8	0.1	0.680	2.36E-11	1.77E-04	4.21E-09	3.16E-02
22fr070	Gmh, hori.	73.4	102.0	6.3	321.0	52.4	14.7	0.1	0.680	2.00E-11	1.50E-04	2.93E-09	2.20E-02
22fr105	Gmh, hori.	109.0	102.0	6.3	407.0	83.9	18.8	0.1	0.680	1.88E-11	1.41E-04	3.53E-09	2.65E-02
22fr150	Gmh, hori.	154.0	102.0	6.3	495.0	123.8	23.8	0.1	0.680	1.74E-11	1.30E-04	4.14E-09	3.10E-02
23fr150	Gmh, diag.	154.0	102.0	6.3	496.0	124.3	23.3	0.1	0.600	1.77E-11	1.33E-04	4.13E-09	3.10E-02
24fr070	Gcpo, hori.	73.4	102.0	6.3	325.0	53.7	13.4	0.1	0.630	2.21E-11	1.65E-04	2.95E-09	2.21E-02
24fr105	Gcpo, hori.	109.0	102.0	6.3	408.0	84.3	18.3	0.1	0.630	1.92E-11	1.44E-04	3.53E-09	2.64E-02
24fr140	Gcpo, hori.	144.0	102.0	6.3	475.0	114.1	23.6	0.1	0.630	1.69E-11	1.27E-04	3.99E-09	2.99E-02
24fr170	Gcpo, hori.	174.0	102.0	6.3	519.0	136.1	31.6	0.1	0.630	1.36E-11	1.02E-04	4.29E-09	3.22E-02
24fr170b	Gcpo, hori.	174.0	102.0	6.3	517.0	135.0	32.6	0.1	0.630	1.31E-11	9.84E-05	4.28E-09	3.21E-02
24fr170c	Gcpo, hori.	174.0	102.0	6.3	513.0	133.0	34.7	0.1	0.630	1.23E-11	9.19E-05	4.25E-09	3.19E-02
25fr070	Gcpo, hori.	73.4	102.0	6.3	355.0	64.0	3.1	0.1	0.630	1.02E-10	7.63E-04	3.16E-09	2.37E-02
25fr105	Gcpo, hori.	109.0	102.0	6.3	447.0	101.1	1.6	0.1	0.630	2.43E-10	1.82E-03	3.80E-09	2.85E-02
25fr140	Gcpo, hori.	144.0	102.0	6.3	525.0	139.2	-1.6	0.1	0.630	-2.79E-10	-2.09E-03	4.33E-09	3.25E-02
25fr140b	Gcpo, hori.	144.0	102.0	6.3	525.0	139.2	-1.6	0.1	0.630	-2.79E-10	-2.09E-03	4.33E-09	3.25E-02
26fr070	Gcpo > Gmpb, vert.	73.4	102.0	6.3	284.0	41.1	26.0	0.1	0.280	9.85E-12	7.39E-05	2.56E-09	1.92E-02
26fr105	Gcpo > Gmpb, vert.	109.0	102.0	6.3	334.0	56.7	46.0	0.1	0.280	6.28E-12	4.71E-05	2.89E-09	2.17E-02
26fr140	Gcpo > Gmpb, vert.	144.0	102.0	6.3	375.0	71.3	66.4	0.1	0.280	4.77E-12	3.58E-05	3.16E-09	2.37E-02
26fr180	Gcpo > Gmpb, vert.	184.0							0.280				
26fr180b	Gcpo > Gmpb, vert.	184.0	102.0	6.3	475.0	114.1	63.6	0.1	0.280	6.02E-12	4.51E-05	3.83E-09	2.87E-02
27fr140	Gcpo < Gmpb, vert.	142.0	102.0	6.3	520.0	136.6	-0.9	0.1	0.280	-4.44E-10	-3.33E-03	4.12E-09	3.09E-02
27fr140b	Gcpo < Gmpb, vert.	141.0	102.0	6.3	517.0	135.0	-0.4	0.1	0.280	-1.13E-09	-8.45E-03	4.10E-09	3.08E-02
27fr160	Gcpo < Gmpb, vert.	146.0	102.0	6.3	520.0	136.6	3.1	0.1	0.280	1.34E-10	1.01E-03	4.12E-09	3.09E-02
28fr070	Gmpb, hori.	73.3	102.0	6.3	248.0	31.4	35.6	0.1	0.380	8.88E-12	4.99E-05	2.37E-09	1.78E-02
28fr105	Gmpb, hori.	109.0	102.0	6.3	318.0	51.4	51.3	0.1	0.380	5.54E-12	4.16E-05	2.84E-09	2.13E-02
28fr140	Gmpb, hori.	144.0	102.0	6.3	389.0	76.7	61.0	0.1	0.380	5.45E-12	4.09E-05	3.32E-09	2.49E-02
28fr190.	Gmpb, hori.	194.0	102.0	6.3	466.0	109.8	77.8	0.1	0.300	4.94E-12	3.70E-05	3.84E-09	2.88E-02
28fr190b	Gmpb, hori.	194.0	102.0	6.3	470.0	111.7	76.0	0.1	0.380	5.09E-12	3.82E-05	3.87E-09	2.90E-02
29fr070	Gmpb, hori.	73.3	102.0	6.3	245.0	30.7	36.3	0.1	0.380	6.47E-12	4.85E-05	2.35E-09	1.76E-02
29fr105	Gmpb, hori.	109.0	102.0	6.3	281.0	40.2	62.4	0.1	0.380	4.15E-12	3.11E-05	2.59E-09	1.94E-02
29fr140	Gmpb, hori.	144.0	102.0	6.3	356.0	64.3	73.3	0.1	0.380	4.22E-12	3.17E-05	3.10E-09	2.32E-02
29fr190	Gmpb, hori.	194.0	102.0	6.3	424.0	91.0	98.6	0.1	0.380	3.68E-12	2.76E-05	3.58E-09	2.67E-02
30fr070	Gmpb > Gcpo, vert.	73.3	102.0	6.3	312.0	49.5	17.5	0.1	0.230	1.55E-11	1.16E-04	2.70E-09	2.02E-02
30fr105	Gmpb > Gcpo, vert.	109.0	102.0	6.3	399.0	80.7	22.0	0.1	0.230	1.48E-11	1.11E-04	3.27E-09	2.45E-02
30fr140	Gmpb > Gcpo, vert.	144.0	102.0	6.3	468.0	110.8	26.9	0.1	0.230	1.38E-11	1.04E-04	3.72E-09	2.79E-02
30fr150	Gmpb > Gcpo, vert.	154.0	102.0	6.3	487.0	119.9	27.6	0.1	0.230	1.38E-11	1.04E-04	3.84E-09	2.88E-02
30fr160	Gmpb > Gcpo, vert.	163.0	102.0	6.3	502.0	127.4	29.3	0.1	0.230	1.34E-11	1.01E-04	3.94E-09	2.95E-02
31fr070	Gmpb < Gcpo, vert.	73.3	102.0	6.3	242.0	29.9	37.0	0.1	0.230	6.05E-12	4.54E-05	2.24E-09	1.68E-02
31fr105	Gmpb < Gcpo, vert.	109.0	102.0	6.3	322.0	52.7	50.0	0.1	0.230	5.53E-12	4.15E-05	2.76E-09	2.07E-02
31fr140	Gmpb < Gcpo, vert.	144.0	102.0	6.3	386.0	75.5	62.1	0.1	0.230	5.12E-12	3.84E-05	3.16E-09	2.39E-02
31fr180	Gmpb < Gcpo, vert.	184.0	102.0	6.3	451.0	102.9	74.8	0.1	0.230	4.82E-12	3.62E-05	3.61E-09	2.70E-02
32fr180c	Gmpb < Gcpo, vert.	184.0	202.0	16.6	399.0	80.7	86.8	0.1	0.230	4.52E-12	3.39E-05	3.92E-09	2.94E-02
33fr070	Gcpo, hori.	73.3	102.0	6.3	373.0	70.6	-3.6	0.1	0.550	-9.09E-11	-6.82E-04	3.27E-09	2.45E-02
33fr105	Gcpo, hori.	109.0	102.0	6.3	465.0	109.4	-6.7	0.1	0.550	-5.83E-11	-4.37E-04	3.90E-09	2.93E-02
33fr140	Gcpo, hori.	144.0	102.0	6.3	524.0	138.7	-1.0	0.1	0.550	-4.19E-10	-3.15E-03	4.31E-09	3.23E-02
33fr140b	Gcpo, hori.	140.0	102.0	6.3	526.0	139.8	-6.1	0.1	0.550	-7.10E-11	-5.33E-04	4.32E-09	3.24E-02
34fr070	Gcpo, hori.	73.4	102.0	6.3	370.0	69.4	-2.4	0.1	0.550	-1.37E-10	-1.03E-03	3.25E-09	2.44E-02
34fr105	Gcpo, hori.	109.0	102.0	6.3	460.0	107.0	-4.4	0.1	0.550	-8.86E-11	-6.64E-04	3.87E-09	2.90E-02
34fr130	Gcpo, hori.	133.0	102.0	6.3	514.0	133.5	-6.8	0.1	0.550	-6.22E-11	-4.67E-04	4.24E-09	3.18E-02
35fr140	Gcpo, hori.	144.0	202.0	16.6	508.0	130.4	-3.0	0.1	0.550	-1.65E-10	-1.23E-03	4.88E-09	3.66E-02

Tab. A7.4: Listing of all measured *in situ* gas pneumatic data, Friedingen, SW Germany, bold: data used in further evaluation

A 7.3 Laboratory Gas Tracer Data

filename	lithofacies	Δp [10² Pa]	Q_{in} [ml/s]	Q_{out} [ml/s]	l [m]	v_a [m/s]	t [m]	Diff [m²/s]	1 dimensional k [m²]	K_f [m/s]
13dp5	Sp, mS	7.80	1.26	212.00	0.76	1.70E-02	5.00E-03	1.69E-05	*8.92E-11*	8.69E-04
13dp10	Sp, mS	12.77	1.26	149.00	0.76	-	-	1.69E-05		
b13dp10	Sp, mS	12.77	1.26	426.92	0.76	3.75E-02	6.00E-03	1.69E-05	*1.20E-10*	9.01E-04
13dp12	Sp, mS	14.99	1.26	524.92	0.76	4.95E-02	5.00E-03	1.69E-05	*1.35E-10*	1.01E-03
13dp15	Sp, mS	17.28	1.29	652.32	0.76	6.35E-02	6.80E-03	1.69E-05	*1.50E-10*	1.13E-03
13dp19	Sp, mS	19.00	1.25	694.18	0.76	6.85E-02	1.00E-02	1.69E-05	*1.48E-10*	1.11E-03
In13dp10	*Sp, mS*	12.78	420.02	423.60	0.76	3.84E-02	7.00E-03	1.69E-05	*1.23E-10*	9.22E-04
14dp10	St, fS	12.73	1.25	151.15	0.76	1.03E-02	2.50E-03	1.69E-05	*3.31E-11*	2.48E-04
14dp20	St, fS	22.82	1.26	305.15	0.76	2.18E-02	3.50E-03	1.69E-05	*3.91E-11*	2.93E-04
14dp30	St, fS	32.91	1.26	458.44	0.76	3.48E-02	4.00E-03	1.69E-05	*4.33E-11*	3.25E-04
14dp40	St, fS	43.01	1.26	610.68	0.76	4.95E-02	4.50E-03	1.69E-05	*4.71E-11*	3.53E-04
14dp48	St, fS	48.77	1.25	695.02	0.76	6.15E-02	7.00E-03	1.69E-05	*5.16E-11*	3.87E-04
In14dp20	St, fS	22.82	298.51	300.46	0.76	2.20E-02	5.50E-03	1.69E-05	*3.94E-11*	2.96E-04
In14dp21	St, fS	22.82	298.94	302.71	0.76	2.19E-02	5.30E-03	1.69E-05	*3.93E-11*	2.95E-04
15dpro1	Gmt	5.48	2.26	702.61	0.76	1.60E-01	7.00E-02	1.69E-05	*1.20E-09*	8.97E-03
15dpr02	Gmt	5.50	1.38	703.20	0.76	1.90E-01	1.50E-01	1.69E-05	*1.41E-09*	1.06E-02
15dpro3	Gmt	5.49	1.95	702.90	0.76	1.70E-01	7.00E-02	1.69E-05	*1.27E-09*	9.50E-03
15dpro4	Gmt	5.41	1.60	702.34	0.76	1.70E-01	4.00E-02	1.69E-05	*1.29E-09*	9.64E-03
16dpro1	Gcpo	1.00	1.26	714.75	2.09	4.50E-01	1.80E-01	1.69E-05	*5.09E-08*	3.82E-01
16dpro2	Gcpo	0.99	1.25	714.16	2.09	4.20E-01	1.80E-01	1.69E-05	*4.78E-08*	3.58E-01
16dpro3	Gcpo	1.01	1.26	714.29	2.09	4.20E-01	1.80E-01	1.69E-05	*4.67E-08*	3.50E-01
In16dpr1	Gcpo	0.71	498.15	597.98	2.09	4.20E-01	1.80E-01	1.69E-05	*6.64E-08*	4.98E-01
In16dpr2	Gcpo	0.82	498.00	601.84	2.09	4.30E-01	1.80E-01	1.69E-05	*5.87E-08*	4.40E-01
17dpro1	Gcpo	0.93	1.28	683.55	2.09	3.00E-01	2.50E-01	1.69E-05	*3.62E-08*	2.72E-01
17dpro2	Gcpo	1.12	1.27	705.11	2.09	2.90E-01	2.70E-01	1.69E-05	*2.90E-08*	2.18E-01
17dpro3	Gcpo	1.13	1.26	706.30	2.09	3.00E-01	2.50E-01	1.69E-05	*2.98E-08*	2.23E-01
17dpro4	Gcpo	1.18	1.25	706.90	2.09	3.40E-01	3.00E-01	1.69E-05	*3.25E-08*	2.43E-01
17dpro5	Gcpo	1.17	1.26	707.10	2.09	3.40E-01	3.00E-01	1.69E-05	*3.27E-08*	2.45E-01
17dpro6	Gcpo	1.18	1.26	707.41	2.09	3.20E-01	3.00E-01	1.69E-05	*3.05E-08*	2.29E-01
18dp10	Gmpb	10.23	1.26	195.13	0.76	2.00E-02	1.00E-02	1.69E-05	*8.00E-11*	6.00E-04
18dp20	Gmpb	20.33	1.27	367.80	0.76	4.00E-02	1.20E-02	1.69E-05	*8.05E-11*	6.04E-04
18dp30	Gmpb	30.42	1.26	538.73	0.76	-	-	1.69E-05		
b18dp30	Gmpb	30.42	1.27	538.17	0.76	6.40E-02	1.50E-02	1.69E-05	*8.61E-11*	6.46E-04
18dp40	Gmpb	39.37	1.26	686.46	0.76	9.35E-02	1.70E-02	1.69E-05	*9.72E-11*	7.29E-04
In18dp20	Gmpb	20.33	355.97	367.14	0.76	4.10E-02	1.30E-02	1.69E-05	*8.25E-11*	6.19E-04
19dp10	Gmpb	10.23	1.26	132.14	0.76	1.35E-02	3.70E-03	1.69E-05	*5.40E-11*	4.05E-04
19dp15	Gmpb	15.40	1.26	195.94	0.76	2.02E-02	5.00E-03	1.69E-05	*5.37E-11*	4.03E-04
19dp30	Gmpb	30.42	1.26	378.67	0.76	4.15E-02	6.00E-03	1.69E-05	*5.58E-11*	4.19E-04
19dp45	Gmpb	45.71	1.26	562.68	0.76	6.75E-02	7.00E-03	1.69E-05	*6.04E-11*	4.53E-04
b19dp45	Gmpb	45.71	1.26	562.55	0.76	6.75E-02	7.00E-03	1.69E-05	*6.04E-11*	4.53E-04
19dp55	Gmpb	55.18	1.25	674.40	0.76	9.30E-02	7.00E-03	1.69E-05	*6.90E-11*	5.17E-04
In19dp30	Gmpb	30.43	369.99	381.42	0.76	4.10E-02	8.00E-03	1.69E-05	*5.51E-11*	4.14E-04
In19dp3b	Gmpb	30.44	370.00	381.73	0.76	4.00E-02	7.00E-03	1.69E-05	*5.38E-11*	4.03E-04

Tab. A7.5: Listing of all measured laboratory gas tracer data, samples from Friedingen and Böhringen, SW Germany

A 7.4 Laboratory Gas Pneumatic Data

filename	lithofacies	Δp [10² Pa]	Q_{in} [ml/s]	Q_{out} [ml/s]	l [m]	r [m]	1 dimensional k [m²]	K_f [m/s]
13dp5	Sp, mS	7.80	1.26	212.00	0.76	0.095	*1.31E-10*	9.81E-04
13dp10	Sp, mS	12.77	1.26	149.00	0.76	0.095		
b13dp10	Sp, mS	12.77	1.26	426.92	0.76	0.095	*1.61E-10*	1.21E-03
13dp12	Sp, mS	14.99	1.26	524.92	0.76	0.095	*1.68E-10*	1.26E-03
13dp15	Sp, mS	17.28	1.29	652.32	0.76	0.095	*1.82E-10*	1.36E-03
13dp19	Sp, mS	19.00	1.25	694.18	0.76	0.095	*1.76E-10*	1.32E-03
In13dp10	Sp, mS	12.78	420.02	423.60	0.76	0.095	*1.59E-10*	1.20E-03
14dp10	St, fS	12.73	1.25	151.15	0.76	0.095	*5.71E-11*	4.28E-04
14dp20	St, fS	22.82	1.26	305.15	0.76	0.095	*6.43E-11*	4.82E-04
14dp30	St, fS	32.91	1.26	458.44	0.76	0.095	*6.70E-11*	5.03E-04
14dp40	St, fS	43.01	1.26	610.68	0.76	0.095	*6.83E-11*	5.12E-04
14dp48	St, fS	48.77	1.25	695.02	0.76	0.095	*6.86E-11*	5.14E-04
In14dp20	St, fS	22.82	298.51	300.46	0.76	0.095	*6.33E-11*	4.75E-04
In14dp21	St, fS	22.82	298.94	302.71	0.76	0.095	*6.38E-11*	4.79E-04
15dpro1	Gmt	5.48	2.26	702.61	0.76	0.095	*6.17E-10*	4.63E-03
15dpr02	Gmt	5.50	1.38	703.20	0.76	0.095	*6.15E-10*	4.62E-03
15dpro3	Gmt	5.49	1.95	702.90	0.76	0.095	*6.16E-10*	4.62E-03
15dpro4	Gmt	5.41	1.60	702.34	0.76	0.095	*6.24E-10*	4.68E-03
16dpro1	Gcpo	1.00	1.26	714.75	2.09	0.050	*3.43E-08*	2.57E-01
16dpro2	Gcpo	0.99	1.25	714.16	2.09	0.050	*3.45E-08*	2.59E-01
16dpro3	Gcpo	1.01	1.26	714.29	2.09	0.050	*3.37E-08*	2.53E-01
In16dpr1	Gcpo	0.71	498.15	597.98	2.09	0.050	*4.01E-08*	3.01E-01
In16dpr2	*Gcpo*	0.82	498.00	601.84	2.09	0.050	*3.49E-08*	2.62E-01
17dpro1	Gcpo	0.93	1.28	683.55	2.09	0.050	*3.50E-08*	2.63E-01
17dpro2	Gcpo	1.12	1.27	705.11	2.09	0.050	*3.00E-08*	2.25E-01
17dpro3	Gcpo	1.13	1.26	706.30	2.09	0.050	*2.98E-08*	2.23E-01
17dpro4	Gcpo	1.18	1.25	706.90	2.09	0.050	*2.86E-08*	2.15E-01
17dpro5	Gcpo	1.17	1.26	707.10	2.09	0.050	*2.88E-08*	2.16E-01
17dpro6	Gcpo	1.18	1.26	707.41	2.09	0.050	*2.86E-08*	2.15E-01
18dp10	Gmpb	10.23	1.26	195.13	0.76	0.095	*9.17E-11*	6.88E-04
18dp20	Gmpb	20.33	1.27	367.80	0.76	0.095	*8.70E-11*	6.53E-04
18dp30	Gmpb	30.42	1.26	538.73	0.76	0.095		
b18dp30	Gmpb	30.42	1.27	538.17	0.76	0.095	*8.51E-11*	6.38E-04
18dp40	Gmpb	39.37	1.26	686.46	0.76	0.095	*8.39E-11*	6.29E-04
In18dp20	Gmpb	20.33	355.97	367.14	0.76	0.095	*8.68E-11*	6.51E-04
19dp10	Gmpb	10.23	1.26	132.14	0.76	0.095	*6.21E-11*	4.66E-04
19dp15	Gmpb	15.40	1.26	195.94	0.76	0.095	*6.12E-11*	4.59E-04
19dp30	Gmpb	30.42	1.26	378.67	0.76	0.095	*5.99E-11*	4.49E-04
19dp45	Gmpb	45.71	1.26	562.68	0.76	0.095	*5.92E-11*	4.44E-04
b19dp45	Gmpb	45.71	1.26	562.55	0.76	0.095	*5.92E-11*	4.44E-04
19dp55	Gmpb	55.18	1.25	674.40	0.76	0.095	*5.88E-11*	4.41E-04
In19dp30	Gmpb	30.43	369.99	381.42	0.76	0.095	*6.03E-11*	4.52E-04
In19dp3b	Gmpb	30.44	370.00	381.73	0.76	0.095	*6.03E-11*	4.52E-04

Tab. A7.6: Listing of all measured laboratory gas pneumatic data, based on gas tracer measurements, samples from Friedingen and Böhringen, SW Germany

sample	k9		k11		k12		k13		k14		k15		k16		k17		k18		k19	
lithofacies	Gcpo		Sh, mS		Sh, fS		Sp, mS		St, fS		Gmt		Gcpo		Gcpo		Gmpb		Gmpb	
l [m]	2.09		0.76		0.76		0.76		0.76		0.76		2.09		2.09		0.76		0.76	
r [m]	0.05		0.095		0.095		0.095		0.095		0.095		0.05		0.05		0.095		0.095	
Q/Δp [10^{-6} m³/Pa.s]	279.49		26.81		8.72		40.39		16.18		41.46		786.87		1002.90		18.26		13.45	
k [m²]	1.30E-08		1.26E-10		4.09E-11		1.89E-10		7.59E-11		1.94E-10		3.66E-08		4.67E-08		8.56E-11		6.31E-11	
K_f [m/s]	9.75E-02		9.43E-04		3.07E-04		1.42E-03		5.69E-04		1.46E-03		2.75E-01		3.50E-01		6.42E-04		4.73E-04	
	Δp	Q	Δp	Q	Δp	Q	Δp	Q	Δp	Q	Δp	Q	Δp	Q	Δp	Q	Δp	Q	Δp	Q
	2.74	6	2.50	3	2.81	4	4.27	43.40	5.74	43	0.50	10	0.26	506	0.49	3	2.27	43	6.30	43
	2.85	503	2.56	3	7.89	44	5.23	83.70	11.30	124	0.91	105	0.52	786	0.65	306	4.68	84	8.70	84
	2.86	730	2.85	43	13.70	84	6.15	124.00	14.00	165	1.69	206	0.41	686	0.72	407	7.07	124	13.00	124
	2.89	750	2.97	43	19.00	124	7.04	164.00	16.60	205	2.82	307	0.66	887	0.76	506	9.41	164	16.10	165
	2.98	770	4.96	84	24.60	165	7.96	205.00	19.20	245	3.49	357	0.79	987	0.90	609	11.70	205	19.40	205
	3.05	790	6.60	124	29.60	205	8.67	245.00	21.80	286	4.21	407	1.07	1180	1.01	709	13.90	245	22.50	245
	3.13	810	8.36	164	35.10	245	9.73	285.00	24.30	326	5.08	458	0.97	1090	1.13	810	16.00	285	25.60	285
	3.30	831	8.94	165	40.20	285	10.60	326.00	26.80	366	5.95	508			1.45	1010	18.30	326	28.90	326
	3.37	851	11.70	245	45.10	326	11.50	366.00	29.30	407	7.06	558					20.50	366	31.60	366
	3.44	871	13.30	285	49.90	366	12.40	407.00	31.80	447	8.18	609					22.90	406	34.70	407
	3.56	891	14.20	316	55.00	407	13.30	447.00	36.70	528	9.36	659					24.90	447	37.70	447
	3.68	912	14.90	326	59.60	447	14.10	487.00	39.20	568	10.70	709					27.20	487	40.70	487
	3.74	932	16.20	366	64.50	487	15.00	528.00	41.60	608	12.00	760					29.40	527	43.60	528
	3.91	972	17.20	386	69.20	528	15.80	568.00	44.10	649	13.40	810					31.40	568	46.60	568
	3.93	952	19.50	447	73.80	568	16.70	608.00	49.00	729	14.60	860					33.60	608	49.60	608
	4.08	1010	21.00	487	78.00	608	17.50	649.00	51.20	769	16.40	911					35.80	648	49.50	608
	4.11	992	22.20	528	82.50	649	18.40	689.00	53.90	810	18.20	961					38.00	689	52.40	649
	4.24	1030	23.80	568	87.30	689	19.30	730.00	56.30	850	20.10	1010					40.20	729	55.40	689
	4.38	1050	25.50	608	91.70	729	20.20	770.00	58.80	891	21.80	1060					42.50	770	58.30	730
	4.50	1070	26.70	649	96.00	770	21.00	810.00	61.10	931	23.70	1110					44.50	810	61.30	770
	4.51	1110	28.40	689	100.00	810	21.90	851.00	63.80	972	25.90	1160					46.80	850	64.10	810
	4.53	1090	29.60	730	104.00	850	22.70	891.00	66.40	1010							48.90	890	67.00	851
	4.79	1130	31.30	770	108.00	891	23.60	932.00									51.40	931	70.00	891
	5.01	1160	32.80	810	113.00	931	24.50	972.00									53.40	971	73.00	931
	5.07	1180	34.20	851	117.00	972	25.40	1010.00									55.70	1010	76.00	972
			35.60	891	121.00	1010											55.80	1010	79.00	1010
			36.60	931	125.00	1050														
			38.00	972	129.00	1090														
			39.50	1010	133.00	1130														
			41.00	1050	138.00	1170														
			42.60	1090																
			44.10	1130																
			45.60	1170																

Tab. A7.7: Listing of all measured laboratory gas pneumatic data, based on gas pneumatic measurements, samples from Friedingen and Böhringen, SW Germany

Annex 8: Collection of 2D Sedimentological Outcrop Studies

This collection of outcrop analysis studies comprises photographic images of Quaternary outcrops in gravel pits in Southwest Germany and their sedimentological interpretation in terms of a lithological facies analysis described in chapter 2 and 7.

The total of 16 outcrops is split up under the three field sites Bittelschieß (11), Hüntwangen (1) and Steißlingen (4).

Outcrop Analysis BITTELSCHIESS BI1

Photograph of Outcrop

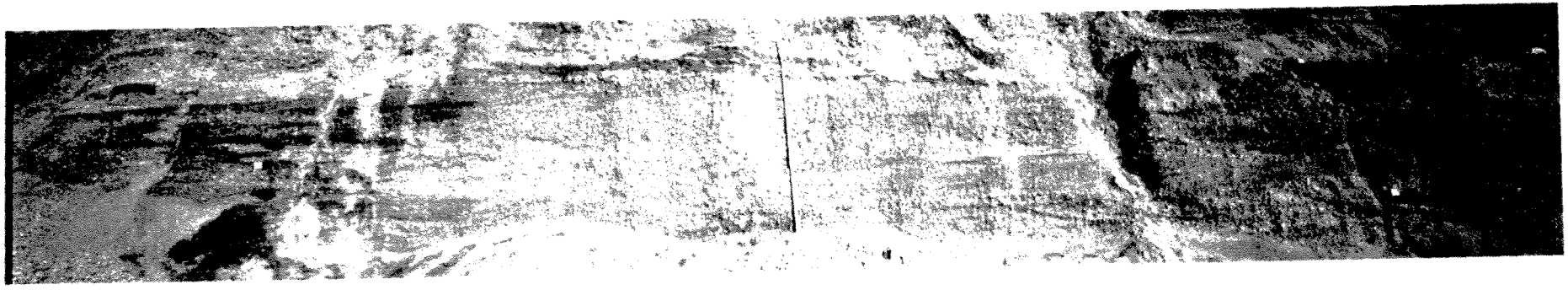

Sedimentological Interpretation

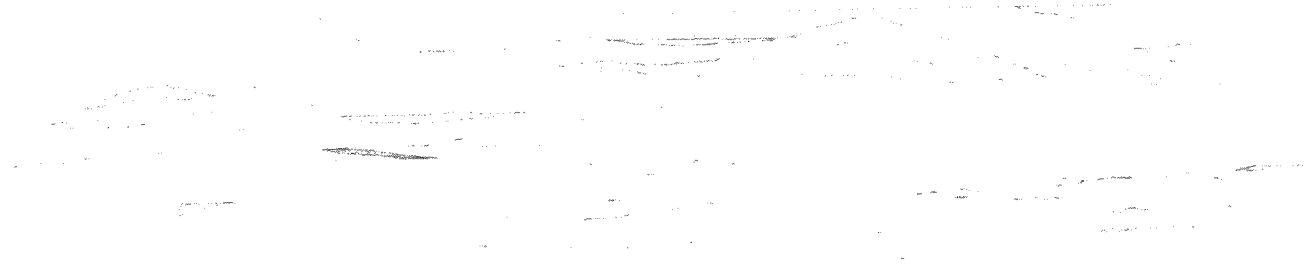

Lithofacies

Gmp	Gcp	Gcpo	Gmtb	Gctb	Gmh	Gch	Gcho	Gcm	Sp	Sh	Sg
Gmpb	Gcpb	Gmt	Gct	Gcto	Gmhb	Gchb	Gmm	Gg	St	Sm	

meters

0 1 2 3 4 5

Outcrop Analysis BITTELSCHIESS BI2

Photograph of Outcrop

Sedimentological Interpretation

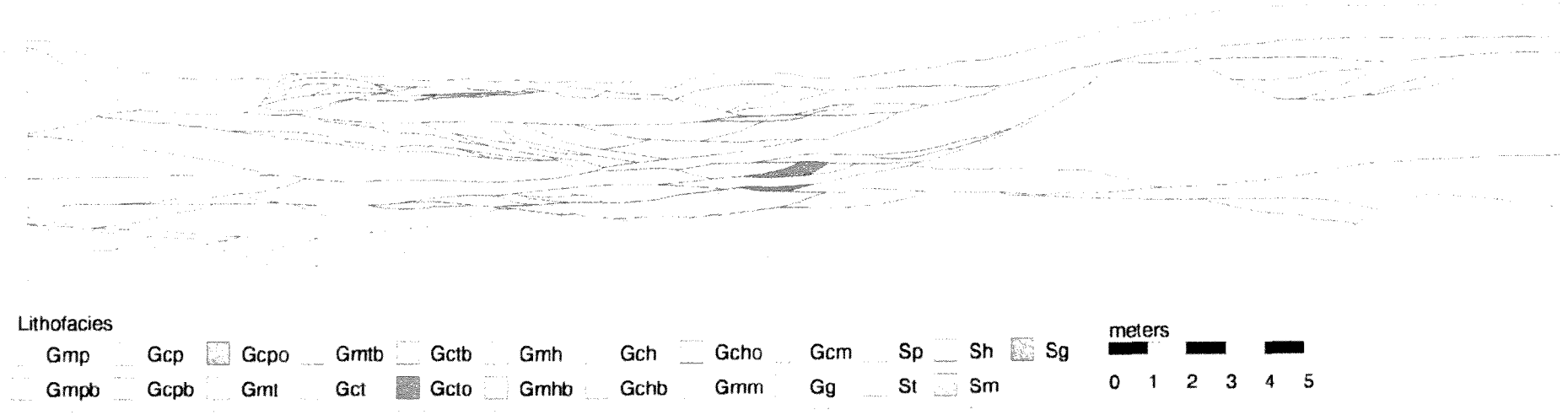

Outcrop Analysis BITTELSCHIESS BI3

Photograph of Outcrop

Sedimentological Interpretation

Lithofacies

Gmp	Gcp	Gcpo	Gmtb	Gctb	Gmh	Gch	Gcho	Gcm	Sp	Sh	Sg
Gmpb	Gcpb	Gmt	Gct	Gcto	Gmhb	Gchb	Gmm	Gg	St	Sm	

meters

0 1 2 3 4 5

Outcrop Analysis BITTELSCHIESS BI4

Photograph of Outcrop

Sedimentological Interpretation

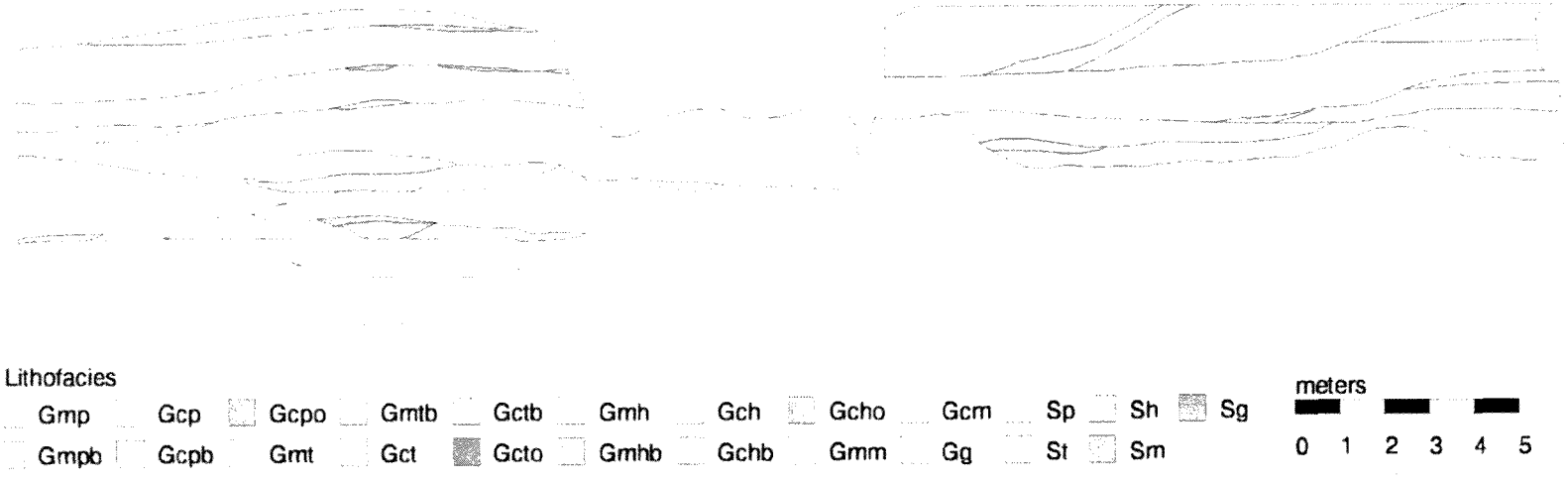

Outcrop Analysis BITTELSCHIESS BI5

Photograph of Outcrop

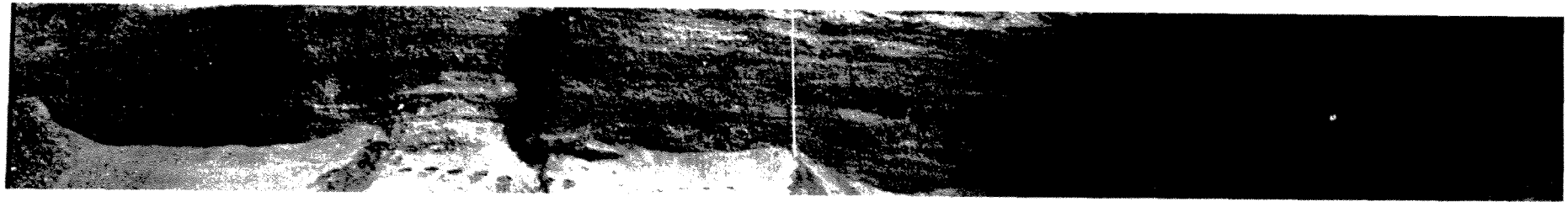

Sedimentological Interpretation

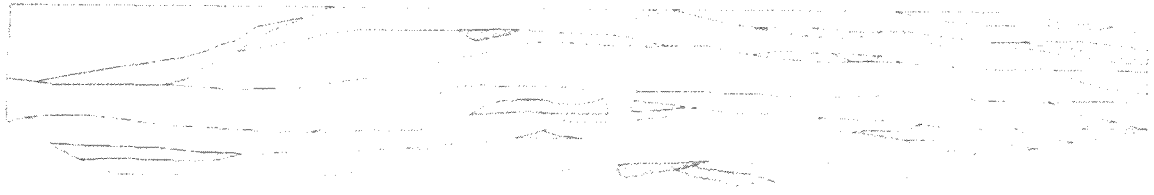

Lithofacies

Gmp	Gcp	Gcpo	Gmtb	Gctb	Gmh	Gch	Gcho	Gcm	Sp	Sh	Sg
Gmpb	Gcpb	Gmt	Gct	Gcto	Gmhb	Gchb	Gmm	Gg	St	Sm	

meters

0 1 2 3 4 5

Outcrop Analysis BITTELSCHIESS BI6

Photograph of Outcrop

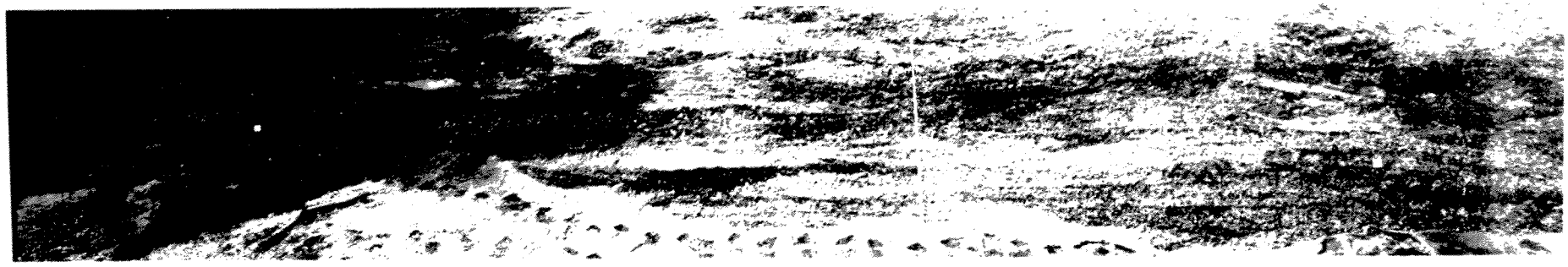

Sedimentological Interpretation

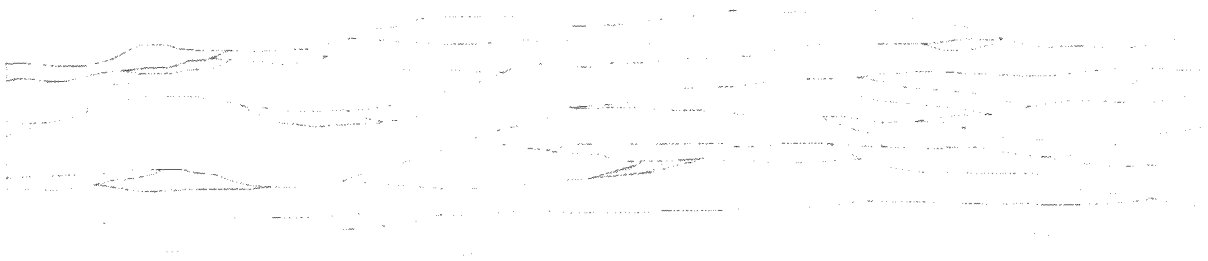

Lithofacies

Gmp	Gcp	Gcpo	Gmtb	Gctb	Gmh	Gch	Gcho	Gcm	Sp	Sh	Sg	
Gmpb	Gcpb	Gmt	Gct	Gcto	Gmhb	Gchb	Gmm	Gg	St	Sm		

meters

0 1 2 3 4 5

Outcrop Analysis BITTELSCHIESS BI7

Photograph of Outcrop

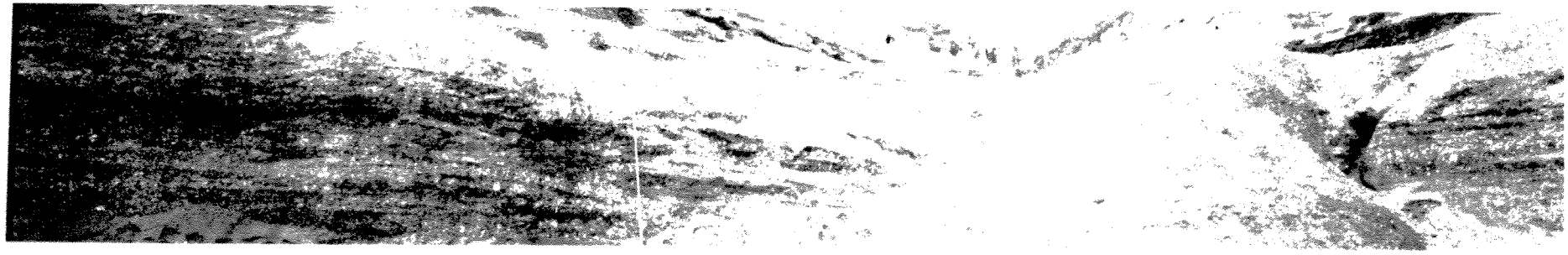

Sedimentological Interpretation

Lithofacies

Gmp	Gcp	Gcpo	Gmtb	Gctb	Gmh	Gch	Gcho	Gcm	Sp	Sh	Sg
Gmpb	Gcpb	Gmt	Gct	Gcto	Gmhb	Gchb	Gmm	Gg	St	Sm	

meters

0 1 2 3 4 5

Outcrop Analysis BITTELSCHIESS BI8

Photograph of Outcrop

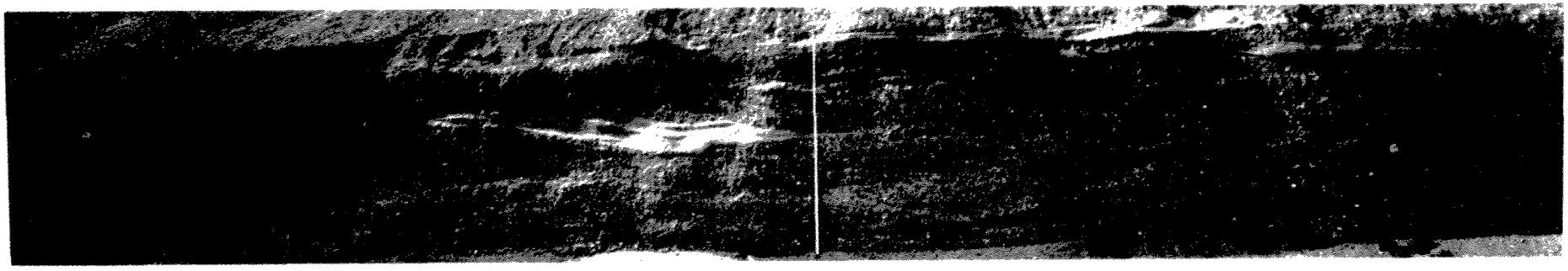

Sedimentological Interpretation

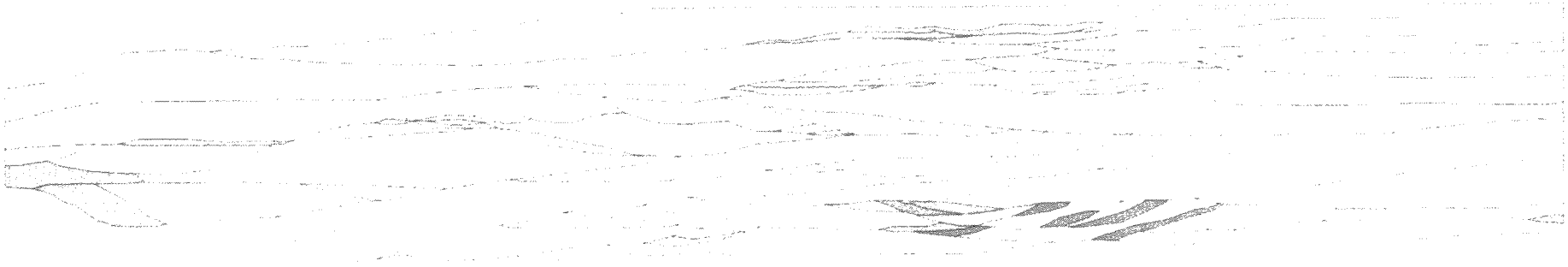

Outcrop Analysis BITTELSCHIESS BI9

Photograph of Outcrop

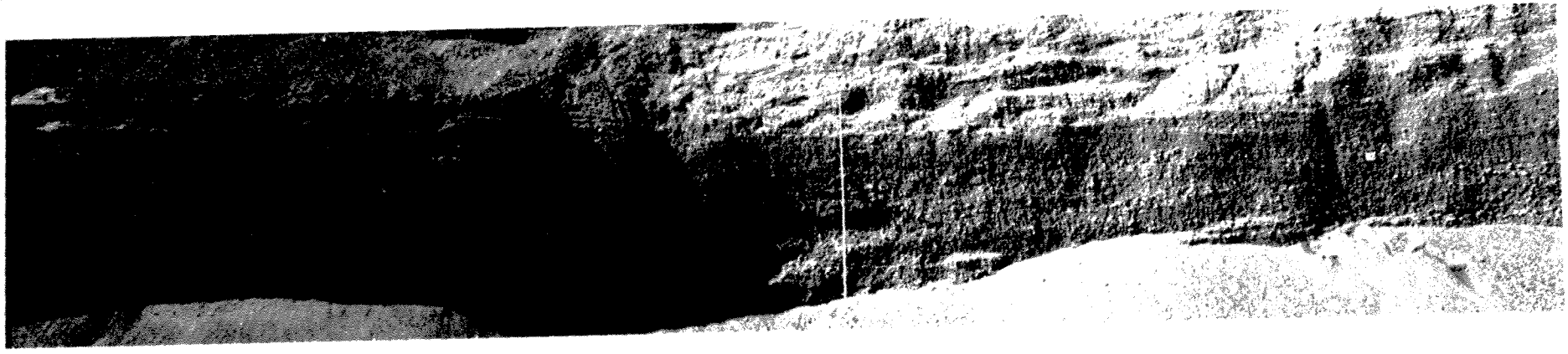

Sedimentological Interpretation

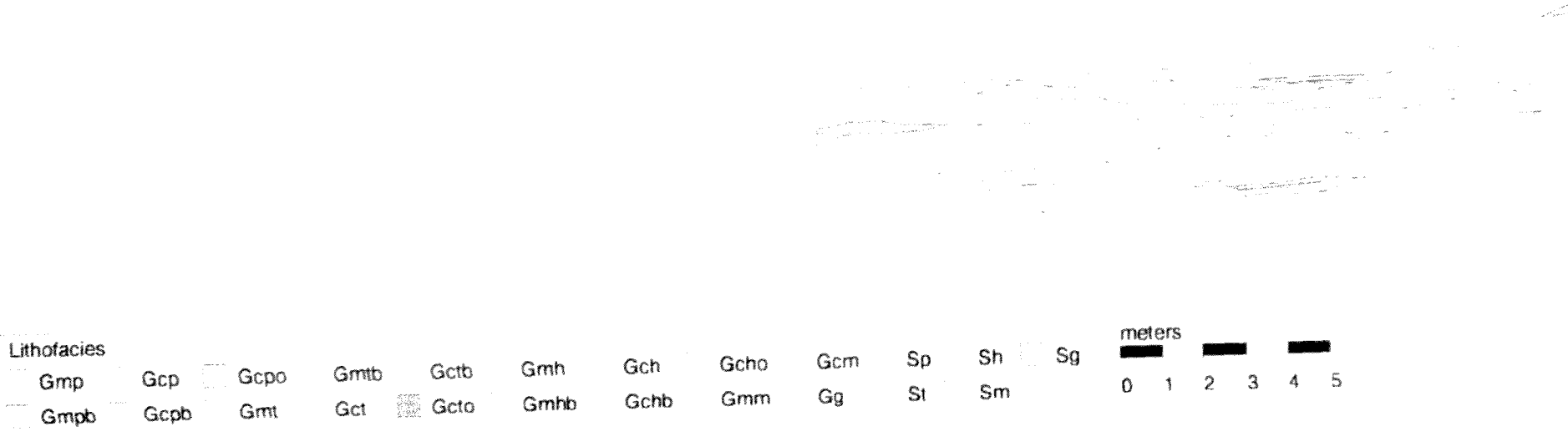

Outcrop Analysis BITTELSCHIESS BI10

Photograph of Outcrop

Sedimentological Interpretation

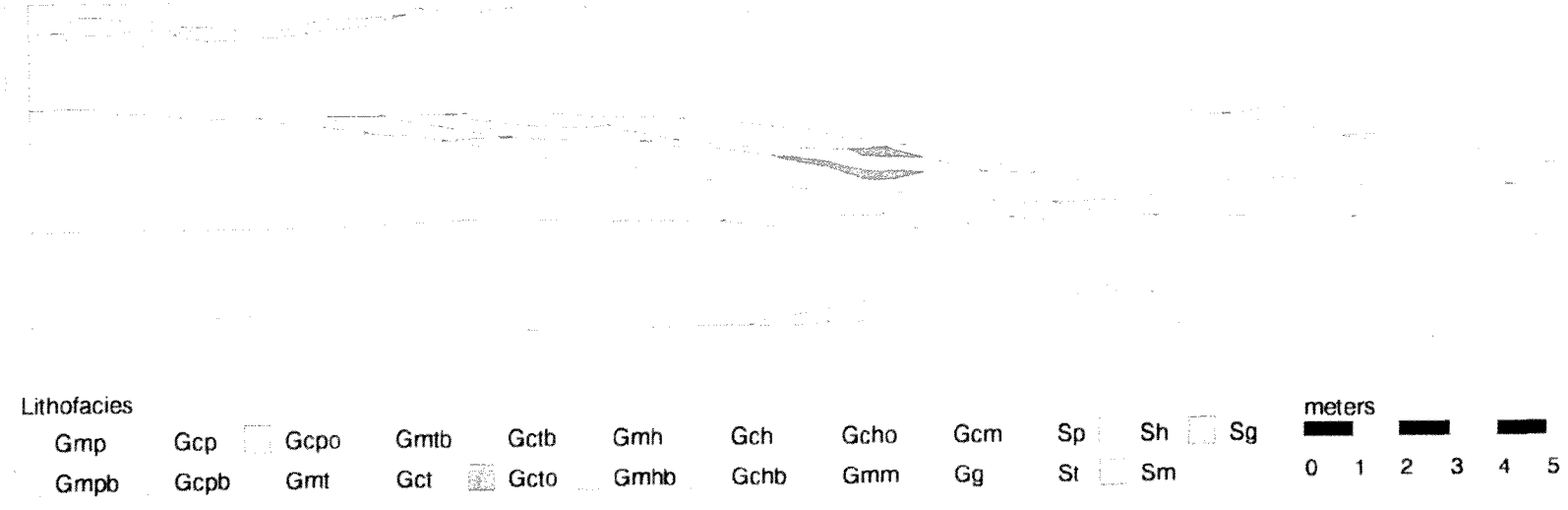

Outcrop Analysis BITTELSCHIESS BI11

Photograph of Outcrop

Sedimentological Interpretation

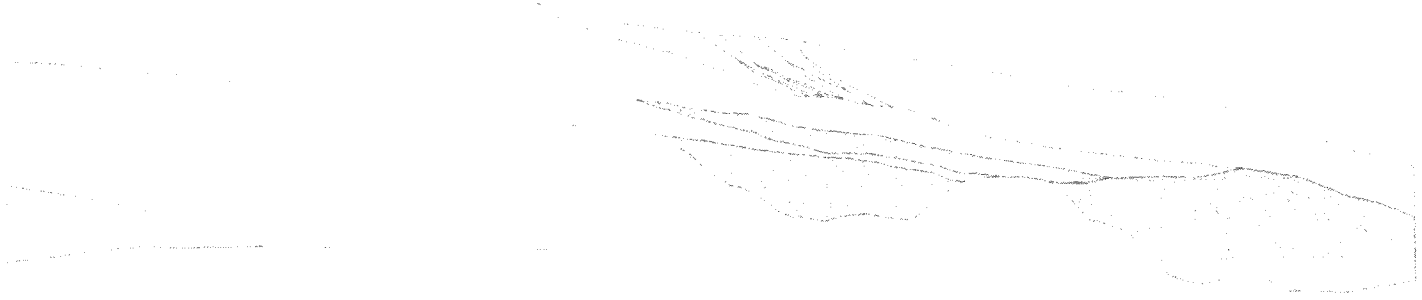

Lithofacies

Gmp	Gcp	Gcpo	Gmtb	Gctb	Gmh	Gch	Gcho	Gcm	Sp	Sh	Sg
Gmpb	Gcpb	Gmt	Gct	Gcto	Gmhb	Gchb	Gmm	Gg	St	Sm	

meters

0 1 2 3 4 5

Outcrop Analysis HUENTWANGEN HU1

Photograph of Outcrop

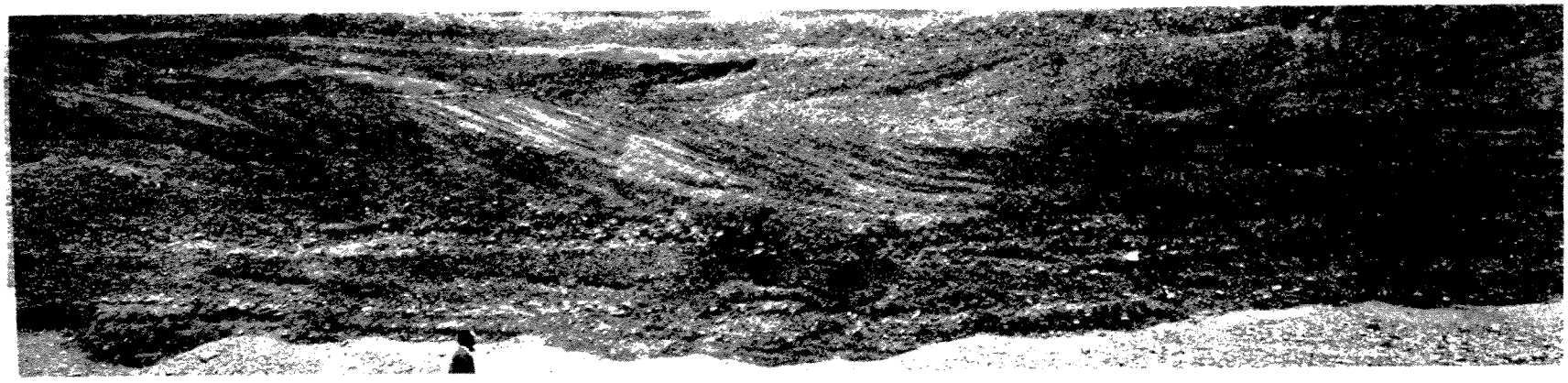

Sedimentological Interpretation

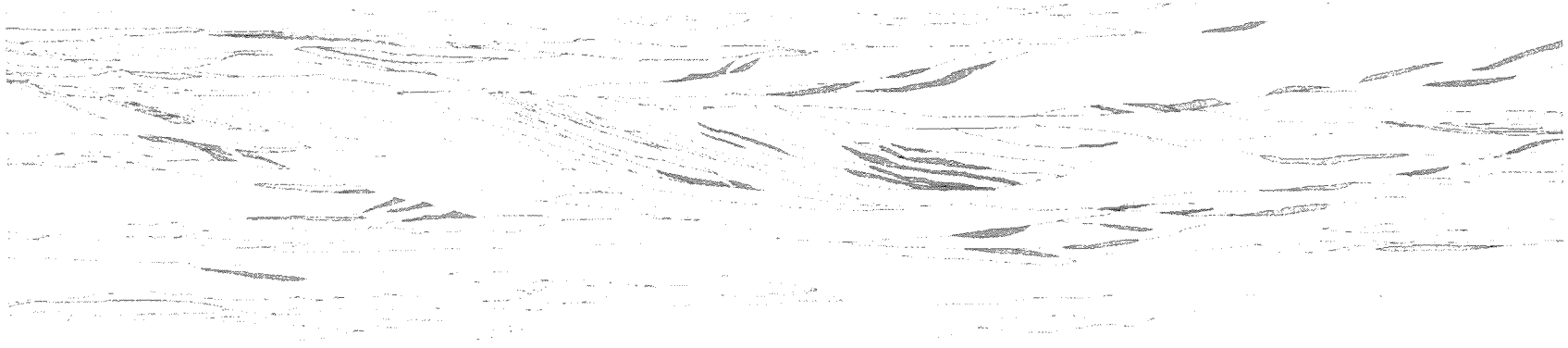

Outcrop Analysis STEISSLINGEN ST1

Photograph of Outcrop

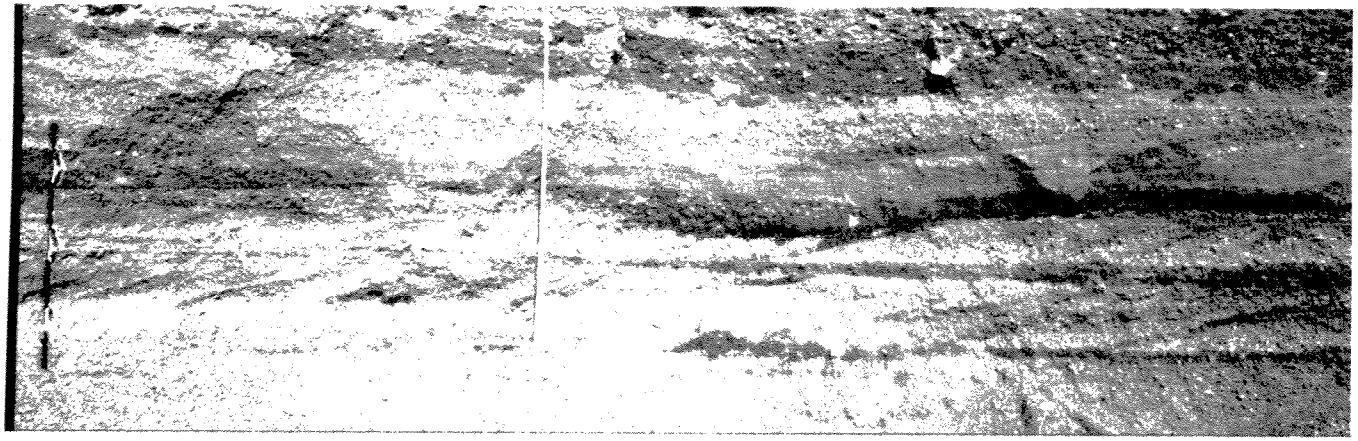

Sedimentological Interpretation

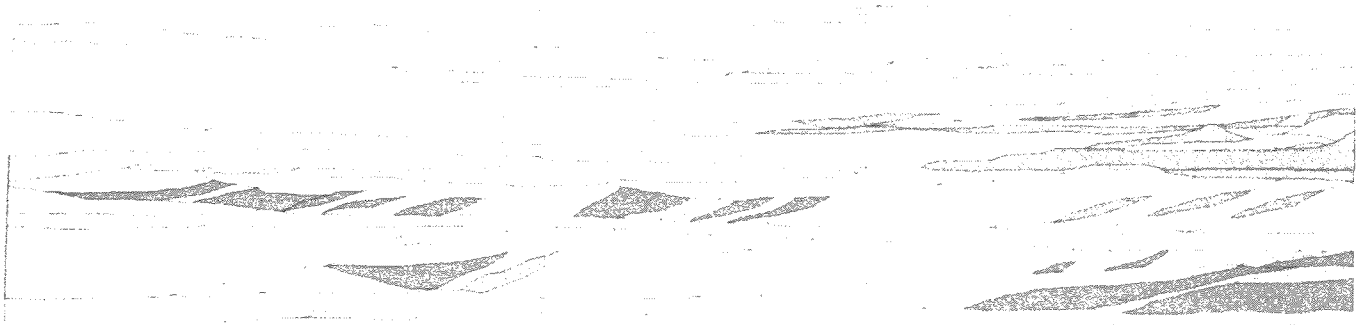

Lithofacies

Gmp	Gcp	Gcpo	Gmtb	Gctb	Gmh	Gch	Gcho	Gcm	Sp	Sh	Sg
Gmpb	Gcpb	Gmt	Gct	Gcto	Gmhb	Gchb	Gmm	Gg	St	Sm	

meters

0 1 2 3 4 5

Outcrop Analysis STEISSLINGEN ST2

Photograph of Outcrop

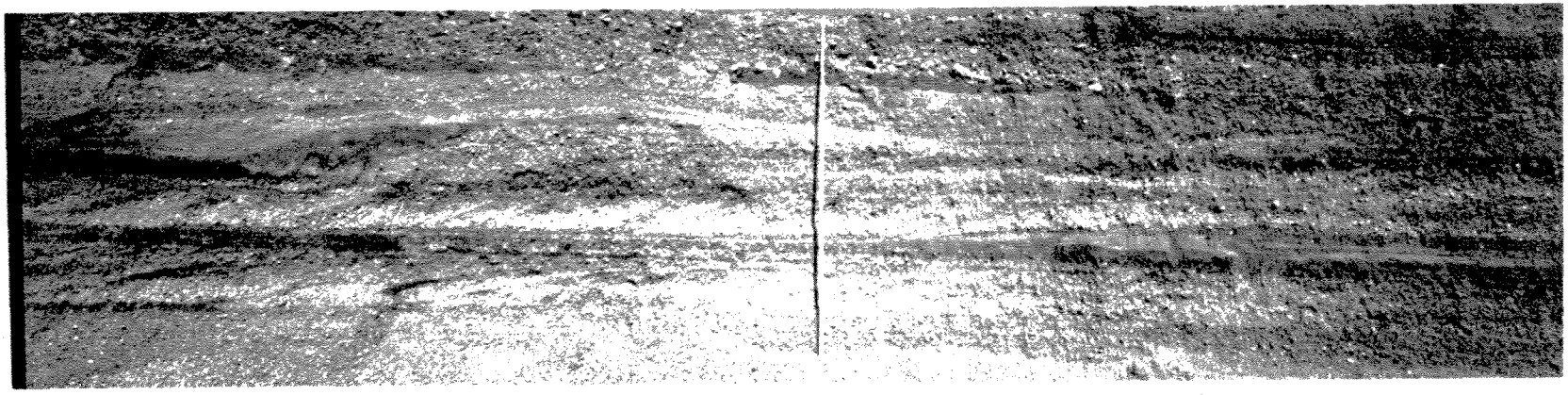

Sedimentological Interpretation

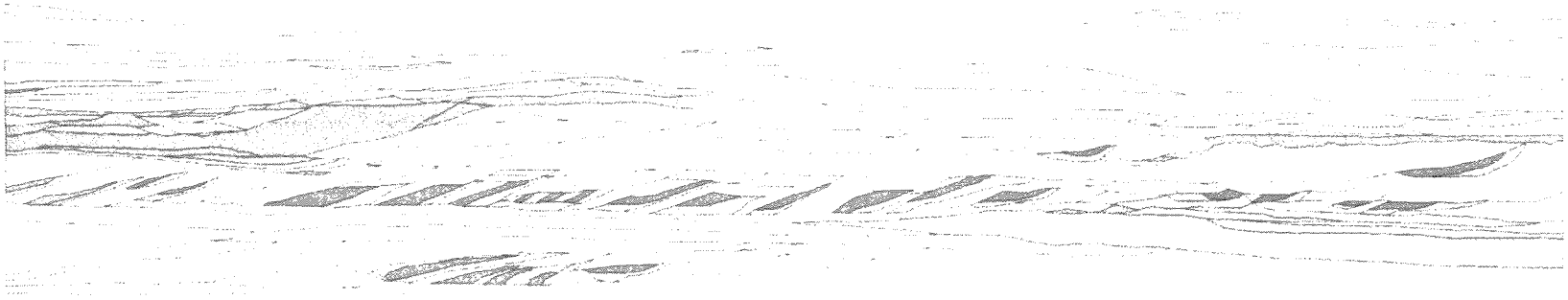

Lithofacies

Gmp	Gcp	Gcpo	Gmtb	Gctb	Gmh	Gch	Gcho	Gcm	Sp	Sh	Sg	
Gmpb	Gcpb	Gmt	Gct	Gcto	Gmhb	Gchb	Gmm	Gg	St	Sm		

metres

0 1 2 3 4 5

Outcrop Analysis STEISSLINGEN ST3

Photograph of Outcrop

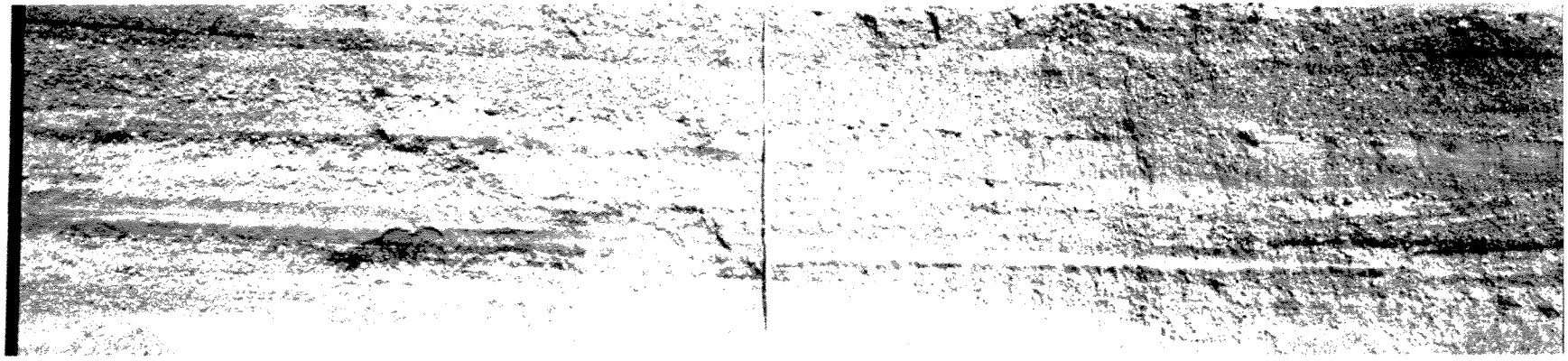

Sedimentological Interpretation

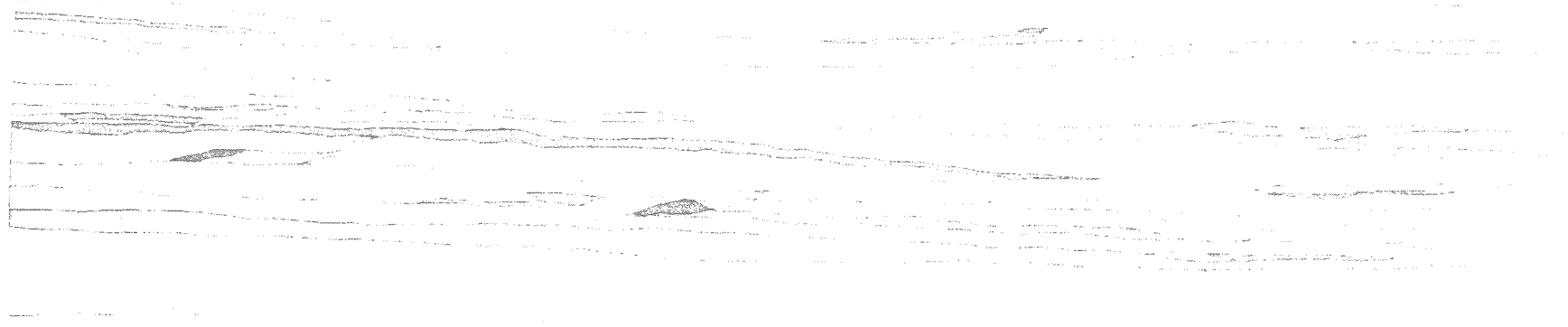

Lithofacies

Gmp	Gcp	Gcpo	Gmtb	Gctb	Gmh	Gch	Gcho	Gcm	Sp	Sh	Sg
Gmpb	Gcpb	Gmt	Gct	Gcto	Gmhb	Gchb	Gmm	Gg	St	Sm	

meters

0 1 2 3 4 5

Outcrop Analysis STEISSLINGEN ST4

Photograph of Outcrop

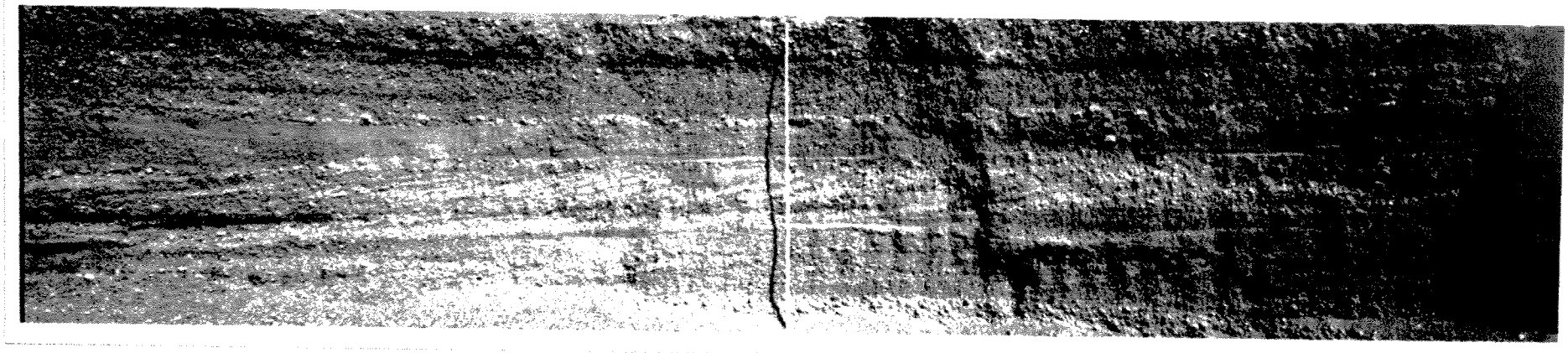

Sedimentological Interpretation

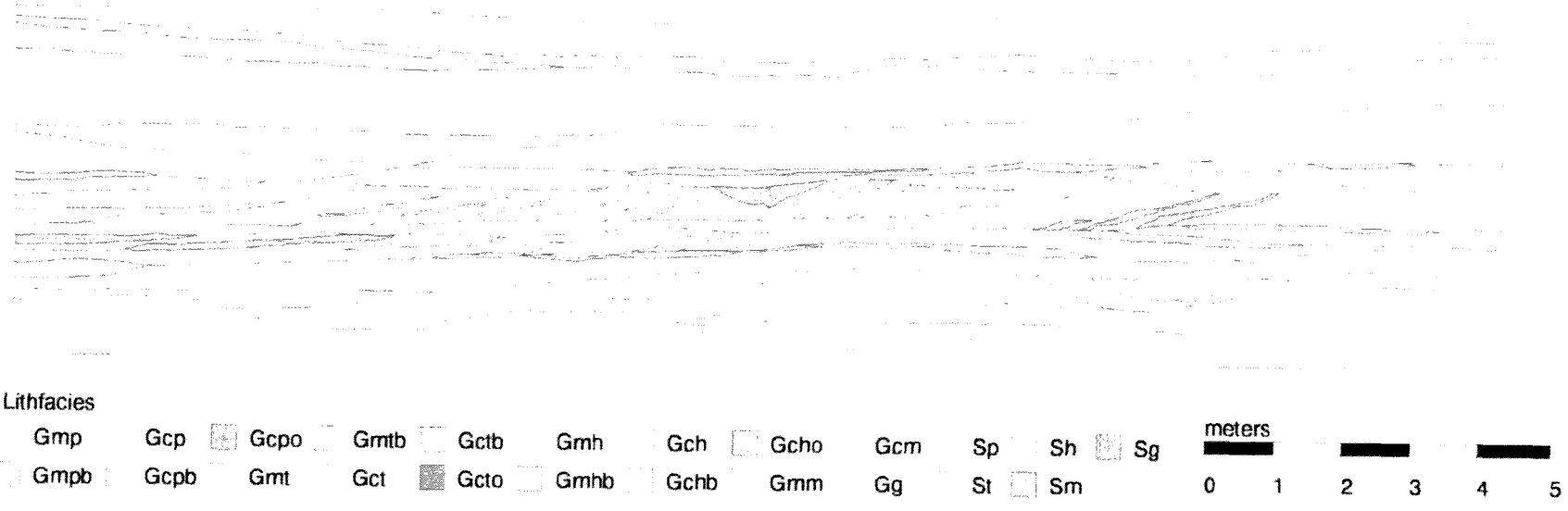

Outcrop Analysis STEISSLINGEN ST3

Photograph of Outcrop

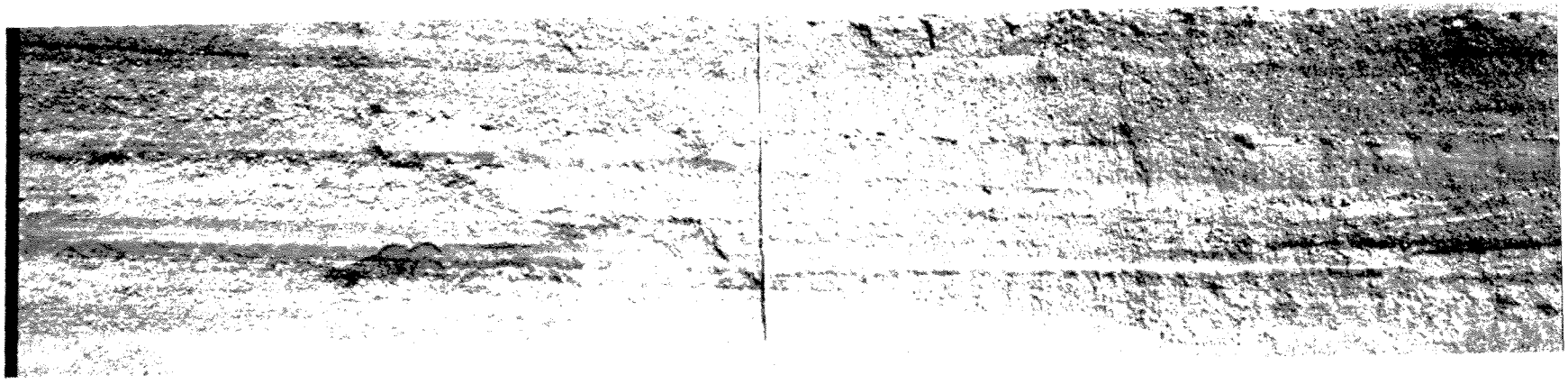

Sedimentological Interpretation

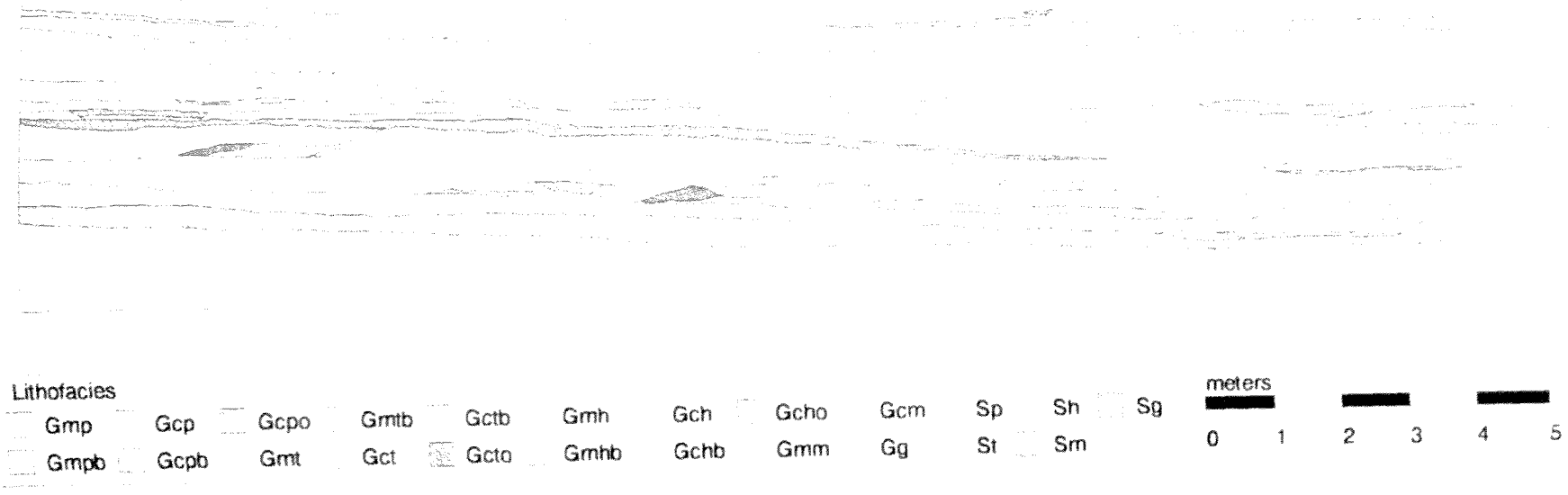

Outcrop Analysis STEISSLINGEN ST4

Photograph of Outcrop

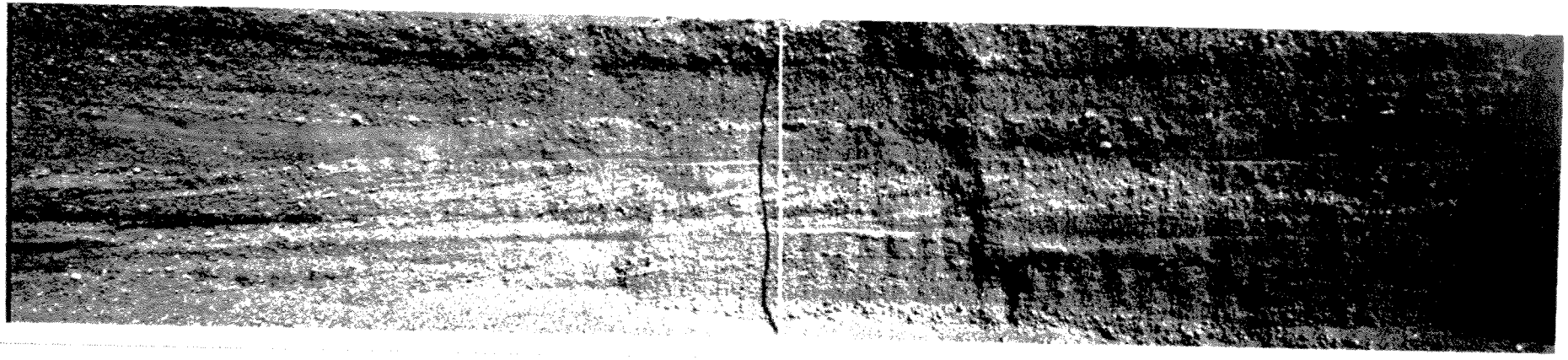

Sedimentological Interpretation

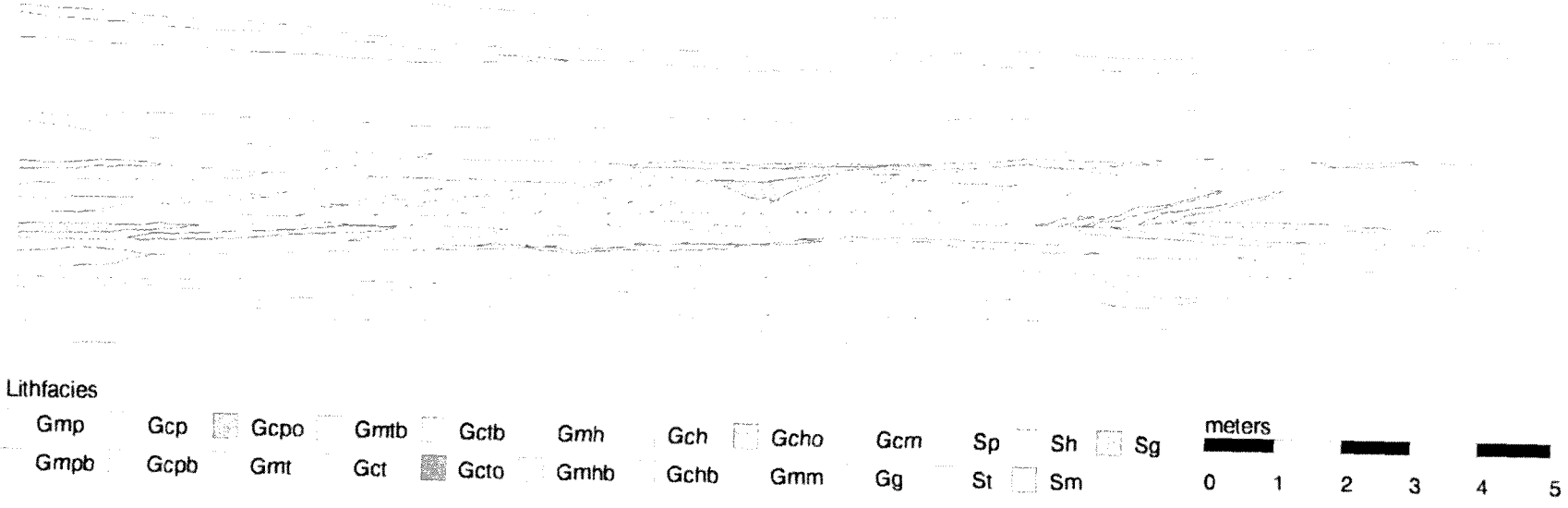

Annex 9: Listing of Program ARCTOGS

```
      PROGRAM ARCTOGS
C
C     Author:       Ralf KLingbeil
C     Version:      1
C     Date:         03.06.96
C     Language:     Fortran 77
C
C     Files:        will be created by the program
C
C     Arrays:       Value (Maxncols, Maxnrows)
C
C     Subroutines:  none
C
C     Functions:    none
C
C     Variables:    filename C path and filename of ARC/INFO (input)- or
C                              GSLIB (output)-file
C                   text     C scrolling parameter, unimportant
C                   Ncols    I No. of columns in x direction
C                   Nrows    I No. of rows in y direction
C                   Inumber  I unimportant No.
C                   Rnumber  R unimportant No.
C
C-----------------------------------------------------------------------
C     this program transfers data written in the format of the GRIDASCII
C     command in ARC/INFO (ARC) into an input file for GSLIB
C-----------------------------------------------------------------------

      INCLUDE 'parameter.inc'

      CHARACTER * 60 filename, text

      REAL Value(Maxncols,Maxnrows)

C      WRITE (*,*)
C      WRITE (*,*) 'Enter path and filename from where to read the'
C      WRITE (*,*) '--> INPUT DATA (e.g. ''path/GRID.IN'')'
C      WRITE (*,*) '    ~~~~~~~~~~'
C      WRITE (*,*)
C      READ (*,9000) filename

C-----------------------------------------------------------------------
C     >>>> START reading from INPUT DATA
C-----------------------------------------------------------------------
C      OPEN (3,FILE=filename)
      OPEN (3,FILE='temp.dat')
      REWIND (3)

C-----------------------------------------------------------------------
C          reading general parameters (incl. Ncols, Nrows)
C-----------------------------------------------------------------------
      READ (3,*) text, Ncols
      READ (3,*) text, Nrows
      READ (3,*) text, Rnumber
      READ (3,*) text, Rnumber
      READ (3,*) text, Rnumber
      READ (3,*) text, Inumber

C      IF ((Ncols .GT. Maxncols) .OR. (Nrows .GT. Maxnrows)) THEN
C        WRITE (*,*)
C        WRITE (*,*) '--> The No. of Columns or Rows exceeds the Max.!'
C        WRITE (*,*) '--> Change PARAMETER.INC, compile & run again.'
C        STOP
C      ENDIF


C-----------------------------------------------------------------------
C          reading Value
C-----------------------------------------------------------------------
      DO 10 J=1,Nrows
         READ (3,*) (Value(I,J),I=1,Ncols)
 10   CONTINUE

      CLOSE (3)

C-----------------------------------------------------------------------
C     >>>> END reading from INPUT DATA
C-----------------------------------------------------------------------

C      WRITE (*,*)
C      WRITE (*,*) 'Enter path and filename to where to write the'
C      WRITE (*,*) '--> OUTPUT DATA (e.g. ''path/GRID.OUT'')'
C      WRITE (*,*) '    ~~~~~~~~~~~'
C      WRITE (*,*)
C      READ (*,9000) filename

C-----------------------------------------------------------------------
C     >>>> START writing OUTPUT DATA
C-----------------------------------------------------------------------
C      OPEN (3,FILE=filename)
      OPEN (3,FILE='temp.out')
      REWIND (3)

C-----------------------------------------------------------------------
C          asking and writing general parameters (incl. title)
C-----------------------------------------------------------------------

C      WRITE (*,*)
C      WRITE (*,*) 'Enter PROJECT TITLE:'
C      WRITE (*,*)
C      READ (*,9000) text
      text='text1'

      WRITE (3,9000) text
      WRITE (3,*) 1

C      WRITE (*,*)
C      WRITE (*,*) 'Enter VARIABLE NAME:'
C      WRITE (*,*)
C      READ (*,9000) text
      text='text2'

      WRITE (3,9000) text

C-----------------------------------------------------------------------
C          writing Values
C-----------------------------------------------------------------------
      DO 20 J=1,Nrows
         JJ=Nrows-J+1
         DO 30 I=1,Ncols
            WRITE (3,*) Value(I,JJ)
 30      CONTINUE
 20   CONTINUE

      CLOSE (3)
C-----------------------------------------------------------------------
C     >>>> END writing OUTPUT DATA
C-----------------------------------------------------------------------

C-----------------------------------------------------------------------
C     formats
C-----------------------------------------------------------------------

9000 FORMAT (A)

      STOP
      END
```

Annex 10: Listing of Program PREMFLOW

```
      PROGRAM PREMFLOW
C ------------------------------------------------------------------
C *** PREPROCESSING FOR MODFLOW AND MODPATH **** 72 columns per line ***
C
C     originally by J. Whittaker
C
C     Version 3 of 05th Mar. 1998, changed by R. Klingbeil
C     Parameters set to maximum of 1100 x 200 cells
C     HEAD GRADIENT is set to  0.002
C ------------------------------------------------------------------
      PARAMETER (NPOLY=100, NTYPE=25, NPOIN=4000, NROW=200, NCOL=1100)
      DOUBLE PRECISION KX(NTYPE), KZ(NTYPE), PORO(NTYPE), RKD(NTYPE)
      INTEGER IGTYP(NROW,NCOL), ICOLOR(NTYPE), IRANK(NTYPE)
      CHARACTER*1 TEXT
C ------------------------------------------------------------------
C --- DIMENSIONS OF DIAGRAM
C
      XMIN=0.0
      XMAX=25.0
      ZMIN=0.0
      ZMAX=5.0
C
      DO 2 I=1,NTYPE
         IRANK(I)=0
         ICOLOR(I)=0
 2    CONTINUE
C ---
C ------------------------------------------------------------------
C --- READING KWERT.DAT
C
      OPEN(3,FILE='kwert.dat')
      nntype = 0
      DO 3 i=1,NTYPE
         READ(3,*,END=4) J,KX(J),KZ(J),PORO(J),RKD(J),IRANK(J),ICOLOR(J)
         nntype = nntype + 1
 3    CONTINUE
 4    CLOSE (3)
C
C ---
C ------------------------------------------------------------------
C --- RUN OPTION 1
C
 5    write(6,*) 'RUN OPTION 1 ?'
      write(6,*) ' (0) read in ARC/INFO ascii file'
      write(6,*) ' (1) read in existing grid'
      write(6,*)
      read(5,*) iopt
      if (iopt.lt.0 .or. iopt.gt.1) goto 5
C
C ---
C ------------------------------------------------------------------
C --- BEGIN OF SORPTION (RUN OPTION 2)
C     creating APPARENT POROSITY
C     by including equilibrium RETARDATION FACTOR ret
C     calculated from EQUILIBRIUM Kd (eq)
C
 6    write(6,*) 'RUN OPTION 2 ?'
      write(6,*) ' (0) only advection'
      write(6,*) ' (1) advection & equilibrium sorption'
      write(6,*)
      read(5,*) iiopt
      if (iiopt.lt.0 .or. iiopt.gt.1) goto 6
C
      if (iiopt.eq.1) then
         rho = 2.7
         do 7 i=1,nntype
            ret = (rho * rkd(i) * (1-poro(i)))/poro(i) + 1.
            poro(i) = poro(i) * ret
 7       continue
      endif
C
C --- END OF SORPTION
C ------------------------------------------------------------------
C --- READ EXISTING GRID INFORMATION
C
      if (iopt.eq.0 .or. iopt.eq.1) then
         call dread(igtyp,nx,nz,dx,dz,nrow,ncol,iopt)
         XMIN=0.0
         XMAX=DX*NX
         ZMIN=0.0
         ZMAX=DZ*NZ
      endif
C
      CALL GROUTE('SEL MX11; PAPER 290.0 200.0; E')
      CALL ROPEN
      CALL GLIMIT(XMIN,XMAX,ZMIN,ZMAX,0.0,0.0)
      CALL GVPORT(20.0,20.0,250.0,160.0)
      CALL GSCALE
C
C ---
C ------------------------------------------------------------------
C --- DISPLAY FINAL GRID
C
      CALL GSEGCR(1)
      CALL GRIDPLOT(NX,NZ,DX,DZ,IGTYP,ICOLOR,NROW,NCOL,NTYPE)
C --- plot frqame
      call gscale
      call gwicol(0.3,1)
      call gvect(0.,0.,0)
      call gvect(XMAX,0.,1)
      call gvect(XMAX,ZMAX,1)
      call gvect(0.,ZMAX,1)
      call gvect(0.,0.,1)
      CALL ANNOTATE(ICOLOR,IRANK,NTYPE)
      CALL GSEGCL(1)
      CALL RCLOSE
C
C ---
C ------------------------------------------------------------------
C --- SAVE GRID INFORMATION IFREQUESTED
C
 50      WRITE(6,*) 'SAVE GRID INFORMATION ?  (Y=YES)'
         READ(5,*) TEXT
         IF (TEXT.EQ.'Y' .OR. TEXT.EQ.'y')
     *      call dsave(igtyp,nx,nz,dx,dz,nrow,ncol)
C
C ---
C ------------------------------------------------------------------
C --- OUTPUT DATA IN FORMAT FOR MODFLOW AND MODPATH
C
      write(6,*) 'data files for modflow and modpath'
      write(6,*) 'option (1) whole grid'
      write(6,*) '       (2) portion of grid'
      read(5,*) iopt2
      if (iopt2.eq.1) then
         jmin=1
         jmax=nx
         imin=1
         imax=nz
         ngx=nx
         ngz=nz
      else
         write(6,*) 'input jmin,imin,ngx,ngz'
         read(5,*) jmin,imin,ngx,ngz
         jmax=jmin+ngx-1
         imax=imin+ngz-1
      endif
      CALL DATOUT(DX,DZ,NX,NZ,IGTYP,NROW,NCOL,NTYPE,imin,imax,jmin,jmax,
     *            ngx,ngz,iopt,iiopt,nntype)
C
C ---
C ------------------------------------------------------------------
      STOP
      END

C ******************************************************************
C *************************    SUBROUTINES   ***********************
C ******************************************************************
C
C ************************ SUBROUTINE DREAD ************************
C
      subroutine dread(igtyp,nx,nz,dx,dz,nrow,ncol,iopt)
      CHARACTER*80 FNAME
      CHARACTER*13 TEMP
      integer igtyp(nrow,ncol)
C
C ------------------------------------------------------------------
C --- read in the file name for reading grid information
C
      write(6,*) 'enter filename for input grid information'
      READ(5,'(A)') FNAME
C
C ---
C ------------------------------------------------------------------
C --- read in data
C
      open(3, file=fname)
C
      if (iopt.eq.1) then
         read(3,*) nx,nz
         read(3,*) dx,dz
         do 10 i=1,nz
            read(3,90) (igtyp(i,j),j=1,nx)
 10      continue
      else
         read(3,*) TEMP, nx
         read(3,*) TEMP, nz
         read(3,*) TEMP, dd
         read(3,*) TEMP, dd
         read(3,*) TEMP, dx
         read(3,*) TEMP, dd
         dz=dx
         icount=0
         do 20 i=1,nz
            read(3,*,end=30) (igtyp(i,j),j=1,nx)
 20      continue
 30   continue
      endif
      close(3)
 90   format(24i3)
C
C ---
C ------------------------------------------------------------------
      return
      end
C
C ************************ SUBROUTINE DSAVE ************************
C
      subroutine dsave(igtyp,nx,nz,dx,dz,nrow,ncol)
      CHARACTER*80 FNAME
      integer igtyp(nrow,ncol)
C
C ------------------------------------------------------------------
C --- read in the file name for saving grid information
C
      write(6,*) 'enter filename for output of grid information'
      READ(5,'(A)') FNAME
C
C ---
C ------------------------------------------------------------------
C --- write out data
C
      open(3, file=fname)
      write(3,*) nx,nz
      write(3,*) dx,dz
      do 10 i=1,nz
         write(3,90) (igtyp(i,j),j=1,nx)
 10   continue
      close(3)
 90   format(24i3)
 91   format(10i5)
C
C ---
C ------------------------------------------------------------------
      return
      end
C
C ********************** SUBROUTINE GRIDPLOT ***********************
C
      SUBROUTINE GRIDPLOT(NX,NZ,DX,DZ,IGTYP,ICOLOR,NROW,NCOL,NTYPE)
      INTEGER IGTYP(NROW,NCOL),ICOLOR(NTYPE)
C
      CALL GSCALE
      DO 10 J=1,NX
         DO 20 I=1,NZ
            XMIN=(J-1)*DX
            ZMIN=(NZ-I)*DZ
            if (igtyp(i,j).ne.0) then
               ICOL=ICOLOR( IGTYP(I,J) )
            else
               icol=1
            endif
            CALL SQUARE(XMIN,ZMIN,DX,DZ,ICOL)
 20      CONTINUE
 10   CONTINUE
C
      RETURN
      END
C
C ********************** SUBROUTINE ANNOTATE ***********************
C
      SUBROUTINE ANNOTATE(ICOLOR,IRANK,NTYPE)
      INTEGER ICOLOR(NTYPE), IRANK(NTYPE)
C
      CALL GSCAMM
      CALL RTXFON('SIMP',0)
      CALL RTXHEI(3.0)
C
      IRANKMAX=0
      DO 5 I=1,NTYPE
         IF (IRANK(I) .GT. IRANKMAX) IRANKMAX=IRANK(I)
 5    CONTINUE
C
      XMIN=12.0
```

```
      DO 10 I=1,IRANKMAX
         DO 20 J=1,IRANKMAX
         IF (IRANK(J) .EQ. I) THEN
            XMIN=XMIN+8.0
            ZMIN=100.0
            ICOL=ICOLOR(J)
            IF (I .EQ. 1) CALL RTX(14,'Bimodal Gravel',XMIN,ZMIN-6.0)
            IF (I .EQ. 7) XMIN=XMIN+8.0
            IF (I .EQ. 7) CALL RTX(14,'Open Framework',XMIN,ZMIN-6.0)
            IF (I .EQ. 11) XMIN=XMIN+8.0
            IF (I .EQ. 11) CALL RTX(12,'P/T/H Gravel',XMIN,ZMIN-6.0)
            IF (I .EQ. 17) XMIN=XMIN+8.0
            IF (I .EQ. 17) CALL RTX(8,'M Gravel',XMIN,ZMIN-6.0)
            IF (I .EQ. 19) XMIN=XMIN+8.0
            IF (I .EQ. 19) CALL RTX(4,'Sand',XMIN,ZMIN-6.0)
            CALL SQUARE2(XMIN,ZMIN,6.0,6.0,ICOL)
         ENDIF
 20      CONTINUE
 10   CONTINUE
C
      CALL RTXHEI(5.0)
      CALL RTX(16,'STEISSLINGEN ST2 ',20.0,120.0)
C
      RETURN
      END
C
C ************************* SUBROUTINE SQUARE *************************
C
      SUBROUTINE SQUARE(XMIN,ZMIN,DXX,DZZ,ICOL)
      REAL XPLOT(5),ZPLOT(5)
C
C --- fillings
      XMAX=XMIN+DXX
      ZMAX=ZMIN+DZZ
      XPLOT(1)=XMIN
      ZPLOT(1)=ZMIN
      XPLOT(2)=XMAX
      ZPLOT(2)=ZMIN
      XPLOT(3)=XMAX
      ZPLOT(3)=ZMAX
      XPLOT(4)=XMIN
      ZPLOT(4)=ZMAX
      XPLOT(5)=XMIN
      ZPLOT(5)=ZMIN
      NP=5
      CALL RSURF(XPLOT,ZPLOT,NP,ICOL,0.0)
C
      RETURN
      END
C
C ************************* SUBROUTINE SQUARE2 *************************
C
      SUBROUTINE SQUARE2(XMIN,ZMIN,DXX,DZZ,ICOL)
      REAL XPLOT(5),ZPLOT(5)
C
C --- fillings
      XMAX=XMIN+DXX
      ZMAX=ZMIN+DZZ
      XPLOT(1)=XMIN
      ZPLOT(1)=ZMIN
      XPLOT(2)=XMAX
      ZPLOT(2)=ZMIN
      XPLOT(3)=XMAX
      ZPLOT(3)=ZMAX
      XPLOT(4)=XMIN
      ZPLOT(4)=ZMAX
      XPLOT(5)=XMIN
      ZPLOT(5)=ZMIN
      NP=5
      CALL RSURF(XPLOT,ZPLOT,NP,ICOL,0.0)
C
C --- frames
      XPLOT(1)=XMIN
      ZPLOT(1)=ZMIN
      XPLOT(2)=XMAX
      ZPLOT(2)=ZMIN
      XPLOT(3)=XMAX
      ZPLOT(3)=ZMAX
      XPLOT(4)=XMIN
      ZPLOT(4)=ZMAX
      XPLOT(5)=XMIN
      ZPLOT(5)=ZMIN
      NP=5
      CALL GWICOL(0.15,1)
      CALL GVECT(XPLOT,ZPLOT,NP)
C
      RETURN
      END
C
C ************************* SUBROUTINE DATOUT *************************
C
      SUBROUTINE DATOUT(DX,DZ,NX,NZ,IGTYP,NROW,NCOL,NTYPE,imin,imax,
     *                  jmin,jmax,ngx,ngz,iopt,iiopt,nntype)
      REAL COND(NROW,NCOL), KX(NTYPE), KZ(NTYPE), K1,K2
      REAL SHEAD(NCOL,NROW), PORO(NTYPE), RKD(NTYPE), POR(NCOL,NROW)
      REAL KFBORE(24,NROW), KFX(NROW,NCOL), KFZ(NROW,NCOL)
      INTEGER IGTYP(NROW,NCOL), IUNIT(24), IBOUND(NCOL,NROW)
      INTEGER IRANK(NTYPE), ICOLOR(NTYPE)
      integer ibtyp(24,NROW)
      integer ikount(25)
      CHARACTER *20 FMTIN
      CHARACTER *80 TEXT
C
C ---------------------------------------------------------------------
C --- OUTPUT THE DATA IN A FORM SUITABLE FOR MODFLOW
C ---------------------------------------------------------------------
C --- assign kf values according to categories
C
        OPEN(3,FILE='kwert.dat')
 10     READ(3,*,END=15) J,KX(J),KZ(J),PORO(J),RKD(J),IRANK(J),
     +      ICOLOR(J)
            GOTO 10
 15     CLOSE(3)
        ITYPE=J
        do 500 i=1,nz
           do 510 j=1,nx
              kfx(i,j)=kx(igtyp(i,j))
              kfz(i,j)=kz(igtyp(i,j))
 510       continue
 500    continue
C
C ---
C ---------------------------------------------------------------------
C --- calculate the geometric mean of all the permeabilities
C
        do 6 i=1,ITYPE
           ikount(i)=0
 6      continue
        do 7 j=jmin,jmax
           do 8 i=imin,imax
              num=igtyp(i,j)
              ikount(num) =ikount(num)+1
 8         continue
 7      continue
        condx=0.0
        condz=0.0
        write(6,*) 'categ   no of cells   percent  -ln(kx)'
        do 9 i=1,ITYPE
           condx=condx+ikount(i)*log(kx(i))
           condz=condz+ikount(i)*log(kz(i))
           percen=100.0* float(ikount(i))/((jmax-jmin+1)*(imax-imin+1))
           write(6,*) i, ikount(i), percen, -log(KX(I))
 9      continue
        condx=condx/((jmax-jmin+1)*(imax-imin+1))
        condx=exp(condx)
        condz=condz/((jmax-jmin+1)*(imax-imin+1))
        condz=exp(condz)
        write(6,*)
        write(6,*) 'geometric mean of conductivities:'
        write(6,*) 'Kg (x-dir), Kg(y-dir)'
        write(6,*)  condx, condz
C
C ---
C ---------------------------------------------------------------------
C --- calculate the arithmetic mean of all the permeabilities
C
        pmean=0.0
        plmean=0.0
        do 11 j=jmin,jmax
           do 12 i=imin,imax
              pmean=pmean+kx(igtyp(i,j))
              plmean=plmean-log(kx(igtyp(i,j)))
 12        continue
 11     continue
        pmean=pmean/((jmax-jmin+1)*(imax-imin+1))
        plmean=plmean/((jmax-jmin+1)*(imax-imin+1))
        var=0.0
        varl=0.0
        skew=0.0
        skewl=0.0
        do 17 j=jmin,jmax
           do 18 i=imin,imax
              var=var+(kx(igtyp(i,j))-pmean)**2
              varl=varl+(-log(kx(igtyp(i,j)))-plmean)**2
              skew=skew+(kx(igtyp(i,j))-pmean)**3
              skewl=skewl+(-log(kx(igtyp(i,j)))-plmean)**3
 18        continue
 17     continue
        var=var/((jmax-jmin+1)*(imax-imin+1))
        varl=varl/((jmax-jmin+1)*(imax-imin+1))
        skew=skew/((jmax-jmin+1)*(imax-imin+1))
        skew=skew/(var**1.5)
        skewl=skewl/((jmax-jmin+1)*(imax-imin+1))
        skewl=skewl/(varl**1.5)
        write(6,*)
        write(6,*) 'arithmetic means of conductivities:'
        write(6,*)
        write(6,*) 'Ka (x-dir) stats:'
        write(6,*) 'mean:',pmean
        write(6,*) 'var: ',var
        write(6,*) 'skew:',skew
        write(6,*)
        write(6,*) '(-ln K)a (x-dir) stats:'
        write(6,*) 'mean:',plmean
        write(6,*) 'var: ',varl
        write(6,*) 'skew:',skewl
C
        pmean=0.0
        plmean=0.0
        do 20 j=jmin,jmax
           do 21 i=imin,imax
              pmean=pmean+kz(igtyp(i,j))
              plmean=plmean-log(kz(igtyp(i,j)))
 21        continue
 20     continue
        pmean=pmean/((jmax-jmin+1)*(imax-imin+1))
        plmean=plmean/((jmax-jmin+1)*(imax-imin+1))
        var=0.0
        varl=0.0
        skew=0.0
        skewl=0.0
        do 22 j=jmin,jmax
           do 23 i=imin,imax
              var=var+(kz(igtyp(i,j))-pmean)**2
              varl=varl+(-log(kz(igtyp(i,j)))-plmean)**2
              skew=skew+(kz(igtyp(i,j))-pmean)**3
              skewl=skewl+(-log(kz(igtyp(i,j)))-plmean)**3
 23        continue
 22     continue
        var=var/((jmax-jmin+1)*(imax-imin+1))
        varl=varl/((jmax-jmin+1)*(imax-imin+1))
        skew=skew/((jmax-jmin+1)*(imax-imin+1))
        skew=skew/(var**1.5)
        skewl=skewl/((jmax-jmin+1)*(imax-imin+1))
        skewl=skewl/(varl**1.5)
        write(6,*)
        write(6,*) 'Ka (y-dir) stats:'
        write(6,*) 'mean:',pmean
        write(6,*) 'var: ',var
        write(6,*) 'skew:',skew
        write(6,*)
        write(6,*) '(-ln K)a (y-dir) stats:'
        write(6,*) 'mean:',plmean
        write(6,*) 'var: ',varl
        write(6,*) 'skew:',skewl
        write(6,*)
C
      ISS=1
      IGFDCB=50
      LAYCON=0
      DELR=DX
      DELC=DZ
      NUNIT=25
      FMTIN='  (7E11.5)'
C
C ---
C ---------------------------------------------------------------------
C --- DATA FILE FOR VARIOGRAM CALCULATION
C
      OPEN(8,FILE='kf.dat')
      WRITE(8,*) 'STEISSLINGEN'
      WRITE(8,*) 2
      WRITE(8,*) 'KX'
      WRITE(8,*) 'KZ'
      DO 13 I=imax,imin,-1
         DO 14 J=jmin,jmax
            WRITE(8,94)  -log(KFX(I,J)) ,-log(KFZ(I,J))
C           WRITE(8,94)  KFX(I,J) , KFZ(I,J)
 14      continue
 13   continue
 94   format(2e14.6)
      close(8)
C
C ---
C ---------------------------------------------------------------------
C --- BOUNDARY CONDITIONS FOR MODFLOW
C
      write(6,*) 'INPUT OPTION:'
      write(6,*) '  1: Confined flow under head gradient'
      write(6,*) '  2: Confined flow under pumping'
      write(6,*) '  3: Slug test'
      read(5,*) ifopt
      iss=1
      if (ifopt.eq.2) then
         write(6,*) 'INPUT OPTION:'
         write(6,*) '  0: Transient Conditions'
```

```
        write(6,*) '  1: Stationary Conditions'
        read(5,*) iss
        write(6,*) 'INPUT JB (WELL CELL NUMBER)'
        read(5,*) jb
      elseif (ifopt.eq.3) then
        iss=0
        write(6,*) 'INPUT JB (WELL CELL NUMBER)'
        read(5,*) jb
      endif
C
C ---
C ------------------------------------------------------------------------
C --- GENERAL FINITE DIFFERENCE FILE - GFD.DAT
C
      OPEN(4,FILE='gfd.dat')
      WRITE(4,900) ISS,IGFDCB
      WRITE(4,900) LAYCON
      WRITE(4,910) 0,DELR
      WRITE(4,910) 0,DELC
C
C --- storage capacity for transient case
C
      IF (IFOPT.EQ.2 .AND. ISS.EQ.0)
     *   WRITE(4,998) 0,3.125E-06
      IF (IFOPT.EQ.3)
     *   WRITE(4,998) 0,3.125E-06
C
C --- horizontal conductivity
C
      WRITE(4,920) NUNIT,1.0,FMTIN,-1
      DO 25 I=IMIN,IMAX
         DO 30 J=JMIN,JMAX-1
            K1=KFX(I,J)
            K2=KFX(I,J+1)
c           COND(I,J)=2.0*K1*K2/(K1+K2)
            COND(I,J)=SQRT(K1*K2)
            COND(I,J)=COND(I,J)*DELC/DELR
   30    CONTINUE
         J=JMAX
         COND(I,J)=0.0
   25 CONTINUE
C
      if (ifopt.eq.2. .or. ifopt.eq.3) then
         do 35 i=imin,imax
            cond(i,jb)=10.0
            cond(i,jb+1)=10.0
            cond(i,jb+2)=10.0
   35    continue
      endif
C
      DO 40 I=IMIN,IMAX
         WRITE(4,930) (COND(I,J),J=JMIN,JMAX)
   40 CONTINUE
C
C --- vertical conductivity
C
      WRITE(4,920) NUNIT,1.0,FMTIN,-1
      DO 50 J=JMIN,JMAX
         DO 60 I=IMIN,IMAX-1
            K1=KFZ(I,J)
            K2=KFZ(I+1,J)
c           COND(I,J)=2.0*K1*K2/(K1+K2)
            COND(I,J)=SQRT(K1*K2)
            COND(I,J)=COND(I,J)*DELR/DELC
            if (COND(I,J).le.0.0) write(6,*) 'help', i,j
   60    CONTINUE
         I=IMAX
         COND(I,J)=0.0
   50 CONTINUE
C
      if (ifopt.eq.2 .or. ifopt.eq.3) then
         DO 65 I=IMIN,IMAX-1
            cond(i,jb)=10.0
            cond(i,jb+1)=10.0
            cond(i,jb+2)=10.0
            cond(i,jb+3)=10.0
   65    continue
      endif
C
      DO 70 I=IMIN,IMAX
         WRITE(4,930) (COND(I,J),J=JMIN,JMAX)
   70 CONTINUE
      CLOSE(4)
C
C ---
C ------------------------------------------------------------------------
C --- BASIC INPUT FILE - BAS.DAT
C
      TEXT='STEISSLINGEN'
      NLAY=1
      NPER=1
      ITMUNI=1
      DO 80 I=1,24
         IUNIT(I)=0
   80 CONTINUE
C --- OUTPUT CONTROL
      IUNIT(12)=22
C --- PCG2
      IUNIT(13)=23
C --- GFD
      IUNIT(15)=25
      if (ifopt.eq.2) then
C ---    WELL DATA
         IUNIT(2)=12
      endif
      IAPART=0
      ISTRT=0
      NUNIT=1
      DO 90 I=IMIN,IMAX
         IBOUND(JMIN,I)=-1
         DO 100 J=JMIN+1,JMAX-1
            IBOUND(J,I)=1
  100    CONTINUE
         IBOUND(JMAX,I)=-1
   90 CONTINUE
      HNOFLO=999.9
C
C --- INITIAL HEADS
C
      if (ifopt.eq.2 .or. ifopt.eq.3) then
         sheb=10.0
      else
C
C --- HEAD GRADIENT OF 0.001 M A METRE
C
c        sheadb=10.0+(ngx-1)*dx*0.001
c     endif
C
C --- HEAD GRADIENT OF 0.002 M A METRE
C
         sheadb=10.0+(ngx-1)*dx*0.002
      endif
      DO 110 I=IMIN,IMAX
         DO 120 J=JMIN,JMAX-1
            SHEAD(J,I)=sheadb
  120    CONTINUE
         SHEAD(JMAX,I)=10.0
  110 CONTINUE
C
C --- SLUG TEST
C
      if (ifopt.eq.3) then
         do 111 I=IMIN,IMAX
            do 112 J=JB,JB+3
               SHEAD(J,I)=sheadb+1.0
  112       continue
  111    continue
      endif
      PERLEN=300.
      NSTP=1
      TSMULT=1.4
      FMTIN='  (24I3)'
C
      OPEN(4,FILE='bas.dat')
      WRITE(4,970) TEXT
      WRITE(4,*)
      WRITE(4,900) NLAY,NGZ,NGX,NPER,ITMUNI
      WRITE(4,940) (IUNIT(J),J=1,24)
      WRITE(4,900) IAPART,ISTRT
      WRITE(4,950) NUNIT,1,FMTIN,-1
      DO 130 I=IMIN,IMAX
         WRITE(4,940) (IBOUND(J,I),J=JMIN,JMAX)
  130 CONTINUE
      WRITE(4,960) HNOFLO
      FMTIN='  (7E11.5)'
      WRITE(4,920) NUNIT,1.0,FMTIN,-1
      DO 140 I=IMIN,IMAX
         WRITE(4,930) (SHEAD(J,I),J=JMIN,JMAX)
  140 CONTINUE
      WRITE(4,960) PERLEN,NSTP,TSMULT
      CLOSE(4)
C
C ---
C ------------------------------------------------------------------------
C --- WELL DATA FILE - WELL.DAT
C
      if (ifopt.eq.2) then
c        NUMBER OF WELLS = 2
         MXWELL=2
         IWELCB=0
         OPEN(4,FILE='well.dat')
         WRITE(4,900) MXWELL,IWELCB
         WRITE(4,900) MXWELL
         QWELL=-0.5e-04
         WRITE(4,995) 1,1,JB+1,QWELL
         WRITE(4,995) 1,1,JB+2,QWELL
         close(4)
      endif
C
C ---
C ------------------------------------------------------------------------
C --- MAIN FILE FOR MODPATH - MAIN.DAT
C
      NCBL=0
      IGRID=1
      DO 150 I=1,6
         IUNIT(I)=0
  150 CONTINUE
      if (ifopt.eq.2) then
C ---    WELL DATA
         IUNIT(2)=15
      endif
      IUNIT(7)=50
      IUNIT(8)=52
      DELZ=1.0
      ZBL1=0.0
      NUNIT=100
      FMTIN='  (24I3)'
C
C -------------------------------------
C --- BEGIN SORPTION
C     new by R Klingbeil
C
      if (iiopt.eq.1) then
         rho = 2.7
         do 155 i=1,nntype
            ret = (rho * rkd(i))/poro(i) + 1
            poro(i) = poro(i) * ret
  155    continue
      endif
C
C --- END SORPTION
C -------------------------------------
C
      if (iopt.lt.3) then
         DO 160 I=IMIN,IMAX
            DO 170 J=JMIN,JMAX
               POR(J,I)=PORO( IGTYP(I,J) )
  170       CONTINUE
  160    CONTINUE
      endif
C
      OPEN(4,FILE='main.dat')
      WRITE(4,900) NGX,NGZ,NLAY,NCBL,IGRID
      WRITE(4,980) (IUNIT(I),I=1,8)
      WRITE(4,990) LAYCON
      WRITE(4,910) 0,DELR
      WRITE(4,910) 0,DELC
      WRITE(4,910) 0,DELZ
      WRITE(4,935) ZBL1
      WRITE(4,950) NUNIT,1,FMTIN,-1
      DO 180 I=IMIN,IMAX
         WRITE(4,940) (IBOUND(J,I),J=JMIN,JMAX)
  180 CONTINUE
      FMTIN='  (7E11.5)'
      WRITE(4,920) NUNIT,1.0,FMTIN,-1
      write(6,*) 'NOT overwriting the porosities'
      DO 190 I=IMIN,IMAX
         WRITE(4,930) (POR(J,I),J=JMIN,JMAX)
  190 CONTINUE
C
C --- set constant porosity=0.2
c     write(6,*) 'overwriting the porosities'
c     WRITE(4,910) 0,0.2
c
  900 FORMAT(5I10)
  910 FORMAT(I10,F10.3)
  920 FORMAT(I10,E10.3,A20,I10)
  930 FORMAT(7E11.5)
  935 FORMAT(E10.4)
  940 FORMAT(24I3)
  950 FORMAT(I10,I10,A20,I10)
  960 FORMAT(F10.1,I10,F10.1)
  970 FORMAT(A80)
  980 FORMAT(8I5)
  990 FORMAT(I2)
  995 FORMAT(3I10,E10.4)
  998 FORMAT(I10,E10.4)
C
C ---
C ------------------------------------------------------------------------
      RETURN
      END
```

Annex 11: Listing of Program RETARD

```
      program retard
C ------------------------------------------------------------------
C     program to calculate the retardation of particles, which have been
C     advectively transported by MODPATH through a 2D section, where
C     flow has been modelled by MODFLOW before, using ENDPOINT or
C     PATHLINE, kwert.dat, gravel.dat, bimodal.dat, openwork.dat,
C     sand.dat and an output file from PREMFLOW, describing the cell
C     parameters for the section.
C     The total travel times of every particle will be calculated and
C     written to the output file t-tot.dat.
C     The travel times of every particle in each hydrofacies will be
C     calculated and written to the output file t-hf.dat.
C     The path length of every particle in each hydrofacies will be
C     calculated and written to the output file p-hf.dat.
C
C     Version 5 of 04th Mar. 1998, by R. Klingbeil
C ------------------------------------------------------------------
C     variables: FNAME    C input file name for grid information
C                IOPT     I run option
C                IIPART   I temporary, to compare with IPART
C                IPART    I actual No of particles
C                ITEMP1-8 I temporary variables
C                ITYPE    I 1 gravel, 2 bimodal, 3 openwork, 4 sand
C                J        I temporary index for lithofacies
C                NCOL     I max. (No columns, No path positions/particle)
C                NLINE    I max. No particles * max. No cells in x/j dir
C                NP       I max. No particles
C                NROW     I max. No rows
C                NT       I max. No Kd values in e.g. bimodal.dat
C                NTYPE    I max. No lithofacies in kwert.dat
C                NX       I No of columns, cells in x/j direction
C                NY       I No of rows, cells in y/i direction
C                RET      R retardation factor
C                RHO      R density (=2.7)
C                RRKD     R actual RKD for particle, time & position
C                TEMP1-5  R temporary variables
C                TOT      R total time/particle (start > arrival)
C                XLC      R actual x coor. of particle at arrival
C                YLC      R actual y coor. of particle at arrival
C
C     arrays:    BMKD   NT        R KD for bimodal
C                BMT    NT        R T for bimodal
C                EKD    NTYPE     R equilibrium Kd per lithofacies
C                GRAVKD NT        R KD for gravel
C                GRAVT  NT        R T for gravel
C                IGTYP  NROW,NCOL I lithofacies code for cell
C                IPOS   NP,NCOL   I cell index in i/y direction
C                JPOS   NP,NCOL   I cell index in j/x direction
C                NPART  NCOL      I No of positions per particle path
C                OWKD   NT        R KD for openwork
C                OWT    NT        R T for openwork
C                PBM    NP        R cum. pathlength of part. in bimodal
C                PCON   NP,NCOL   R pathlength in specific cell
C                PGRAV  NP        R cum. pathlength of part. in gravel
C                PORO   NTYPE     R porosity of lithofacies
C                POW    NP        R cum. pathlength of part. in openwork
C                PSAND  NP        R cum. pathlength of part. in sand
C                RKD    NT        R real Kd (TTAB) for actual ITYPE
C                SANDKD NT        R KD for sand
C                SANDT  NT        R T for sand
C                TCON   NP,NCOL   R contact time of part. in cell
C                TCUM   NP,NCOL   R cumulative time of part. in cell
C                TGRAV  NP        R cumulative time of part. in gravel
C                TOW    NP        R cumulative time of part. in openwork
C                TSAND  NP        R cumulative time of part. in sand
C                TTAB   NT        R time int. for real Kd in table
C                TTOT   NP        R total time/part. (start > arrival)
C                XCON   NP,NCOL   R pathlength in specific cell in x/j
C                XPOS   NP,NCOL   R pos. of particle in x/j dir
C                YCON   NP,NCOL   R pathlength in specific cell in y/i
C                YPOS   NP,NCOL   R pos. of particle in y/i dir
C
C ==================================================================
C --- RUN OPTIONS
C
      parameter (NCOL=1500, NP=500, NROW=250, NT=2000, NTYPE=25)
      double precision BMKD(NT), BMT(NT), EKD(NTYPE), GRAVKD(NT),
     +                 GRAVT(NT), OWKD(NT), OWT(NT), PBM(NP),
     +                 PCON(NP,NCOL), PGRAV(NP), PORO(NTYPE), POW(NP),
     +                 PSAND(NP), RKD (NT), SANDKD(NT), SANDT(NT),
     +                 TBM (NP), TCON (NP,NCOL), TCUM (NP,NCOL),
     +                 TGRAV (NP), TOW (NP), TSAND (NP), TTAB (NT),
     +                 TTOT (NP), XCON (NP,NCOL), XPOS(NP,NCOL),
     +                 YCON(NP,NCOL), YPOS(NP,NCOL)
      integer IGTYP(NROW,NCOL), IIPART, IPART, IPOS (NP,NCOL), ITYPE,
     +        IOPT, ITEMP1, ITEMP2, ITEMP3, ITEMP4, ITEMP5, ITEMP6,
     +        ITEMP7, ITEMP8, JPOS (NP,NCOL), NPART (NCOL)
      character*80 FNAME
C
      NLINE = NP * NCOL
C
 5    write(6,*) 'RUN OPTION ?'
      write(6,*) ' (0) advection only, faster, using ENDPOINT'
      write(6,*) ' (1) advection only, slower, using PATHLINE'
      write(6,*) ' (2) advection & sorption with equilibrium'
      write(6,*) '     Kd(eq, lithofacies)'
      write(6,*) ' (3) advection & sorption with contact time '
      write(6,*) '     dependent Kd(t, lithofacies)'
      write(6,*)
      read(5,*) IOPT
      if (IOPT.lt.0 .or. IOPT.gt.3) goto 5
C
C ---
C ==================================================================
C     ADVECTION ONLY (IOPT = 0)
C     using only total time per particle from ENDPOINT column 9
C ------------------------------------------------------------------
C ---
C
      if (IOPT.eq.0) then
         open(3,file='t-tot.dat')
         write(3,*) 'arrival times [d]'
         write(3,*) 3
         write(3,*) 'x'
         write(3,*) 'z'
         write(3,*) 't'
C
         open(4,file='ENDPOINT')
 20      read(4,900,end=10) ITEMP1,ITEMP2,ITEMP3,ITEMP4,XLC,YLC,TEMP1,
     +                      TEMP2,TOT,TEMP3,TEMP4,TEMP5,ITEMP5,ITEMP6,
     +                      ITEMP7,ITEMP8
C
C --- conversion of tot from seconds to days
C
         TOT = TOT / (60.0*60.0*24.0)
C
C --- data output to t-tot.dat
C
         write(3,910) XLC,YLC,TOT
         goto 20
 10      continue
         close(3)
         close(4)
C
C ---
C ==================================================================
C     ADVECTION ONLY (IOPT = 1)
C     For each particle:
C     a) reading actual cell position (j,i) from PATHLINE column 7, 8
C        and contact time for cell (j,i) as difference from cumulative
C        times from PATHLINE column 6,
C     b) looking up IGTYP for actual cell position (j,i) from FNAME,
C     c) setting retardation factor to 1.0, contact time within
C        particular cell for particular particle remains constant,
C     d) adding up all contact times for each particle path
C     e) adding up all contact times for each particle path in each
C        hydrofacies
C     f) adding up all path length for each particle path in each
C        hydrofacies
C ==================================================================
C     ADVECTION WITH EQUILIBRIUM SORPTION (IOPT = 2)
C     For each particle:
C     a) reading actual cell position (j,i) from PATHLINE column 7, 8
C        and contact time for cell (j,i) as difference from cumulative
C        times from PATHLINE column 6,
C     b) looking up IGTYP for actual cell position (j,i) from FNAME,
C     c) reading equilibrium Kd values from table kwert.dat depending on
C        IGTYP of actual cell position of particle,
C     d) calculating equilibrium retardation factor and adjusting
C        contact time within particular cell for particular particle,
C     e) adding up all newly calculated contact times for each particle
C        path
C     f) adding up all contact times for each particle path in each
C        hydrofacies
C     g) adding up all path length for each particle path in each
C        hydrofacies
C ==================================================================
C     ADVECTION WITH SORPTION DEPENDING ON CONTACT TIME (IOPT = 3)
C     For each particle:
C     a) reading actual cell position (j,i) from PATHLINE column 7, 8
C        and contact time for cell (j,i) as difference from cumulative
C        times from PATHLINE column 6,
C     b) looking up IGTYP for actual cell position (j,i) from FNAME,
C     c) reading particular Kd values from table for this particular
C        IGTYP (lithofacies) and contact time: gravel.dat, bimodal.dat,
C        sand.dat or openwork.dat,
C     d) calculating actual retardation factor and adjusting contact
C        time within particular cell for particular particle,
C     e) adding up all newly calculated contact times for each particle
C        path
C     f) adding up all contact times for each particle path in each
C        hydrofacies
C     g) adding up all path length for each particle path in each
C        hydrofacies
C ------------------------------------------------------------------
C ---
C
      elseif ((IOPT.eq.1).or.(IOPT.eq.2).or.(IOPT.eq.3)) then
C
C --- reading equilibrium Kd EKD and porosity PORO for lithofacies
C     (index J=1,23)
C
         open(4,file='kwert.dat')
         do 30 i=1,NTYPE
            read(4,*,END=40) J,TEMP1,TEMP2,PORO(J),EKD(J),ITEMP1,ITEMP2
 30      continue
 40      close (4)
C
C --- reading all data from PATHLINE
C
         open(4,file='PATHLINE')
         N = 0
         IIPART = 1
 50      N = N+1
         read(4,920,end=60) IPART,XPOS(IPART,N),YPOS(IPART,N),TEMP1,
     +                      TEMP2,TCUM(IPART,N),JPOS(IPART,N),
     +                      IPOS(IPART,N),ITEMP1
C
C     same particle: continue
C
         if (IPART.eq.IIPART) goto 50
C
C     next particle: 1. correct, 2. start again
C
         NPART(IPART-1) = N-1
         XPOS(IPART,1) = XPOS(IPART,N)
         YPOS(IPART,1) = YPOS(IPART,N)
         TCUM(IPART,1) = TCUM(IPART,N)
         JPOS(IPART,1) = JPOS(IPART,N)
         IPOS(IPART,1) = IPOS(IPART,N)
         N = 1
         IIPART = IPART
         goto 50
 60      NPART(IPART) = N-1
         close(4)
C
C --- reading all lithofacies codes for section
C --- read in the file name for reading grid information
C
         write(6,*) 'input filename for grid information'
         READ(5,'(A)') FNAME
C
C --- read in all data from FNAME
C
         open(4,file=FNAME)
         read(4,*) NX,NY
         read(4,*) TEMP1,TEMP2
         do 70 i=1,NY
            read(4,930) (IGTYP(i,j),j=1,NX)
 70      continue
         close(4)
C
C ---    reading Kd and TTAB from files into tables
C
         open(4,file='gravel.dat')
         NGRAV = 0
         do 72 l=1,NT
            read(4,*,end=73) GRAVT(l), GRAVKD(l)
            NGRAV = NGRAV + 1
 72      continue
 73      close(4)
C
         open(4,file='bimodal.dat')
         NBM = 0
         do 74 l=1,NT
            read(4,*,end=75) BMT(l), BMKD(l)
            NBM = NBM + 1
 74      continue
 75      close(4)
C
         open(4,file='openwork.dat')
         NOW = 0
         do 76 l=1,NT
            read(4,*,end=77) OWT(l), OWKD(l)
```

```
            NOW = NOW + 1
 76       continue
 77       close(4)
C
          open(4,file='sand.dat')
          NSAND = 0
          do 78 l=1,NT
             read(4,*,end=79) SANDT(l), SANDKD(l)
             NSAND = NSAND + 1
 78       continue
 79       close(4)
C
C --- transfering cumulative times TCUM to residence times TCON per cell
C --- transfering positions XPOS to pathlength XCON per cell
C --- transfering positions YPOS to pathlength YCON per cell
C --- calculating pathlength per cell from XCON and YCON
C
          do 80 i=1,IPART
             do 90 j=1,NPART(i)-1
                TCON(i,j)=TCUM(i,j+1)-TCUM(i,j)
                XCON(i,j)=XPOS(i,j+1)-XPOS(i,j)
                YCON(i,j)=YPOS(i,j+1)-YPOS(i,j)
                PCON(i,j)=SQRT(XCON(i,j)*XCON(i,j)+YCON(i,j)*YCON(i,j))
 90          continue
             TCON(i,NPART(i))=0.0
             XCON(i,NPART(i))=0.0
             YCON(i,NPART(i))=0.0
 80       continue
C
C --- writing out min., aver., max. contact times per lithofacies
C
          open(4,file='tcon.dat')
          write(4,*) 'LF-No, No, min., average, max. contact time [s]'
          do 95 k=1,23
             TMAX = 0.0
             TMIN = 10000000.0
             TSUM = 0.0
             NCOUNT = 0
             do 96 i=1,IPART
                do 97 j=1,NPART(i)
                   if (IGTYP(IPOS(i,j),JPOS(i,j)).eq.k) then
                      if (TCON(i,j).gt.TMAX) TMAX = TCON(i,j)
                      if (TCON(i,j).lt.TMIN) TMIN = TCON(i,j)
                      TSUM = TSUM + TCON (i,j)
                      NCOUNT = NCOUNT + 1
                   endif
 97             continue
 96          continue
             TAVER = TSUM / NCOUNT
             write(4,*) k, NCOUNT, TMIN, TAVER, TMAX
 95       continue
          close(4)
C
C --- retardation calculations
C
          RHO = 2.7
          do 100 i=1,IPART
             TTOT(i) = 0.0
             TGRAV(i) = 0.0
             TBM(i) = 0.0
             TOW(i) = 0.0
             TSAND(i) = 0.0
             PGRAV(i) = 0.0
             PBM(i) = 0.0
             POW(i) = 0.0
             PSAND(i) = 0.0
             do 110 j=1,NPART(i)
C
C               looking up IGTYP for each particle position
                k = IGTYP(IPOS(i,j),JPOS(i,j))
C
C ---           resorting of IGTYP to ITYPE
C
C
                gravel
                if ((k.eq.1).or.(k.eq.3).or.(k.eq.6).or.
     +              (k.eq.8).or.(k.eq.11).or.(k.eq.13)
     +              .or.(k.eq.16).or.(k.eq.17)) ITYPE = 1
C
C               bimodal
                if ((k.eq.2).or.(k.eq.4).or.(k.eq.7).or.
     +              (k.eq.9).or.(k.eq.12).or.(k.eq.14))
     +              ITYPE = 2
C
C               openwork
                if ((k.eq.5).or.(k.eq.10).or.(k.eq.15)
     +              .or.(k.eq.18)) ITYPE = 3
C
C               sand
                if ((k.eq.19).or.(k.eq.20).or.(k.eq.21)
     +              .or.(k.eq.22).or.(k.eq.23)) ITYPE = 4
C
C ---           different retardatio options
C
                if (IOPT.eq.1) then
C
C                  no retardation, only advection
                   RET = 1.0
C
                elseif (IOPT.eq.2) then
C
C                  taking EKD and PORO value for specific IGTYP
C                  calculating retardation RET
                   RET = 1.0 + RHO * EKD(k) * (1.0-PORO(k)) / PORO(k)
C
                elseif (IOPT.eq.3) then
C
C ---              reading Kd and TTAB from table for ITYPE
C
                   if (ITYPE.eq.1) then
                      N = NGRAV
                      do 120 l=1,NT
                         TTAB(l) = GRAVT(l)
                         RKD(l) = GRAVKD(l)
 120                  continue
                   elseif (ITYPE.eq.2) then
                      N = NBM
                      do 121 l=1,NT
                         TTAB(l) = BMT(l)
                         RKD(l) = BMKD(l)
 121                  continue
                   elseif (ITYPE.eq.3) then
                      N = NOW
                      do 122 l=1,NT
                         TTAB(l) = OWT(l)
                         RKD(l) = OWKD(l)
 122                  continue
                   elseif (ITYPE.eq.4) then
                      N = NSAND
                      do 123 l=1,NT
                         TTAB(l) = SANDT(l)
                         RKD(l) = SANDKD(l)
 123                  continue
                   endif
C
C                  finding real Kd for contact time TCON
                   if (TTAB(1).ge.TCON(i,j)) then
                      RRKD = RKD(1)
                      goto 140
                   elseif (TTAB(N).le.TCON(i,j)) then
                      RRKD = RKD(N)
                      goto 140
                   endif
                   do 130 l=2,N
                      if ((TTAB(l).gt.TCON(i,j))
     +                    .and.(TTAB(l-1).le.TCON(i,j))) then
                         RRKD = RKD(l-1)
                         goto 140
                      endif
 130               continue
C
C                  taking RRKD and PORO value for specific IGTYP
C                  calculating retardation RET
 140               RET = 1.0 + RHO * RRKD * (1.0-PORO(k)) / PORO(k)
                endif
C
C               multiplying contact time TCON with retardation RET for
C               real TCON
                TCON(i,j) = TCON(i,j) * RET
C
C ---           summing up TCON per particle to TTOT
                TTOT(i) = TTOT(i) + TCON(i,j)
C
C ---           summing contact time and pathlength per HF and part
C
                if (ITYPE.eq.1) then
                   TGRAV(i) = TGRAV(i) + TCON(i,j)
                   PGRAV(i) = PGRAV(i) + PCON(i,j)
                elseif (ITYPE.eq.2) then
                   TBM(i) = TBM(i) + TCON(i,j)
                   PBM(i) = PBM(i) + PCON(i,j)
                elseif (ITYPE.eq.3) then
                   TOW(i) = TOW(i) + TCON(i,j)
                   POW(i) = POW(i) + PCON(i,j)
                elseif (ITYPE.eq.4) then
                   TSAND(i) = TSAND(i) + TCON(i,j)
                   PSAND(i) = PSAND(i) + PCON(i,j)
                endif
 110         continue
C
C               conversion of times TTOT from seconds to days
             TTOT(i) = TTOT(i) / (60.0*60.0*24.0)
C
C               conversion of times TGRAV, TBM, TOW, TSAND
C               from seconds to days
             TGRAV(i) = TGRAV(i) / (60.0*60.0*24.0)
             TBM(i) = TBM(i) / (60.0*60.0*24.0)
             TOW(i) = TOW(i) / (60.0*60.0*24.0)
             TSAND(i) = TSAND(i) / (60.0*60.0*24.0)
 100      continue
C
C --- data output to t-tot.dat, t-hf.dat, p-hf.dat
C
          open(3,file='t-tot.dat')
          write(3,*) 'arrival times [d]'
          write(3,*) 3
          write(3,*) 'x'
          write(3,*) 'z'
          write(3,*) 't'
C
          open(4,file='t-hf.dat')
          write(4,*) 'contact times per particle and HF [d]'
          write(4,*) 5
          write(4,*) 'tbm'
          write(4,*) 'tow'
          write(4,*) 'tgrav'
          write(4,*) 'tsand'
          write(4,*) 'tsum'
C
          open(7,file='p-hf.dat')
          write(7,*) 'pathlengths per particle and HF [m]'
          write(7,*) 5
          write(7,*) 'pbm'
          write(7,*) 'pow'
          write(7,*) 'pgrav'
          write(7,*) 'psand'
          write(7,*) 'psum'
C
          do 150 i=1,IPART
             TSUM = TBM(i) + TOW(i) + TGRAV(i) + TSAND(i)
             PSUM = PBM(i) + POW(i) + PGRAV(i) + PSAND(i)
             write(3,910) XPOS(i,NPART(i)),YPOS(i,NPART(i)),TTOT(i)
             write(4,940) TBM(i),TOW(i),TGRAV(i),TSAND(i),TSUM
             write(7,940) PBM(i),POW(i),PGRAV(i),PSAND(i),PSUM
 150      continue
          close(3)
          close(4)
          close(7)
       endif
C
C ---
C ---------------------------------------------------------------------
C
       stop
 900   format(4i5,8e12.5,4i5)
 910   format(3e20.12)
 920   format(i5,5e20.12,3i5)
 930   format(24i3)
 940   format(5e20.12)
       end
```

In der Reihe C der Tübinger Geowissenschaftlichen Arbeiten (TGA) sind bisher erschienen:

Nr. 1: Grathwohl, Peter (1989): Verteilung unpolarer organischer Verbindungen in der wasserungesättigten Bodenzone am Beispiel der leichtflüchtigen aliphatischen Chlorkohlenwasserstoffe. 102 S.

Nr. 2: Eisele, Gerhard (1989): Labor- und Felduntersuchungen zur Ausbreitung und Verteilung leichtflüchtiger chlorierter Kohlenwasserstoffe (LCKW) im Übergangsbereich wasserungesättigte/wassergesättigte Zone. 84 S.

Nr. 3: Ehmann, Michael (1989): Auswirkungen atmogener Stoffeinträge auf Boden- und Grundwässer sowie Stoffbilanzierungen in drei bewaldeten Einzugsgebieten im Oberen Buntsandstein (Nordschwarzwald). 134 S.

Nr. 4: Irouschek, Thomas (1990): Hydrogeologie und Stoffumsatz im Buntsandstein des Nordschwarzwaldes. 144 S.

Nr. 5: Sanns, Matthias (1990): Experimentelle Untersuchungen zum Ausbreitungsverhalten von leichtflüchtigen Chlorkohlenwasserstoffen (LCKW) in der wassergesättigten Zone. 122 S. **(Vergriffen!)**

Nr. 6: Seeger, Thomas (1990): Abfluß- und Stofffrachtseparation im Buntsandstein des Nordschwarzwaldes. 154 S.

Nr. 7: Einsele, Gerhard & Pfeffer, Karl-Heinz (Hrsg.) (1990): Untersuchungen über die Auswirkungen des Reaktorunfalls von Tschernobyl auf Böden, Klärschlamm und Sickerwasser im Raum von Oberschwaben und Tübingen. 151 S.

Nr. 8: Douveas, Nikon G. (1990): Verwitterungstiefe und Untergrundabdichtung beim Talsperrenbau in dem verkarsteten Nord-Pindos-Flysch (Projekt Pigai-Aoos, NW-Griechenland). 165 S.

Nr. 9: Schlöser, Heike (1991): Quantifizierung der Silikatverwitterung in karbonatfreien Deckschichten des Mittleren Buntsandsteins im Nordschwarzwald. 93 S.

Nr. 10: Köhler, Wulf-Rainer (1992): Beschaffenheit ausgewählter, nicht direkt anthropogen beeinflußter oberflächennaher und tiefer Grundwasservorkommen in Baden-Württemberg. 144 S.

Nr. 11: Bundschuh, Jochen (1991): Der Aquifer als thermodynamisch offenes System. - Untersuchungen zum Wärmetransport in oberflächennahen Grundwasserleitern unter besonderer Berücksichtigung von Quellwassertemperaturen (Modellversuche und Geländebeispiele). 100 S.

Nr. 12: Herbert, Mike (1992): Sorptions- und Desorptionsverhalten von ausgewählten polyzyklischen aromatischen Kohlenwasserstoffen (PAK) im Grundwasserbereich. 111 S.

Nr. 13: Sauter, Martin (1993): Quantification and forecasting of regional groundwater flow and transport in a karst aquifer (Gallusquelle, Malm, SW-Germany. 150 S.

Nr. 14: Bauer, Michael (1993): Wasserhaushalt, aktueller und holozäner Lösungsabtrag im Wutachgebiet (Südschwarzwald). 130 S.

Nr. 15: Einsele, Gerhard & Ricken, Werner (Hrsg.) (1993): Eintiefungsgeschichte und Stoffaustrag im Wutachgebiet (SW-Deutschland). 215 S.

Nr. 16: Jordan, Ulrich (1993): Die holozänen Massenverlagerungen des Wutachgebietes (Südschwarzwald). 132 S.

Nr. 17: Krejci, Dieter (1994): Grundwasserchemismus im Umfeld der Sonderabfalldeponie Billigheim und Strategie zur Erkennung eines Deponiesickerwassereinflusses. 121 S.

Nr. 18: Hekel, Uwe (1994): Hydrogeologische Erkundung toniger Festgesteine am Beispiel des Opalinustons (Unteres Aalenium). 170 S.

Nr. 19: Schüth, Christoph (1994): Sorptionskinetik und Transportverhalten von polyzyklischen aromatischen Kohlenwasserstoffen (PAK) im Grundwasser - Laborversuche. 80 S.

Nr. 20: Schlöser, Helmut (1994): Lösungsgleichgewichte im Mineralwasser des überdeckten Muschelkalks in Mittel-Württemberg. 76 S.

Nr. 21: Pyka, Wilhelm (1994): Freisetzung von Teerinhaltsstoffen aus residualer Teerphase in das Grundwasser: Laboruntersuchungen zur Lösungsrate und Lösungsvermittlung. 76 S.

Nr. 22: Biehler, Daniel (1995): Kluftgrundwässer im kristallinen Grundgebirge des Schwarzwaldes – Ergebnisse von Untersuchungen in Stollen. 103 S.

Nr. 23: Schmid, Thomas (1995): Wasserhaushalt und Stoffumsatz in Grünlandgebieten im württembergischen Allgäu. 145+ 92 S.

Nr. 24: Kretzschmar, Thomas (1995): Hydrochemische, petrographische und thermodynamische Untersuchungen zur Genese tiefer Buntsandsteinwässer in Baden-Württemberg. 142 S.

Nr. 25: Hebestreit, Christoph (1995): Zur jungpleistozänen und holozänen Entwicklung der Wutach (SW-Deutschland). 88 S.

Nr. 26: Hinderer, Matthias (1995): Simulation langfristiger Trends der Boden- und Grundwasserversauerung im Buntsandstein-Schwarzwald auf der Grundlage langjähriger Stoffbilanzen. 175 S.

Nr. 27: Körner, Johannes (1996): Abflußbildung, Interflow und Stoffbilanz im Schönbuch Waldgebiet. 206 S.

Nr. 28: Gewald, Thomas (1996): Der Einfluß der Desorptionskinetik bei der Freisetzung von Trichlorethen (TCE) aus verschiedenen Aquifersanden. 67 S.

Nr. 29: Schanz, Ulrich (1996): Geophysikalische Untersuchungen im Nahbereich eines Karstsystems (westliche Schwäbische Alb). 114 S.

Nr. 30: Renner, Sven (1996): Wärmetransport in Einzelklüften und Kluftaquiferen - Untersuchungen und Modellrechnungen am Beispiel eines Karstaquifers. 89 S.

Nr. 31: Mohrlok, Ulf (1996): Parameter-Identifikation in Doppel-Kontinuum-Modellen am Beispiel von Karstaquiferen. 125 S.

Nr. 32: Merkel, Peter (1996): Desorption and Release of Polycyclic Aromatic Hydrocarbons (PAHs) from Contaminated Aquifer Materials. 76 S.

Nr. 33: Schiedek, Thomas (1996): Auftreten und Verhalten von ausgewählten Phthalaten in Wasser und Boden. 112 S.

Nr. 34: Herbert, Mike & Teutsch, Georg (Hrsg.) (1997): Aquifersysteme Südwestdeutschlands - Eine Vorlesungsreihe an der Eberhard-Karls-Universität Tübingen. 162 S.

Nr. 35: Schad, Hermann (1997): Variability of Hydraulic Parameters in Non-Uniform Porous Media: Experiments and Stochastic Modelling at Different Scales. 233 S.

Nr. 36: Herbert, Mike & Kovar, Karel (Eds.) (1998): GROUNDWATER QUALITY 1998: Remediation and Protection - Posters -.- Proceedings of the GQ'98 conference, Tübingen, Sept. 21-25, 1998, Poster Papers. 146 S.

Nr. 37: Klein, Rainer (1998): Mechanische Bodenbearbeitungsverfahren zur Verbesserung der Sanierungseffizienz bei in situ Maßnahmen.- 106 S.

Nr. 38: Schollenberger, Uli (1998): Beschaffenheit und Dynamik des Kiesgrundwassers im Neckartal bei Tübingen.- 74 S.

Nr. 39: Rügner, Hermann (1998): Einfluß der Aquiferlithologie des Neckartals auf die Sorption und Sorptionskinetik organischer Schadstoffe.- 78 S.

Nr. 40: Fechner, Thomas (1998): Seismische Tomographie zur Beschreibung heterogener Grundwasserleiter.- 113 S.

Nr. 41: Kleineidam, Sybille (1998): Der Einfluß von Sedimentologie und Sedimentpetrographie auf den Transport gelöster organischer Schadstoffe im Grundwasser.- 82 S.

Nr. 42: Hückinghaus, Dirk (1998): Simulation der Aquifergenese und des Wärmetransports in Karstaquiferen.- 124 S.